

**APPLICATION OF NONLINEAR SYSTEM
FREQUENCY ANALYSIS AND DESIGN TO
VIBRATION ISOLATION AND ENERGY
HARVESTING**

Diala. H. Uchenna



Primary supervisor: Professor Zi-Qiang Lang

Submitted in fulfilment of the requirements for the degree of
Doctor of Philosophy

Department of Automatic Control and Systems Engineering (ACSE)
Faculty of Engineering
University of Sheffield
2019

Keywords

Vibration Isolation System, Vibration Energy Harvester, Output Frequency Response Function (OFRF), Associated Linear Equations (ALE), Electromagnetic vibration energy harvesters, Electromagnetic Damper

Abstract

Vibration is naturally present in the environment including engineering systems and structures. The presence of vibration can be beneficial or destructive, depending on the nature of the affected system and also the level of vibration. Vibrations at dangerously high levels can be reduced by the addition of some energy dissipation elements (dampers) or/and energy storage elements (springs). Energy dissipation elements, such as dampers, dissipate some of these destructive mechanical vibrations as heat. However, mechanical spring systems absorb and store this mechanical vibration energy as potential energy.

Nonlinear analysis is primarily applied in system analysis and design of engineering systems. Many methods are available to perform this purpose including averaging method, perturbation method, harmonic balance and the recently developed Output frequency response function (OFRF).

The studies presented in this thesis focus on the application of nonlinear system frequency domain analysis and design to vibration isolation and energy harvesting systems. The OFRF method is the analytical and design tool adopted for all studies presented in this thesis. This method is chosen due to its advantage over other methods. This is because the OFRF reveals a significant relationship between the system output spectrum and the parameters that define the system nonlinearities. Therefore, it can facilitate a systematic analysis, design and optimisation process which other approaches are unable to realize.

The first study considered in this thesis is a frequency domain analysis, design and optimisation of a vehicle suspension system which is illustrative of a vibration isolation system. In this study, the suspension system is analysed and designed based on a performance criterion. The main aim of the study is to minimise the transmitted vibration force to a tolerable level. At the specified level, some of the vibration energy is dissipated as heat by the damping system. However, this energy can be harvested into electricity, a process known as energy harvesting. This leads to subsequent studies in this thesis.

The next study considers a vibration energy harvester system with nonlinear cubic damping characteristic. In this study, a concept is investigated, using the OFRF method, which increases the average power harvested by the harvesting device compared to an equivalent linear harvester. An extension of this study is further considered with the addition of a nonlinear hardening stiffness element to primarily broaden the operational bandwidth of the harvesting device.

A final study is then considered where a dual-function system is investigated. The primary function of the system is vibration isolation while its secondary function is energy harvesting. The system is therefore called a dual-function vibration isolation and energy harvester system. This system is optimised for the best dual-function performance subject to existing constraints.

For all the systems considered in this thesis, nonlinearities have been integrated into the existing systems to improve their performance, correspondingly, based on a selected criterion. In addition, the OFRF method has been employed in the analysis, design and optimisation of all the systems considered.

Table of Contents

Keywords	i
Abstract	ii
Table of Contents	iv
List of Figures	viii
List of Tables.....	xv
List of Abbreviations.....	xvi
Statement of Original Authorship	xvii
Acknowledgements	xviii
Research Publications.....	i
Chapter 1: Introduction	1
1.1 Introduction.....	1
1.1.1 Background.....	1
1.1.2 Vibration Isolation	2
1.1.3 Vibration Energy Harvesting	4
1.2 Context.....	6
1.3 Research Aims and Objectives.....	8
1.4 Significance and Scope	11
1.5 Summary of contributions.....	12
1.6 Thesis Outline	13
1.7 Assumptions considered in this thesis.....	14
Chapter 2: Literature Review	17
2.1 Background	17
2.2 Review on Vibration Isolation Systems.....	18
2.3 Review on vibration energy harvesting systems	24
2.4 Output Frequency Response Function (OFRF).....	29

2.4.1	Introduction	29
2.4.2	Volterra series representation of nonlinear systems in the time and frequency domain	30
2.4.3	Determination of the OFRF.....	31
2.4.4	Limitations of the OFRF method	33
2.5	Summary.....	34
Chapter 3: Analysis and design of a nonlinear vibration isolation system...		37
3.1	Introduction	37
3.2	Model formulation.....	39
3.3	Determination of the OFRF representation	41
3.3.1	Determination of the OFRF monomials	41
3.3.2	Determination of the OFRF coefficients	42
3.4	System optimisation.....	46
3.5	Numerical Studies.....	49
3.6	Energy dissipation analysis.....	51
3.6.1	Hysteresis Curves for a nonlinear viscous-elastic model	59
3.7	Conclusions	61
Chapter 4: Analysis, design and optimisation of a vibration energy harvester with damping nonlinearity		65
4.1	Introduction	65
4.2	Model formulation.....	67
4.3	System analysis, design and optimisation.....	69
4.3.1	Determination of the OFRF.....	69
4.3.2	Optimisation of an unconstrained VEH system	73
4.3.3	Optimisation of a constrained VEH system	73
4.4	Electromechanical coupling of the nonlinear vibration energy harvester.....	79
4.5	Parameter estimation of coil and load resistances of the nonlinear VEH system.....	82

4.6	Conclusions.....	90
Chapter 5: Analysis and design of a vibration energy harvester with damping and stiffness nonlinearities 93		
5.1	Introduction.....	93
5.2	Device modeling.....	95
5.2.1	Effect of Nonlinear Stiffness on the harvester power.....	96
5.3	Determination of the OFRF Structure.....	97
5.4	Evaluation of the Associated Linear Equations.....	98
5.5	Determination of the OFRF using the ALES.....	101
5.6	Results and Discussion.....	103
5.6.1	Effects of hardening spring on VEH systems with cubic damping.....	106
5.6.2	Optimisation of an unconstrained nonlinear VEH system.....	108
5.7	Conclusions.....	110
Chapter 6: Analysis, design and optimisation of a dual-function vibration isolation and energy harvesting system..... 111		
6.1	Introduction.....	111
6.2	Model formulation.....	113
6.3	VI-EH System Analysis.....	115
6.4	Experiment for model validation.....	120
6.4.1	Device.....	120
6.4.2	Determination of system parameters.....	122
6.4.3	Model validation against measured data.....	124
6.5	System design and optimisation.....	127
6.6	Effects of load resistance on performance metrics.....	135
6.7	Conclusions.....	137
Chapter 7: Conclusions and Future work 139		
7.1	Conclusions.....	139

7.2	Highlights of main contributions	142
7.3	Recommendations and Future works.....	143
7.3.1	Ongoing fabrication work of a VEH test rig	143
7.3.2	Extensions of research works for future consideration	146
	Bibliography	147

List of Figures

Figure 1.1: Schematic diagram of a (a) force-excited (b) base-excited vibration isolation system.....	2
Figure 1.2: Schematics of vibration isolation methods (a) passive (b) fully active and (c) semi-active.	4
Figure 1.3: Schematic diagram of (a) electrostatic (b) piezoelectric (c) electromagnetic transducers	6
Figure 2.1: Schematic of a base-excited vibration isolation system	21
Figure 2.2: Schematic diagram of a quasi-zero-stiffness vibration isolation system.....	23
Figure 2.3: Principles of Electromagnetic induction.....	25
Figure 2.4: A representation of a typical emVEH with a load resistance, R_L	25
Figure 2.5: A typical dual-function vibration isolation and energy harvesting system with load resistance, R_L	28
Figure 3.1: Schematic of the nonlinear suspension system under a base excitation.....	39
Figure 3.2: Comparison between OFRF and numerical simulation for (a) $Z(j\omega_r)$ and (b) $F_{trans}(j\omega_r)$, output spectra of system (3.4) respectively.	45
Figure 3.3: Output spectrum of the transmitted force, $ F_{trans}(j\omega_r) $	47
Figure 3.4: Contour map of the Output spectrum of the transmitted force, $ F_{trans}(j\omega_r) $	47
Figure 3.5: Comparison of the system output response, at resonance, under linear and nonlinear conditions.	48
Figure 3.6: Comparison of the system output spectrum under linear and nonlinear conditions across the entire frequency range.	49

Figure 3.7: Effect of linear damping characteristic parameter on the system output spectra across the entire frequency range with $c_2 = 10\text{N.s.m}^{-3}$ and $k_2 = 100\text{N.m}^{-3}$	50
Figure 3.8: Effect of nonlinear stiffness characteristic parameter on the system output spectra across the entire frequency range with $c_1 = 0.5\text{N.s.m}^{-1}$ and $c_2 = 10\text{N.s.m}^{-3}$	50
Figure 3.9: Effect of nonlinear damping characteristic parameter on the system output spectra across the entire frequency range with $c_1 = 0.5\text{N.s.m}^{-1}$ and $k_2 = 100\text{N.m}^{-3}$	50
Figure 3.10: Relationship between the Energy dissipation and design parameters at $\Omega = 1$	53
Figure 3.11: Energy dissipation plot for sets of design parameters at $\Omega = 1$	53
Figure 3.12: Energy dissipation levels for different combinations of design parameters at $\Omega = 0.4$	54
Figure 3.13: Energy dissipation levels for different combinations of design parameters at $\Omega = 2$	54
Figure 3.14: Contours of energy dissipation levels for sets of design parameters.	55
Figure 3.15: Effect of linear damping characteristic parameter on the energy dissipation level across all frequency range with $c_2 = 10\text{N.s.m}^{-3}$ and $k_2 = 100\text{N.m}^{-3}$	56
Figure 3.16: Effect of nonlinear damping characteristic parameter on the energy dissipation level across all frequency range with $c_1 = 0.5\text{N.s.m}^{-1}$ and $k_2 = 100\text{N.m}^{-3}$	56
Figure 3.17: Effect of nonlinear stiffness characteristic parameter on the energy dissipation level across all frequency range with $c_1 = 0.5\text{N.s.m}^{-1}$ and $c_2 = 10\text{N.s.m}^{-3}$	57

Figure 3.18: Variation of energy dissipated and force transmitted by the suspension system with respect to k_2 at $c_1 = 1.5 \text{ N.s.m}^{-1}$ and $c_2 = 23.9 \text{ N.s.m}^{-3}$	58
Figure 3.19: Variation of energy dissipated and force transmitted by the suspension system with respect to c_2 at $c_1 = 1.5 \text{ N.s.m}^{-1}$ and $k_2 = 164.2 \text{ N.m}^{-3}$	58
Figure 3.20: Variation of suspension damper force and energy dissipated by the suspension system with frequency at $c_1 = 0.5 \text{ N.s.m}^{-1}$ and $c_2 = 10 \text{ N.s.m}^{-3}$	59
Figure 3.21: Comparison of the Hysteresis curves for the vibration isolation system having different combinations of nonlinear parameters at resonance. (b) is shown in Figure 3.22.	60
Figure 3.22: Enlarged origin of the hysteresis curves in Figure 3.21.	61
Figure 4.1: SDOF base-excited vibration energy harvester with a nonlinear damper.....	67
Figure 4.2: Comparison between OFRF analytical and Runge-Kutta numerical solution: a) relative mass displacement, b) Average power.....	72
Figure 4.3: Comparison of the output frequency response of system (4.3) determined using analytical (OFRF) method and numerical simulations.	75
Figure 4.4: Comparison of the average power of the VEH system of Eq. (4.6) determined using analytical (OFRF) method and numerical simulations.	75
Figure 4.5: Comparison of the system performances under the non-optimised and optimised cases. (a) time history and (b) Output response curves for the relative displacement of the VEH system.	76
Figure 4.6: Comparison of the average harvestable power obtained under the non-optimised and optimised cases.....	77

Figure 4.7: Average harvestable power obtained at different excitation frequencies, $\Omega = \omega/\omega_r$ and nonlinear damping parameter values, c_3 .	78
Figure 4.8: Contour plot for the average harvestable power obtained at different excitation frequencies, $\Omega = \omega/\omega_r$ and nonlinear damping parameter values, c_3 .	78
Figure 4.9: Schematic representation of a vibration-based energy harvester with a nonlinear resistive load.	79
Figure 4.10: Comparison between the force-velocity characteristics for the desired damping force and estimated electrical damping force, respectively.	82
Figure 4.11: Simulink implementation of the VEH system.	83
Figure 4.12: Comparison between the time histories of the desired damping force (blue solid) and the actual electrical damping force (red dash).	85
Figure 4.13: Relative displacement for the linear and nonlinear VEH systems at maximum excitation, Y_{\max} .	85
Figure 4.14: Average power for the linear and nonlinear VEH systems at maximum excitation, Y_{\max} .	86
Figure 4.15: Relative displacement for the linear and nonlinear VEH systems at an excitation of $0.1Y_{\max}$.	86
Figure 4.16: Average power for the linear and nonlinear VEH systems at an excitation of $0.1Y_{\max}$.	87
Figure 4.17: Time histories of the VEH circuit currents for the linear (blue dash) and nonlinear (red solid) VEH systems.	88
Figure 4.18: Time histories of the actual damping forces for the linear (blue dot) and nonlinear (red solid) VEH systems.	88
Figure 4.19: Time histories of the induced open circuit voltages for the linear (blue dash) and nonlinear (red solid) VEH systems.	89

Figure 4.20: Time histories of the voltages across the load resistance for the linear (blue dash) and nonlinear (red solid) VEH system.	89
Figure 5.1: SDOF of a vibration energy harvester with nonlinear stiffness and damping.	95
Figure 5.2: Effect of nonlinear stiffness on the resonant frequency	96
Figure 5.3: A representation of the individual ALE contributions to the general output response of system (5.2).	100
Figure 5.4: Graph of individual nth-order ALE contributions to the output response of system (5.2) at the fundamental frequency.	100
Figure 5.5: ALE-OFRF vs numerical simulation results for the output spectra and average power respectively at $c_3 = 0.45$ and $k_3 = 250$	104
Figure 5.6: ALE-OFRF vs numerical simulation results for the output spectra and average power respectively at $c_3 = 0.25$ and $k_3 = 270$	105
Figure 5.7: Effect of hardening stiffness on the output spectrum and average power of the nonlinear VEH system.	107
Figure 5.8: Output spectrum of system (5.2) versus a variation of c_3 and k_3 at $\Omega = 1$	108
Figure 5.9: Average power of VEH versus a variation of c_3 and k_3 at $\Omega = 1$	109
Figure 5.10: Y-X view of the Average power of VEH for a variation of c_3 and k_3 at $\Omega = 1$	109
Figure 6.1: Model schematic of the dual-function VI-EH system.	113
Figure 6.2: Comparison between the OFRF analytical and Runge-Kutta numerical solution: a) Transmissibility, b) Output power, and c) Energy conversion efficiency at four acceleration levels 0.25g, 0.50g, 0.75g, and 1.0g [m.s ⁻²].	119
Figure 6.3: The representative dual-function VI-EH device fabricated and adopted in this work: a) Fully fabricated and assembled VI-EH device,	

b) Cross-sectional view of the VI-EH device, and c) 2D sketch of the VI-EH device with detailed geometries and dimensions.	121
Figure 6.4: Experiment setup used to estimate restoring forces of the VI-EH device.	123
Figure 6.5: Measured total restoring force of the VI-EH device.	123
Figure 6.6: Apparatus used for dynamic characterization of the VI-EH device.	125
Figure 6.7: Measured and modelled simulated displacement transmissibility of the VI-EH device at 0.5g [m.s ⁻²].	126
Figure 6.8: Measured and modelled output power from the VI-EH device at 0.5g [m.s ⁻²].	126
Figure 6.9: Model simulation of the performance of the VI-EH system subject to variation in linear damping, c_1 while keeping k_3 fixed: a) Transmissibility, b) Output power, and c) Energy conversion efficiency at 4 acceleration levels 0.25g, 0.50g, 0.75g, and 1.0g [m.s ⁻²].	129
Figure 6.10: Design criteria for the nonlinear stiffness coefficient, k_3 : a) Transmissibility, b) Output power, and c) Energy conversion efficiency at four acceleration levels 0.25g, 0.50g, 0.75g, and 1.0g [m.s ⁻²].	134
Figure 6.11: The Output power of the VI-EH system as a function of R_L while keeping k_3 fixed at the optimum value for four acceleration levels 0.25g, 0.5g, 0.75g and 1.0g [m.s ⁻²].	136
Figure 6.12: Effect of the Energy conversion efficiency of the VI-EH system to variation in R_L while keeping k_3 fixed at the optimum value for four acceleration levels 0.25g, 0.5g, 0.75g and 1.0g [m.s ⁻²].	136
Figure 7.1: CAD model of (a) geometric and (b) right-side views of the proposed vibration energy harvester test rig.	144
Figure 7.2: Electromagnetic damper by Aerotech, Inc.	144

Figure 7.3: CAD models (a) and actual assembly (b) of the vibration energy

harvester test rig 145

List of Tables

Table 2.1: Established facts of earlier studies for linear SDOF emVEHs	26
Table 3.1: Results from the optimisation problem.....	46
Table 4.1: Maximum average harvestable power attainable at $\omega = 6.3 \text{ rad s}^{-1}$ ($\Omega = 1$) subject to the system constraint, $Z_{\max} = 2.5 \text{ m}$	74
Table 5.1: Simulation (Training) values of model design parameters	101
Table 6.1: Systems parameters and properties of the fabricated multi-function VI-EH device.	124
Table 6.2: Maximum energy conversion efficiency attainable at specific nonlinear stiffness value subject to the system constraints at predetermined base accelerations	130
Table 6.3: Maximum energy conversion efficiency attainable at specific nonlinear stiffness value subject to the system constraints considering the normalized weight contribution of each excitation.....	132
Table 7.1: Shaker device specifications	143

List of Abbreviations

ALE	Associated Linear Equations
CAD	Computer Aided Design
EMD	Electromagnetic Damper
emVEHs	Electromagnetic vibration energy harvesters
GA	Genetic Algorithm
HBM	Harmonic Balance Method
HSLDS	High-Static-Low-Dynamic Stiffness
MDOF	Multiple Degrees of Freedom
MEMS	Micro-Electro-Mechanical Systems
MR	Magnetorheological
NDE	Nonlinear Differential Equation
OFRF	Output Frequency Response Function
QZS	Quasi-Zero-Stiffness
SDOF	Single Degree of Freedom
SIMO	Single Input Multiple Output
SMA	Shape Memory Alloy
VEH	Vibration Energy Harvester
VEHs	Vibration Energy Harvesters
VI-EH	Vibration Energy Harvester
VIS	Vibration Isolation System

Statement of Original Authorship

The work contained in this thesis has not been previously submitted to meet requirements for an award at this or any other higher education institution. To the best of my knowledge and belief, the thesis contains no material previously published or written by another person except where due reference is made.

Signature: _____

Date: _____

Acknowledgements

My utmost gratitude goes to the Almighty God, for his guidance, wisdom and understanding he bestowed on me throughout this doctoral programme. I also thank him for his blessings on my family.

I also wish to thank my beautiful wife, Amara, for her immense support and encouragement for the duration of my doctoral programme. I also acknowledge my gorgeous children, Tziona and Jaden who are always ready to put a smile on my face when I feel fatigued from work.

I would like to thank my supervisor, Professor Zi-Qiang Lang for his outstanding supervision, constructive criticisms and immense support throughout the duration of my doctoral programme.

I would also love to appreciate my colleagues and dear friends that have made this journey a memorable one.

Research Publications

Some of the studies presented in this thesis have been published as outlined below.

- *Nonlinear Design and Optimisation of a Vibration Energy Harvester*; Diala U., Gunawardena R., Zhu Y. and Lang Z.Q. in 2018 UKACC 12th International Conference on Control (CONTROL 2018), pp. 180-185. IEEE, 2018.
- *Geometric Nonlinear Damper Design – A frequency-based approach*; Diala U.H., Okafor K.C. and Lang Z.Q., in Proc. IEEE 3rd Int. Conf. on Electro-Technology for National Development (NIGERCON 2017), Vol. 2, pp.500-503, 2017.
- *Analysis and Design of a Nonlinear Vibration-based Energy Harvester – A frequency-based approach*; Diala U.H., Pope S.A. and Lang Z.Q., in Proc. IEEE Int. Conf. on Advanced Intelligent Mechatronics (AIM 2017), Munich, pp.1550 - 1555, 2017.
- *Analysis, Design and Optimisation of a Nonlinear Energy Harvester*; Diala U.H., Pope S.A., and Lang Z.Q., in the 24th International Congress on Sound and Vibration (ICSV24), London, 23-27 July 2017.
- *Analysis and Optimal Design of a Vibration Isolation System Combined with Electromagnetic Energy Harvester*; Diala U. H., Mofidian S. M., Lang Z. Q. and Bardaweel H.; Journal of Intelligent Material Systems and Structures (2019), 30(16), pp.2382-2395.

Chapter 1: Introduction

This chapter outlines the background in Section 1.1, the context of the research in Section 1.2 and the research objectives in Section 1.3. Section 1.4 describes the significance and scope of this research and provides definitions of terms used. Finally, Section 1.6 includes an outline of the remaining chapters of the thesis.

1.1 INTRODUCTION

1.1.1 Background

Vibration can be described as the repetitive motion of a body relative to a nominal position of equilibrium [1]. It is a natural phenomenon occurring in different aspects of life. For example, the human body naturally vibrates at varying frequencies. The heart and lung undergo low frequency vibrations while the ear undergoes high frequency vibration. Inanimate objects like machines with rotating parts can vibrate due to an unbalanced dynamic system structure during normal operations [2]. Such vibrations are undesirable as they can cause harmful effects to the machines or the user. Examples of machines that exhibit vibrations include washing machines, ventilators, turbines etc.

Structures such as buildings and bridges also experience vibrations for different reasons which could include; presence of operational machinery in the environment, movements of vehicles and people, earthquakes and wind. These stress oscillations due to vibrations can lead to fatigue failure of the structural assembly. Structures such as buildings and bridges, can suffer a collapse under severe vibrations caused by earthquakes and wind. Similarly, machines such as automobiles and washing machines can experience a fault due to vibration effects over a period of time.

Micro-vibrations are low amplitude vibrations generated in structures such as Space systems. These vibrations need to be isolated as they can severely degrade the performance of sensitive machines on Space stations and shuttles. Such effects can happen while taking high precision space measurements using precision instruments like an electron microscope, special sensors etc. Such vibrations could result to poor measurement readings and eventually poor results from data analysis [1], [2].

1.1.2 Vibration Isolation

Vibration isolation involves the reduction in the levels of unwanted and undesirable vibrations transmitted within engineering structures and machineries. For several decades, this has been a challenging task for engineers. A vibration isolation system (VIS) consists of the body being isolated, the supporting foundation and the vibration isolators positioned between the body and the foundation [3].

To quantify the effectiveness or performance of a VIS, a key performance index called ‘transmissibility’ is used. Under harmonic excitation, for a force-excited VIS, force transmissibility is the ratio of the magnitudes of the force transmitted to the base structure, $f_o(t)$, to the excitation force, $f_{in}(t)$, i.e. $T_f = |f_o|/|f_{in}|$. Similarly, for a base-excited VIS, the absolute displacement transmissibility is the ratio of the magnitudes of the mass-displacement, $x(t)$, to the base-structure displacement, $y(t)$, i.e. $T_d = |x|/|y|$, at a specific frequency of interest [4]. Figure 1.1 illustrates both excitation types.

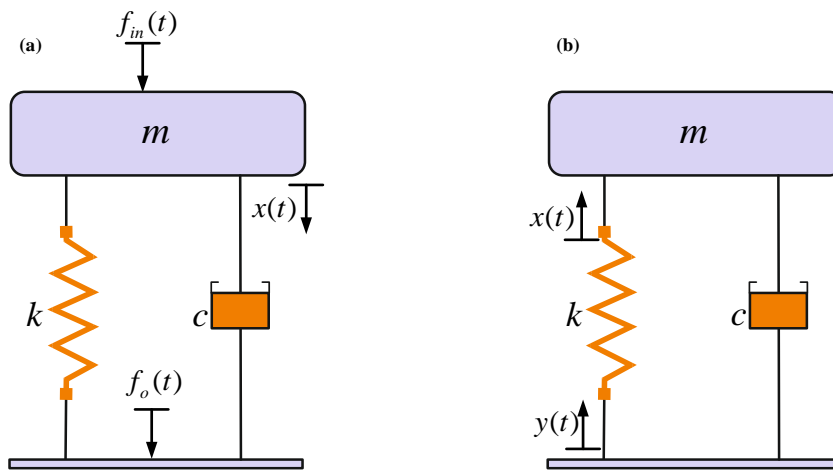


Figure 1.1: Schematic diagram of a (a) force-excited (b) base-excited vibration isolation system

Many vibration isolation methods have been proposed and designed; however, three major methods have been widely studied. These methods include; Passive, semi-active isolation and fully active. These methods are now discussed in turn.

Passive vibration isolation

This vibration isolation method refers to the mitigation of vibration disturbances using passive techniques such as rubber pads, elastomers, mechanical springs, fluids

or negative-stiffness components. Implementation of a passive isolation system requires no external power source for its functionality. A conventional passive vibration isolator also includes a high performance damper such as visco-elastic composite dampers or viscous fluid dampers [5] which dissipates the vibration energy as heat. Though this method of isolation performs well at high frequencies as it prevents the transmission of high frequency disturbances, its performance at low frequency range is quite poor [3][6]. The amplification at resonance can be reduced by increasing the damping of the system, however, high frequency isolation is degraded [7]. This inherent limitation of the passive isolation method motivated the investigation of controlled suspension systems like the active and semi-active methods. A schematic diagram of a typical passive vibration isolation system is shown in Figure 1.2(a).

Active vibration isolation

This method aims at improving vibration isolation performance with the application of an actuator in the isolation interface and sensors at the end of the transmission route with a feedback control law guiding the actuator. The actuators and sensors are used to provide control force and feedback signals respectively thereby ensuring a good isolation performance at both low and high frequency regions. In this isolation method, the isolator stiffness and damping are made adjustable to improve the isolation performance through active feedback control [8]–[11]. However, this method has some limitations such as complexity, cost (due to the need for conditioning electronics for the sensors and power electronics for the actuator) and external power source for the actuators. A schematic of a typical fully active vibration isolation system is shown in Figure 1.2(b).

Semi-active isolation

In this isolation method, the benefits of both passive and active isolation methods are combined while avoiding their drawbacks. Semi-active isolation elements provide the adaptability of active isolation elements with no external power requirement. In a semi-active vibration isolator, for example, the damper is typically replaced by a controllable, electromechanical, adjustable-orifice valve with dissipative characteristic [12]–[16]. As a result of its high reliability, minimal cost and comparable performance to the active isolators, they are more widely accepted in the automotive industry. A schematic of a typical semi-active vibration isolation system is shown in Figure 1.2(c).

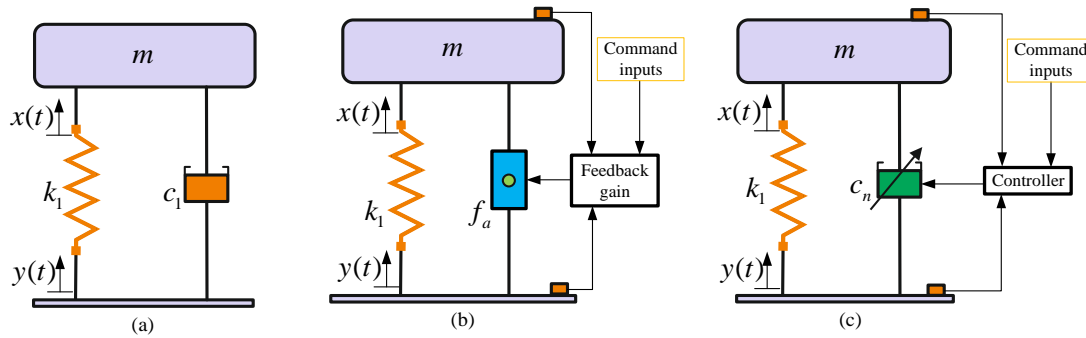


Figure 1.2: Schematics of vibration isolation methods (a) passive (b) fully active and (c) semi-active.

Vibration isolation elements generally comprise a spring and damper and are both assumed to be massless. The vibration energy generated by the seismic disturbance is absorbed by the spring as potential energy but dissipated by the damper as heat energy. However, the vibration energy can also be converted from its mechanical form to a useful form such as electrical energy. This conversion process, known as vibration energy harvesting, is a subset of energy harvesting which is the process of garnering electrical energy from ambient energy. Vibration energy harvesting employs one or more of three main transduction mechanisms as discussed in Section 1.1.2.

1.1.3 Vibration Energy Harvesting

Energy harvesting is the conversion of ambient energy from the environment to electrical energy. Some ambient energy sources include heat, radio wave, light energy, vibration etc. In recent years, energy harvesting has received considerable attention due to advances in power electronics and low-powered wireless sensors [17]. The interest in energy harvesting is growing since the era of the Internet of Things (IoT) which targets microelectronics and wearable technologies. Although there are many different ambient sources of energy, this study focuses on ambient vibration as a source of energy.

Vibration sources such as human motion, ocean waves, seismic activities are capable of delivering harvestable mechanical energy that can be used for powering miniature electronics [18]. This energy can be extracted by utilizing one or an integration of different transduction mechanisms. There are three basic transduction

mechanisms namely; electrostatic, piezoelectric, and electromagnetic energy harvesting.

Electrostatic energy harvesting

The Electrostatic transduction technology employs a variable capacitive device and exploits the relative movement between the electrically isolated capacitor plates to produce energy. The distance between the plates of the variable capacitor vary (or the area of the plates are adjusted) in response to external motions inducing an application of mechanical energy [19], [20]. The effect of the variation in distance between the plates causes a change in capacitance thus causing an increase in voltage in a constrained charge system or an increase in charge in a constrained voltage system [20]. This enables the conversion of mechanical energy, generated from the relative motion, to electrical energy according to the principle of electrostatics. A schematic of a typical Electrostatic energy harvester is shown in Figure 1.3(a).

Piezoelectric energy harvesting

Piezoelectricity is a coupling method between the mechanical and electrical behaviours of a specific class of ceramics and crystals (known as active materials). A piezoelectric material generates an electric field when under mechanical stress/strain [21]. This transduction mechanism as shown in Figure 1.3(b) has recently received the greatest attention compared to the other two. This is largely due to their large power densities and ease of application compared to the other transduction mechanisms [22]. Another benefit of the piezoelectric transduction mechanism over the other two is the possibility of producing piezoelectric devices in macro- as well as micro-scale due to its well-established thick and thin-film production techniques.

Electromagnetic energy harvesting

Most electromagnetic generators operate on the basic principle of Faraday's Law of electromagnetic induction. Electromagnetic induction is the generation of electric current within a conductor placed across a magnetic field. Faraday's law states that the rate of change of the magnetic flux linkage of the circuit is proportional to the electromotive force (EMF) or voltage induced in a circuit [23]. This is typically realised using a device as described in Figure 1.3(c). The concept of realisation enables a permanent magnet to be excited by the ambient vibration thus causing a relative motion between the magnet and the coil wound around the outer block of the device.

The relative motion causes a time-varying magnetic flux which results to an EMF being generated across the coil terminals.

In this thesis, the discourse on energy harvesters will focus on electromagnetic energy harvesters and accordingly a significant part of the literature review will concern this transduction mechanism.

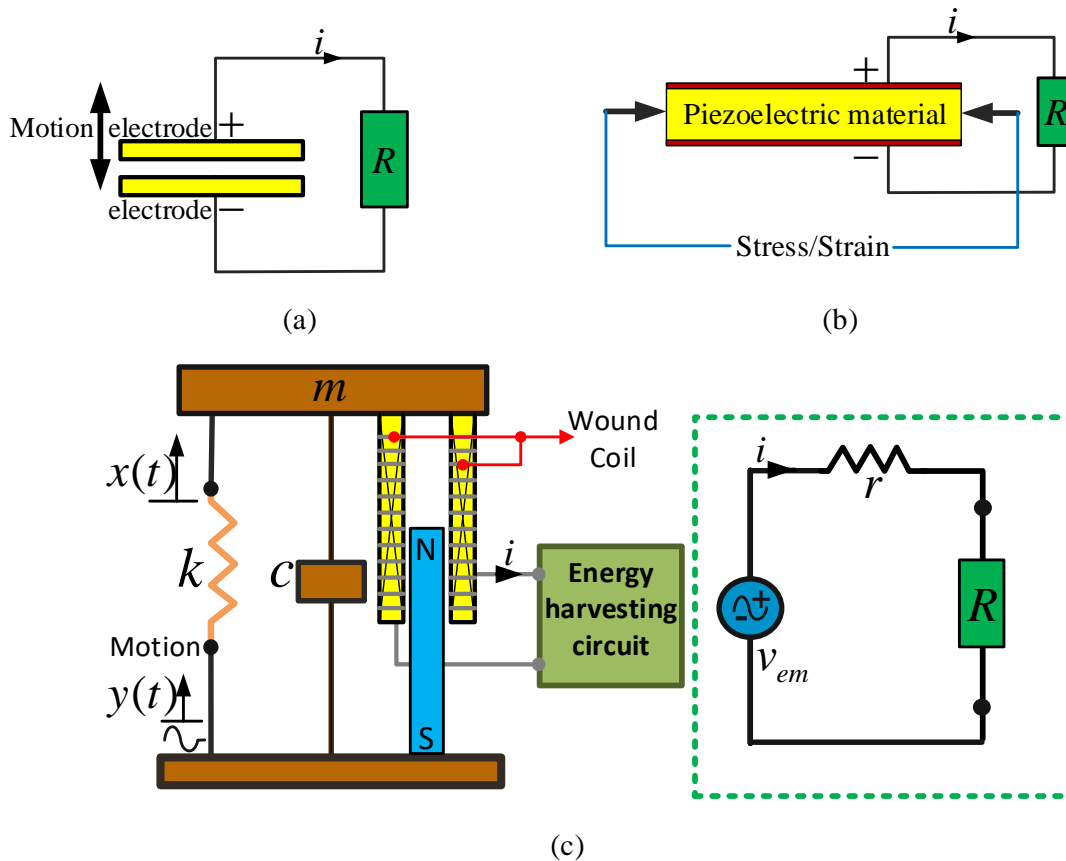


Figure 1.3: Schematic diagram of (a) electrostatic (b) piezoelectric (c) electromagnetic transducers

1.2 CONTEXT

Vibration isolation and energy harvesting involve two processes. The first encompasses the isolation of an object from the adverse effect of ambient vibration using several configurations of isolation elements. The second (energy harvesting) entails the conversion of vibration energy to electrical energy. Vibration isolation systems are usually designed for frequencies within the isolation range ($\omega > \omega_n \sqrt{2}$)

whereas vibration energy harvester (VEH) systems are typically designed to operate within the resonant region where maximum power is harvested.

The focus of this thesis is concerned with three studies which are:

(a) Analytical study, design and optimisation of a Vibration Isolation System (VIS) e.g. a vehicle suspension system. In this study, a VIS is designed in the form of a vehicle suspension system whereby the main objective is to minimise the transmission of vibration force from the source of vibration to the object to be protected.

(b) Analysis, design and optimisation of a Vibration Energy Harvester (VEH) system with nonlinear damping characteristic. This study comprises the investigation of an approach to increase the average power harvested by a VEH system by integrating a cubic damping characteristic. A further extension to this study was considered by including a nonlinear stiffness characteristic to broaden the operational frequency range.

(c) The final study considered a dual-function system - a Vibration Isolation and Energy Harvester (VI-EH) system. The proposed system has a primary function of isolating vibration and a secondary function of harvesting any available energy. The need for dual-function systems capable of isolating vibrations and simultaneously harvesting available energy has received significant interest lately. This is majorly due to advancement in micro-electro-mechanical systems (MEMS) application.

For all three studies, the effect of deliberately integrating nonlinearities in the dynamic characteristics of each corresponding system of interest is explored. This is conducted to improve the performance of the system of concern based on selected performance metrics. Therefore, the studies considered in this work can be classified into; Vibration isolation systems, Vibration energy harvesting systems and Dual-purpose vibration isolation and energy harvesting systems. These are explored comprehensively in Chapters 3-6, respectively.

The generic models of these systems are of the Nonlinear Differential Equation (NDE) form. Analytical tools employed for the study of such systems include the methods of averaging [24], perturbation [25], multiple scales [26], [27] and Harmonic Balance [28], [29]. For the studies proposed in this thesis, a frequency domain analysis, design and optimisation will be conducted using the recently developed Output

Frequency Response Function (OFRF) method [30], [31]. The use of the OFRF approach is more beneficial as it defines, analytically, a relationship between the output spectrum of the system and the system parameters. Therefore, it facilitates a systematic analysis, design and optimisation process.

1.3 RESEARCH AIMS AND OBJECTIVES

The adverse effects of environmental vibration on engineering structures has been established and several techniques have been developed to efficiently isolate these vibrations. However, recently, there has been more focus on developing efficient methods of converting the vibration energy into useful electrical energy. The studies investigated in this thesis focus on both isolation of environmental vibration energy from engineering structures and also the conversion of this energy into electricity. Therefore, the research goals of this work are to investigate approaches to improve the performances of a vibration isolation system, vibration energy harvesting system and a dual-purpose vibration isolation and energy harvesting system. Each chapter investigates a different system. However, while Chapter 3 considers a vehicle suspension system, Chapters 4 and 5 considers primarily vibration energy harvesters and, finally, a dual-function device is considered in Chapter 6. The objectives required to realise these goals are highlighted as follows.

- **Vibration isolation system:** This study examines a vehicle suspension system which is representative of a vibration isolation system. Although previous studies have investigated a similar system, little attention has been given to the energy dissipation process of such a system. Therefore, the main objective of this study is to investigate the energy dissipation process of the proposed suspension system based on the derived OFRF model. It is demonstrated that, using the OFRF model of the suspension system, an estimate of the energy dissipation level, of the designed suspension system, can be obtained. The tasks involved for this study are outlined as follows:
 - Derive an OFRF representation of the output spectra of the system of interest.
 - Demonstrate the accuracy of the OFRF representation in describing the actual system.

- Analyse, design and optimise the vibration suppression performance with respect to the design parameters (using the OFRF representation).
- Ensure the design criteria is met under existing constraints.
- Compare and demonstrate that the designed system outperforms the corresponding linear suspension system.
- Derive an OFRF representation of the energy dissipation level of the suspension system.
- Analyse the energy dissipation level of the proposed suspension system using the OFRF representation.
- Demonstrate the effects of the design parameters on the energy dissipation level of the suspension system.

The vibration energy that is dissipated as heat, by the suspension system, can be harvested into electricity. This is known as vibration energy harvesting and it is examined in Chapter 4.

- **Vibration energy harvesting system:** This study investigates, firstly, an approach to increase the average power harvested within a constrained bandwidth. The objective of this study is to employ the OFRF method, for the first time, in the analysis, design and optimisation of a VEH system with nonlinear damping characteristics. In addition, a systematic design procedure will be demonstrated, from analysis to implementation stage, for the design of the VEH system. The following tasks are proposed to achieve the objective of this study.
 - Derive an OFRF representation of the VEH system of interest. Demonstrate that the derived OFRF representation precisely describes the output characteristics of the real system.
 - Analyse, design and optimise the VEH system with respect to a nonlinear damping characteristic parameter integrated into the system. This is to be conducted for two cases; without constraint and with constraint.
 - Compare and demonstrate that the nonlinear design outperforms an equivalent linear device by harvesting more power at several excitation levels.

- Further develop an electromechanical representation of the actual VEH system. Show the electrical characteristics of the VEH design.

An extension of this study is also presented with the integration of a nonlinear hardening stiffness characteristic parameter. This is required to extend the operational bandwidth of the VEH system. This is the first effort, to the best of the author's knowledge, to investigate a VEH system simultaneously integrated with both nonlinear cubic damping and stiffness characteristics. The following tasks are proposed for this study.

- Derive an OFRF representation of the output spectra of the actual system using the Associated Linear Equation (ALE) decomposition method.
 - Demonstrate the effectiveness of the derived ALE generated OFRF (ALE-OFRF) representation. Show it accurately describes the system output characteristics.
 - Analyse, design and optimise the system using the design parameters and performance metrics of interest.
 - Show the effect of the integrated hardening stiffness parameter on the operational bandwidth of the VEH device with respect to the average power harvested.
- **Dual-purpose vibration isolation and energy harvesting system:** This study proposes a dual-function device capable of isolating vibration (primary function) and also harvesting available energy (secondary function). This study is motivated by the increasing interest in self-powering devices. The objective here is to analytically investigate the dual-function VI-EH device, which is, to the best of the author's knowledge, the first effort to consider this. The required tasks for the proposed study are outlined below.
 - Determine the OFRF representation of the output spectra of the actual system for each excitation level. Demonstrate that the OFRF representation correctly defines the actual system characteristics.
 - Validate that the analytical model (OFRF) matches the experimental model.
 - Analyse, design and optimise the system using the design parameters and considering each excitation level.

- Investigate a comprehensive optimisation process while considering all excitation levels simultaneously.
- Show the effects of the resistive load on the desired performance metrics of the VEH system.

It should be noted that the systems considered in this thesis are analysed, designed and optimised for the chosen parameter(s) of interest to achieve an improved performance based on the chosen performance metrics. In addition, only odd order stiffness and damping nonlinearities are considered due to their established effectiveness in nonlinear system design.

1.4 SIGNIFICANCE AND SCOPE

Several sources of vibration such as wind, human motion, machines etc. can generate pulsations that are capable of either adversely affecting the performance of a device or causing destructive effects on engineering structures. These unwanted vibrations can cause problems like measurement errors in sensitive measuring devices, rotation imbalance in rotating machinery, dynamic instability or fatigue cracking in engineering structures. The need to develop efficient methods for the isolation of these unwanted vibrations cannot be emphasized enough. While different isolation techniques have been developed to mitigate the effects of these unwanted vibrations, methods have been established to capture and utilise the vibration energy. The significance of the research studies reported in this thesis is that it investigates ways to enhance the performances of vibration isolation systems and vibration energy harvesting systems. These systems are represented in diverse configurations depending on its key function. For example, the study reported in Chapter 3, which is a vehicle suspension system is representative of a vibration isolation system. The suspension system considered is analysed, designed and optimised based on desired design criteria to improve its isolation performance. In addition to this, an energy dissipation analysis is also performed which can be employed as a performance metric as well. The systems considered in Chapters 4 and 5 are representative of a vibration energy harvesting system. However, based on the specific model formulation which is dependent on the enhancements needed, certain nonlinear components are introduced to realize the desired performance. In Chapter 4, a nonlinear damping parameter is

introduced to increase the dynamic range of the device. However, in Chapter 5, a nonlinear hardening stiffness was introduced to a model similar to that formulated in Chapter 4, to extend the operating bandwidth of the device. In Chapter 6, a dual-purpose device is formulated to concurrently perform the functions of a vibration isolation system (primary) and a vibration energy harvesting system (secondary). The system is designed and optimised to provide the best performance possible.

1.5 SUMMARY OF CONTRIBUTIONS

A brief summary of contributions in this thesis are outlined as follows:

❖ Chapter 3

The major contribution of the study presented in this chapter is the novel investigation of the Energy dissipation level of a designed vehicle suspension system using the OFRF method. This also involved a Hysteresis analysis of the vehicle suspension system based on the OFRF design. Using the OFRF method, it was demonstrated that the energy dissipation level, for a designed vehicle suspension system, can be estimated. The effect of each nonlinear design parameter was also demonstrated.

❖ Chapter 4

The major contribution of the research work presented in this chapter, is the novel application of the OFRF method in the analysis, design and optimisation of a nonlinear VEH system. In this study, a cubic damping characteristic was considered and a systematic way of proceeding from the design stage to implementation stage, is demonstrated.

❖ Chapter 5

In this chapter, and for the first time, a VEH device is investigated with the integration of both damping and stiffness nonlinearities. Furthermore, a novel application of the OFRF method was employed. However, in this study, the OFRF model was derived using the ALE decompositions of the actual system model.

❖ Chapter 6

This chapter considered a dual-function vibration isolation and energy harvesting system. The novel OFRF method was employed in the analysis, design and optimisation of the dual-function VI-EH system. The system was optimised for the

nonlinear stiffness parameter. This work is the first effort to tackle the issue of simultaneous vibration isolation and energy harvesting system using an analytical approach (the OFRF method).

1.6 THESIS OUTLINE

The rest of this thesis is structured as follows:

Chapter 2 gives a comprehensive discussion of previous studies of related systems considered in this thesis. These include; vibration isolation systems, vibration energy harvesting systems and dual-purpose vibration isolation and energy harvesting systems. Early works on the major vibration isolation schemes comprising passive, semi-active and fully active isolation schemes, are considered. The incorporation of nonlinear components to the dynamic models of several configurations of vibration isolation system are surveyed. Integration of nonlinear characteristics due to inherent design and geometric formation are equally explored. Moreover, for vibration energy harvesting systems, a significant part of the work discussed are that of the electromagnetic transduction method. The improvements in the energy harvesting capability of the devices using nonlinear dynamic components, are also covered in this chapter.

In Chapter 3, a frequency domain analysis, design and optimisation of a vehicle suspension system descriptive of a vibration isolation system is presented. The OFRF method is employed for this study as it facilitates the analysis and design of nonlinear systems. This is because it explicitly expresses the output spectrum of the system of interest in terms of the design parameters. Furthermore, a novel application of the OFRF method in the analysis of the energy dissipation level of the designed suspension system is also provided. The effect of the design parameters on this performance metric is also examined. The conclusions in this chapter lead to the study in Chapter 4.

Chapter 4 provides a novel application of the OFRF method in the analysis, design and optimisation of a vibration energy harvester. For the system considered in this study, a nonlinear cubic damping characteristic is introduced as a result of the resistive load characteristics in the energy harvesting circuit. It is also demonstrated that the nonlinear vibration energy harvester performs better than an equivalent linear device. The Chapter also shows an electromechanical system representative of the

actual energy harvester which can be used to simulate the dynamic characteristic of the real system.

Chapter 5 presents an extension of the study reported in Chapter 4. In this chapter, a second nonlinear component i.e. hardening stiffness, is integrated into a VEH system with cubic damping characteristic. This is expected to broaden the bandwidth of the VEH system. In this study, the Associated Linear Equations (ALE) method is briefly introduced and subsequently, the ALE decomposition of the VEH dynamic model is used to determine the OFRF of the model. The ALE-generated-OFRF representation is further used for analysis and design of the system of interest. The effect of the nonlinear hardening stiffness is also presented.

In Chapter 6, a dual-purpose vibration isolation and energy harvesting system is studied. This system is capable of isolating unwanted vibration as well as harvesting available energy. The dual-purpose vibration isolation and energy harvesting system provides a primary function of isolating vibration while the energy harvesting capability is secondary. The system is analysed, designed and optimised with respect to a hardening stiffness parameter. In addition to optimising the system based on specific excitation levels, a broad optimisation process is conducted while concurrently assessing all available excitation levels.

Chapter 7 finally delivers concluding remarks as well as highlights of the studies covered in this thesis. Also discussed in this chapter is a nearly completed ongoing fabrication work on a vibration energy harvesting test rig. Schematic diagrams of an integrated model of the test-rig developed using SolidWorks and a physical assembly of the test rig are also shown. The Chapter ends with recommendations of how to extend the research outcomes presented in this thesis.

1.7 ASSUMPTIONS CONSIDERED IN THIS THESIS

The following assumptions have been considered in the studies presented in this thesis:

- All systems considered, belong to the class of nonlinear systems stable at zero equilibrium and which can be defined by a Volterra series. The OFRF method is only applicable for stable nonlinear systems.

- Only single degree of freedom (SDOF) systems, have been considered here. This is mainly to demonstrate a proof of concept especially using the OFRF method.

Chapter 2: Literature Review

This chapter begins with a brief historical background on vibration isolation systems and vibration energy harvesting systems (Section 2.1). A review of the literature on the following is then presented accordingly; vibration isolation systems (Section 2.2) wherein past studies on key isolation techniques are discussed; vibration energy harvesting systems (Section 2.3) comprising, mostly, previous works on electromagnetic energy harvesters and efforts made to solve important limitations to existing techniques with regards to performance and output power. Furthermore, the Output Frequency Response Function (Section 2.4) is described, which is the adopted tool used herein for the analytical study, design and optimisation of the different vibration isolation and energy harvesting models considered in this work. Finally, Section 2.5 highlights a summary and some implications of the literature reviewed.

2.1 BACKGROUND

Many vibration isolation methods have been developed over the years as a result of the desire for better vibration isolation performance for engineering machines and structures. One of the earliest approaches for suppressing vibrations due to, for example, seismic waves and wind, is to design structures with enough strength and deformation capacity in a malleable mode [2]. A combination of these structural characteristics (strength and deformation capacity) ensured ancient structures withstood fierce wind and seismic actions, though with some degree of degradation. Modifications of these structural systems towards vibration mitigation led to the concept of Structural Control. With this concept, the structure is seen as a dynamic system with time-dependent state variables, (e.g. displacement, velocity and acceleration) and having mechanical properties, such as stiffness, damping, that can be made adjustable to reduce, to acceptable limits, the dynamic effects on a payload [2], [32]. Besides, rather than suppressing or isolating this vibration energy using isolation elements, part of the vibration is converted to a useful form such as electrical energy. This concept is called energy harvesting.

The emergence of smart wireless systems (e.g. sensors) in the last decade and its essentiality in our daily life, improving comfort, security and efficiency in various

applications such as the automotive, electronics and oil and gas industry etc., triggered an interest in energy harvesting [33]. This was motivated by the quest for complete autonomy of power supply for these devices which is possible due to the ubiquitous presence of ambient vibration. This was a good way to put the high, unacceptable levels of vibration energy into good use by converting it into useful electrical energy. A number of brilliant review articles have been published on Energy harvesting covering an extensive range of mechanisms and techniques [22], [34]–[41]. Three main transduction mechanisms exist; electrostatic, piezoelectric and electromagnetic which has been concisely discussed in Subsection 1.1.2 of Chapter 1. However, this work only considers the electromagnetic transduction mechanism therefore previous works on this transduction mechanism will be mainly reviewed herein.

2.2 REVIEW ON VIBRATION ISOLATION SYSTEMS

A vibration isolation system is a device inserted between a source of undesired vibration and the object to be protected from vibration, to minimise the amount of vibration energy transmitted [2][42]. Several vibration isolation schemes have been investigated and implemented but they all generally fall into three categories; passive, semi-active and fully active [43]. Conventional passive isolation schemes have been employed in aerospace engineering, where a linear spring and damper system was successfully deployed on an aircraft, with good stability performance and no external power needed [44]. However, there are two trade-offs with respect to the stiffness and damping design [45]. To ensure low transmissibility is achieved over the entire spectrum, the elastic stiffness of the isolation system needs to be very small. However, this will cause the static and quasi-static displacements to be large which is harmful to supported objects. Secondly, with a high elastic stiffness, a high damping element is used to reduce the transmissibility at resonance i.e. region of greatest displacement. This may increase the transmissibility over high frequencies i.e. beyond resonance [46]. To mitigate the limitations of conventional passive isolation systems, efficient techniques, based on semi/adaptive passive (involves tuning of a passive isolation system), semi active and fully active approaches have been widely deployed. It should be noted however, due to high complexity, cost and power requirements, the fully active approach has not been as extensively deployed in practice as the semi passive and semi-active techniques.

An extension of the passive isolation method is the Adaptive Passive Vibration Control which was investigated in [47]. This method involves the combination of a tuneable Shape Memory Alloy (SMA) device, with their variable material properties, governed by a robust tuning strategy. The SMA device offers an adaptive mechanism through its ability to modify its elastic modulus on the application of heat. When applied to a system, the tuned isolation system is able to attenuate the vibration well across a wide band of frequency compared to a manually tuned vibration absorber. However, this method achieves control using a human-operator-in-the-loop which is a manual tuning approach. The same authors, in [48], proposed an improved version of the adaptive passive vibration control method with an SMA device which uses a nonlinear Proportional-Integral (PI) control strategy for its tuning.

The semi-active isolation method has been extensively studied by Liu et al. [49], as it delivers the same versatility, adaptability and performance as the fully active technique but requiring a significantly lesser amount of power. The vibration isolation characteristics of four semi-active damping control strategies were studied in [49] based on the skyhook technique and compared to that of a passive isolation system. The results confirmed the superior performance of the semi-active system over the conventional passive system at frequencies beyond resonance. Several studies have been reported on improved semi-active control strategies [39]–[48].

Karnopp, in [15], discussed the benefits of the active isolation scheme. In their study, the active isolation method was described as a complex system comprising, basically, a sensor, feedback actuator, and a control unit with the last two devices requiring an external power source and an amplifier. The external power requirement, coupled with its complexity, physical actuator limitations and high cost, unfortunately, makes the active vibration isolation scheme unattractive.

There have been studies to improve the performance of passive isolation systems by integrating nonlinearities in the dynamic characteristics of the isolation elements [49]–[61].

The concept of nonlinear vibration isolation has enjoyed significant development due to the need to protect engineering machines and structures from vibration disturbances [61]. Several innovative isolation methods, for example, nonlinear damping and nonlinear quasi-zero stiffness, have been developed based on nonlinear dynamics concept. These methods show good isolation performance and

stability over a desired frequency range. Earlier examples include [61], [62] and recently [63]–[69], where a systematic frequency-domain approach for nonlinear analysis and design is established using the Output Frequency Response Function (OFRF). More studies on the OFRF concept can be found in [70]–[77] and are further discussed in Section 2.4.

Many techniques employing nonlinear viscous damping techniques have been proposed and developed. Jing et al. [63] proposed a novel method for the analysis and design of a pure cubic nonlinear damping controller for the suppression of periodic disturbance using nonlinear feedback. In this work specifically, the authors proffered a systematic frequency domain method which can exploit the benefits of system nonlinearities to realize a desired frequency domain performance of an isolation system. Indeed, the results showed that the proposed isolation system outperforms that of an equivalent linear damping system. A similar study was done by Jing and Lang [64] using a dimensionless mass-spring damping system and the results reinforced those of [63]. A theoretical study was done by Lang et al. in [78] to investigate the use of the OFRF in analysing the effects of nonlinear viscous damping on vibration isolation of a SDOF system and the results conformed with that obtained in [63]. In a more relatively recent study, Carmen et al. [32] [65], investigated the gains of nonlinear viscous cubic damping on the transmissibility of a Duffing-type vibration isolation system. In these studies, it was observed that the system exhibited undesired jumps and super-harmonics due to light damping levels but the jumps can be suppressed by heavy linear damping. However, the drawbacks of substantial linear damping make its use unpopular. The authors therefore confirmed the application of a nonlinear cubic viscous damping as a better alternative in the suppression of the resonant peak while reducing the hostile characteristics of nonlinear stiffness. This was done without any compromise on the force transmissibility over the desired isolation region.

Peng et al. [79] investigated the effect of cubic nonlinear damping on a typical SDOF vibration isolation system using the harmonic balance method (HBM). The effect of the cubic damping was observed to be dependent on the type of disturbance force causing the vibration. It was also shown to be negligible at high frequency range for both force and displacement transmissibility if the system is force-excited. It was similarly shown that if the disturbance force is base-excited, an increase in the cubic

nonlinear damping slightly reduced the relative displacement transmissibility but increased the absolute displacement transmissibility and significantly increased the force transmissibility. This revealed the effectiveness of the pure cubic viscous damper for force-excited systems. In another study, a nonlinear vehicle suspension system was investigated by Chen et al. [80] using the frequency domain analysis and optimisation method. Optimal values of the nonlinear damping parameters were designed for a desired isolation performance of the suspension system. An investigative comparison was carried out for the force transmissibility and results showed a better performance was obtained compared to an equivalent linear damping over all frequency range. A similar system was considered by Xiao et al. in [81] where it was theoretically shown that the cubic order nonlinear damping provides better isolation performance under both force and base displacement excitation. Figure 2.1 shows a schematic diagram of a SDOF vibration isolation system with different integrations of damping nonlinearities recently employed in literature [31], [63], [80]–[86]. These nonlinear viscous damping characteristics have been implemented using a Magnetorheological damper (MR damper) which provides a controllable damping characteristic for vibration isolation [87]–[90].

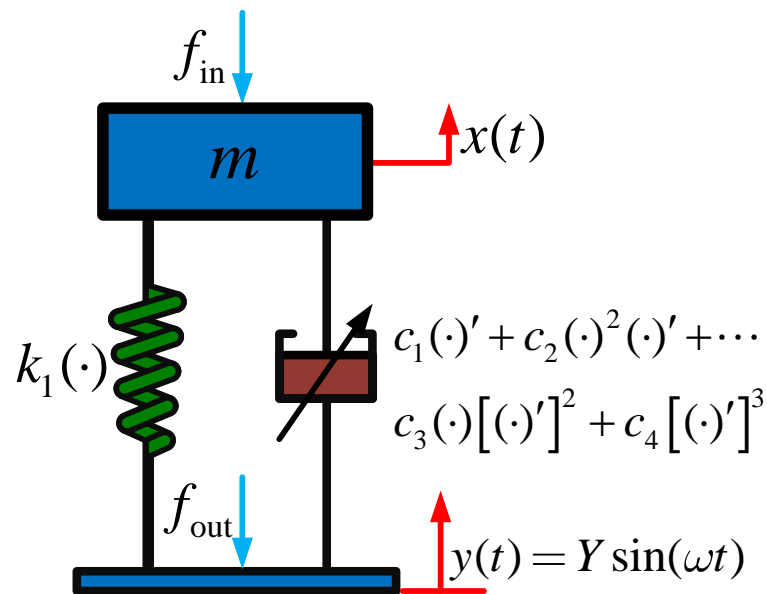


Figure 2.1: Schematic of a base-excited vibration isolation system

Furthermore, the effects of nonlinear stiffness characteristics in vibration isolation performance have also been extensively studied [84]–[95]. The duffing

equation has been broadly used to model a wide range of systems. Some examples include beams with stiffness nonlinearity and nonlinear vibrations in cables. More examples can be found in the book by Kovacic and Brennan [101]. The performance of a vibration isolation system is strictly limited by the degree of the system stiffness but should be capable of providing a high-static load mount. A common method of achieving low frequency vibration isolation is by employing a near-zero stiffness isolator. Such isolators are known as quasi-zero-stiffness (QZS) vibration isolators. Such isolators employ linear springs geometrically configured in such a way as to create a nonlinear stiffness behaviour. The QZS structure composes of a suspension mass connected to the foundation by two horizontal springs and a vertical spring. This geometric configuration enables the system to achieve a high-static-low-dynamic stiffness (HSLDS) isolation so as to realise a good isolation performance. Magnetic springs have been widely employed in realizing the QZS structure [94], [102]–[105]. A schematic diagram of a quasi-zero-stiffness vibration isolation system is shown in Figure 2.2. Kovacic et al. [60] studied the characteristics of a nonlinear vibration isolator with a quasi-zero stiffness. The isolation system comprise a vertical linear stiffness and two nonlinear pre-stressed oblique springs which integrate the auxiliary spring design idea of Alabudzev et al. [106]. Two kinds of nonlinearities are inherent in the system design, viz. geometric and physical nonlinearities. The geometric nonlinear stiffness introduces a softening parameter resulting to a quasi-zero dynamic stiffness at the equilibrium position. A similar study was carried out by Carrella et al. [107]–[109], where the QZS mechanism was shown to facilitate the design of nonlinear vibration isolation systems possessing a high-static-low-dynamic stiffness. This was accomplished by a combination of both positive and negative stiffness elements.

According to [108], a high-static stiffness characteristic is desired in a vibration isolation system to enable the isolators to withstand static loads without experiencing a large displacement. However, a low-dynamic stiffness characteristic is desired in a vibration isolation system to enable the reduction in the value of the natural frequency of the system. The natural frequency of the system is desired to be as low as it can get which results in an increase in the isolation region. This design earlier proposed by [106] was reinforced in [108] where Carrella et al. revealed how the application of a nonlinear isolation system with a stiffness element configured in a certain way can

improve isolation performance where the static stiffness far exceeds the dynamic stiffness. In this study, analysis showed that the dynamic stiffness increases monotonically with displacement on any side of the equilibrium position. However, a better performance was obtained when the inclined angles of the oblique springs were around 48-57 degrees. It was also revealed that the force-displacement characteristics of the system can be approximated by a cubic stiffness. Brennan et al. [110] presented non-dimensional estimated expressions and their equivalent displacement amplitudes at the jump-up and jump-down frequencies of a lightly damped duffing oscillator. Two methods, the harmonic balance method and the perturbation method were employed in the analytical derivations and their results were then compared. It was discovered that while the jump-down frequency depended on both the degrees of stiffness nonlinearity and the damping present in the system, the jump-up frequency was majorly dependent on the stiffness nonlinearity and weakly dependent on the system damping.

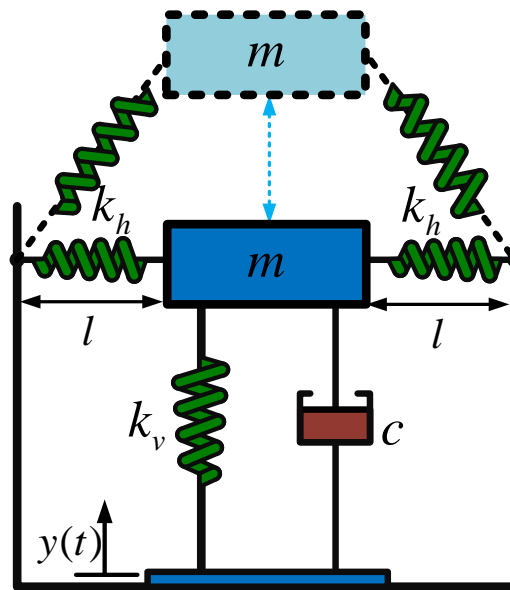


Figure 2.2: Schematic diagram of a quasi-zero-stiffness vibration isolation system.

In summary, this section has explored the previous studies on vibration isolation systems, especially methods incorporating nonlinearities contributed by damper or/and spring elements. Some of the attenuated vibration energy can be harvested and used to operate low-power electronics. This concept is termed vibration energy harvesting. In the next section, some past works on vibration energy harvesting will be reviewed.

2.3 REVIEW ON VIBRATION ENERGY HARVESTING SYSTEMS

As mentioned in Chapter 1, vibration energy harvesting is classified into three basic transduction mechanisms namely; piezoelectric, electrostatic and electromagnetic. However, the review in this section will almost entirely focus on the electromagnetic transduction methodology which is the main subject of the studies performed in this thesis.

Energy harvesting involves the conversion of ambient energy generated from ambient sources such as solar energy, temperature, radio frequency, kinetic energy etc., to electrical energy. Vibration energy harvesters (VEHs), which are energized by ambient mechanical vibrations, are a subclass of the broader class of kinetic energy harvesters. VEHs convert vibration energy to electrical energy [111]. Energy harvesting approaches have recently become an active area of research because of the emergence of low-power electronic devices. This has contributed immensely to the recent comprehensive study of energy harvesters. Popular applications of VEHs include wireless sensors used in structural health monitoring procedures to ascertain the health status of engineering structures and provision of energy to low-powered autonomous systems [112] such as Unmanned Aerial Vehicles and MEMS. Human-related motions have also been harvested for electrical power [113] such as in the case of pacemakers which require small quantities of power to function. In [18], large-scale energy harvesters were employed for harvesting large-scale vibration energy ranging from 1W to 100kW. Applications ranging from human motion, vehicular and machine motion, civil and mechanical structures were also discussed therein.

Electromagnetic vibration energy harvesters (emVEHs) employ the electromagnetic transduction technique and therefore converts mechanical energy inherent in vibratory motions to electrical energy. The electromagnetic transduction method operates based on Faraday's law of induction and a simple design consists of a permanent magnet and a coil. One is made to move relative to the other causing the coil to cut across the magnetic field generated by the magnet. This results in a voltage induced across the coil terminals [23] as illustrated in Figure 2.3. Current flows through the wire once an electrical load is connected across the wire thus leading to the generation of electrical power. This transduction method is implemented in an electromagnetic damper (EMD or EM damper) and employed in emVEHs. Many studies involving design and fabrication, have been done to improve the performance

of emVEHs [115]–[120]. A typical emVEH, as represented in Figure 2.4, consists of a coil, magnet, mechanical spring and an enclosing frame. The magnet or coil is usually supported by the spring to enable the relative motion of one about the other. As a result of this motion, a mechanical damping characteristic is created because of the air resistance and surface friction within the enclosure while an electrical damping is formed on account of the flow of current in the coil [121].

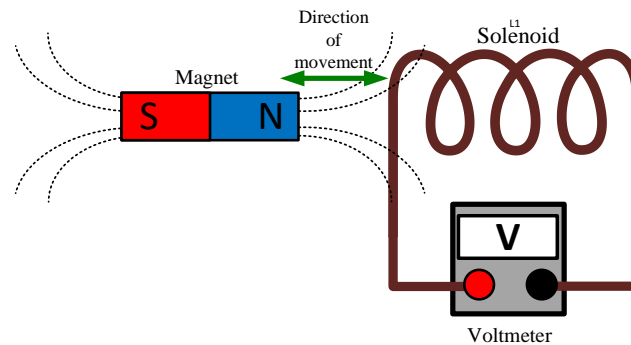


Figure 2.3: Principles of Electromagnetic induction.

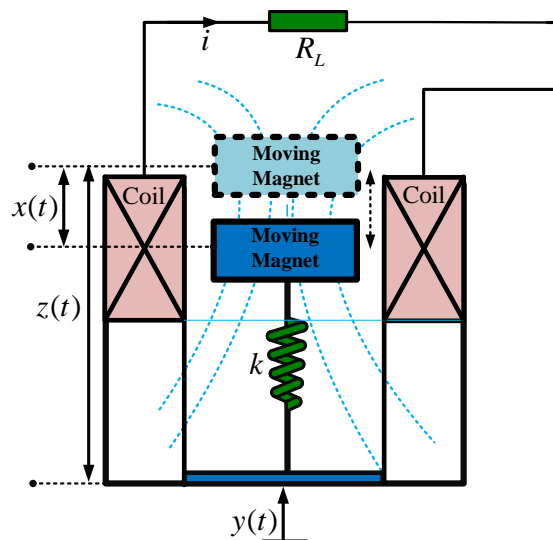


Figure 2.4: A representation of a typical emVEH with a load resistance, R_L .

Comparing the output voltage of emVEHs with that of electrostatic and piezoelectric energy harvesters, the voltage order ranges from a few μV to some mV. Nevertheless, their low output impedance enables them to produce high current levels

[122]. Most previous studies on linear resonant energy harvesters have established some major facts. These are presented in Table 2.1.

Table 2.1: Established facts of earlier studies for linear SDOF emVEHs

S/N	Facts established	Reference
1	When excited at resonance, maximum power is generated.	[112] , [113], [123], [124]
2	Increase in damping (associated with electromechanical coupling) results to an increase in operational bandwidth of an emVEH.	[33], [112], [124]
3	A large mass (of magnet) fitted in the containing frame is required.	[112] , [123], [124], [125]
4	The maximum output power is dependent on the maximum permissible mass displacement due to device size and geometry.	[112] , [113], [123], [124]

Most publications in literature have literally identified two major design limitations of energy harvesting systems. The first established fact on Table 2.1 is the foremost limitation of linear VEHs which implies that energy harvesters are designed to function at a selected band of frequencies, usually the region of resonance. Therefore, excitations having frequencies outside this band are untapped which affects the efficiency of the harvester system. However several nonlinear design concepts have been reported in literature to increase the excitation frequency range over which the harvester system is operational [126].

Investigations in [127] revealed various strategies on how the excitation frequency range, over which the vibration energy harvester functions, can be increased. The first strategy which was studied in [128] proposed adjusting or tuning the resonant frequency of a generator to always match the frequency of the ambient vibration hence maximizing power harvested. It was shown that this could be achieved by either adjusting the mechanical properties of the structure (i.e. mechanical tuning) as examined in [129] or adjusting the electrical load (i.e. electrical tuning) as investigated and reported in [130]. The second strategy employed in [131] involved expanding the bandwidth of the generator. This was also revealed to be achieved by employing either of the following; an array of structures with different resonant frequencies, coupled oscillators, bi-stable structures, an amplitude limiter, nonlinear springs or a large inertial mass. The application of a nonlinear softening spring proposed in [132] was

employed to effect the adjustment of the resonant frequency as it was also shown that this improved the bandwidth of the energy harvester over which power can be harvested. A similar study was carried out in [133] using a bi-stable nonlinear spring termed a snap-through mechanism which quickly moved the sprung mass between two stable states in order to steepen the displacement-time response curve resulting in an increase in the velocity for a specific excitation hence improving the harvested power. A second mechanism was also employed in this study using a hardening-type stiffness to widen the operational bandwidth of the harvester hence increasing the frequency range over which power can be harvested.

Besides increasing the operational bandwidth of emVEHs, it has been recently revealed in [134], using the harmonic balance method (HBM), that the dynamic range of an emVEH can be improved as well. This was achieved by introducing a cubic damping nonlinearity which is purely velocity-dependent. Its performance was compared to an emVEH with an equivalent linear damper which causes the same mass displacement response, at resonance, as the cubic nonlinear damped emVEH. It was demonstrated that when the system is excited at the resonant frequency, both systems harvested the same amount of energy. However, when excited below the maximum acceptable excitation level, the nonlinear harvester performed better compared to its linear counterpart i.e. harvested more power. Nevertheless, mechanical viscous damping was not considered by the authors. The authors of [135] investigated the effect of the coil resistance on the energy harvester with a cubic resistance using the same concept as in [134]. It was established that the internal resistance provided an upper limit for the electrical damping of a VEH with cubic load resistance. The same authors also demonstrated in [136] how the dynamic range of an emVEH can also be extended using a variable load resistance. This technique was proposed to have a successful application in locations with varying excitation levels. In [137], it was demonstrated that when the energy harvester includes a parasitic damping characteristic, due to inherent damping, the output power is depleted. Nonetheless, the cubic damping system still outperforms the equivalent linear damping system. It should be noted that for an emVEH, the characteristic of its electrical damping is dependent on the characteristic of the load resistance connected across it. This implies that a linear load resistance generates a linear electrical damping force while a nonlinear load resistance generates a nonlinear electrical damping force.

The vibration isolation and energy harvesting system described in Figure 2.5 show the EM damper with its electrical elements. These include the back emf, v_{em} (v), the coil resistance, R_c (Ω), and inductance, L (H). The coil inductance is often negligible because of their very small values due to low vibration frequencies of engineering structures [35], [130], [138], [139]. Though the energy harvesting circuit can be represented with a constant resistor as observed in Figure 2.4, it can also be represented with different interface circuits such as the form shown in Figure 2.5 as long as it can be modelled as a resistive load. Typically, a DC-DC charging circuit can be modelled as a resistive load [135], [139]–[142].

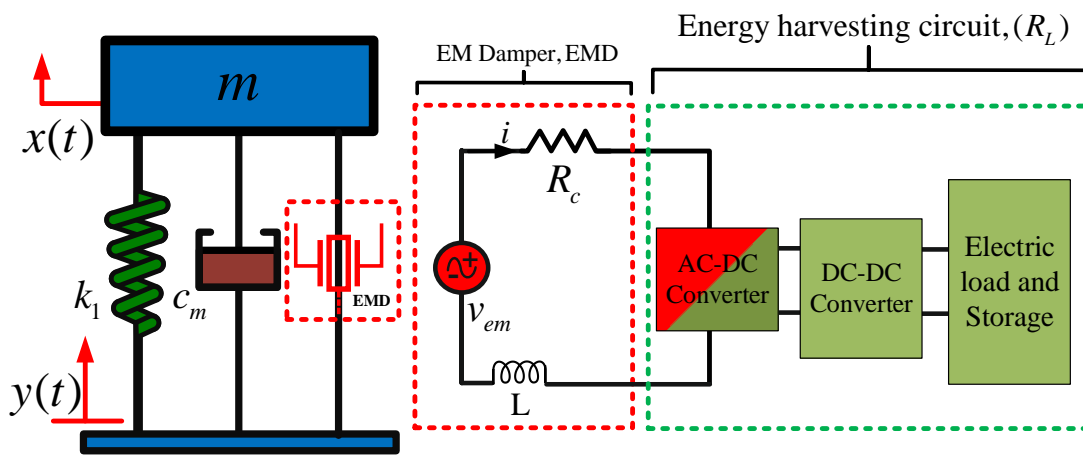


Figure 2.5: A typical dual-function vibration isolation and energy harvesting system with load resistance, R_L .

Nonlinear vibration isolation and nonlinear energy harvesting systems, whose equation of motion can be represented using a nonlinear differential equation (NDE), have been studied using several analytical methods. These include the method of multiple scales [143], direct numerical integration [144], nonlinear normal forms [145] and the harmonic balance method [146], [147]. Although the recently developed Output Frequency Response Function (OFRF) [30], [31], has been previously used for the analysis and design of several nonlinear vibration isolation systems, it has never been employed for the analysis nor design of an energy harvester. In this work, the OFRF method is the preferred method for the analysis and design of the nonlinear systems investigated herein. The OFRF method is beneficial compared to other methods as it provides an explicit analytical relationship between the design objectives

and system parameters. This can significantly facilitate system design and optimisation. The OFRF concept will be comprehensively discussed in the next section.

2.4 OUTPUT FREQUENCY RESPONSE FUNCTION (OFRF)

2.4.1 Introduction

Lang and Billings [30] derived an expression for the output frequency response of nonlinear systems in a way that explains how the fundamental nonlinear mechanisms operate on the input spectra resulting in system output frequency effects. The findings in [30] led to the derivation of an expression for the output frequency response that defines, analytically, a relationship between the output spectrum and the system parameters. This expression, established in [31], is known as the output frequency response function (OFRF) of the system. Jing et al. in [148] investigated the parametric characteristics of the frequency response functions of nonlinear systems.

The OFRF concept, according to [31] shows that for a wide set of nonlinear systems, there exists a basic polynomial relationship between the output response and the system nonlinear parameters. To determine the structure (monomials) of the OFRF, a symbolic operation method was proposed by Peng and Lang in [149]. This method is an efficient algorithm that can be used to determine the monomials in the OFRF representation of the output frequency response of a nonlinear system. The efficiency of the algorithm was demonstrated as it was used in the analysis of the output frequency response of a passive engine mount. In [85], a new systematic approach was proposed for the analysis and design of the output response of a Volterra system using the OFRF method. The study in [149] was extended by the same authors in [150] to the multiple degrees of freedom (MDOF) case. Using the OFRF method, the force transmissibility of a vibration isolation system, with a nonlinear anti-symmetric viscous damping, was theoretically investigated. The conclusions show that the anti-symmetric nonlinear viscous damping can significantly suppress the force transmissibility over the regions of resonance. Similarly, as in [149], Peng et al. [151], [152] used the OFRF, estimated from numerical simulation responses, to obtain an explicit analytical relationship between the transmissibility and nonlinear characteristic parameters. A broad pattern of how the nonlinear parameters affect the

force and displacement transmissibility was investigated for the vibration isolation system.

It was established in [65], [79] that the OFRF is only effective for the analysis and design of systems that belong to a class of nonlinear systems stable at zero equilibrium and can be described in the neighbourhood of the equilibrium by a convergent Volterra series. However, the OFRF cannot be used to represent strongly nonlinear/unstable systems with characteristics such as chaos, limit cycles, bifurcations, and jump phenomenon. For the cases where strong nonlinear behaviours, such as jump phenomena, can be observed, the OFRF concept cannot be applied [65] and other analytical methods should be employed.

2.4.2 Volterra series representation of nonlinear systems in the time and frequency domain

The OFRF concept and its parametric characteristics is described here.

Consider the class of nonlinear systems stable at zero equilibrium and can be defined in the neighbourhood of the equilibrium by the Volterra series

$$y(t) = \sum_{n=1}^N \int_{-\infty}^{\infty} \cdots \int_{-\infty}^{\infty} h_n(\tau_1, \dots, \tau_n) \prod_{i=1}^n u(t - \tau_i) d\tau_i \quad (2.1)$$

where $y(t)$ and $u(t)$ are the respective output and input of the system, $h_n(\tau_1, \dots, \tau_n)$ is the n th-order Volterra kernel and N represents the maximum order of the system nonlinearity. An expression for the output frequency response of this class of nonlinear system to a general input has been derived by Lang and Billings [30] and given as

$$\begin{cases} Y(j\omega) = \sum_{n=1}^N Y_n(j\omega) & \forall \omega \\ Y_n(j\omega) = \frac{1}{\sqrt{n}(2\pi)^{n-1}} \int_{\omega_1 + \dots + \omega_n = \omega} H_n(j\omega_1, \dots, j\omega_n) \prod_{i=1}^n U(j\omega_i) d\sigma_{\omega_n} \end{cases} \quad (2.2)$$

where $Y_n(j\omega)$ denotes the n th-order output frequency response, $Y(j\omega)$ is the output spectra, $U(j\omega)$ is the input excitation with a continuous spectrum, $d\sigma_{\omega_n}$ is the area of a minute element on the hyperplane $\omega = \omega_1 + \dots + \omega_n$ and $H_n(j\omega_1, \dots, j\omega_n)$, is the n th-order generalised frequency response function (GFRF) given as

$$H_n(j\omega_1, \dots, j\omega_n) = \int_{-\infty}^{\infty} \cdots \int_{-\infty}^{\infty} h_n(\tau_1, \dots, \tau_n) e^{-j(\omega_1\tau_1 + \dots + \omega_n\tau_n)} d\tau_1 \dots d\tau_n \quad n=1,2,\dots \quad (2.3)$$

The Volterra series can approximate the input-output relationship of nonlinear systems up to any high order N [153].

2.4.3 Determination of the OFRF

Consider the Volterra systems which can also be described by the following differential equation

$$\sum_{\bar{m}=1}^M \sum_{p=0}^{\bar{m}} \sum_{l_1, \dots, l_{\bar{m}}=0}^L c_{p, \bar{m}-p}(l_1, \dots, l_{\bar{m}}) \prod_{i=1}^p \frac{d^{l_i} y(t)}{dt^{l_i}} \prod_{i=p+1}^{\bar{m}} \frac{d^{l_i} u(t)}{dt^{l_i}} = 0 \quad (2.4)$$

where L is the order of the derivative and M is the maximum degree of nonlinearity in terms of the system input and output, $u(t)$ and $y(t)$ respectively. According to the OFRF method [31], [85], [148], the output frequency response of system (2.4) can be represented by a polynomial function in terms of the system nonlinear characteristic parameters as

$$Y(j\omega) = \sum_{j_1=0}^{m_1} \cdots \sum_{j_{S_N}=0}^{m_{S_N}} \phi_{(j_1, \dots, j_{S_N})}(j\omega) \xi_1^{j_1} \dots \xi_{S_N}^{j_{S_N}} \quad (2.5)$$

where m_i are the maximum order of ξ_i , $i = 1, \dots, S_N$ in the polynomial expression of the output spectrum, $Y(j\omega)$ of system (2.5). The notations $\phi_{(j_1, \dots, j_{S_N})}(j\omega)$ are complex-valued frequency functions (also called OFRF coefficients) dependent on the system input and linear characteristic parameters, where $j_i = 0, \dots, m_i$ and $i = 1, \dots, S_N$. Furthermore, $\xi_1^{j_1} \dots \xi_{S_N}^{j_{S_N}}$ is a set of monomials (i.e. the OFRF structure) in terms of the system nonlinear characteristic parameters. It should be noted that $\phi_{(j_1, \dots, j_{S_N})}(j\omega)$ represents the coefficients of $\xi_1^{j_1} \dots \xi_{S_N}^{j_{S_N}}$ with the same dimension and needs to be evaluated in order to obtain the OFRF representation of system (2.4). However, firstly the monomials need to be determined using a recursive algorithm discussed in Jing et al. [148] and Peng et al. [149]. For a Single-Input-Multiple-Output (SIMO) system, an elaborate procedure has been described by Zhu and Lang in [68].

A. Determination of the OFRF structure

Let the set of monomials in the OFRF representation of the n th-order output spectrum be denoted as \mathfrak{M} and the frequency function vector be denoted as $\Phi(j\omega)$, then the OFRF can be described as

$$Y(j\omega) = \mathfrak{M} \cdot \Phi(j\omega)^T \quad (2.6)$$

where

$$\mathfrak{M} = \bigcup_{n=1}^N M_n \quad (2.7)$$

Here, the monomials, M_n can be determined using [149]

$$M_n = \left[\bigcup_{l_1, \dots, l_n=0}^L [c_{0,n}(l_1, \dots, l_n)] \right] \cup \left[\bigcup_{\bar{m}=p=1}^{n-1} \bigcup_{p=1}^{n-(\bar{m}-p)} \bigcup_{l_1, \dots, l_n=0}^L [c_{p,(\bar{m}-p)}(l_1, \dots, l_{\bar{m}})] \otimes M_{n-(\bar{m}-p),p} \right] \cup \left[\bigcup_{p=2}^n \bigcup_{l_1, \dots, l_n=0}^L [c_{p,0}(l_1, \dots, l_{\bar{m}})] \otimes M_{n,p} \right] \quad (2.8)$$

where

$$M_{n,p} = \bigcup_{i=1}^{n-p+1} M_i \otimes M_{n-i,p-1}, \quad M_{n,1} = M_n, \quad M_1 = 1 \quad (2.9)$$

The character ‘ \otimes ’ is the Kronecker product.

Then the set of monomials can be obtained as $\mathfrak{M} = \bigcup_{n=1}^N M_n$

B. Determination of the OFRF coefficients

To determine the set of OFRF coefficients $\Phi(j\omega)$, the next steps are taken as described in Section 3.2 of [85] and also in Refs [148], [31]. This is done assuming no measurement error or data noise [85].

A1. Select α series of different values of the system nonlinear parameters of interest to form a series of vectors $\psi_1 \cdots \psi_\alpha$.

A2. Using the same input to excite the system under different values of nonlinear parameters $\psi_1 \cdots \psi_\alpha$ and record the corresponding time domain output responses $y(t)_1 \cdots y(t)_\alpha$ for each case.

A3. Lastly, using the FFT method, obtain a series of corresponding output frequency response $Y(j\omega)_1 \cdots Y(j\omega)_\alpha$ of the time domain responses.

Following steps (A2-A3) it can be deduced from (2.6) that

$$\mathfrak{M} \cdot \Phi(j\omega)^T = \begin{bmatrix} \psi_1 \\ \psi_2 \\ \vdots \\ \psi_\alpha \end{bmatrix} \cdot \Phi(j\omega)^T = \begin{bmatrix} Y(j\omega)_1 \\ Y(j\omega)_2 \\ \vdots \\ Y(j\omega)_\alpha \end{bmatrix} =: \tilde{Y}(j\omega) \quad (2.10)$$

The least square method can then be employed to obtain $\Phi(j\omega)^T$ as

$$\Phi(j\omega)^T = \mathfrak{M}^T \mathfrak{M}^{-1} \mathfrak{M}^T \cdot \tilde{Y}(j\omega) \quad (2.11)$$

so as to determine the OFRF (2.6). The OFRF thus obtained can be used in the design of the parameter(s) of interest in \mathfrak{M} given a desired output response, $Y^*(j\omega)$. To do this, at a frequency of interest, ω , the OFRF representation derived is solved for the nonlinear parameter(s) and optimized such that $|Y(j\omega) - Y^*(j\omega)|$ can be minimised to the lowest possible value. This analytical method will be employed for most of the nonlinear models considered in this study.

2.4.4 Limitations of the OFRF method

The OFRF method has also got some limitations and these are outlined as follows;

- It only works for the class of nonlinear systems stable at zero equilibrium.
- It performs poorly for nonlinear systems that experience the jump phenomenon.
- It performs poorly for strongly nonlinear systems that shows nonlinear characteristics such as chaos, bifurcation, limit cycles etc.

For such strongly nonlinear systems, alternative methods such as multiple scales [143], direct numerical integration [144], the nonlinear normal forms [145], harmonic balance method [146], and power flow analysis [147] etc., can be employed.

2.5 SUMMARY

In this chapter, a brief background on vibration isolation systems and also vibration energy harvesting systems were discussed. Major vibration isolation methods which have been proposed in the literature were reviewed and their strengths as well as weaknesses highlighted. The limitations of the conventional passive isolation method led to the development of more efficient techniques. However, improvements were made to the passive method enabling the tuning of the isolation elements. The fully active method, although can provide excellent performance in theory, it is unpopular due to its complexity, cost and power requirement. In contrast to the fully active approach, the semi-active technique has been widely accepted and deployed in many engineering vibration systems. The semi-active technique has been widely implemented using the MR damper which enables the controllability of its damping characteristic.

Several studies have been done to improve the linear vibration isolation method by incorporating some forms of nonlinearities in the system dynamic model. This has led to a strong interest in the design of nonlinear vibration isolation systems. This remains an interesting and active research area due to the need to isolate engineering machines and structures from destructive vibration disturbances. The incorporation of nonlinear components in the dynamic models of vibration isolation systems have shown to improve, immensely, its isolation performance. Some studies have been concerned with integrating nonlinear stiffness components while some have concentrated on nonlinear damping. Others have combined both damping and stiffness nonlinearities as such designs have shown to perform much better than using only either one of the nonlinear component [32], [67], [149], [154], [155]. However, most of the vibration energy injected into a system is dissipated away as heat by the vibration isolation elements. Recently, little attention has been given to the estimation of the energy dissipation level of the designed vibration isolation elements. This has been considered in Chapter 3, using the OFRF method. It has been demonstrated that the energy dissipation level for a designed suspension system can be estimated for a set of design parameters. Furthermore, the need for self-powered devices has led to the research area comprising the conversion of these vibration energies to electrical energy, a concept known as vibration energy harvesting.

Vibration energy harvesting is a concept involving the conversion of kinetic energy (from mechanical vibration) to electrical energy. It involves three transduction approaches namely piezoelectric, electrostatic and electromagnetic. The electromagnetic transduction method is based on the Faradays' law of electromagnetic induction and basically consists of a coil and a permanent magnet. This transduction method is implemented using an electromagnetic damper which can be integrated in an oscillating system primarily for either vibration isolation, energy harvesting or a hybrid of both. An oscillating motion causes one of either the coil or magnet to move relative to the other thereby inducing a voltage across the terminals of the coil. The induced voltage can be stored as electrical energy using an energy harvesting circuit which can be modelled as a resistive load.

Nonlinear design of vibration energy harvesters has recently become an interesting research area because of the need to increase the power output efficiency. Two design limitations have been acknowledged in literature and several solutions have been explored. The first limitation, which concerns bandwidth limitation of the VEH, led to many works focused on expanding the bandwidth of VEHs. The second limitation relates to extending the dynamic range of a VEH and, until recently barely enjoyed any attention. Both limitations have been explored by considering integration of nonlinearities in the system dynamic characteristics. Several nonlinear analytical methods exist for the analysis and design of nonlinear systems however for most of the studies in this thesis, the recently developed Output Frequency Response Function (OFRF) method is considered. This is because it offers a clear analytical association between the design objectives and system parameters. It should be noted that this is the first effort in the application of the OFRF method for the analysis, design, and optimisation of an energy harvester.

In Chapter 4, the current gap in literature, where no clear design-to-implementation procedure has been demonstrated, is exploited in this study. The use of the OFRF method is also the first effort in investigating energy harvesters. An extension of Chapter 4 is also presented in Chapter 5 whereby, in addition to the nonlinear damping characteristics present in the VEH system, a nonlinear stiffness element is incorporated into the system. This additional integration is intended to expand the bandwidth of the VEH system. To the best of the author's knowledge, this is the first attempt in considering both nonlinear damping and stiffness characteristics,

simultaneously, in an energy harvesting system. Finally, Chapter 6 considers the analytical investigation of a dual-function vibration isolation and energy harvesting system. To the best of the author's knowledge, this has not been considered in a previous study, which implies this work is the first effort to do this. The study proposes a dual-function device whereby vibration isolation is the primary function and energy harvesting is the secondary function.

In the next chapter, a vehicle suspension system is investigated. An analysis, design, and optimisation of the isolation elements with nonlinear characteristics is explored. The nonlinear damping and stiffness parameters are designed for a desired system output response and the energy dissipation level, of the designed suspension system, is estimated using the derived OFRF model.

Chapter 3: Analysis and design of a nonlinear vibration isolation system

3.1 INTRODUCTION

A vibration isolation system (VIS) is a device fixed between an equipment that requires protection from vibration and the source of vibration. A vehicle suspension system is an application of such a system comprising a spring, damper and frames/linkages [156]–[159]. A major significance of isolation springs is its ability to absorb and store energy from motion bumps and acceleration with ease. However, isolation springs such as rubber, coil and leaf springs are not capable of dissipating the absorbed energy easily. This can result in unacceptable spring performances before eventual failure which makes the need for an adequately designed damping system paramount [160]. The damper plays a vital role in vehicle vibration isolation as it damps out vertical motions and ensures the life cycle of the spring is extended. The design of a good isolation system is important in vehicle suspension systems to ensure a decent ride comfort [160]. In [158], the transmissibility of linear isolation systems were analytically associated with the mass, spring and damping ratios and thereafter the optimised parameters were linked to the resonant characteristics of the system. Linear isolation designs of engine mounts have been widely reported in literature [151]–[155]. In [159], the damping and stiffness parameters of an isolation system were optimised using the root-mean-square method which was done by minimising objective functions representative of relative displacement and absolute acceleration. In [157], the force transmitted from the engine to the base was minimised using the method of sequential quadratic programming used to choose the stiffness value as well as the positioning of the engine mount. Due to the inherent nonlinearity present in all shock and vibration isolation systems, more interests have been shown in nonlinear vibration isolation systems [58], [149], [161]. Several analytical methods exist for the study of nonlinear suspension systems such as the harmonic balance methods [162], [163], averaging methods [164], [165] and describing function methods [166], [167]. However, these methods do not evidently reveal the relationship between the vehicle

suspension performance metrics and system parameters. The recently developed output frequency response function (OFRF) method is a systematic frequency domain approach that enables the derivation of the system output spectrum in terms of the nonlinear parameters of interest. This method will be employed in the present study as it facilitates system analysis and design.

A model for a single degree of freedom (SDOF) passive vibration isolation system with cubic nonlinearities in stiffness and damping was studied in [168] where the consequence of the system nonlinear parameters on the relative and absolute displacement transmissibility were explored. A similar system was investigated in [161] which employed related damping and stiffness nonlinearities. The method of averaging perturbation was used to observe the effects of nonlinearities on the dynamic behaviour of the system. The same nonlinear passive mount, employed in [161], was considered by Peng and Lang in [149]. However, the OFRF method was applied in the study, to theoretically analyse the output frequency response behaviour with respect to the system nonlinearities and subsequently verified by simulation studies.

In this chapter, a vehicle suspension system, as shown in Figure 3.1 and similar to that in [149], [161] and [168] is described. It should be noted that the nonlinear cubic damping characteristics of the suspension systems, employed in these studies, are a function of both the displacement and velocity of the corresponding suspension system. Such a nonlinear damping structure has been chosen because it has proved to perform better than pure velocity-dependent cubic damping, for base-excited systems [82]. However, in the present study, an analysis and design of the suspension system was conducted using the OFRF method. Optimal values of the design parameters were obtained for a desired design specification and the designed parameters were validated using numerical simulation. Furthermore, for the first time, the energy dissipation performance of the designed suspension system was investigated using the OFRF method. The effects of the suspension system nonlinearities on the energy dissipated by the isolation elements were explored. An investigation was then performed using the OFRF method where nonlinear system parameters were designed for a desired energy dissipation level for the suspension system. A summary of the major objectives in this chapter is highlighted below:

- Design and optimisation of system parameters for a design specification required for ride comfort.

- Investigation of the energy dissipation level for the designed suspension system.

The rest of the chapter is organised as follows: Section 3.2 provides the model formulation of the suspension system to be investigated; Section 3.3 describes the determination of the OFRF representation of the system output spectra; Section 3.4 presents the system design and optimisation process for a desired design specification; Section 3.5 demonstrates, with numerical simulation studies, the effects of the system parameters; Section 3.6 analyses the energy dissipation level of the designed suspension system as well as the effects of system nonlinearities on the dissipation level; Section 3.7 summarises the chapter with some concluding remarks.

3.2 MODEL FORMULATION

A schematic diagram of the nonlinear SDOF suspension system considered in this study, is shown in Figure 3.1 [161]. This includes a suspended oscillating mass, m representing e.g. the quarter mass of a vehicle body, with an absolute displacement of $x(t)$ due to a base motion of $y(t)$. The suspension system has two nonlinear isolation components comprising nonlinear damping (c_1, c_2) and nonlinear stiffness (k_1, k_2) elements.

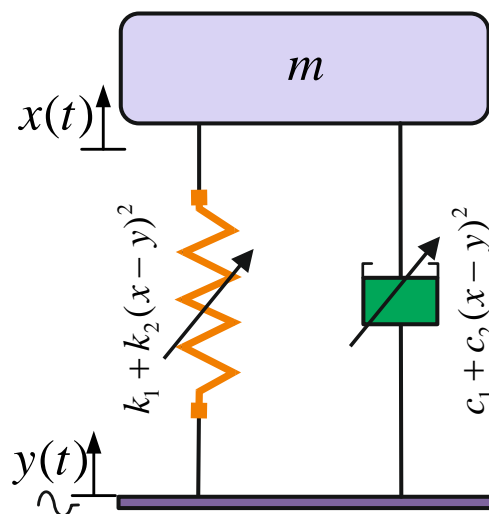


Figure 3.1: Schematic of the nonlinear suspension system under a base excitation.

The equation of motion for the suspension system is given by

$$m\ddot{z} + c\dot{z} + kz = -m\ddot{y} \quad (3.1)$$

where $z = x - y$ is the relative displacement between the base and the sprung mass, c is the damping function and k is the stiffness function. The damping and stiffness functions are described as

$$\begin{cases} k = k_1 + k_2 z^2 \\ c = c_1 + c_2 z^2 \end{cases} \quad (3.2)$$

Assuming the base excitation is harmonic that is

$$y = Y \sin(\omega t) \quad (3.3)$$

then system (3.1) becomes

$$\begin{cases} m\ddot{z} + (c_1 + c_2 z^2)\dot{z} + (k_1 + k_2 z^2)z = m\omega^2 Y \sin(\omega t) \\ f_{\text{trans}} = (c_1 + c_2 z^2)\dot{z} + (k_1 + k_2 z^2)z \end{cases} \quad (3.4)$$

where ω and Y are the excitation frequency and amplitude of the base displacement respectively and f_{trans} is the force transmitted through the vibration isolators (parallel combination of spring and damper).

To ensure ride comfort, the minimisation of the transmitted force is required. The transmitted force output spectrum is maximum at the resonant frequency, ω_r . Consequently, ω_r becomes the frequency of interest and the objective will be to minimise f_{trans} . The procedure outlined by Zhu and Lang in [68] for the analysis and design of a SIMO system using the OFRF, will be employed here.

In Section 3.3, the OFRF method will be used to derive an analytical relationship between the output spectra of system (3.4) and its nonlinear parameters of interest. Thereafter, a system analysis and design will be performed in order to obtain the nonlinear parameters for the desired performance metrics based on design specifications. The effects of the nonlinear parameters, c_2 and k_2 on the system output spectra are also explored using numerical simulations.

3.3 DETERMINATION OF THE OFRF REPRESENTATION

In this section, the OFRF representation of the output spectra of system (3.4) is obtained in terms of the nonlinear parameters of interest c_2 and k_2 . As indicated in Eq. (2.5) of subsection 2.4.3 in Chapter 2, the OFRF of nonlinear system (2.4) is a polynomial function of the nonlinear characteristic parameters of the system. The coefficients of the OFRF are the functions of the output frequency of the system, determined by the specific structure of Eq. (2.4), the system input spectrum and the linear characteristic parameters of the system. To enable the use of the OFRF representation of system (3.4) for system analysis and design, its coefficients and monomials have to be determined first.

The following analysis has been performed using these system parameters which have been carefully chosen so as not to drive the system output response to an unstable condition; $m = 0.2 \text{ kg}$, $c_1 = 1.5 \text{ N.s.m}^{-1}$, $k_1 = 500 \text{ N.m}^{-1}$, $Y = 0.05 \text{ m}$. It should be noted that these practical values have been prudently selected for this study as a future work (not reported in this thesis) will involve some experimental studies to validate the results established in this study. It can be inferred that the system in Eq. (3.4) is the instance of system (2.4) with $c_{0,1}(0) = -m\omega^2 Y$, $c_{1,0}(2) = m$, $c_{1,0}(0) = k_1$, $c_{1,0}(1) = c_1$, $c_{3,0}(0,0,1) = c_2$, $c_{3,0}(0,0,0) = k_2$, else $c_{p,q}(\bullet) = 0$.

3.3.1 Determination of the OFRF monomials

To determine the OFRF representation, the algorithm described in **A** of subsection 2.4.3 in Chapter 2 as well as in [68], for SIMO systems, is employed. The recursive algorithm therein is applied to system (3.4) to determine the set of monomials, \mathfrak{M} up to the $N=7^{\text{th}}$ order which yields

$$\mathfrak{M} = \bigcup_{n=1}^7 M_n = [1 \ c_2 \ k_2 \ c_2^2 \ c_2 k_2 \ k_2^2 \ c_2^3 \ c_2^2 k_2 \ c_2 k_2^2 \ k_2^3] \quad (3.5)$$

It should be noted, that the same set of monomials is obtained for both outputs of system (3.4). This implies the OFRF of the outputs of system (3.4) can be expressed as

$$\begin{cases} Z(j\omega) = \mathfrak{M} \cdot \underline{\Phi}(j\omega) \\ F_{\text{trans}}(j\omega) = \mathfrak{M} \cdot \underline{\Phi}(j\omega) \end{cases} \quad (3.6)$$

where $\underline{\Phi}(j\omega)$ and $\underline{\Phi}(j\omega)$ are the OFRF coefficients of the output spectra of system (3.4), $Z(j\omega)$ and $F_{\text{trans}}(j\omega)$ respectively. Next, the OFRF coefficients are determined.

3.3.2 Determination of the OFRF coefficients

To determine the coefficients of the OFRFs for the system outputs, $Z(j\omega)$ and $F_{\text{trans}}(j\omega)$, the steps outlined in **B** of subsection 2.4.3 in Chapter 2 are followed. The least square approach is used to determine $\underline{\Phi}(j\omega)$ and $\underline{\Phi}(j\omega)$ as

$$\begin{cases} \underline{\Phi}(j\omega)^T = \psi^T \psi^{-1} \psi^T \cdot \tilde{Z}(j\omega) \\ \underline{\Phi}(j\omega)^T = \psi^T \psi^{-1} \psi^T \cdot \tilde{F}_{\text{trans}}(j\omega) \end{cases} \quad (3.7)$$

where

$$\begin{aligned} \underline{\Phi}(j\omega)^T &= \begin{bmatrix} \underline{\phi}_{0,0}(j\omega) \\ \underline{\phi}_{1,0}(j\omega) \\ \vdots \\ \underline{\phi}_{0,3}(j\omega) \end{bmatrix}, & \underline{\Phi}(j\omega)^T &= \begin{bmatrix} \phi_{0,0}(j\omega) \\ \phi_{1,0}(j\omega) \\ \vdots \\ \phi_{0,3}(j\omega) \end{bmatrix}, \\ \tilde{Z}(j\omega) &= \begin{bmatrix} Z(j\omega)_{(1)} \\ Z(j\omega)_{(2)} \\ \vdots \\ Z(j\omega)_{(P)} \end{bmatrix}, & \tilde{F}_{\text{trans}}(j\omega) &= \begin{bmatrix} F_{\text{trans}}(j\omega)_{(1)} \\ F_{\text{trans}}(j\omega)_{(2)} \\ \vdots \\ F_{\text{trans}}(j\omega)_{(P)} \end{bmatrix} \end{aligned} \quad (3.8)$$

and

$$\psi = \begin{bmatrix} 1 & c_{2(1)} & k_{2(1)} & c_{2(1)}^2 & c_{2(1)}k_{2(1)} & k_{2(1)}^2 & c_{2(1)}^3 & c_{2(1)}^2k_{2(1)} & c_{2(1)}k_{2(1)}^2 & k_{2(1)}^3 \\ & & & & & \vdots & & & & \\ 1 & c_{2(P)} & k_{2(P)} & c_{2(P)}^2 & c_{2(P)}k_{2(P)} & k_{2(P)}^2 & c_{2(P)}^3 & c_{2(P)}^2k_{2(P)} & c_{2(P)}k_{2(P)}^2 & k_{2(P)}^3 \end{bmatrix}$$

$Z(j\omega)_{(i)}$ and $F_{\text{trans}}(j\omega)_{(i)}$ represents the output spectra of system (3.4) when $c_{2(i)} = c_2(i)$ and $k_{2(i)} = k_2(i)$ for $i = 1, 2, \dots, P$ where $P = 25$ for a varied set of $c_2 \in [0, 28] \text{ N.s.m}^{-3}$ and $k_2 \in [0, 2] \times 10^2 \text{ N.m}^{-3}$. The varied sets of nonlinear parameters, c_2 and k_2 have been selected to ensure the system remains stable for all

combinations of the parameters, as the OFRF method is only applicable for stable nonlinear systems. Therefore, considering $N=7$, the OFRF representations of the output spectra of system (3.4) can be expressed as

$$\left. \begin{aligned}
 Z(j\omega) &= \sum_{\bar{n}=0}^3 \sum_{\bar{m}=0}^{\bar{n}} \phi_{\bar{m}, \bar{n}-\bar{m}}(j\omega) c_2^{\bar{m}} k_2^{\bar{n}-\bar{m}} \\
 &= \phi_{0,0}(j\omega) + \phi_{1,0}(j\omega) c_2 + \phi_{0,1}(j\omega) k_2 + \phi_{2,0}(j\omega) c_2^2 \\
 &\quad + \phi_{1,1}(j\omega) c_2 k_2 + \phi_{0,2}(j\omega) k_2^2 + \phi_{3,0}(j\omega) c_2^3 + \phi_{2,1}(j\omega) c_2^2 k_2 \\
 &\quad + \phi_{1,2}(j\omega) c_2 k_2^2 + \phi_{0,3}(j\omega) k_2^3 \\
 \text{and} \\
 F_{\text{trans}}(j\omega) &= \sum_{\bar{n}=0}^3 \sum_{\bar{m}=0}^{\bar{n}} \phi_{\bar{m}, \bar{n}-\bar{m}}(j\omega) c_2^{\bar{m}} k_2^{\bar{n}-\bar{m}} \\
 &= \phi_{0,0}(j\omega) + \phi_{1,0}(j\omega) c_2 + \phi_{0,1}(j\omega) k_2 + \phi_{2,0}(j\omega) c_2^2 \\
 &\quad + \phi_{1,1}(j\omega) c_2 k_2 + \phi_{0,2}(j\omega) k_2^2 + \phi_{3,0}(j\omega) c_2^3 + \phi_{2,1}(j\omega) c_2^2 k_2 \\
 &\quad + \phi_{1,2}(j\omega) c_2 k_2^2 + \phi_{0,3}(j\omega) k_2^3
 \end{aligned} \right\} \quad (3.9)$$

Given the output spectra in terms of the nonlinear parameters of interest, as in Eq. (3.9), parameter optimisation can be easily conducted. For example, the resonant frequency, which is the frequency where the maximum displacement of the suspension system occurs (frequency of interest), and measured as $\omega_r = 50 \text{ rad.s}^{-1}$, the OFRF representations of the system output spectra are determined as

$$\begin{aligned}
 Z(j\omega_r) &= (-0.1585 - 0.2344i) + (0.0022 + 0.0040i)c_2 \\
 &\quad + (2.6195 \times 10^{-4} - 1.6383 \times 10^{-4}i)k_2 + (-3.7058 \times 10^{-5} - 1.2109 \times 10^{-4}i)c_2^2 \\
 &\quad + (-1.2745 \times 10^{-5} + 5.3623 \times 10^{-6}i)c_2 k_2 + (7.1624 \times 10^{-8} + 2.6437 \times 10^{-7}i)k_2^2 \\
 &\quad + (1.1426 \times 10^{-7} + 1.6910 \times 10^{-6}i)c_2^3 + (2.3307 \times 10^{-7} - 4.9742 \times 10^{-8}i)c_2^2 k_2 \\
 &\quad + (3.8650 \times 10^{-10} - 9.5687 \times 10^{-9}i)c_2 k_2^2 + (-1.9915 \times 10^{-10} + 1.2264 \times 10^{-11}i)k_2^3
 \end{aligned} \quad (3.10)$$

and

$$\begin{aligned}
 F_{\text{trans}}(j\omega_r) &= (-6.1703 \times 10^1 - 1.2908 \times 10^2 i) + (1.1198 + 2.0110i)c_2 \\
 &\quad + (0.1309 - 0.0820i)k_2 + (-0.0186 - 0.0606i)c_2^2 + (-0.0064 + 0.0027i)c_2 k_2 \\
 &\quad + (3.5977 \times 10^{-5} + 1.3211 \times 10^{-4}i)k_2^2 + (5.7607 \times 10^{-5} + 8.4602 \times 10^{-4}i)c_2^3 \\
 &\quad + (1.1653 \times 10^{-4} - 2.4955 \times 10^{-5}i)c_2^2 k_2 + (1.9106 \times 10^{-7} - 4.7826 \times 10^{-6}i)c_2 k_2^2 \\
 &\quad + (-9.9691 \times 10^{-8} + 6.3415 \times 10^{-9}i)k_2^3
 \end{aligned} \quad (3.11)$$

respectively.

In this case, the output spectra, $|Z(j\omega_r)|$ and $|F_{\text{trans}}(j\omega_r)|$ of system (3.4) are plotted for a varied set of $c_2 \in [0, 35] \text{N.s.m}^{-3}$ while keeping $k_2 = 240 \text{N.m}^{-3}$ fixed and presented in Figure 3.2.

The results, as presented in Figure 3.2, are obtained using the OFRFs of the output spectra as given in Eqs. (3.10) and (3.11) respectively and compared with results obtained from numerical simulations. Note that some of these results have been achieved for parameters beyond those used to determine the OFRFs. The outcome shows a good match between the OFRF-based results and results obtained from numerical simulations.

This indicates the usefulness of the OFRF method and, as revealed, it also shows it provides a good representation of the actual system output spectra. The implication of this is that the OFRF representations of the output spectra of system (3.4) can be used for the analysis and design of the system output spectra. This is because, using the OFRF, an explicit association of the system performance metrics with the system design parameters can be established.

It should be noted that a poor OFRF representation of the actual system output spectra will provide poor analytical results. Such poor representations can be as a result of large numerical errors generated during the determination of the OFRF coefficients. This typically occurs when the parameters are chosen to be large values with large numerical difference among them and also when the set of parameters selected cover a wide range. This will cause the values of the elements in the matrix \mathfrak{M} to be extremely large. Computational errors may result when the inverse of matrix \mathfrak{M} is computed in MATLAB. Such a problem can be solved by following the directives described in [85] and [68].

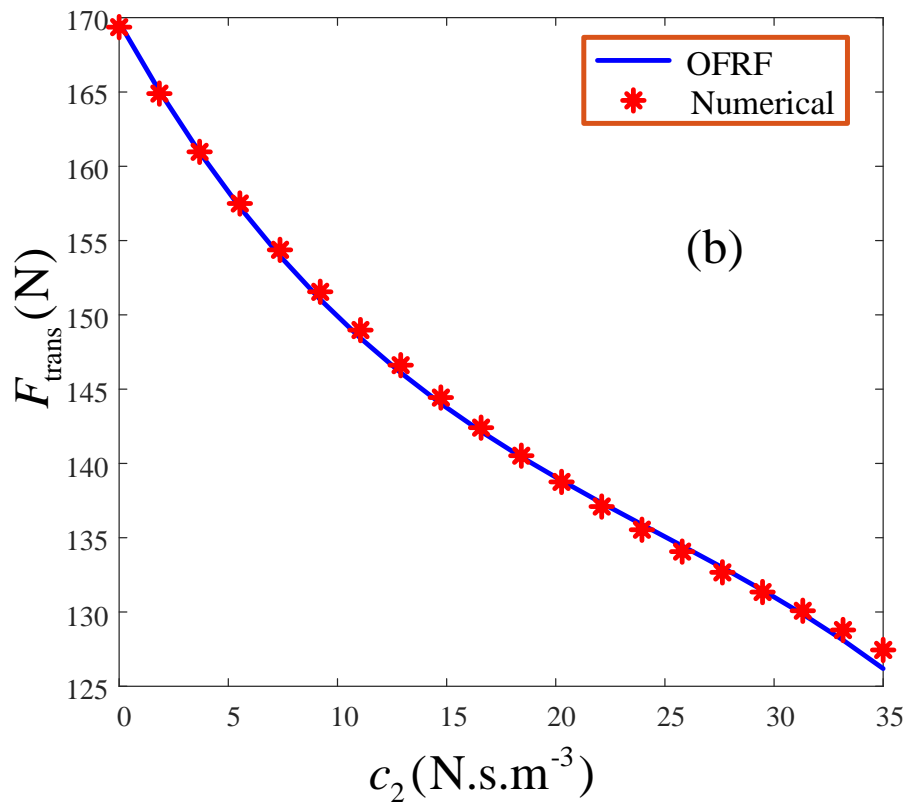
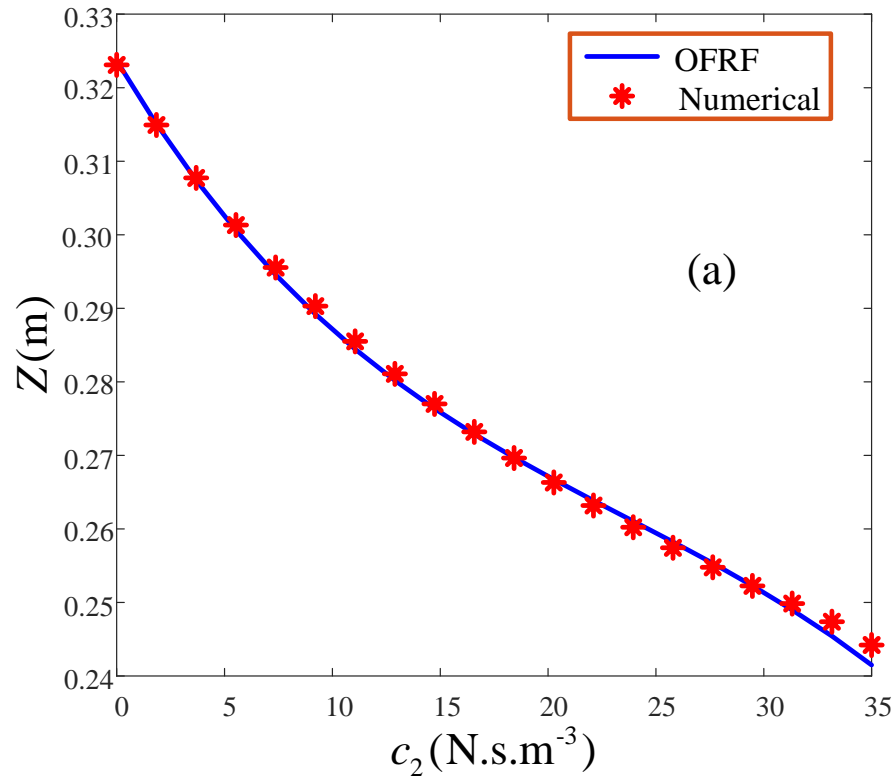


Figure 3.2: Comparison between OFRF and numerical simulation for (a) $Z(j\omega_r)$ and (b) $F_{trans}(j\omega_r)$, output spectra of system (3.4) respectively.

3.4 SYSTEM OPTIMISATION

The objective now is to minimise the unwanted force transmitted at the resonant frequency, $|F_{\text{trans}}(j\omega_r)|$ through the isolation elements (damper and spring) to acceptable limits. Let $|\mathbb{F}_{\text{trans}}(j\omega_r)|$ be the specified force that is transmitted through the vibration isolator, then the optimisation problem can be formulated as

$$\begin{aligned} \min_{c_2, k_2} & \quad |F_{\text{trans}}(j\omega_r) - \mathbb{F}_{\text{trans}}(j\omega_r)| \\ \text{s.t.} & \quad \begin{cases} c_2 - 35 \leq 0 \\ k_2 - 2.4 \times 10^2 \leq 0 \end{cases} \end{aligned} \quad (3.12)$$

Using the OFRF of Eq. (3.11), the relationship between the design parameters, c_2 and k_2 and the output spectrum, $F_{\text{trans}}(j\omega_r)$ is established and provided in Figure 3.3 and Figure 3.4. Looking at Figure 3.4, it is apparent that the contour map can be used as a design guide. The results of two design specifications are presented in Table 3.1. To determine the actual output response, $F_{\text{trans}}(j\omega_r)$, the designed parameters are substituted into the system model (3.4) and simulated numerically using the *Runge-Kutta 4* algorithm.

Table 3.1: Results from the optimisation problem

Desired output response, $ \mathbb{F}_{\text{trans}}(j\omega_r) (\text{N})$	Selected $k_2(\text{N.m}^{-3})$	Corresponding $c_2(\text{N.s.m}^{-3})$	Actual output response, $ F_{\text{trans}}(j\omega_r) (\text{N})$	Percentage error (%) $\left[\frac{ \mathbb{F}_{\text{trans}}(j\omega_r) - F_{\text{trans}}(j\omega_r) }{ F_{\text{trans}}(j\omega_r) } \right] \times 100$
135	150	23.9	134.8924	7.9767×10^{-2}
130	220	31	130.1583	-1.2162×10^{-1}

It should be noted that the second design specification was achieved for parameter values beyond the OFRF-determined range of parameters, i.e. $c_2 \in [0, 28] \text{N.s.m}^{-3}$ and $k_2 \in [0, 2] \times 10^2 \text{N.m}^{-3}$. In Table 3.1, it is observed that the actual output responses obtained using the designed parameters, c_2 and k_2 clearly matches the specified output responses with insignificant percentage errors. This reaffirms the effectiveness of the OFRF-based optimal design.

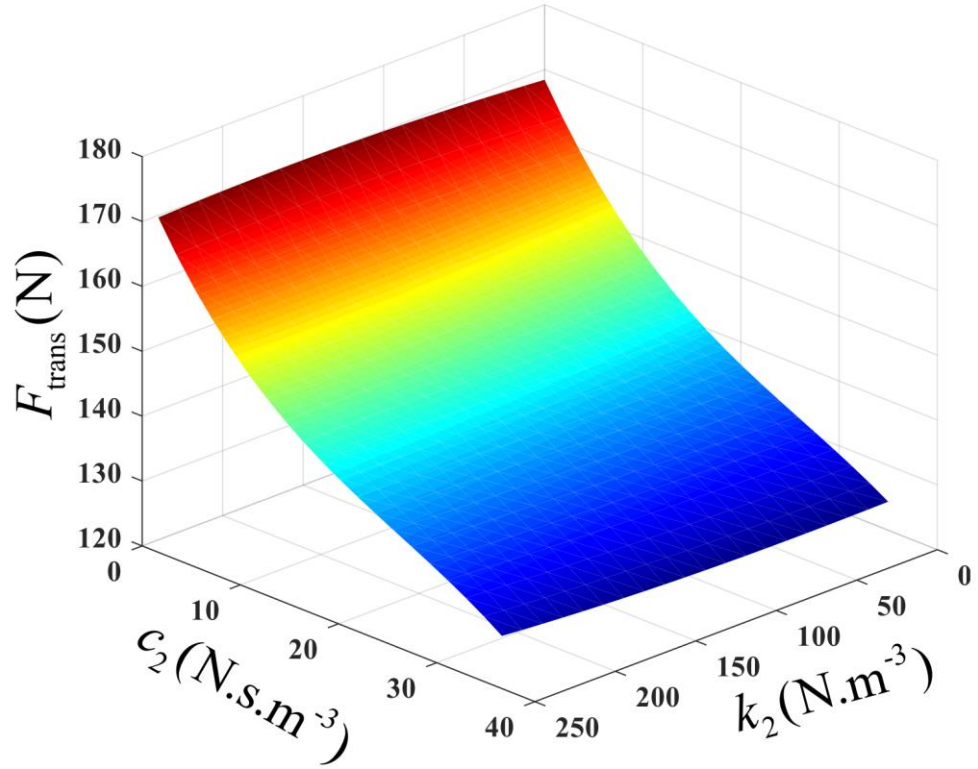


Figure 3.3: Output spectrum of the transmitted force, $|F_{\text{trans}}(j\omega_r)|$.

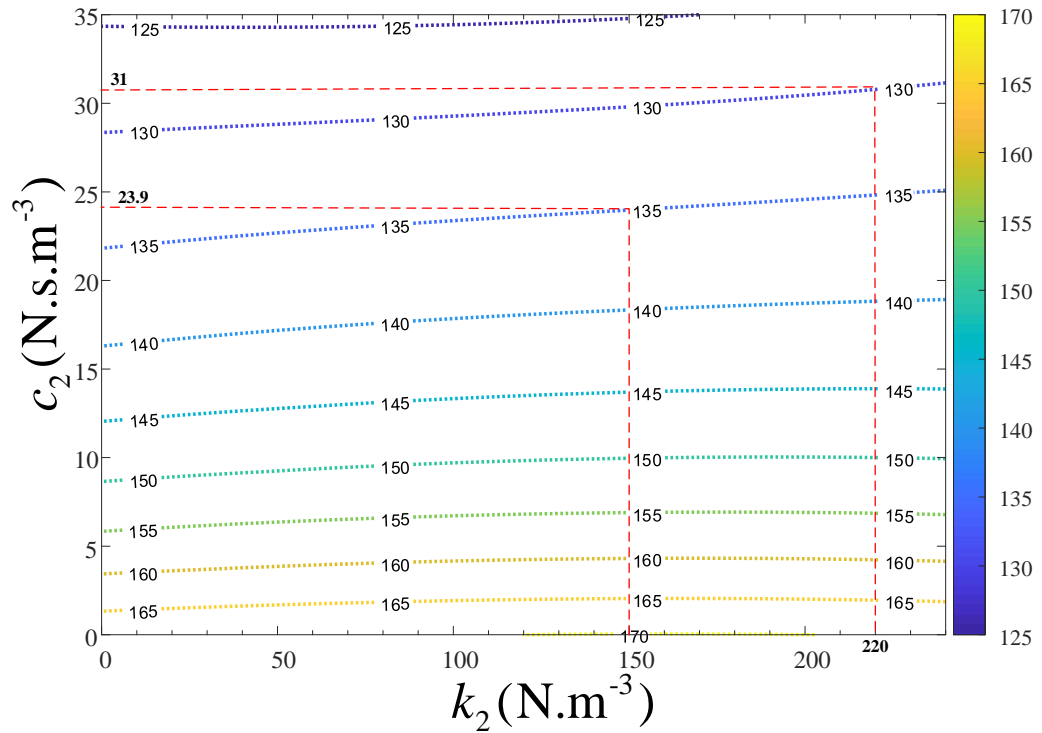


Figure 3.4: Contour map of the Output spectrum of the transmitted force, $|F_{\text{trans}}(j\omega_r)|$.

Looking at the time histories of the force transmitted at the resonant frequency in Figure 3.5, it is obvious that the designed nonlinear vibration isolation system performs better compared to the corresponding linear counterpart (where the nonlinear characteristic parameters, $c_2 = k_2 = 0$). Moreover, a close observation of the time history of the transmitted force due to the designed nonlinear isolation system reveals that the desired transmitted force, at the resonant frequency, is achieved. It should be noted that minimising the force transmitted along the isolation elements, $|F_{\text{trans}}(j\omega_r)|$ results in a decrease in the system output spectrum, $|Z(j\omega_r)|$.

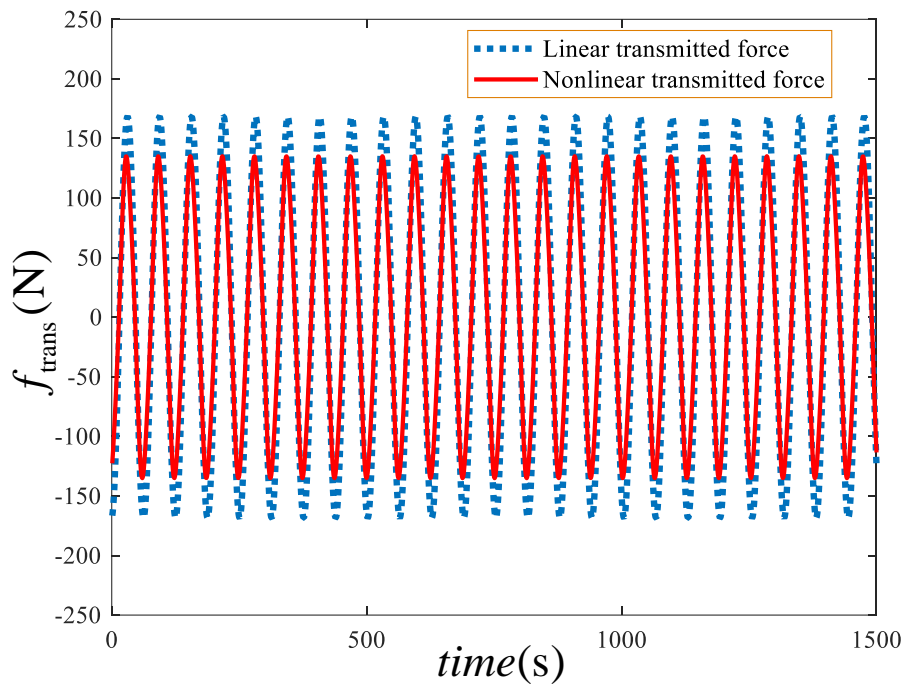


Figure 3.5: Comparison of the system output response, at resonance, under linear and nonlinear conditions.

Furthermore, though the system design has been performed at the resonant frequency, it is imperative to verify that the designed nonlinear optimal parameters maintain the same performance on the system output spectrum across the entire frequency range. This is verified in Figure 3.6 which compares the performance of the nonlinear design to its corresponding linear counterpart (i.e. when $c_2 = k_2 = 0$) on the system output spectrum. It is apparent that not only do the designed optimal parameters achieve a specified output spectrum at the resonant frequency, they are also adequate at suppressing the vibration levels over other frequencies.

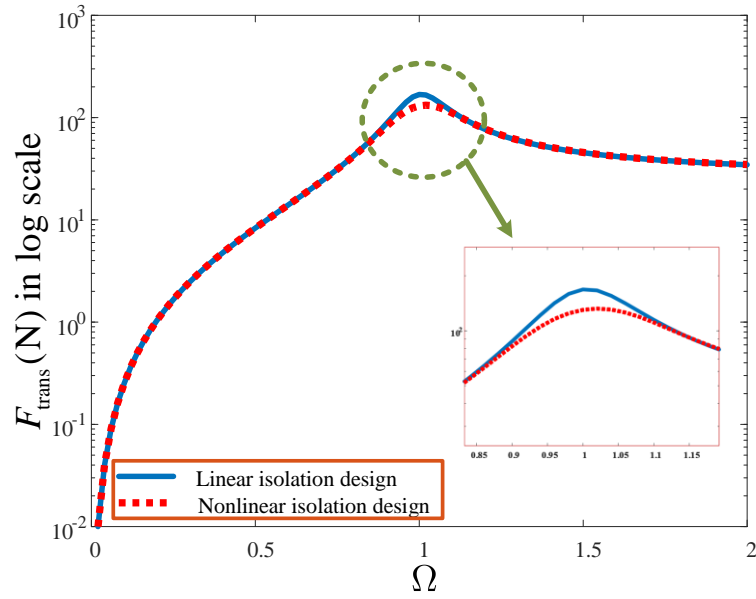


Figure 3.6: Comparison of the system output spectrum under linear and nonlinear conditions across the entire frequency range.

The above system analysis and design have been performed using the OFRF method. It is evident that this method facilitates a systematic analysis and design of nonlinear Volterra systems unlike other methods.

The next section shows the individual effect of the system parameters on the output spectra of the system considered in this study. Each parameter is varied while fixing others. These have been performed using numerical simulations.

3.5 NUMERICAL STUDIES

To demonstrate the effects of c_1 , c_2 , and k_2 on the output spectra of system (3.4), numerical studies were performed and the results presented in Figure 3.7, Figure 3.8 and Figure 3.9. Figure 3.7 shows the well-known influence of linear damping characteristic parameter on the output spectra of system (3.4) where a good isolation performance is witnessed over the resonant region. However, its detrimental effect over the region where isolation is required ($\Omega \gg 1$) when high damping level is employed suggests the need for the integration of nonlinear damping. In Figure 3.8, the effect of k_2 is evident around the resonant region. It is apparent that as k_2 increases, the resonant frequency, ω_r is increased beyond the natural frequency however, its harmful effect (instability) is controlled by an increased damping characteristic. Besides, the effect of increasing the nonlinear viscous damping characteristic

parameter, c_2 is observed, in Figure 3.9, to suppress the vibration at the resonant region. However, the vibration at the non-resonant regions (i.e. at low and high frequency ranges) remain unaffected.

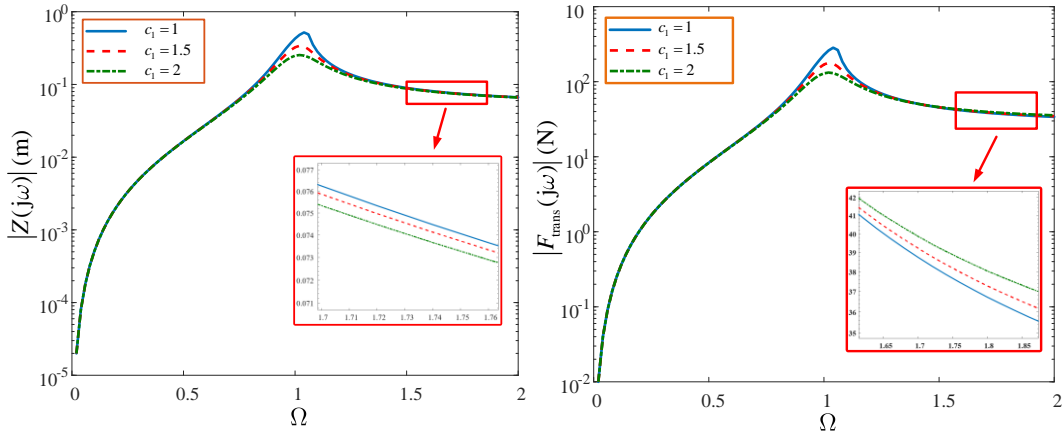


Figure 3.7: Effect of linear damping characteristic parameter on the system output spectra across the entire frequency range with $c_2 = 0.1 \text{ N.s.m}^{-3}$ and $k_2 = 100 \text{ N.m}^{-3}$.

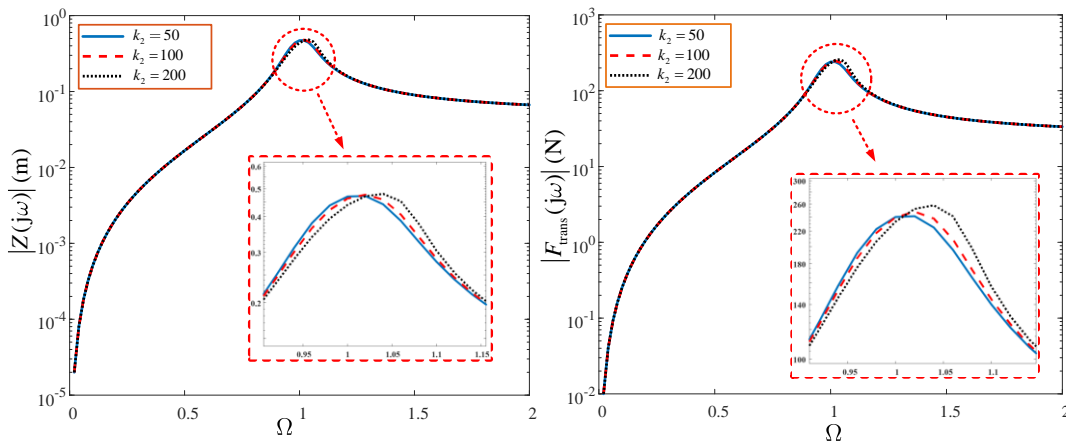


Figure 3.8: Effect of nonlinear stiffness characteristic parameter on the system output spectra across the entire frequency range with $c_1 = 0.5 \text{ N.s.m}^{-1}$ and $c_2 = 10 \text{ N.s.m}^{-3}$.

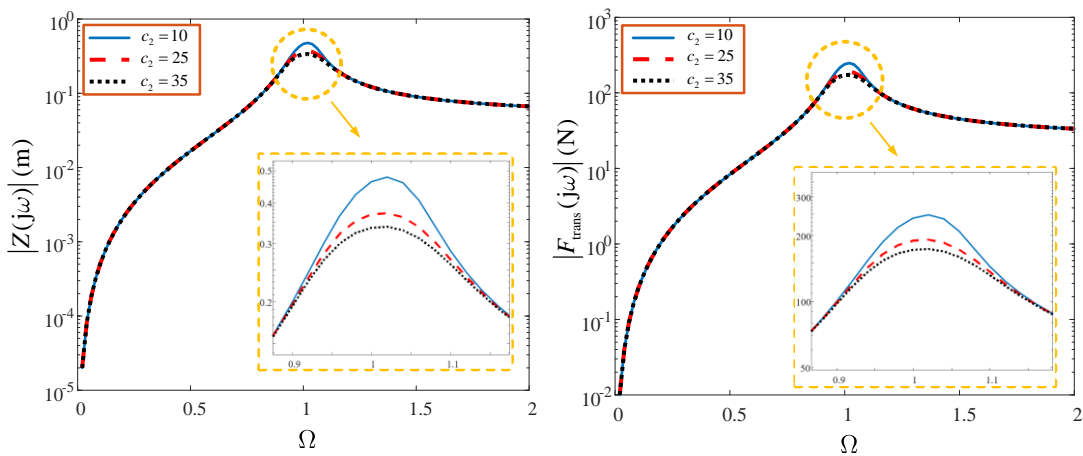


Figure 3.9: Effect of nonlinear damping characteristic parameter on the system output spectra across the entire frequency range with $c_1 = 0.5 \text{ N.s.m}^{-1}$ and $k_2 = 100 \text{ N.m}^{-3}$.

3.6 ENERGY DISSIPATION ANALYSIS

For the SDOF system described in Figure 3.1, the vibration isolation elements (spring and damper) experience energy loss due to their dissipative characteristics. The power dissipated at any instant is $f_{\text{trans}}\dot{z}$, and the energy lost over one complete cycle, E_d , is given as

$$\begin{aligned} E_d &= \int_0^{2\pi/\omega} f_{\text{trans}}\dot{z} dt \\ &= \int_0^{2\pi/\omega} [(c_1\dot{z} + c_2z^2\dot{z} + k_1z + k_2z^3) \cdot \dot{z}] dt \end{aligned} \quad (3.13)$$

Let the relative displacement, $z = Z \sin(\omega t)$, then $\dot{z} = \omega Z \cos(\omega t)$. Equation (3.13) becomes

$$E_d = \int_0^{2\pi/\omega} \left[\begin{array}{l} c_1\omega Z \cos(\omega t) + c_2\omega Z^3 \sin^2(\omega t) \cos(\omega t) \\ + k_1Z \sin(\omega t) + k_2Z^3 \sin^3(\omega t) \end{array} \right] \cdot \omega Z \cos(\omega t) dt \quad (3.14)$$

which yields

$$\begin{aligned} E_d &= \pi c_1 \omega Z^2 + \frac{1}{4} \pi c_2 \omega Z^4 \\ &= \pi \omega Z^2 (c_1 + \frac{1}{4} c_2 Z^2) \\ &= \pi \omega Z^2 (c_1 + c_e) \\ &= \pi c_{eq} \omega Z^2 \end{aligned} \quad (3.15)$$

where $c_{eq} = c_1 + c_e$ and $c_e = \frac{1}{4} c_2 Z^2$

It is observed from Eq. (3.15) that the energy dissipation of the vibration isolation elements is due to the damping characteristics only. The OFRF of the energy lost by the suspension system over one complete cycle can be derived by substituting Eq. (3.9a) into Eq. (3.15) which yields

$$E_d(\omega, c_2, k_2) = \pi c_1 \omega |Z|^2 + \frac{1}{4} \pi c_2 \omega |Z|^4 \quad (3.16)$$

Equation (3.16) indicates E_d is a function of c_1 , ω , Z and the design parameters, c_2 and k_2 (since Z is also a function of the design parameters). This indicates that the OFRF of the energy dissipated can be derived in terms of the design parameters.

Just as the OFRF representation of the output spectrum, Z of system (3.4) was determined and presented in Eq. (3.9a), the OFRFs of the squared and quartic magnitudes of Z are also derived as

$$\begin{cases} |Z|^2 = \sum_{\bar{n}=0}^{\lfloor(N-1)/2\rfloor} \sum_{\bar{m}=0}^{\bar{n}} P_{\bar{m},\bar{n}-\bar{m}}(\omega) c_2^{\bar{m}} k_2^{\bar{n}-\bar{m}} \\ |Z|^4 = \sum_{\bar{n}=0}^{\lfloor(N-1)/2\rfloor} \sum_{\bar{m}=0}^{\bar{n}} Q_{\bar{m},\bar{n}-\bar{m}}(\omega) c_2^{\bar{m}} k_2^{\bar{n}-\bar{m}} \end{cases} \quad \text{and} \quad (3.17)$$

where $N = 7$ while $P_{\bar{m},\bar{n}-\bar{m}}$ and $Q_{\bar{m},\bar{n}-\bar{m}}$ are functions of frequency and represent the OFRF coefficients of $|Z|^2$ and $|Z|^4$ respectively. Substituting Eq. (3.17) into Eq. (3.16) yields

$$\begin{aligned} E_d(\omega, c_2, k_2) = & \pi c_1 \omega \cdot \sum_{\bar{n}=0}^{\lfloor(N-1)/2\rfloor} \sum_{\bar{m}=0}^{\bar{n}} P_{\bar{m},\bar{n}-\bar{m}}(\omega) c_2^{\bar{m}} k_2^{\bar{n}-\bar{m}} \\ & + \left(\frac{1}{4} \pi \omega \right) \cdot \sum_{\bar{n}=0}^{\lfloor(N-1)/2\rfloor} \sum_{\bar{m}=0}^{\bar{n}} Q_{\bar{m},\bar{n}-\bar{m}}(\omega) c_2^{\bar{m}+1} k_2^{\bar{n}-\bar{m}} \end{aligned} \quad (3.18)$$

Equation (3.18) indicates that an estimate of the energy dissipated per cycle by the vibration isolation elements can be determined for a set of design parameters. The relationship between the energy dissipation and the design parameters at the resonant frequency, $\Omega = 1$ is provided in Figure 3.10. It is seen in Figure 3.11 that a large amount of energy is dissipated when a linear vibration isolator is used (when $c_2 = 0, k_2 = 0$) however, the energy dissipated reduces with the integration of nonlinear damping and stiffness characteristics. This is due to the impact of the nonlinear components on the relative displacement of the suspension system. The relative displacement decreases as the nonlinearities increase which, consequently, reduces the force transmitted and energy dissipated by the vibration isolation elements. It is also evident that the energy dissipation level is very sensitive to the nonlinear damping characteristic and less sensitive to the nonlinear hardening stiffness characteristic. Surface plots between the energy dissipation and the design parameters beyond the resonant region, that is, at $\Omega = 0.4$ and $\Omega = 2$ are presented in Figure 3.12 and Figure 3.13 respectively.

Besides, Eq. (3.18), which is the OFRF of the energy dissipation of the isolation system, can be used to estimate the energy dissipated by a set of optimal design

parameters, c_2 and k_2 . An estimation guide can be developed using an OFRF-generated contour map which can facilitate the selection of design parameters for a specified energy dissipation level as illustrated in Figure 3.14.

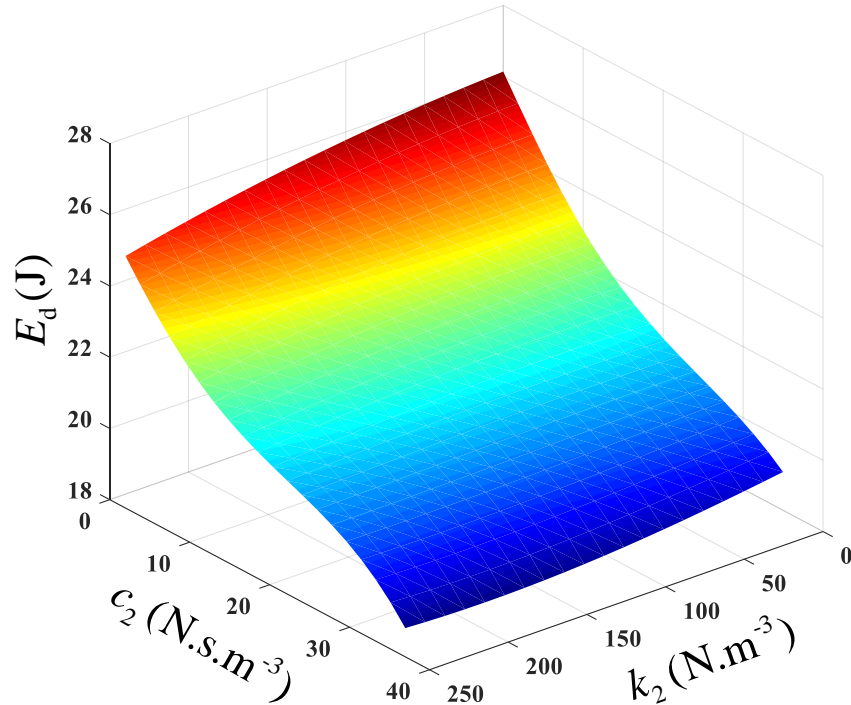


Figure 3.10: Relationship between the Energy dissipation and design parameters at $\Omega = 1$.

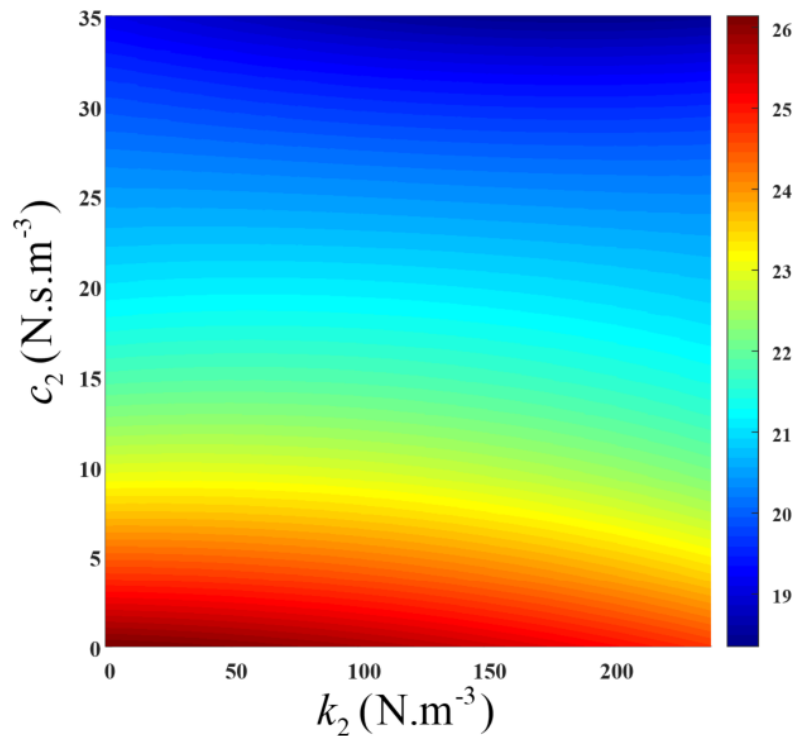


Figure 3.11: Energy dissipation plot for sets of design parameters at $\Omega = 1$.

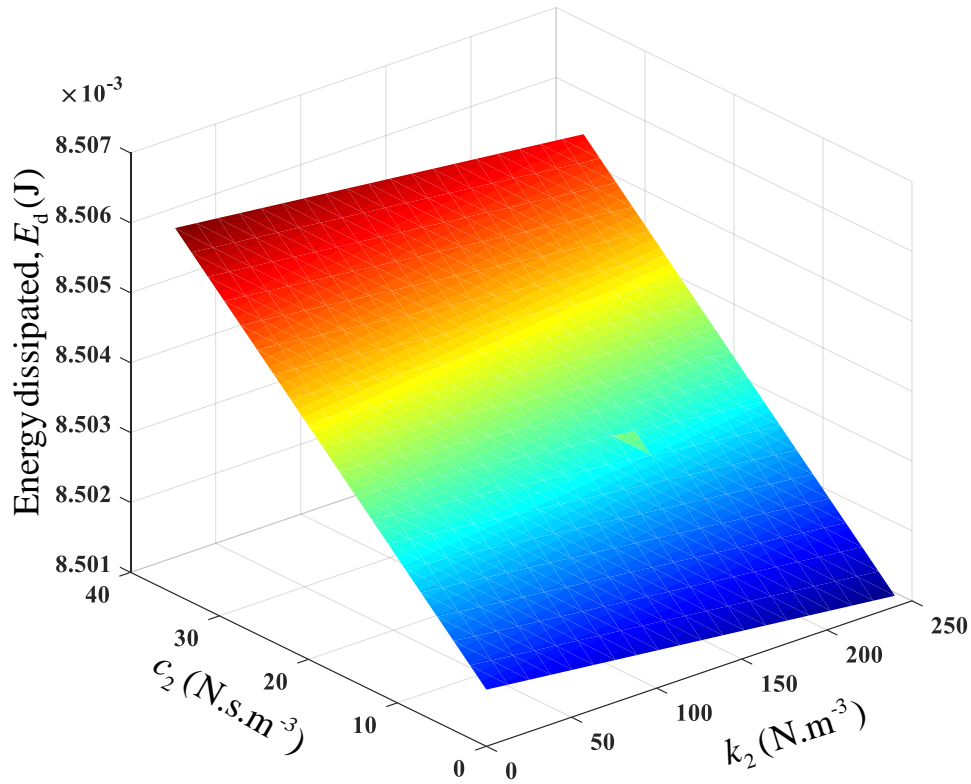


Figure 3.12: Energy dissipation levels for different combinations of design parameters at $\Omega = 0.4$.

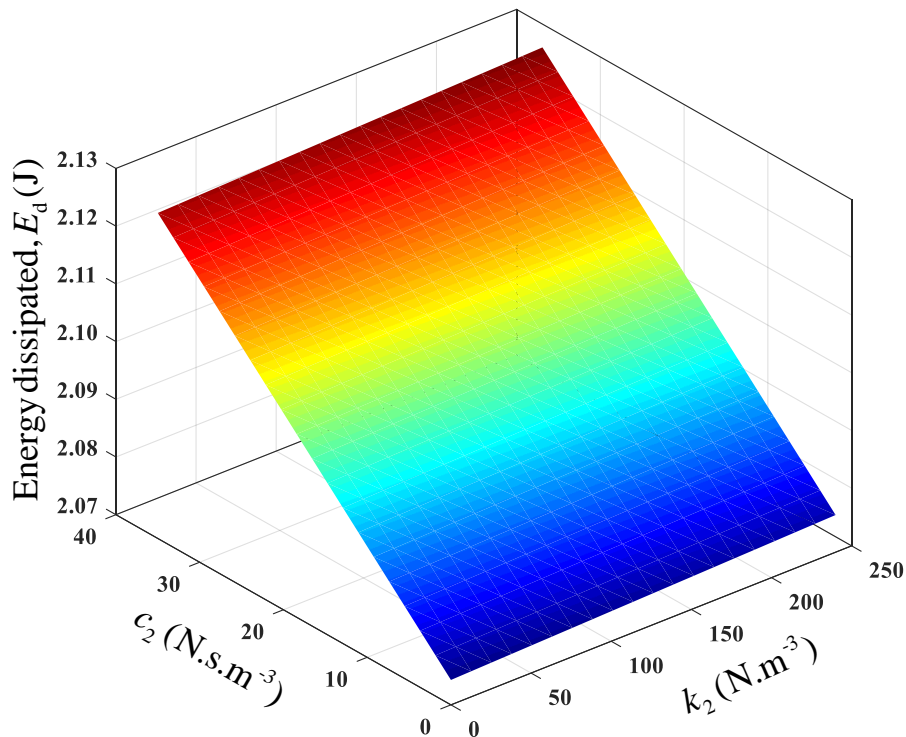


Figure 3.13: Energy dissipation levels for different combinations of design parameters at $\Omega = 2$.

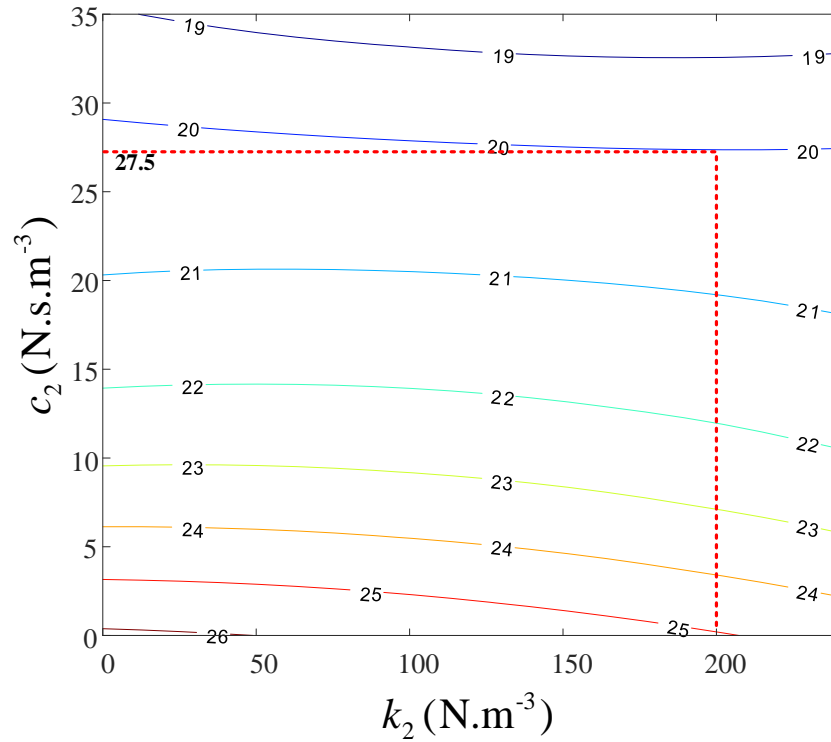


Figure 3.14: Contours of energy dissipation levels for sets of design parameters.

Choosing $k_2 = 200 \text{ N}\cdot\text{m}^{-3}$ along the contour line of 20J gives a corresponding nonlinear damping value of $c_2 = 27.5 \text{ N}\cdot\text{s}\cdot\text{m}^{-3}$. Substituting c_2 and k_2 into system (3.4) and solving for the energy dissipation level, numerically, yields a value of 21.08J which matches the design requirement well with a percentage error of -5.1%.

The results from numerical studies to show the individual effects of system parameters on the energy dissipation level of the suspension system, over the entire spectrum, are presented in Figure 3.15, Figure 3.16 and Figure 3.17. This was done by varying either one of the parameters, c_1 , c_2 or k_2 while keeping the other two fixed. In Figure 3.15, the unwanted impact of linear damping over the high frequency region, experienced by the output spectra of system (3.4), is also apparent for the energy dissipation spectra. It is seen that while an increase in linear damping reduces the energy dissipation over the resonant region, it increases the energy dissipation significantly across the non-resonant regions. Likewise, increasing the nonlinear damping minimises the energy dissipation at the resonant region. However, unlike linear damping, the corresponding increase in the energy dissipation in the non-resonant regions is far less significant as illustrated in Figure 3.16.

The influence of hardening stiffness, as shown in Figure 3.17 is similar to the effect it has on the output spectra of system (3.4). In this case, as nonlinear stiffness is increased, the resonant peak of the energy dissipation level is reduced at $\Omega = 1$. This is due to a resonant-shift effect of k_2 on the resonant energy beyond the natural frequency.

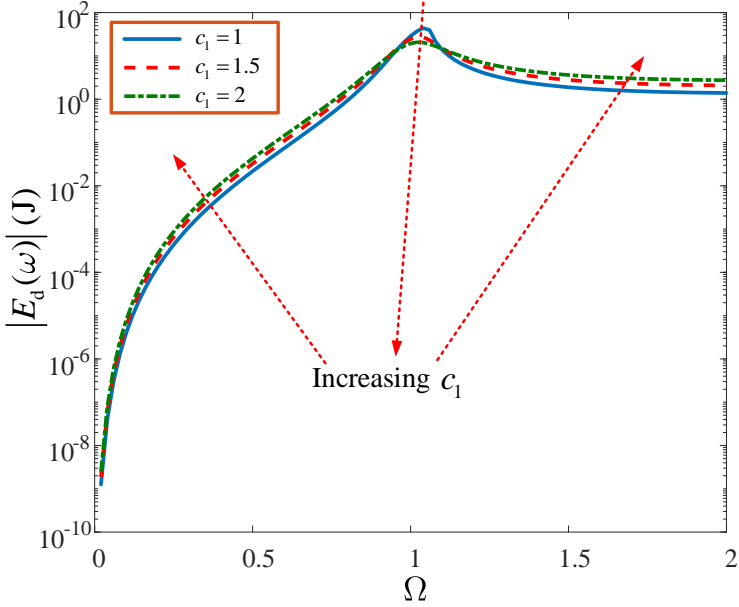


Figure 3.15: Effect of linear damping characteristic parameter on the energy dissipation level across all frequency range with $c_2 = 1 \text{ N.s.m}^{-3}$ and $k_2 = 100 \text{ N.m}^{-3}$.

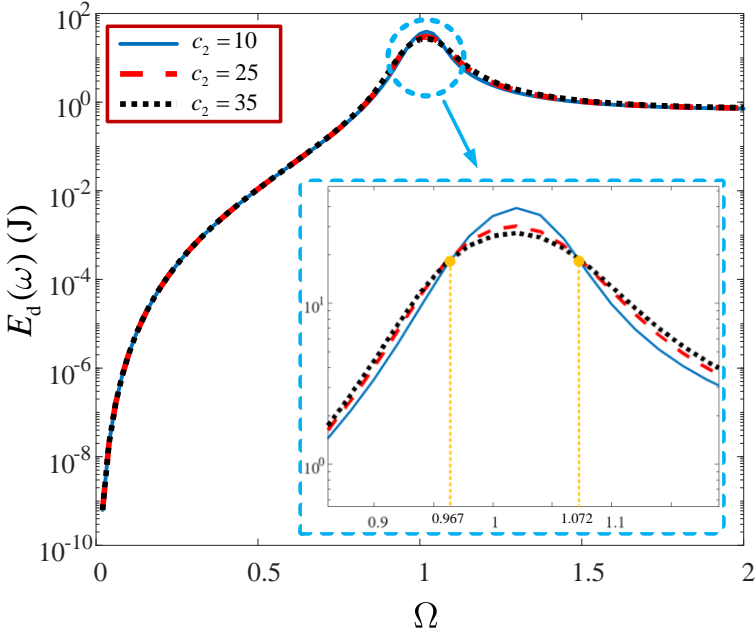


Figure 3.16: Effect of nonlinear damping characteristic parameter on the energy dissipation level across all frequency range with $c_1 = 0.5 \text{ N.s.m}^{-1}$ and $k_2 = 100 \text{ N.m}^{-3}$.

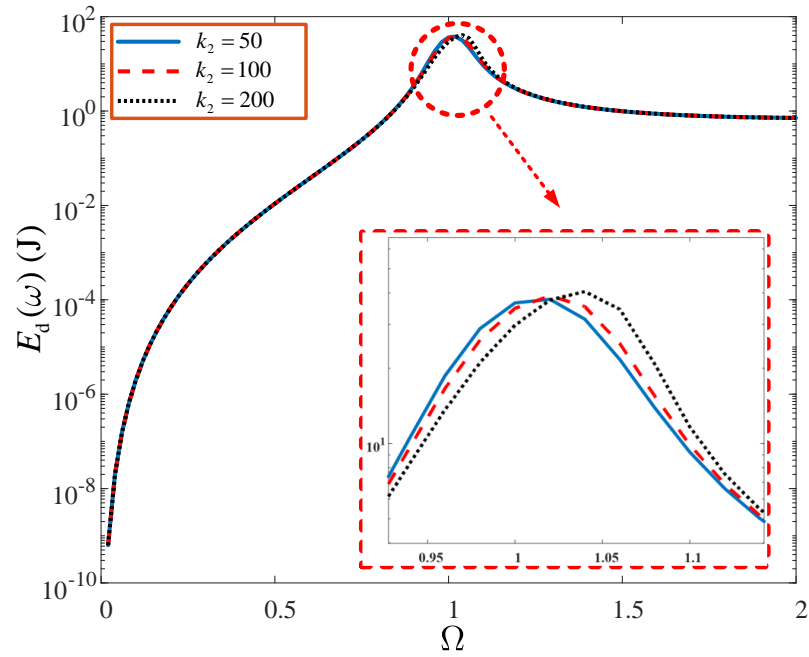


Figure 3.17: Effect of nonlinear stiffness characteristic parameter on the energy dissipation level across all frequency range with $c_1 = 0.5 \text{ N.s.m}^{-1}$ and $c_2 = 10 \text{ N.s.m}^{-3}$.

Using the OFRF representations derived, the variations of both the energy dissipated and force transmitted by the suspension system as a function of the nonlinear stiffness parameter, k_2 are shown in Figure 3.18. It is observed that while the force transmitted by the suspension system is less sensitive to k_2 , the sensitivity of the energy dissipated to k_2 is insignificant. This reaffirms the deduction made from Figure 3.11. This deduction is largely because the spring element stores potential energy when compressed/stretched and dissipates insignificant amounts of energy. It is also seen that for a fixed c_2 , increasing k_2 causes an insignificant decrease in the energy dissipated per cycle however the vibration force transmitted is increased. Similarly, the results illustrated in Figure 3.19 are the variations of both the energy dissipated and force transmitted by the suspension system as a function of the nonlinear damping parameter, c_2 . In this case, it is apparent that both performance metrics are significantly sensitive to c_2 . Both performance metrics also progressively decrease as c_2 increases. This is because the relative displacement of the vehicle suspension system decreases as c_2 increases and this causes a decrease in both the force transmitted and energy dissipated by the suspension system.

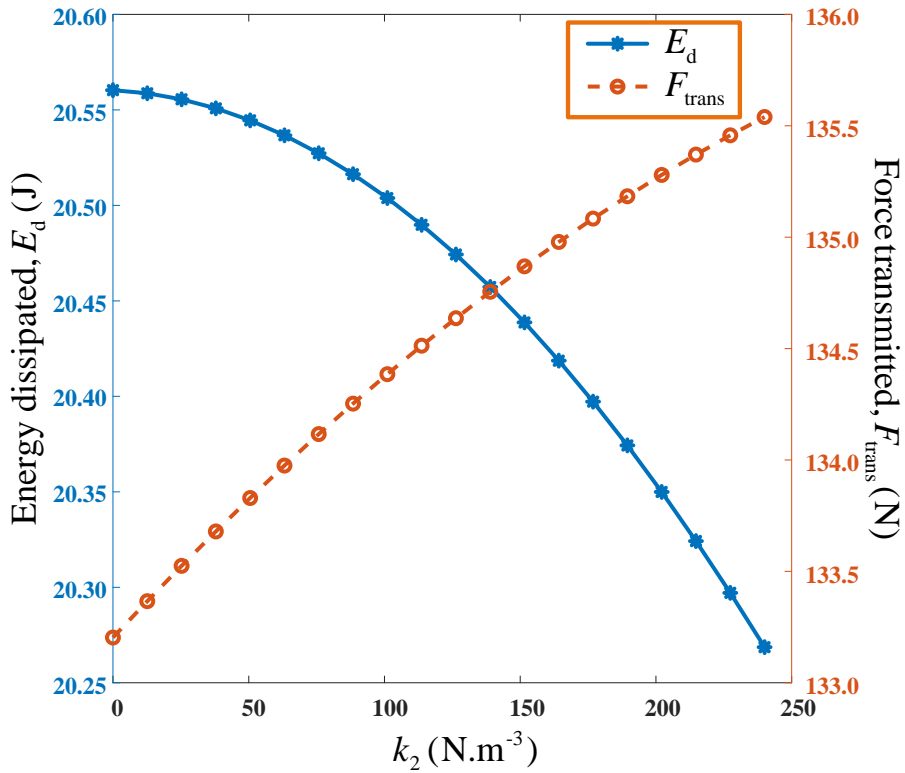


Figure 3.18: Variation of energy dissipated and force transmitted by the suspension system with respect to k_2 at $c_1 = 1.5 \text{ N.s.m}^{-1}$ and $c_2 = 23.9 \text{ N.s.m}^{-3}$.

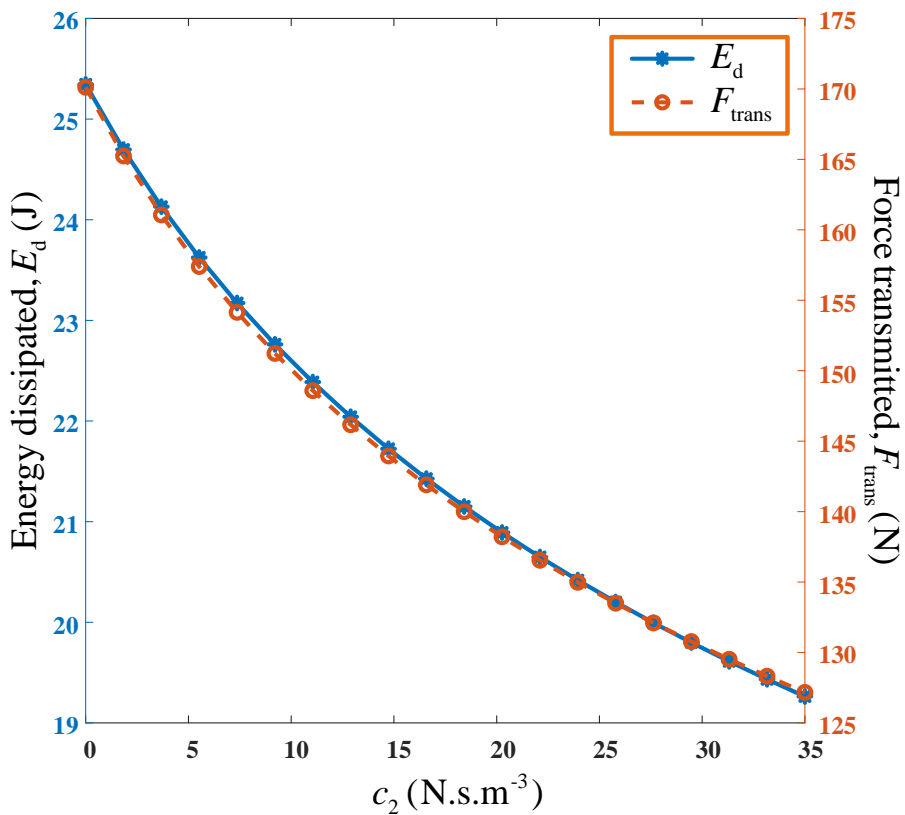


Figure 3.19: Variation of energy dissipated and force transmitted by the suspension system with respect to c_2 at $c_1 = 1.5 \text{ N.s.m}^{-1}$ and $k_2 = 164.2 \text{ N.m}^{-3}$.

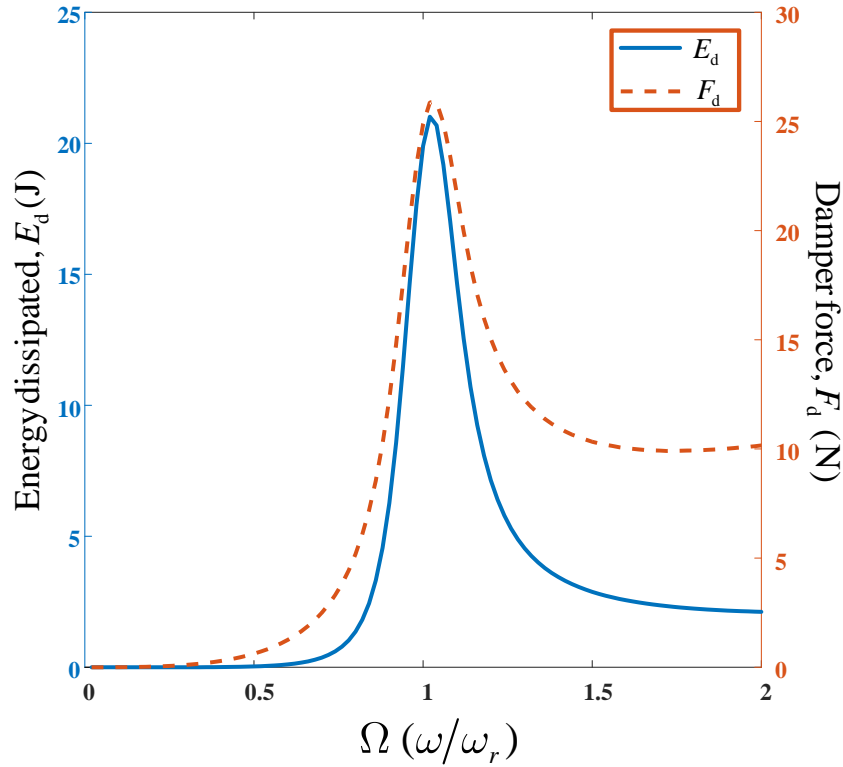


Figure 3.20: Variation of suspension damper force and energy dissipated by the suspension system with frequency at $c_1 = 0.5 \text{ N.s.m}^{-1}$ and $c_2 = 10 \text{ N.s.m}^{-3}$.

Illustrated in Figure 3.20 are the variations of the suspension damper force, F_d (N) and the energy dissipated by the suspension system, E_d (J) with excitation frequency. It is observed that both quantities attain maximum values at the resonant frequency, ($\Omega = 1$). This is expected as a high damping force is desired at resonance (i.e. region of maximum displacement) which corresponds to a high energy dissipation level by the suspension system. However, the amount of energy dissipated at the high frequency region, (i.e. $\Omega \geq 1$) is large and not proportionate to the low level of damping force applied in this region, unlike the proportionality observed in the low frequency region (i.e. $\Omega \leq 1$). This is due to the suppressed relative displacement experienced at the high frequency region due to the high damping level.

3.6.1 Hysteresis Curves for a nonlinear viscous-elastic model

Four hysteresis curves (A, B, C, and D) are presented in Figure 3.21 from different combinations of the designed nonlinear parameters of system (3.4). For a vibration isolation system, the area of the Force-displacement curve ($F_{\text{trans}} - Z$) gives an indication of the energy dissipated per cycle by the isolation system, at any frequency

of interest (typically the resonant frequency). It is observed that the hysteresis curves C and D produced, due to the contribution of a nonlinear damping characteristic by the suspension system, shows a smaller displacement span compared to those with only linear damping (i.e. hysteresis curves A and B). This is due to the superior vibration isolation performance of the nonlinear damping characteristics compared to the corresponding linear case (when $c_2 = 0$). This is because the magnitude of the relative displacement, Z is reduced considerably for the suspension system with nonlinear damping characteristics.

It should be noted that compared to linear dampers, nonlinear dampers dissipate, significantly, more amount of energy for equal excitation and relative displacement [169]. However, such a comparison has not been considered here. Furthermore, while for a linear suspension system configuration, the hysteresis curve assumes an elliptic shape, this is not the case for a nonlinear suspension system.

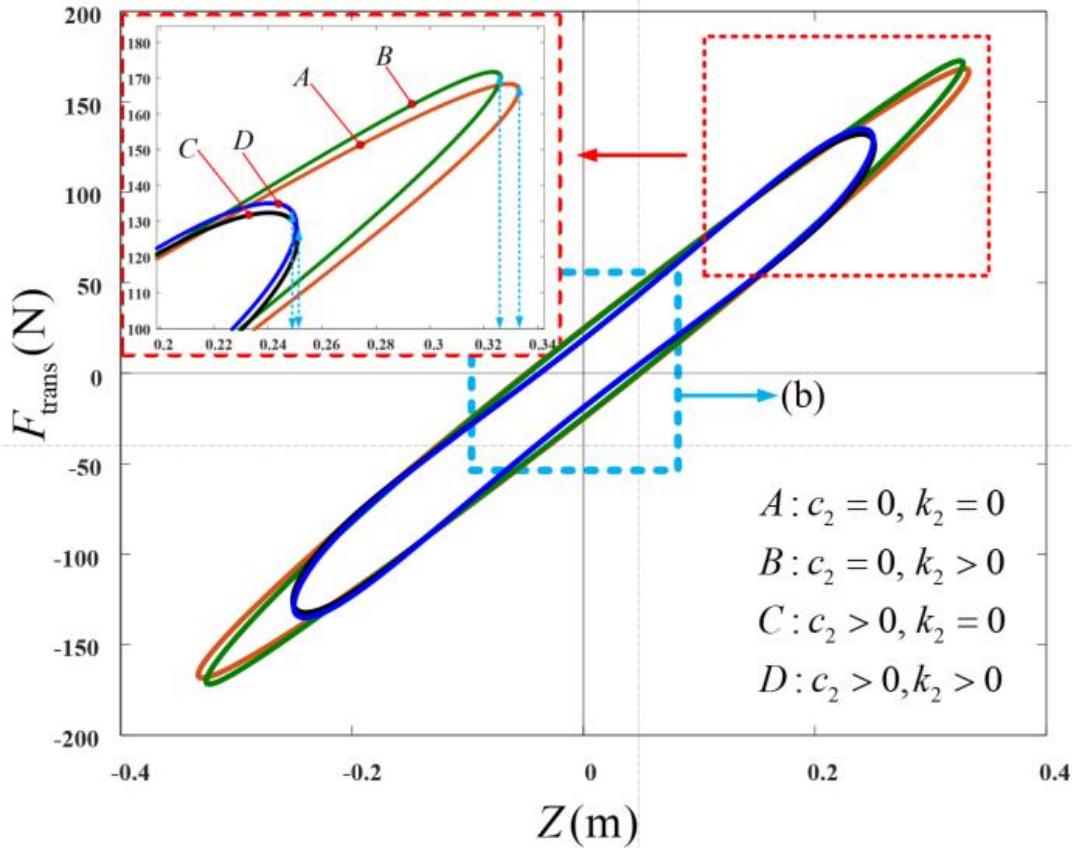


Figure 3.21: Comparison of the Hysteresis curves for the vibration isolation system having different combinations of nonlinear parameters at resonance. (b) is shown in Figure 3.22.

The effect of c_2 on curves C and D, with intercept $c_1 Z_{C,D} \omega_r = 18.75$ N on the vertical axis, is apparent compared to the curves A and B (with intercept, $c_1 Z_{A,B} \omega_r = 24.96$ N) without the effect of c_2 as shown in Figure 3.22. This is seen to be as a result of the influence of c_2 on the system output response, Z , which is a function of the nonlinear damping characteristics, c_2 .

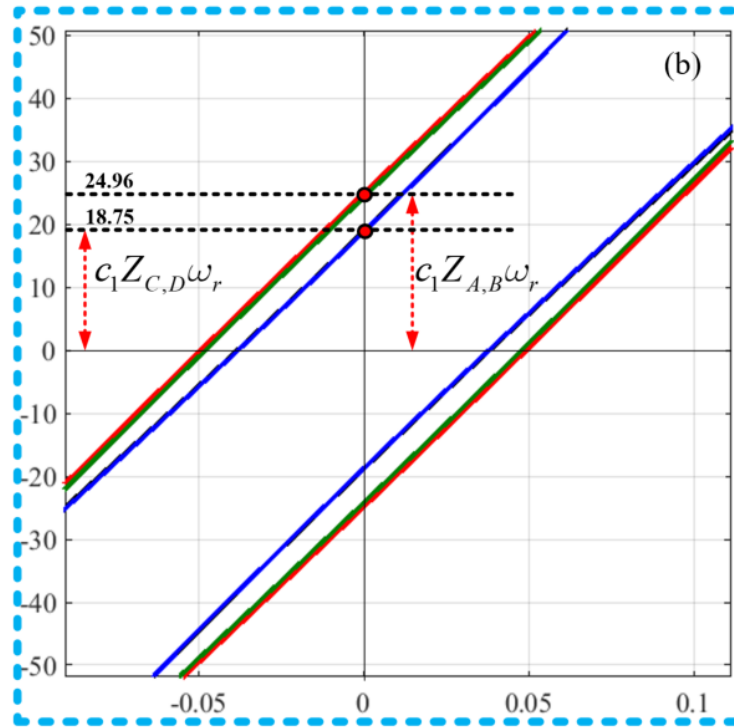


Figure 3.22: Enlarged origin of the hysteresis curves in Figure 3.21.

3.7 CONCLUSIONS

In this chapter, the vibration isolation performance of a vehicle suspension system modelled as a SDOF vibration isolation system has been studied. The Output Frequency Response Function (OFRF) method was the analytical tool employed for the analysis and design of the suspension system based on the design criteria. This method was used because of its ability to explicitly express the system performance metrics in terms of the design parameters of interest. The results obtained from the analytical and simulation studies demonstrate the effectiveness of this method in the analysis and design of vibration isolation systems. To demonstrate the extensive effects of the designed nonlinear system parameters, a comparative study was

conducted between the nonlinear system model and the corresponding linear system (where the nonlinear components are fixed to zero). The outcome reveals the influence of the system nonlinearities especially at the resonant region as the resonant peak is largely reduced without a detrimental effect on the higher range of frequencies. This demonstrates the vibration isolation capability of nonlinear VIS compared to the linear case.

Furthermore, the energy dissipated per cycle by the designed suspension system was investigated also using the OFRF method. Using the OFRF method, a relationship between the Energy dissipation level of the nonlinear suspension system and the design parameters was derived. This polynomial relationship has facilitated the estimation of an energy dissipation level for a set of system nonlinear parameters. The results obtained demonstrated the advantage of employing a nonlinear suspension system compared to the corresponding linear counterpart. Numerical studies were conducted to demonstrate the effects of system parameters on the energy dissipation level of the suspension system. A brief study was also conducted on the energy dissipation level of the suspension system using hysteresis curves as the effects of the system nonlinear parameters on the shape of the loop was investigated. The sensitivity of the energy dissipation level to the nonlinear damping characteristic compared to nonlinear stiffness characteristics was evident. The results in this chapter reveal the vibration suppression advantage of nonlinear suspension systems over the corresponding linear counterpart.

The key contribution of this study is the novel investigation of the Energy dissipation level of a designed vehicle suspension system using the OFRF method. This also involved a Hysteresis analysis of the vehicle suspension system based on the OFRF design. By employing the OFRF method, it was revealed that the energy dissipation level, for a designed vehicle suspension system, can be estimated. The effect of each nonlinear design parameter was also demonstrated. In addition, the energy dissipated as heat by the suspension system can be converted to a beneficial form of energy such as electricity. A suspension system, comprising a viscous damper and spring converts vibration energy to heat energy. However, employing an electromagnetic generator/damper in place of or alongside a mechanical viscous damper enables the conversion of some of the vibration energy to electrical energy.

This is known as vibration energy harvesting and this will be studied in following chapters.

Chapter 4: Analysis, design and optimisation of a vibration energy harvester with damping nonlinearity

4.1 INTRODUCTION

In the previous chapter, a vibration isolation system was designed as a vehicle suspension system. The mechanical energy injected into the system by the base-excitation force is majorly dissipated as heat energy by the vibration isolation elements. However, this mechanical energy can be converted to a beneficial form, which is electrical energy. The conversion of ambient vibration energy to electrical energy is known as vibration energy harvesting [114].

Energy harvesting from environmental vibration has recently received substantial consideration due to the rapid developments in technologies such as low-power wireless sensors, microelectromechanical systems (MEMS) etc. [33], [170]. It has been established that two major limitations exist for most of the vibration energy harvesters studied in the literature. The first and more considered limitation in literature is the operational bandwidth of a vibration energy harvester. Vibration energy harvesters are typically designed to operate at their natural frequencies. This implies excitation frequencies beyond the natural frequency reduces the efficiency of the harvester [124], [171]. The second limitation concerns the constrained physical enclosure of the vibration energy harvester which causes the suspended mass to oscillate within a specified span [172], [173]. Therefore, for best performance, the maximum excitation level is considered at the design stage. However, excitations below the maximum value reduces the effectiveness of the harvester. It has been shown recently in [134], that a nonlinear cubic electrical damping can be employed to extend the harvestable power of an energy harvester. It was established that such a nonlinear harvester outperformed one with an equivalent linear electrical damping. The results of the [134] indicates that at maximum excitation, the same relative displacement of the VEH system and hence average power, are provided by both linear and nonlinear VEH system. Nevertheless, at excitations below maximum level, the nonlinear VEH

system provided more energy compared to its linear counterpart. This assertion was corroborated in [135] which also demonstrated the effect of the harvester coil resistance on its harvestable power level. These studies have been conducted using the harmonic balance method.

In this chapter, the study focuses on the analysis and design of a vibration energy harvester (VEH) with nonlinear electrical damping. A mathematical model of the nonlinear VEH (VEH) system is developed and analysed for the first time, with the Output Frequency Response Function (OFRF) method recently proposed for frequency analysis of nonlinear systems. Performance metrics of the VEH system such as average power, are expressed in terms of the parameter of interest using the OFRF method. An optimisation process is then conducted to maximize the energy harvested by the VEH system. Results indicated an excellent match between numerical and analytical results. Finally, an electromechanical system is simulated, based on the design, to emulate a practical implementation of the VEH system.

A summary of the main contributions in this chapter is highlighted below:

- Analysis and design of a nonlinear vibration energy harvester using the OFRF method.
- Formulation of an electromechanical system based on the designed mechanical analogy and estimation of coil and nonlinear load resistances from the mechanical analogy.
- Investigation of the effect of nonlinear electrical cubic damping on the average power harvested by the VEH system.

Subsequent sections of the chapter are organized as follows: Section 4.2 describes the model formulation of the system to be considered; Section 4.3 demonstrates the analysis, design and optimisation of the system model; Section 4.4 presents the electromechanical implementation of the mechanical analogy of the system considered; Section 4.5 provides an estimation of the electrical parameters of the system; Section 4.6 summarises the chapter with some concluding remarks.

4.2 MODEL FORMULATION

In this work, a base excited single degree-of-freedom (SDOF) vibration energy harvester is considered as illustrated in Figure 4.1. The SDOF system is seen to have an oscillating mass, m , base-displacement $y(t)$, spring stiffness k_1 , the relative displacement between the oscillating mass and the support-base of the harvester $z(t) = x(t) - y(t)$, equivalent linear viscous damping coefficient c_1 and nonlinear cubic damping coefficient c_3 .

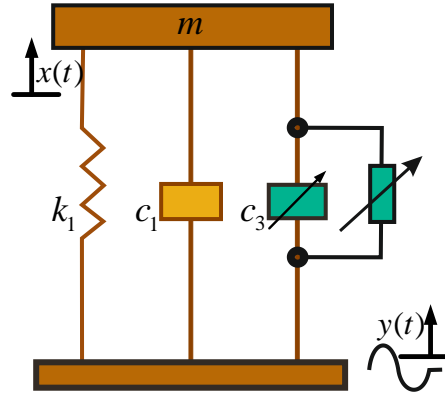


Figure 4.1: SDOF base-excited vibration energy harvester with a nonlinear damper.

The dynamic equation is therefore given as

$$m\ddot{z} + c_1\dot{z} + c_3\dot{z}^3 + k_1z = -m\ddot{y} \quad (4.1)$$

Supposing a harmonic base excitation $y(t)$ is assumed with magnitude, Y , frequency, ω and zero phase shift

$$y(t) = Y\sin(\omega t) \quad (4.2)$$

Then the dynamic equation of the SDOF VEH can be expressed as

$$m\ddot{z} + c_1\dot{z} + c_3\dot{z}^3 + k_1z = m\omega^2 Y\sin(\omega t) \quad (4.3)$$

The damping force due to the electromagnetic damper (EMD) is given as $f_{emd} = c_3\dot{z}^3$. The instantaneous power absorbed by the damping system, in watts, is the product of the instantaneous damping force exerted by the damping system and the relative velocity of the harvester system. Nonetheless, the average power of the damping system is then given by

$$P_{av} = \frac{1}{T} \int_0^T (c_1 \dot{z}) \cdot \dot{z} dt + \frac{1}{T} \int_0^T (c_3 \dot{z}^3) \cdot \dot{z} dt \quad (4.4)$$

Considering a general mono-frequency oscillation, Eq. (4.4) becomes

$$\begin{aligned} P_{av} &= P_{av|c_1} + P_{av|c_3} \\ &= \frac{1}{2} c_1 \omega^2 Z^2 + \frac{3}{8} c_3 \omega^4 Z^4 \end{aligned} \quad (4.5)$$

It should be noted that the first term of Eq. (4.5) is regarded as a loss based on the dissipative power of parasitic damping [137]. This form of damping arises due to the various mechanical losses present. Examples of such losses include, inherent structural damping heat dissipation, friction loss, iron loss etc. For such losses, c_1 is the equivalent viscous damping coefficient for the parasitic damping [139]. The second term of Eq. (4.5) provides harvestable power. Moreover, the cubic damping characteristics of Eq. (4.4) arises due to the nonlinear resistive load characteristics of the practical VEH system.

Furthermore, in practical VEH systems, the relative displacement of the oscillating mass is restricted by the physical enclosure of the system. This, subsequently, implies that the magnitude of the relative displacement is constrained to a certain maximum value, Z_{max} . This physical constraint however limits the maximum harvestable power as it is seen in Eq. (4.5) that the power harvested is a function of Z , and also, Z is a function of the excitation frequency, ω [112]. Therefore, it is important that the damping parameter, c_3 , to be designed, should be able to restrain the oscillations of the suspended mass within a tolerable span as constrained by the enclosing case. However, it should also be able to maximise the energy harvested.

To facilitate the optimal design process, the average maximum excitation level of the environment where the VEH system is to be installed, should be known. The span limit of the suspended mass should also be known. The maximum excitation level of an environment is measured by computing the mean of past vibration measurements collected over time. In this study, the design objective is to maximise the harvestable power

$$P_{av|c_3} = \frac{3}{8} c_3 \omega^4 Z^4 \quad (4.6)$$

The OFRF based approach will be utilised, in this work, for the analysis of the dynamic model of the VEH system (4.3). The parameter of interest, c_3 , will also be designed and optimised to ensure the realization of the maximum harvestable power, subject to existing constraints. The benefit of the OFRF is that the method can provide an explicit analytical relationship between the design objective, $P_{av|c_3}$ and system parameter of interest, c_3 . This can significantly simplify the system design and optimisation. The performance metrics sought in this work are the relative displacement, Z and harvestable power, $P_{av|c_3}$.

In section 4.3, the OFRF representations of the output response, Z and average harvestable power, $P_{av|c_3}$ of the VEH system, will be derived in terms of the parameter of interest, c_3 .

4.3 SYSTEM ANALYSIS, DESIGN AND OPTIMISATION

This section deals with the analytical study of the VEH system described by Eq. (4.3) using the OFRF method. The design of an optimum nonlinear cubic damping parameter that enables the VEH system to harvest the maximum energy available, subject to existing constraints, is also described. Firstly, the OFRF representations of the output response of system (4.3), $Z(j\omega)$ and harvestable power of Eq. (4.5), $P_{av|c_3}$ are determined in terms of the design parameter, c_3 . The subsequent analysis and simulations have been performed using the following model parameters, $m = 1\text{kg}$, $c_1 = 0.35\text{ N.s.m}^{-1}$, $k_1 = 4\pi^2\text{ N.m}^{-1}$, $Y_{\max} = 0.4\text{m}$ [134]. It is observed that system (4.3) belongs to the class of the Volterra system of Eq. (2.4) in subsection 2.4.3 of Chapter 2, with $M = 3$ and $L = 2$. The system parameters are identified as $c_{1,0}(2) = m$, $c_{1,0}(1) = c_1$, $c_{3,0}(111) = c_3$, $c_{1,0}(0) = k$, and $c_{0,1}(0) = -m\omega^2 Y$ while other parameters are zero. To derive the OFRF representation of system (4.3), the OFRF structure \mathfrak{M} and frequency function vector $\Theta(j\omega)$ are derived first.

4.3.1 Determination of the OFRF

To determine the OFRF representation, the systematic procedure outlined in subsection 2.4.3 of Chapter 2, is applied. Applying the algorithm for obtaining the

OFRF structure (monomials), \mathfrak{M} (see subsection 2.4.3 of Chapter 2) to system (4.3) up to the 11th-order i.e. $N = 23$, yields the following monomials;

$$\mathfrak{M} = \bigcup_{n=1}^{23} M_n = [1, c_3, c_3^2, c_3^3, \dots, c_3^9, c_3^{10}, c_3^{11}] \quad (4.7)$$

Twenty-one different values of c_3 are chosen for training dataset. The range of c_3 values used as the training dataset is $c_3 \in [0, 0.01]$. While exciting the system using the same input, each value of c_3 is used to compute a time domain output response $z(t)$ of system (4.3). The corresponding Fast Fourier Transform for each time domain response is obtained at the frequency of interest (the resonant frequency, ω_r). The OFRF coefficient $\Theta(j\omega)$ is then obtained using the least squares' algorithm, as in [31], thus;

$$\Theta(j\omega) = \begin{bmatrix} \theta_0(j\omega) \\ \theta_1(j\omega) \\ \vdots \\ \theta_{10}(j\omega) \\ \theta_{11}(j\omega) \end{bmatrix} = \Lambda^T \Lambda^{-1} \Lambda^T \cdot \begin{bmatrix} Z(j\omega)|_{c_3(1)} \\ Z(j\omega)|_{c_3(2)} \\ \vdots \\ Z(j\omega)|_{c_3(20)} \\ Z(j\omega)|_{c_3(21)} \end{bmatrix} \quad (4.8)$$

where

$$\Lambda = \begin{bmatrix} 1 & c_3(1) & \dots & c_3^{11}(1) \\ 1 & c_3(2) & \dots & c_3^{11}(2) \\ \vdots & \vdots & \ddots & \vdots \\ 1 & c_3(21) & \dots & c_3^{11}(21) \end{bmatrix} \quad (4.9)$$

and $Z(j\omega)|_{c_3(i)}$ represents the output spectrum of the system when $c_3 = c_3(i)$.

Therefore, the OFRF of system (4.3) derived is given as

$$Z(j\omega) = \theta_0(j\omega) + \theta_1(j\omega)c_3 + \theta_1(j\omega)c_3^2 + \dots + \theta_{10}(j\omega)c_3^{10} + \theta_{11}(j\omega)c_3^{11} \quad (4.10)$$

The OFRF representation of system (4.3) at resonance ($\omega = \omega_r$), since the maximum response of the VEH is reached at this frequency, is given as

$$\begin{aligned}
Z(j\omega|_{\omega=\omega_r}) = & (-5.1797 + 2.8125i) + (5.6215 \times 10^3 - 4.3256 \times 10^3 i)c_3 \\
& (-3.668 \times 10^6 - 7.162 \times 10^6 i)c_3^2 + (3.138 \times 10^9 + 6.151 \times 10^9 i)c_3^3 \\
& (-1.691 \times 10^{12} - 3.327 \times 10^{12} i)c_3^4 + (5.965 \times 10^{14} + 1.176 \times 10^{15} i)c_3^5 \\
& (-1.408 \times 10^{17} - 2.781 \times 10^{17} i)c_3^6 + (2.241 \times 10^{19} + 4.428 \times 10^{19} i)c_3^7 \\
& (-2.369 \times 10^{21} - 4.684 \times 10^{21} i)c_3^8 + (1.594 \times 10^{23} + 3.152 \times 10^{23} i)c_3^9 \\
& (-6.173 \times 10^{24} - 1.221 \times 10^{25} i)c_3^{10} + (1.047 \times 10^{26} + 2.073 \times 10^{26} i)c_3^{11}
\end{aligned} \tag{4.11}$$

The output frequency response, Z is a function of ω and c_3 as seen in Eq. (4.10) therefore can be written as $Z(j\omega; c_3)$. It should be noted that the objective here is to design c_3 that provides the maximum power harvested by the VEH with respect to existing constraint. It is observed in Eq. (4.6) that the average power harvested is also a function of the output response, Z . However, a further expression can be derived to obtain the squared and fourth powered magnitudes of the OFRF of the system output response i.e. $|Z(j\omega; c_3)|^2$ and $|Z(j\omega; c_3)|^4$. This is computed using the algorithm derived in [85] thus

$$\begin{aligned}
|Z(j\omega; c_3)|^2 &= \theta_0 \theta_0^* + \sum_{\ell=1}^{11} \left(c_3^\ell \sum_{ii=0}^{\ell} \theta_{ii} \theta_{\ell-1} \right) \\
&:= \sum_{ii=0}^{22} c_3^{ii} \rho_{ii}
\end{aligned} \tag{4.12}$$

where ρ_{ii} are coefficients of the OFRF representation of $|Z(j\omega; c_3)|^2$

The same algorithm in (4.12) is employed further to obtain

$$|Z(j\omega; c_3)|^4 = \sum_{ii=0}^{44} c_3^{ii} \psi_{ii} \tag{4.13}$$

where ψ_{ii} are coefficients of the OFRF representation of $|Z(j\omega; c_3)|^4$

Substituting Eq. (4.13) into Eq. (4.6), the OFRF of the average harvestable power becomes

$$P_{av|c_3} = \frac{3}{8} c_3 \omega^4 |Z(j\omega; c_3)|^4 \tag{4.14}$$

The OFRF is a polynomial representation of the system performance. A comparison of the OFRF results with that obtained using the Runge-Kutta 4 algorithm (ODE45 in MATLAB) over the system parameter value outside the OFRF training set (in this case, $c_3 = 0.0101 \text{N.s}^3.\text{m}^{-3}$) is shown in Figure 4.2. This indicates that the OFRF provides a very good representation for the actual system performance.

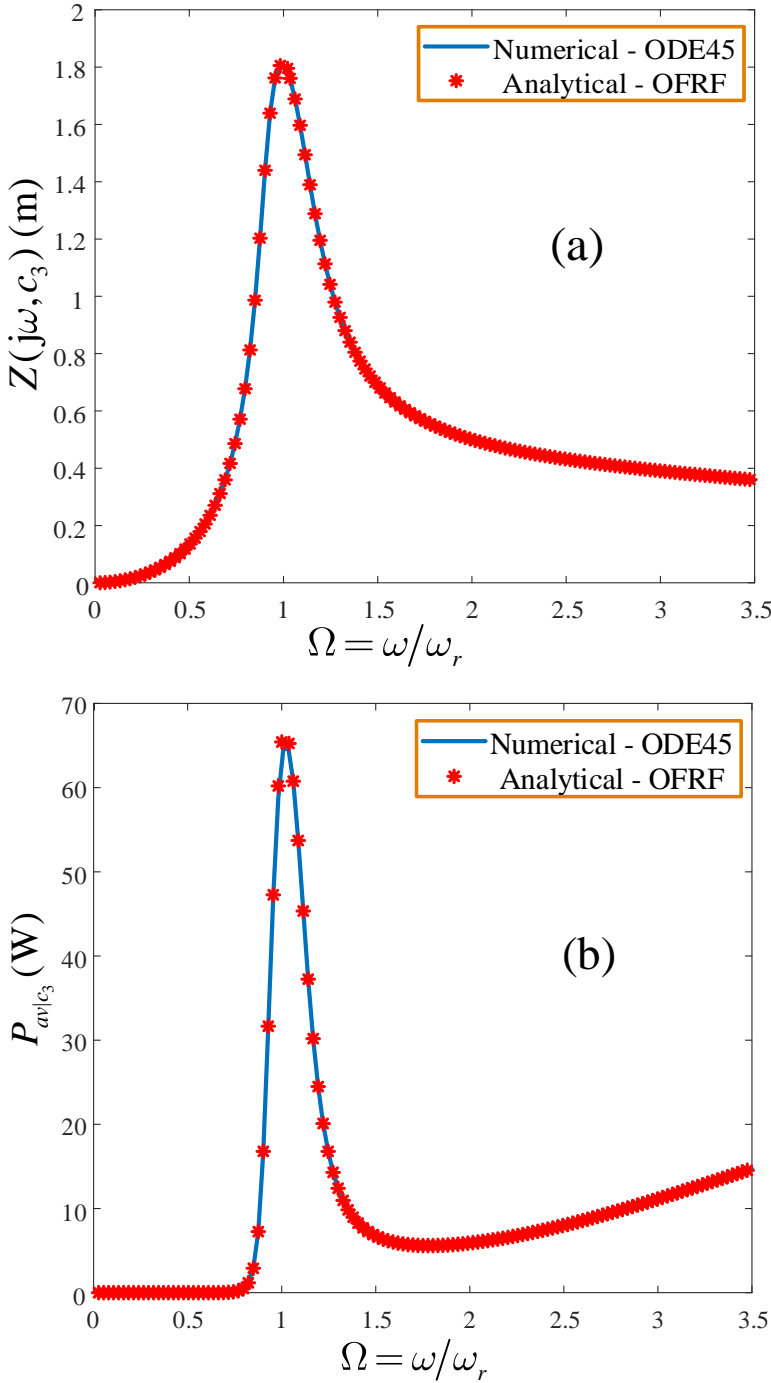


Figure 4.2: Comparison between OFRF analytical and Runge-Kutta numerical solution: a) relative mass displacement, b) Average power.

4.3.2 Optimisation of an unconstrained VEH system

It should be noted that in the absence of a mass displacement constraint in the VEH system, the optimal value of c_3 required to maximise the energy harvested, $P_{av|c_3}$ can be obtained by evaluating the zero of the derivative of (4.14). This gives

$$\frac{dP_{av|c_3}}{dc_3} = 0 \quad (4.15)$$

Though there are several solutions to Eq. (4.15), the minimum, non-negative real solution is selected which is evaluated as $c_3^{\text{opt1}} = 0.0015 \text{ N.s}^3.\text{m}^{-3}$. This value can be substituted into Eqs. (4.11) and (4.14) to obtain the corresponding mass displacement $|Z(j\omega_r; c_3)| = 3.035 \text{ m}$ and average harvestable power $P_{av|c_3, \text{max1}} = 76.68 \text{ W}$ of the VEH system considering no constraints. However, practical VEH systems are constrained in their relative displacement, Z hence posing a constrained optimisation problem.

4.3.3 Optimisation of a constrained VEH system

From the OFRF representations for the average harvestable power and the output frequency response obtained in subsection 4.3.1, the optimisation problem for the nonlinear parameter, c_3 , subject to a constraint, can be formulated as;

$$\begin{aligned} \max_{c_3} \quad & P_{av|c_3}(\omega_r, c_3) \\ \text{s.t.} \quad & \begin{cases} |Z(j\omega_r; c_3)| - Z_{\text{max}} \leq 0 \\ c_3 - 1 \times 10^{-2} \leq 0 \end{cases} \end{aligned} \quad (4.16)$$

where $\omega_r = 6.3 \text{ rad.s}^{-1}$, $Z_{\text{max}} = 2.5 \text{ m}$ is the maximum relative displacement of the VEH system and the design parameter, $c_3 \in [0, 0.01]$. The optimisation problem in Eq. (4.16) is solved using the MATLAB *fmincon* function. The optimal cubic damping is obtained as $c_3^{\text{opt2}} = 0.0032 \text{ N.s}^3.\text{m}^{-3}$. Substituting this value into Eqs. (4.11) and (4.14) yields $|Z(j\omega_r)| = 2.500 \text{ m}$ and $P_{av} = 75.07 \text{ W}$. To demonstrate the effectiveness of the OFRF method, the optimal damping solution, c_3^{opt2} is substituted into system (4.3) and Eq. (4.6) which yields an output spectrum and corresponding average power as $|Z(j\omega_r)| = 2.501 \text{ m}$ and $P_{av} = 74.98 \text{ W}$ respectively.

Table 4.1: Maximum average harvestable power attainable at $\omega = 6.3 \text{ rad s}^{-1}$ ($\Omega = 1$) subject to the system constraint, $Z_{\max} = 2.5 \text{ m}$

Constraint present?	Mass displacement of VEH system, Z (m)	Max. average harvestable Power, $P_{av c_3 \max}$ (W)	Nonlinear damping, $c_3^{\text{opt}} (\text{Ns}^3 \text{m}^{-3}) \times 10^{-3}$
No	3.035	76.68	1.5
Yes	2.500	75.07	3.2

Table 4.1 shows the maximum average power harvestable by the VEH system, while considering both the absence and presence of the VEH mass displacement constraint. It is observed that the maximum average harvestable power of the VEH system, considering the relative mass displacement constraint of the VEH system, $Z = 2.500 \text{ m}$, is determined as $P_{av|c_3 \max 2} = 75.07 \text{ W}$ for $c_3^{\text{opt}2} = 0.0032 \text{ N.s}^3 \text{.m}^{-3}$. This implies, the optimal damping force of the EMD, f_{emd}^* required to extract the maximum average power, $P_{av|c_3 \max 2}$ is given as

$$f_{emd}^* = c_3^{\text{opt}2} \dot{z}^3 \quad (4.17)$$

Figure 4.3 and Figure 4.4 show the effects of a nonlinear cubic damping characteristics on the relative displacement, Z and average power, $P_{av|c_3}$ of the VEH system respectively. These graphs were obtained with respect to a variation of nonlinear cubic damping, $c_3 \in [0, 0.01] \text{ N.m}^{-3} \text{.s}^3$ at the resonant frequency, $\omega = \omega_r$. In Figure 4.3, it is observed that Z decreases monotonically as c_3 increases. There exists an inverse relationship between both parameters. That is, Z decreases as c_3 increases and vice versa. However, in Eq. (4.6), it is observed that the average harvestable power is a function of both parameters (Z and c_3). Therefore, since $P_{av|c_3}$ is a function of Z and c_3 , it is obvious that $P_{av|c_3}$ becomes zero if either of these parameters is zero. This implies

If $c_3 \rightarrow \infty$, then $Z \rightarrow 0$, hence, $P_{av|c_3} \rightarrow 0$

If $c_3 \rightarrow 0$, then $Z \rightarrow \infty$, hence, $P_{av|c_3} \rightarrow 0$

Therefore, as revealed in Figure 4.4, an optimal value of the nonlinear damping parameter needs to be designed in order to determine the maximum average harvestable power subject to any existing constraint.

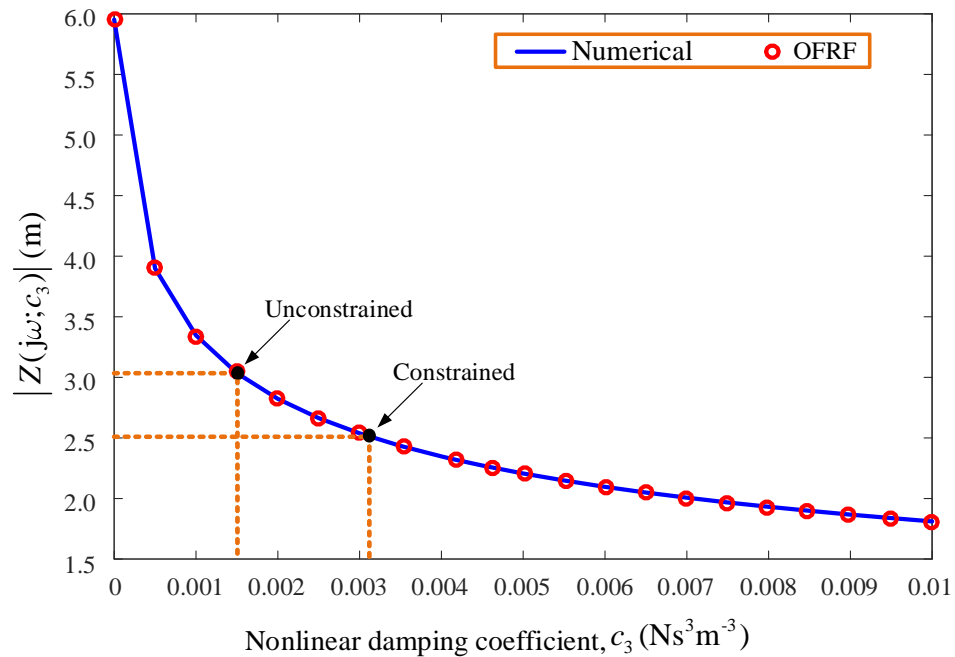


Figure 4.3: Comparison of the output frequency response of system (4.3) determined using analytical (OFRF) method and numerical simulations.

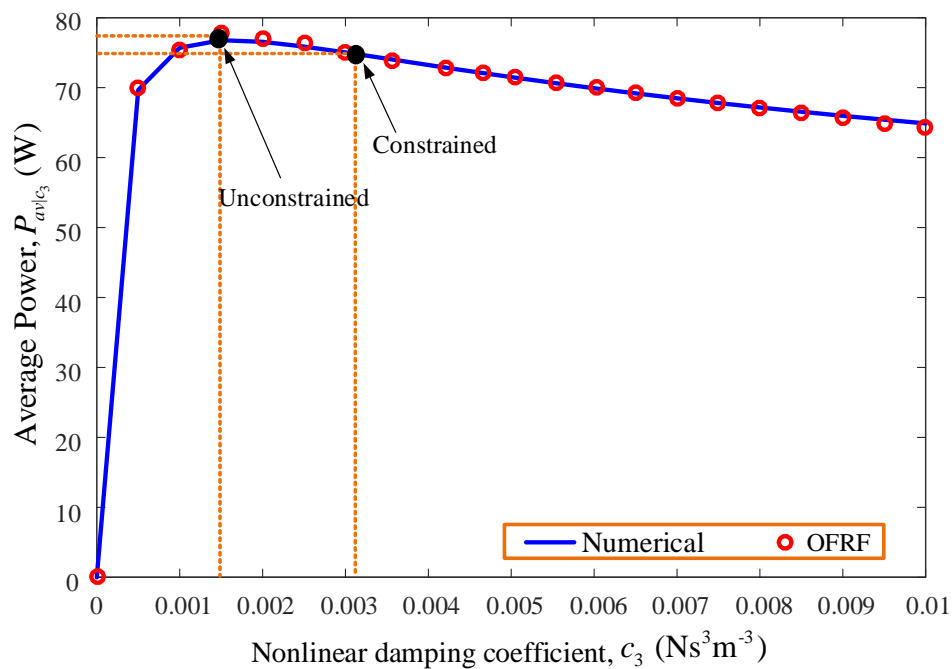


Figure 4.4: Comparison of the average power of the VEH system of Eq. (4.6) determined using analytical (OFRF) method and numerical simulations.

Figure 4.5 represents the (a) time history and (b) output frequency response curves of the relative mass displacement of the VEH obtained for the designed c_3 subject to unconstrained and constrained conditions. Similarly, in Figure 4.6, the corresponding average harvestable power obtained for the designed c_3 under the same conditions, as in Figure 4.5, is shown.

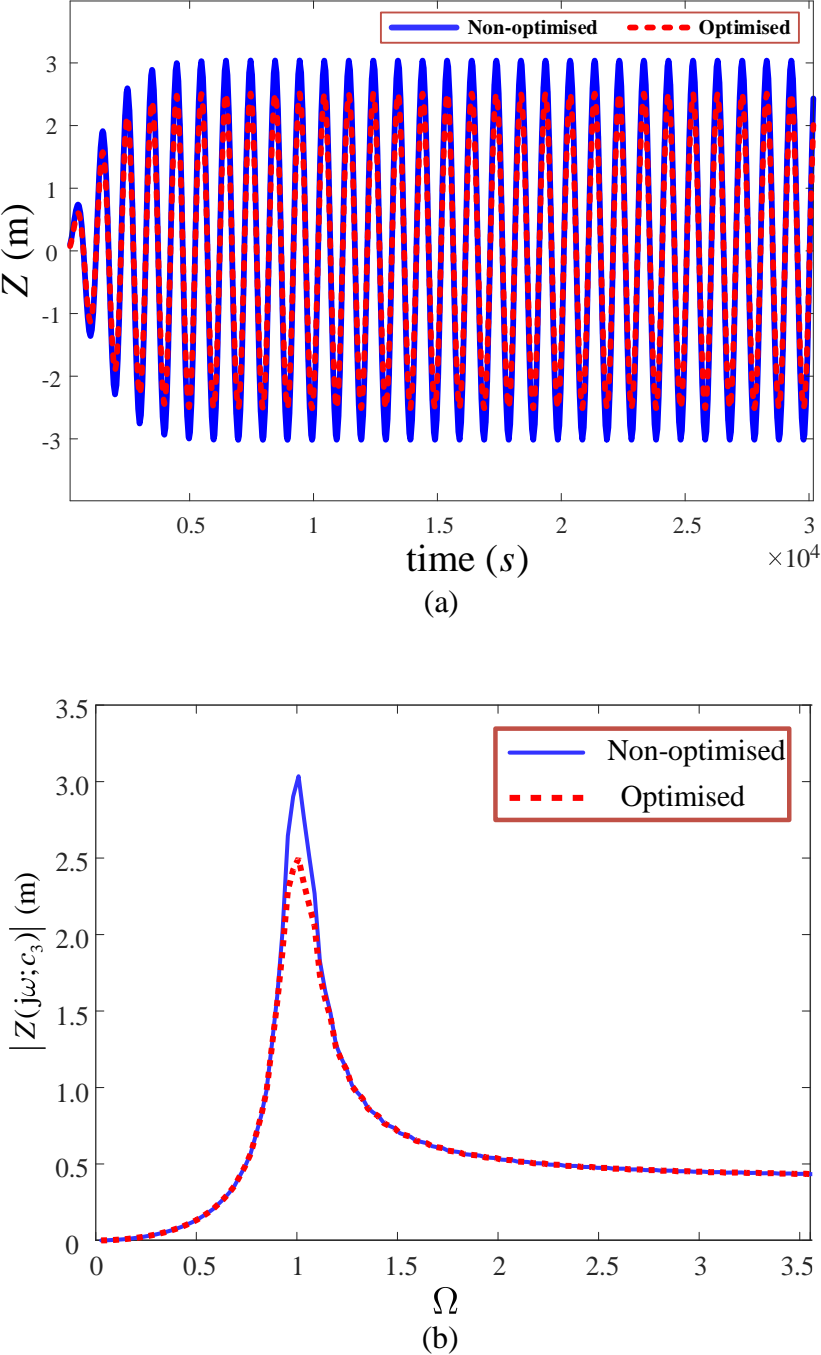


Figure 4.5: Comparison of the system performances under the non-optimised and optimised cases. (a) time history and (b) Output response curves for the relative displacement of the VEH system.

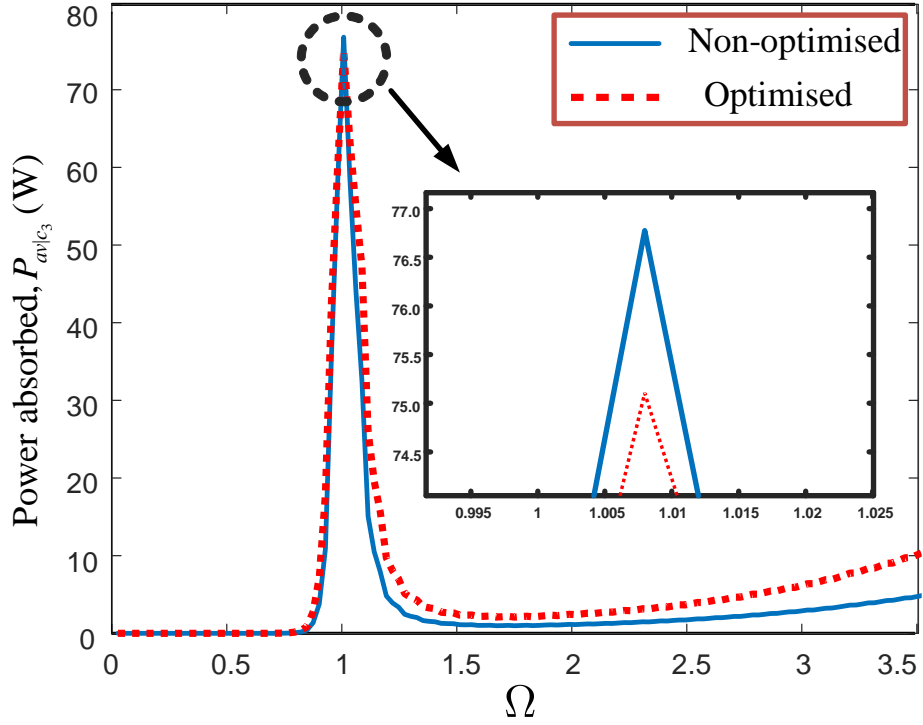


Figure 4.6: Comparison of the average harvestable power obtained under the non-optimised and optimised cases.

In Figure 4.7 and its corresponding top view in Figure 4.8, it is observed that there is an optimal nonlinear damping parameter, c_3^{opt1} and normalised excitation frequency, Ω , at which the maximum average power, $P_{av|c_3 \text{ max1}}$ is attained, considering no constraint. The global maximum average power, $P_{av|c_3 \text{ max1}} = 76.68\text{W}$ when $c_3^{\text{opt1}} = 0.0015 \text{ N.s}^3.\text{m}^{-3}$ at $\Omega = 1$. It is also apparent that the average power, $P_{av|c_3}$ decreases rapidly with the decrease in c_3 when the actual damping coefficient is lesser than c_3^{opt1} . Additionally, $P_{av|c_3}$ decreases steadily with the increase in c_3 when the actual damping coefficient is greater than c_3^{opt1} . This implies that the average power is more sensitive to c_3 when it is less than c_3^{opt1} , and less sensitive to c_3 when it is greater than c_3^{opt1} . Considering these observations, it is recommended that a damping parameter greater than the optimal damping parameter is preferable if the optimal damping parameter is difficult to implement practically.

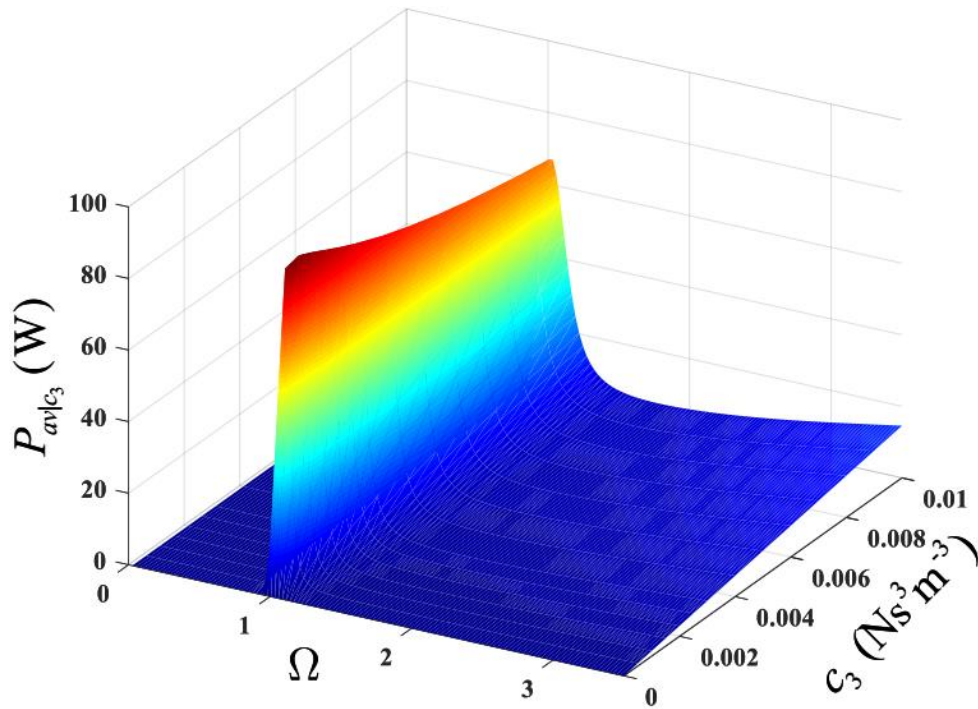


Figure 4.7: Average harvestable power obtained at different excitation frequencies, $\Omega = \omega/\omega_r$, and nonlinear damping parameter values, c_3 .

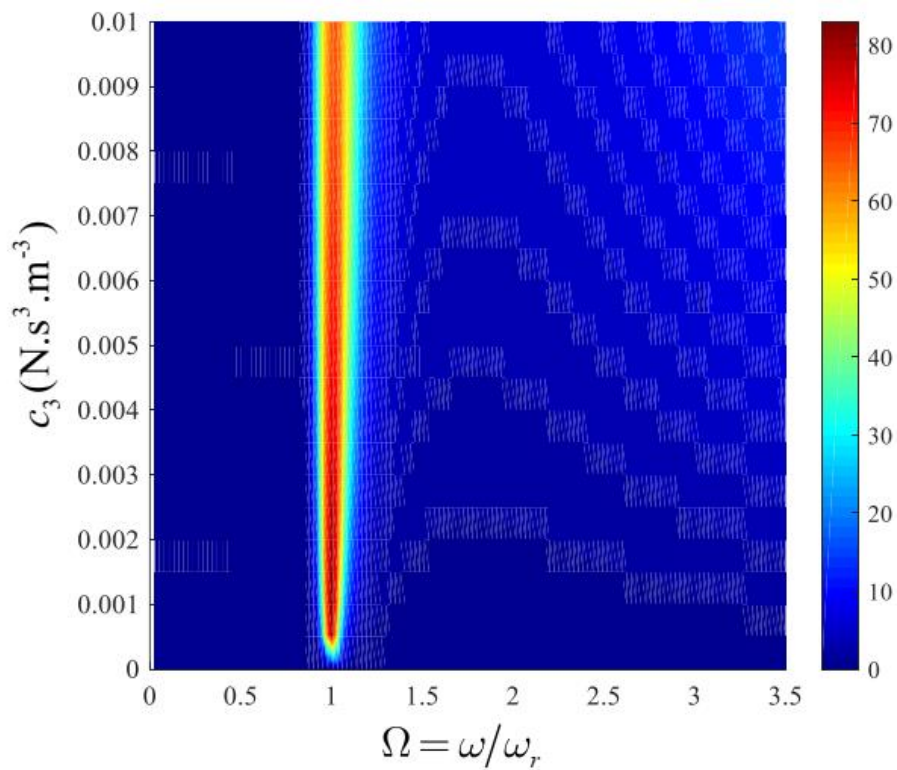


Figure 4.8: Contour plot for the average harvestable power obtained at different excitation frequencies, $\Omega = \omega/\omega_r$, and nonlinear damping parameter values, c_3 .

In the next section, the electromechanical coupling of the VEH system based on the designed optimal nonlinear damping parameter, $c_3^{\text{opt}2}$ and the desired nonlinear damping force, f_{emd}^* , will be discussed.

4.4 ELECTROMECHANICAL COUPLING OF THE NONLINEAR VIBRATION ENERGY HARVESTER

In the implementation process, the VEH uses an electromagnetic transducer i.e. EM damper (EMD), with an internal coil resistance R_c to couple the electrical subsystem to the mechanical subsystem. A schematic representation of the electromechanically coupled system is shown in Figure 4.9.

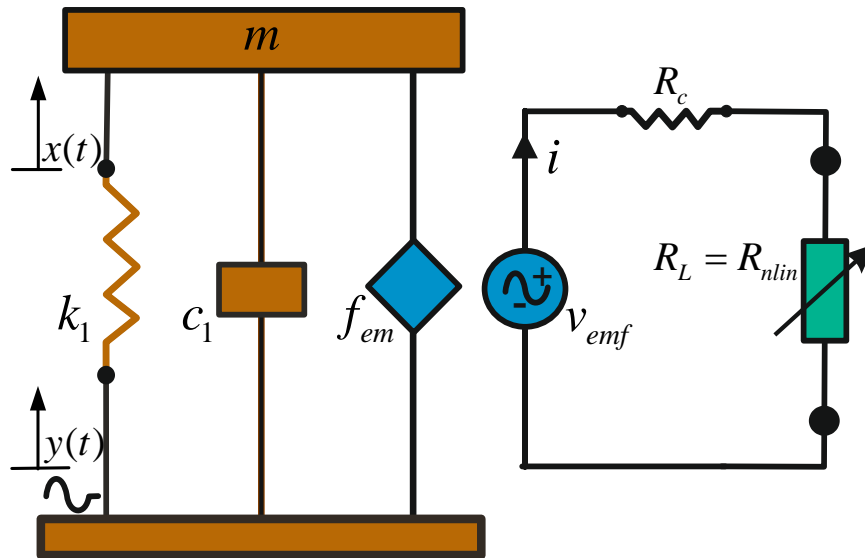


Figure 4.9: Schematic representation of a vibration-based energy harvester with a nonlinear resistive load.

Under base input excitation, a voltage known as the back emf v_{emf} is generated across the coil in the EMD which is, according to Faraday's law of induction, proportional to the velocity of the EMD. The induced voltage (or open circuit voltage) is given by

$$v_{emf} = \kappa \dot{z} \quad (4.18)$$

where κ is the coupling coefficient which is dependent on the geometric and magnetic properties of the EMD [112]. Connecting a shunt load resistance R_L across the circuit causes the back emf to drive a current i along the circuit. The flow of current causes a force f_{em} , known as electromotive force, which is proportional to the current, to be redirected back into the mechanical subsystem. This force opposes the direction of motion of the subsystem and can be expressed as

$$f_{em} = -\kappa i \quad (4.19)$$

If the shunt load resistance of the VEH system is linear, i.e. $R_L = R_{lin}$, this implies

$$v_{emf} = v_c + v_{lin} = iR_c + iR_{lin} \quad (4.20)$$

and the current flowing in the electrical subsystem is given by

$$i = \frac{v_{emf}}{R_c + R_{lin}} = \frac{\kappa \dot{z}}{R_c + R_{lin}} \quad (4.21)$$

Therefore, the linear electromotive force is expressed as

$$f_{em} = \kappa i = \frac{\kappa^2}{R_c + R_{lin}} \dot{z} \quad (4.22)$$

However, in this study, a nonlinear damping parameter, c_3^{opt2} is designed and which yields the desired nonlinear damping force, f_{emd}^* . This suggests that a nonlinear shunt load resistance is required, i.e. $R_L = R_{nlin}$. This is because the characteristics of the load resistance, R_L , determines the characteristics of the electrical damping force.

To implement the nonlinear cubic damping force characteristics, the current flowing through the nonlinear load should be proportional to the cube of the voltage across it [135]. This implies, $v^3 \propto i$, then applying Kirchhoff's voltage law, the total induced voltage becomes

$$v_{emf} = v_c + v_{nlin} = iR_c + (iR_{nlin})^{\frac{1}{3}} \quad (4.23)$$

Then the current in the electrical circuit becomes

$$\begin{aligned}
i = & \frac{1}{6} \frac{12^{1/3} \left(R_{nlin} R_c^2 \left(-9v_{emf} + \sqrt{3} \sqrt{\frac{4R_{nlin} + 27R_c v_{emf}^2}{R_c}} \right) \right)^{1/3}}{R_c^2} \\
& - \frac{1}{6} \frac{12^{2/3} R_{nlin}}{R_c \left(R_{nlin} R_c^2 \left(-9v_{emf} + \sqrt{3} \sqrt{\frac{4R_{nlin} + 27R_c v_{emf}^2}{R_c}} \right) \right)^{1/3}} \\
& + \frac{v_{emf}}{R_c}
\end{aligned} \tag{4.24}$$

Substituting (4.24) into (4.19), the electromotive force, f_{em} becomes

$$\begin{aligned}
f_{em} = & \frac{12^{1/3} \kappa \left(R_{nlin} R_c^2 \left(-9(\kappa \dot{z}) + \sqrt{3} \sqrt{\frac{4R_{nlin} + 27R_c (\kappa \dot{z})^2}{R_c}} \right) \right)^{1/3}}{6R_c^2} \\
& - \frac{12^{2/3} \kappa R_{nlin}}{6R_c \left(R_{nlin} R_c^2 \left(-9(\kappa \dot{z}) + \sqrt{3} \sqrt{\frac{4R_{nlin} + 27R_c (\kappa \dot{z})^2}{R_c}} \right) \right)^{1/3}} \\
& + \frac{\kappa^2 \dot{z}}{R_c}
\end{aligned} \tag{4.25}$$

The objective here is to estimate the coil and nonlinear load resistances, R_c and R_{nlin} required by the VEH system to generate an electrical damping force, f_{em} with the same nonlinear characteristics as the desired damping force (f_{emd}^*) in Eq. (4.17). This is achieved with the nonlinear characteristics of the force-velocity profile of the desired damping force at the frequency of interest and using the same system input. This poses an optimisation problem as the values of R_c and R_{nlin} that minimizes the error $\sum [f_{emd}^*(\dot{z}, \omega_r, c_3^{opt2}) - f_{em}(\dot{z}, \omega_r, \kappa, R_c, R_{nlin})]^2$ is required to be estimated. These estimates can be obtained using the genetic algorithm optimisation method and for the parameters, $\kappa = 3.2 \text{V.s.m}^{-1}$ and $\omega_r = 6.3 \text{rad.s}^{-1}$. In the next section, the optimisation problem is solved and discussed.

4.5 PARAMETER ESTIMATION OF COIL AND LOAD RESISTANCES OF THE NONLINEAR VEH SYSTEM

To determine the estimates of the coil and nonlinear load resistances of the VEH, the genetic algorithm (GA) optimisation method is employed. The GA optimisation algorithm, which is based on natural selection, is chosen due to its ability to solve optimisation problems in which the objective function is strongly nonlinear and nondifferentiable which applies in this case. The optimisation problem can be formulated as

$$\arg \min_{R_c, R_{nlin} \in \mathbb{R}} \sum \left[f_{emd}^*(\dot{z}, \omega_r, c_3^{opt2}) - f_{em}(\dot{z}, \omega_r, \kappa, R_c, R_{nlin}) \right]^2 \quad (4.26)$$

Equation (4.26) is evaluated using the genetic algorithm (*ga*) MATLAB function available in the MATLAB Global Optimisation toolbox. The estimates determined for the coil and nonlinear load resistances are $R_c = 0.434\Omega$ and $R_{nlin} = 2.995 \times 10^4\Omega$ with $\kappa = 3.2\text{Vsm}^{-1}$ and $\omega_r = 6.3\text{rad.s}^{-1}$. Figure 4.10 presents a comparison between the force-velocity characteristics of the desired and the estimated damping force.

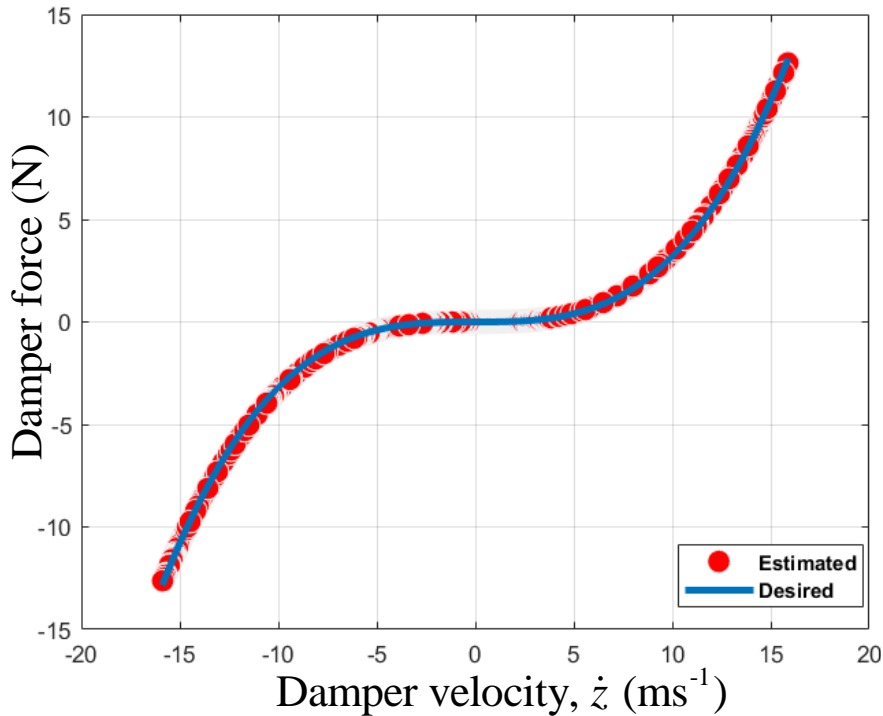


Figure 4.10: Comparison between the force-velocity characteristics for the desired damping force and estimated electrical damping force, respectively.

The estimated values of the coil and nonlinear load resistances are substituted in Eq. (4.25) to determine the electrical damping force, f_{em} . The same values of the mechanical parameters, used during the design process, are also used here. A Simulink electromechanical implementation of the practical VEH system is presented in Figure 4.11 using the estimated coil and nonlinear load resistances.

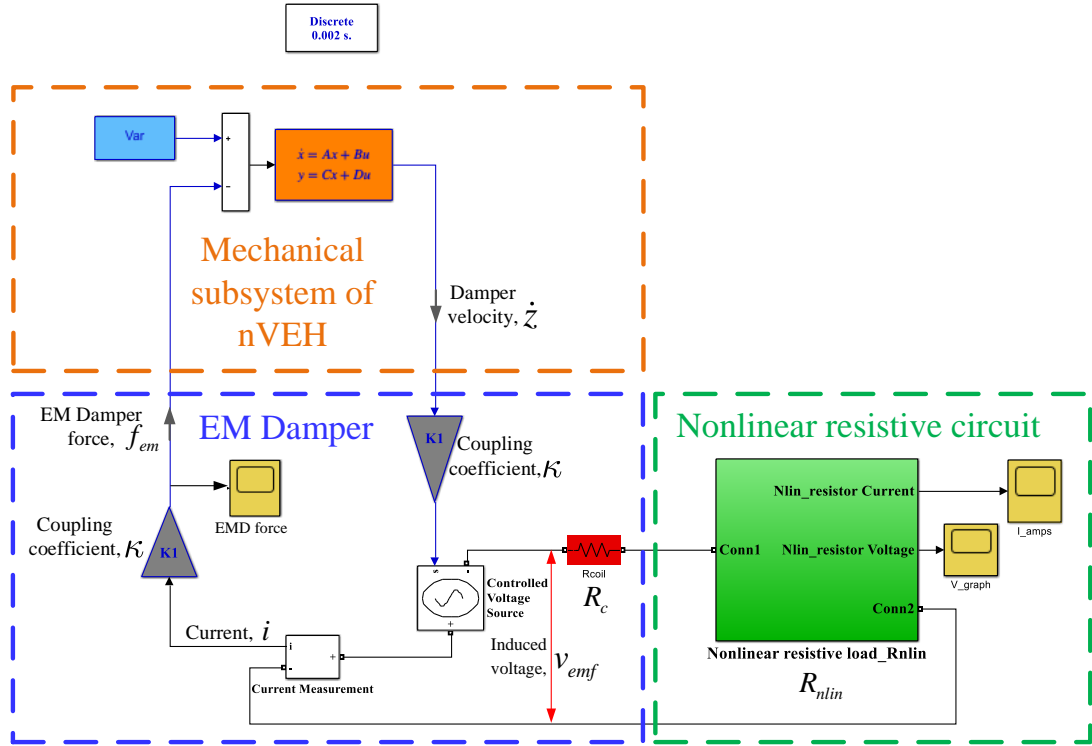


Figure 4.11: Simulink implementation of the VEH system.

The actual electrical damping force was measured out through the ‘EMD force’ scope as seen in the ‘EM Damper’ section of Figure 4.11. A comparison is provided in Figure 4.12, between the time histories of the desired EM damping force, f_{emd}^* and the actual electrical damping force, f_{em} at the resonant frequency. It is observed that there is a good match between the desired and the actual EM damping force.

To determine the equivalent linear load resistance (i.e. when $R_L = R_{lin}$ in Figure 4.9) which causes the same mass displacement of the VEH as the nonlinear load resistance, R_{nlin} at maximum excitation, the equivalent linear damping coefficient, c_{eq} is first determined. This is accomplished using the relationship

$$c_{eq} = \frac{3}{4} c_3 \omega_r^2 Z_{\max}^2 \quad (4.27)$$

where $Z_{\max} = 2.5 \text{ m}$, $c_3 = 0.0032 \text{ N.s}^3.\text{m}^{-3}$ and $\omega_r = 2\pi \text{ rad.s}^{-1}$

The equivalent linear damping coefficient obtained from Eq. (4.27) can be employed as the electrical damping coefficient in the mechanical domain of the VEH system. This implies that it can be used to determine the corresponding linear load resistance, R_{lin} which causes the same mass displacement of the VEH system as the nonlinear load resistance, R_{nlin} thus

$$c_{eq} = \frac{\kappa^2}{R_c + R_{lin}} \quad (4.28)$$

where $\kappa = 3.2 \text{ V.s.m}^{-1}$ and $R_c = 0.434 \Omega$.

With Eq. (4.28), the linear load resistance is determined as $R_{lin} = 16.01 \Omega$. The electromechanical model presented in Figure 4.11 is subsequently used to obtain the output spectrum, Z and corresponding average power, P_{av} of the VEH system. This is initially performed at maximum excitation, Y_{\max} for both linear (where $R_L = R_{lin}$) and nonlinear (where $R_L = R_{nlin}$) load resistances. Then the same process is performed at an excitation level below the maximum e.g. $0.1Y_{\max}$.

It is observed that both the linear and nonlinear load resistances produce the same relative displacement span, Z and average power, P_{av} at maximum excitation, Y_{\max} as shown in Figure 4.13 and Figure 4.14 respectively. Nonetheless, at excitations below the maximum level such as $0.1Y_{\max}$, the nonlinear load resistance delivers a significantly greater relative displacement span, and therefore produce more harvestable power compared to its linear equivalent. These are demonstrated in Figure 4.15 and Figure 4.16 respectively.

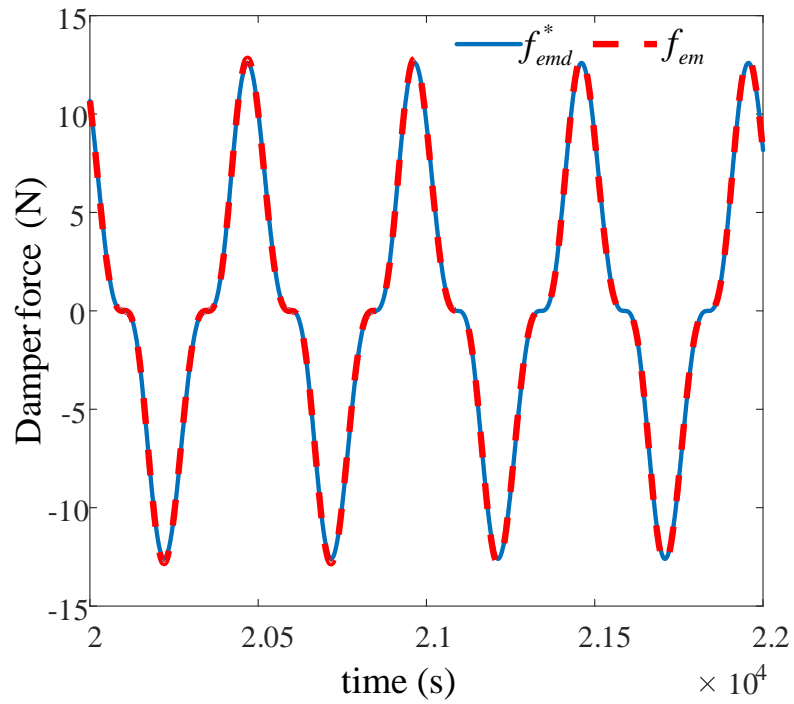


Figure 4.12: Comparison between the time histories of the desired damping force (blue solid) and the actual electrical damping force (red dash).

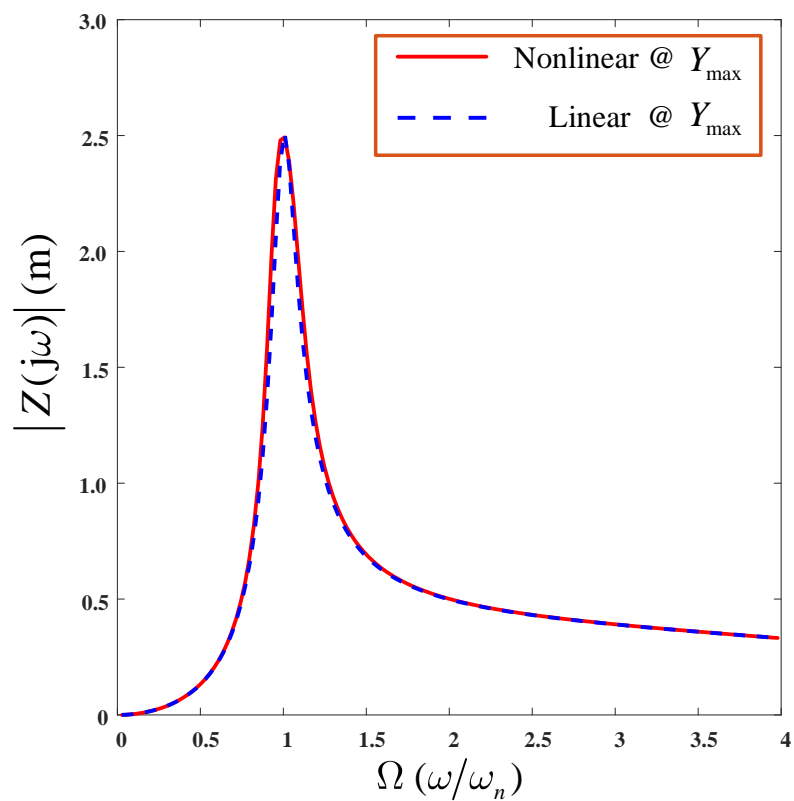


Figure 4.13: Relative displacement for the linear and nonlinear VEH systems at maximum excitation, Y_{max} .

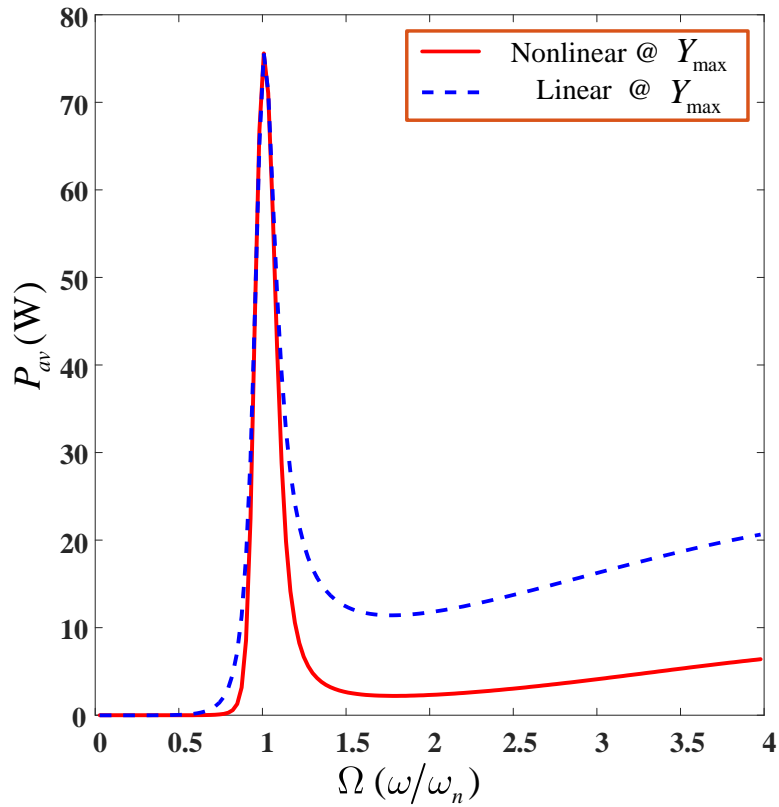


Figure 4.14: Average power for the linear and nonlinear VEH systems at maximum excitation, Y_{\max} .

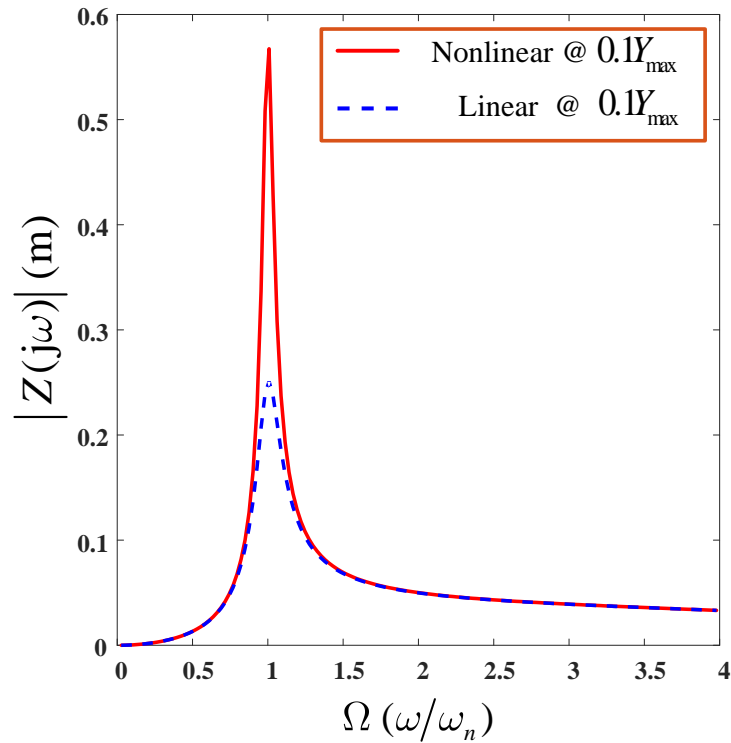


Figure 4.15: Relative displacement for the linear and nonlinear VEH systems at an excitation of $0.1Y_{\max}$.

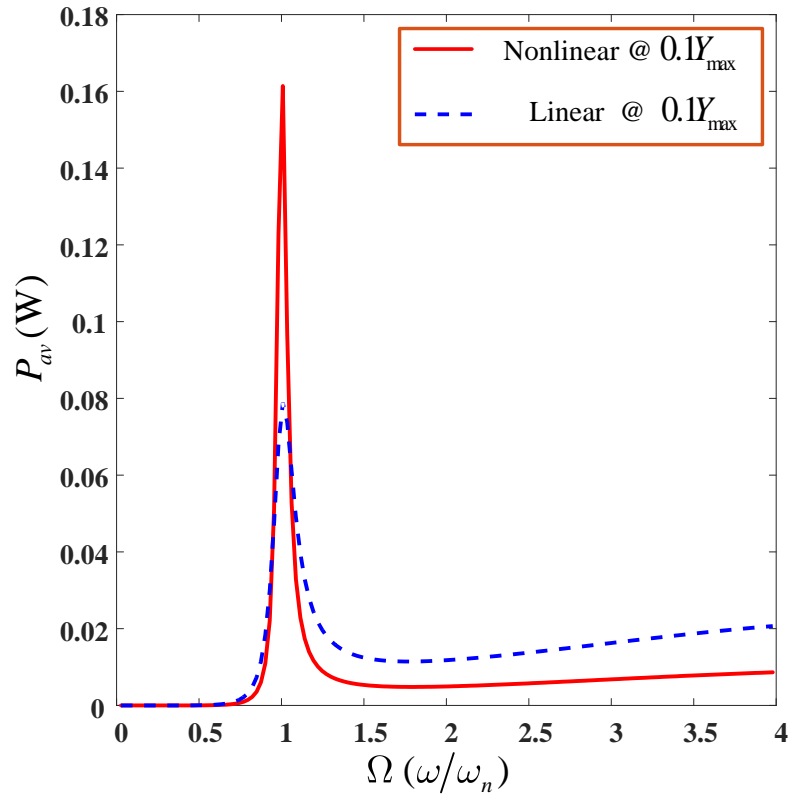


Figure 4.16: Average power for the linear and nonlinear VEH systems at an excitation of $0.1Y_{\max}$.

The electrical damping force, f_{em} is a function of the current, i flowing through the energy harvesting circuit and it is also proportional to it, as expressed in Eq. (4.22). This also implies that the characteristics of the electrical damping force is influenced by that of the current. Similarly, the characteristics of the current is dependent on the characteristics of the load resistance, R_L as indicated in Eq. (4.21). This, therefore, indicates the influence of R_L on f_{em} as deduced from Eq. (4.22). This explains the nonlinear characteristics observed, while employing a nonlinear load resistance, in the VEH circuit current and consequently electrical damping force as seen in Figure 4.17 and Figure 4.18 respectively. However, both linear and nonlinear load resistances provide the same level and characteristic of induced open circuit voltage, v_{emf} at maximum excitation levels as shown in Figure 4.19. This causes both linear and nonlinear VEH systems to attain the same relative displacement span and consequently, to provide the same level of power. In Figure 4.20, the load voltage across both linear and nonlinear load resistances are presented. It should be noted that the sum of the voltages across the coil resistance and load resistance (load voltage)

yields the induced open circuit voltage when the load resistance is connected across it, as given in Eq. (4.20). This is independent of the characteristics of the load resistance.

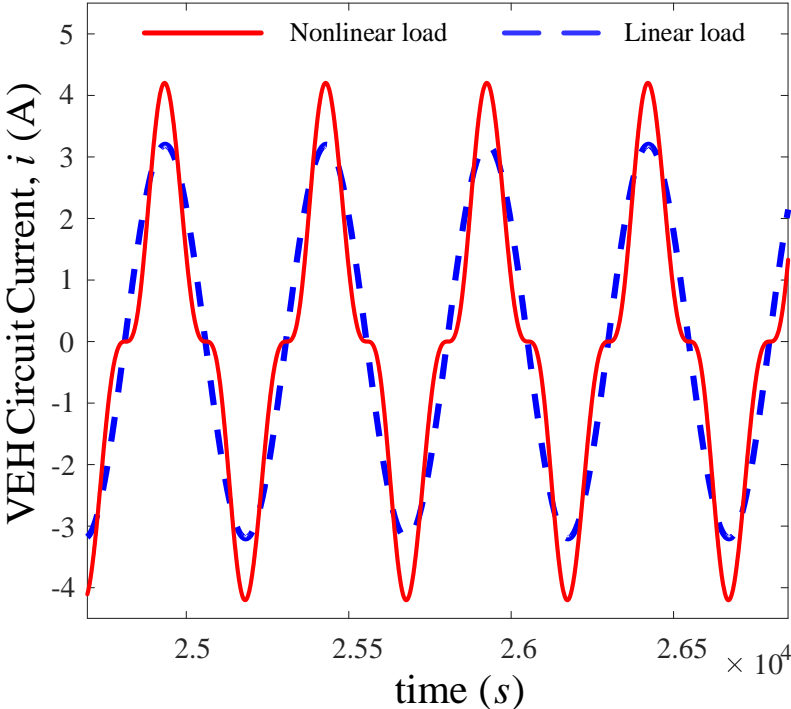


Figure 4.17: Time histories of the VEH circuit currents for the linear (blue dash) and nonlinear (red solid) VEH systems.

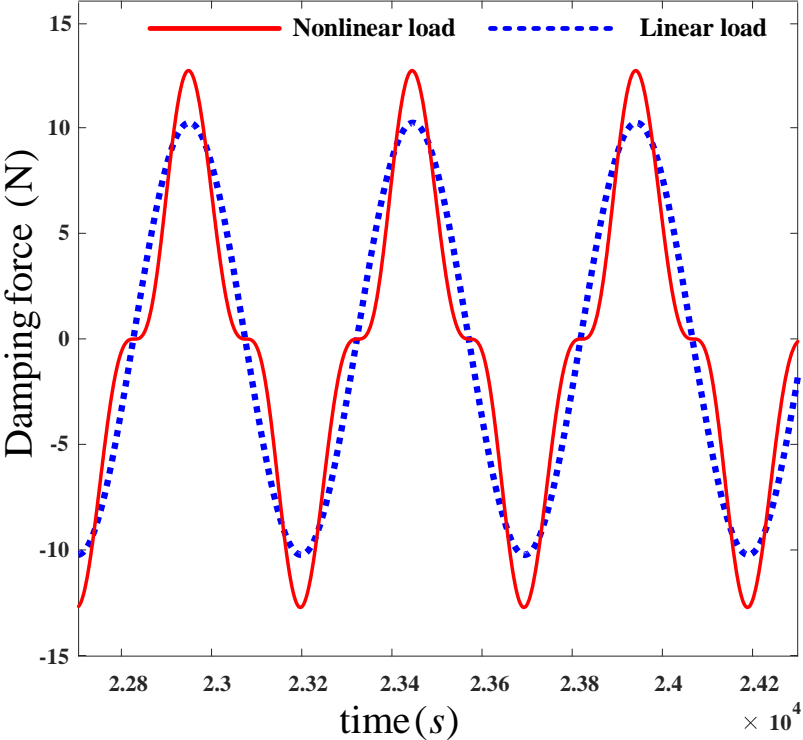


Figure 4.18: Time histories of the actual damping forces for the linear (blue dot) and nonlinear (red solid) VEH systems.

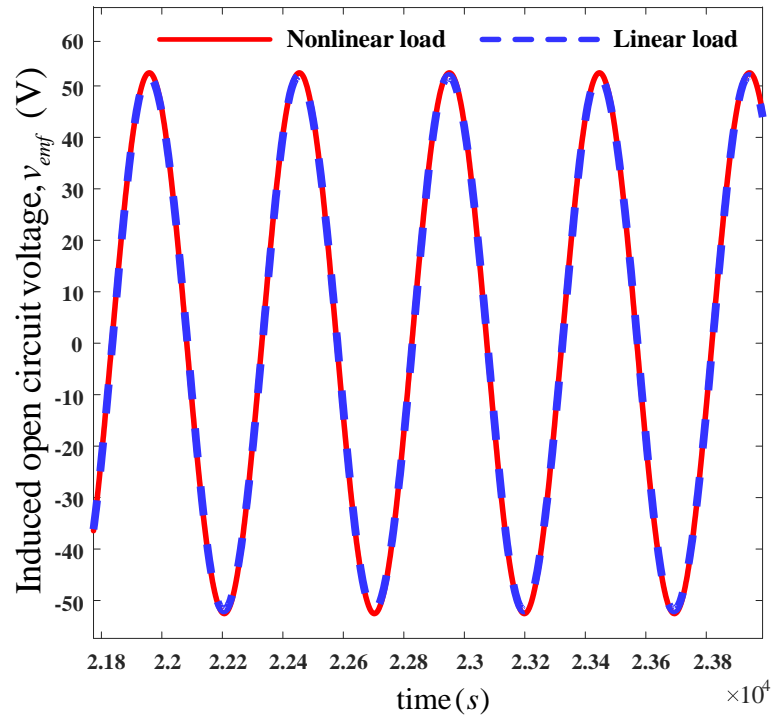


Figure 4.19: Time histories of the induced open circuit voltages for the linear (blue dash) and nonlinear (red solid) VEH systems.

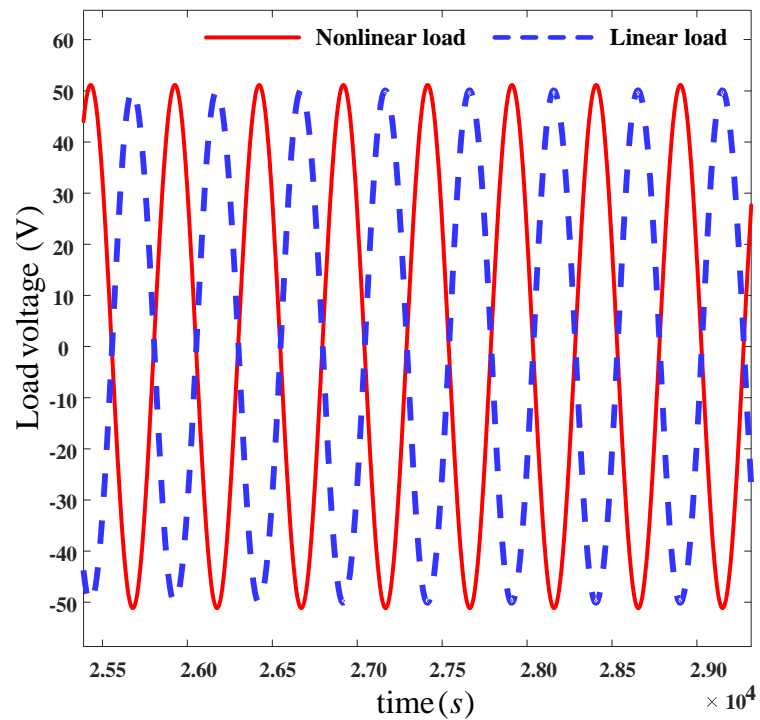


Figure 4.20: Time histories of the voltages across the load resistance for the linear (blue dash) and nonlinear (red solid) VEH system.

Furthermore, while the currents across the nonlinear load resistance and its equivalent linear load resistance are in phase, as shown in Figure 4.17, the voltages across them are out of phase by 180° , as seen in Figure 4.20. This is due to the nonlinear characteristics of the nonlinear load, which is usually an active device such as diodes and transistors. Such devices are used in switching applications thus providing a nonlinear behaviour in power electronics. For a linear load, the voltage and current are proportional hence obeys Ohm's law. However, for a nonlinear load, this is not the case as harmonics are induced into the current flowing in the circuit.

4.6 CONCLUSIONS

Motivated by the desire to improve the performance of vibration energy harvesters, this work has focused on the analysis, design and Simulink implementation of a nonlinear vibration energy harvesting system. The nonlinear VEH system proposed here introduces a nonlinear cubic damping characteristic into the mechanical subsystem and its energy harvesting performance was compared with an equivalent linear VEH. It was established that at maximum excitation level, a nonlinear VEH system, and its linear equivalent, harvest the same amount of power. However, at excitations below the maximum excitation level, the nonlinear VEH outperforms its linear counterpart. That is, it harvests significantly more power at the resonant frequency compared to its linear equivalent. A design of the mechanical subsystem of the VEH system was conducted and subsequently a Simulink model of the electromechanical system was developed. However, prior to the Simulink implementation of the nonlinear VEH system, an analytical study, design and optimisation of the system was initially conducted.

A mathematical model of the nonlinear VEH system was formulated and analysed using a nonlinear system frequency analysis approach known as Output Frequency Response Function (OFRF). Subject to existing system constraint, Z_{\max} , a nonlinear damping parameter, $c_3^{\text{opt}2}$ was designed to enable the nonlinear VEH harvest the maximum average power, $P_{av|c_3 \max 2}$ possible. With the designed damping parameter, the corresponding (desired) damping force, f_{emd}^* was determined at the resonant frequency. The desired damping force characteristics was used to estimate the resistive

elements required to implement an electromechanical VEH system with the desired damping characteristics. With the estimated coil and load resistances, an electromechanical system of the nonlinear VEH system was simulated using the MATLAB Simulink program. The simulated electromechanical system provides clarity of the electrical domain characteristics of the nonlinear VEH system. This study provides an insight into the electromechanical design and implementation of a nonlinear VEH system. Future works will focus on the electrical load design and practical implementation, using DC-DC converters. It is expected that the proposed implementation will provide the same electrical characteristics as the nonlinear load resistance discussed in this work. It is noteworthy that the characteristics of the electrical damping force of a VEH system depends on the characteristics of the load resistance of the VEH system. This implies that a linear resistive load will generate a linear damping characteristic while a nonlinear resistive load will generate a nonlinear damping characteristic.

In this chapter, the design and implementation of a nonlinear VEH system with damping nonlinearity was considered. It was demonstrated that integrating cubic damping nonlinearity to the dynamic model of the VEH system improved its effectiveness by increasing the available power. The system model here incorporated only damping nonlinearity, however, in the next chapter, both damping and stiffness nonlinearities will be considered.

The key contribution of this research work is the novel application of the OFRF method in the analysis, design and optimisation of a nonlinear VEH system. In this study, a cubic damping characteristic was considered and a systematic way of proceeding from the design stage to implementation stage, was demonstrated.

Chapter 5: Analysis and design of a vibration energy harvester with damping and stiffness nonlinearities

5.1 INTRODUCTION

In the previous chapter, the study focused on the optimisation of a nonlinear vibration energy harvester with damping nonlinearity. An optimisation process was carried out to maximize the energy harvested by the VEH system. However, in this study, both damping and stiffness nonlinearities will be considered.

Several works have been done towards broadening the operational frequency range of a VEH system beyond the resonant region [128], [133], [174]–[178]. To broaden the operational bandwidth of a VEH system, [121] proposed the use of active tuning actuators to tune the frequency at resonance to the excitation frequency as long as the actuator does not require an external power source. Ramlan et al. in [126], demonstrated the possible benefits of nonlinear stiffness in energy harvesters. Two types of nonlinear stiffness were considered in the study. Using a bi-stable snap-through mechanism, it was shown that more power was harvested compared to a tuned linear device for a given input excitation. However, with the second type, using a hardening spring, it was demonstrated that the bandwidth was extended further compared to an equivalent linear device. Su et al. showed in [168] that though a nonlinear Duffing energy harvester provides a wider bandwidth that it can also be optimised to maximise the available power. The authors in [175] suggested tuning the resonant frequency of a VEH system to align with that of the excitation frequency and the electrical damping set equal to the parasitic damping. Power electronics were employed here capable of adjusting the damping and resonant frequency thus improving its efficiency. Studies in [176] and [177] have focused on the comparison of the bandwidth for a Duffing-type energy harvester and a linear harvester. The results also confirmed the nonlinear harvester provided a larger bandwidth than the linear type. Most of the published works have compared the Duffing-type VEH and the linear

type. Moreover, several parameter optimisations have been suggested to achieve the desired results such as mechanical damping [176], electrical load [168], [177].

Based on the findings in [134], as discussed in the last chapter, an analysis, design and optimisation of a nonlinear VEH system was conducted in [179] and [180]. While no mass-displacement constraint was considered in [179], this was considered in [180]. In these studies, an optimum cubic damping parameter was designed for a desired harvester energy, using the OFRF method. The OFRF of a nonlinear system is determined based on the nonlinear differential equation (NDE) of the system and it shows the relationship between the output spectrum of the system and its nonlinear parameters. It, thus, describes the system characteristics. The OFRF representation of the system studied in the previous chapter, was determined using the Least-Squares (LS) approach. However, this method requires several numerical simulations using a training set of values of the system design parameters, to obtain the respective system output responses [85].

Vazquez et al. in [181], based on the characteristic of the n th-order Volterra operator being a multi-linear function of a combination of input signals, modelled the behaviour of the Volterra operators by Associated Linear Equations (ALEs). These ALEs, as discussed in [181], [182], can be used as an analytical tool for the Volterra class of nonlinear systems. Based on this, it was further revealed in [183] that the ALEs for a Volterra class of nonlinear systems can be used to determine a more accurate OFRF representation of the system using a significantly lesser number of numerical simulations compared to the LS approach.

In this study, an analysis and design of a nonlinear VEH system is explored using OFRF representations of the system output spectra which are determined from the ALE decompositions of the nonlinear VEH model. In addition to using a nonlinear damping component to extend the average power of the VEH, a stiffness nonlinearity is also integrated to extend the frequency range of the harvester.

A summary of key contributions in this chapter is highlighted below:

- Investigation of a VEH system with both cubic and stiffness nonlinearities using the OFRF method.
- Determination of an OFRF representation using ALE decompositions for the output spectrum and average power of a nonlinear VEH system.

- Demonstration of the effect of a nonlinear stiffness term on a nonlinear VEH system with cubic damping.

Subsequent sections of this chapter are organised as follows: Section 5.2 presents the model formulation of the device; Section 5.3 shows the determination of the OFRF structure; Section 5.2 discusses the evaluation of the ALEs; Section 5.5 shows the determination of the OFRF using the ALEs; Section 5.6 provides results of the study and discussion and finally Section 5.7 concludes the chapter.

5.2 DEVICE MODELING

Given a single degree-of-freedom (SDOF) vibration-based energy harvester, as illustrated in Figure 5.1, having a suspended mass, m and an oscillating support-base with displacement $y(t)$. The mass is isolated from the base by an isolation system modelled as a nonlinear damping system connected parallel to a nonlinear spring. The damping system comprises a mechanical viscous damping, c_1 and an electrical damping, c_3 . The electrical damping arises from the electromagnetic force generated by virtue of the cubic load resistance connected across the EM damper. The linear and cubic stiffness coefficients are k_1 and k_3 respectively.

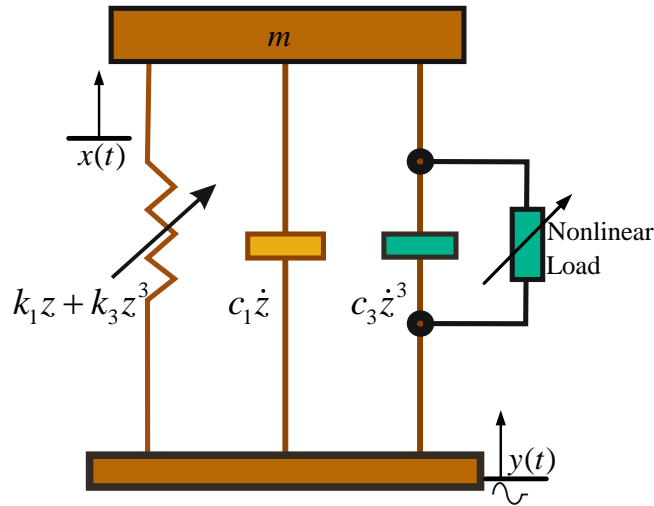


Figure 5.1: SDOF of a vibration energy harvester with nonlinear stiffness and damping.

The model of the SDOF VEH is an NDE and the equation of motion of the mass with respect to the relative displacement $z = x - y$ is given as

$$m\ddot{z} + c_1\dot{z} + c_3\dot{z}^3 + k_1z + k_3z^3 = -m\ddot{y} \quad (5.1)$$

For a harmonic base displacement with amplitude, Y , frequency, ω and zero phase shift, the base displacement is given as $y = Y \sin(\omega t)$. Therefore Equation (5.1) becomes

$$m\ddot{z} + c_1\dot{z} + c_3\dot{z}^3 + k_1z + k_3z^3 = m\omega^2Y \sin(\omega t) \quad (5.2)$$

The nonlinear damping device absorbs an instantaneous power equal to the product of the instantaneous damper force and relative velocity of the VEH [112]. Nonetheless, it yields an average power given as

$$P_{av} = \frac{1}{T} \int_0^T (c_3\dot{z}^3) \cdot \dot{z} dt \quad (5.3)$$

For a single-frequency harmonic oscillation, where $z = Z \sin(\omega t)$, this yield

$$P_{av} = \frac{3}{8} c_3 \omega^4 Z^4 \quad (5.4)$$

In addition, it can be deduced that since the output frequency response, Z of system (5.2) is a function of ω and the nonlinear parameters, c_3 and k_3 , therefore, P_{av} given in Eq. (5.4) is also a function of c_3 , k_3 and ω . The resonant frequency is the frequency of focus here as it is the frequency where maximum power absorption occurs.

5.2.1 Effect of Nonlinear Stiffness on the harvester power

It has been established in literature [128], [130], [133], [174] that a nonlinear hardening spring ($k_3 > 0$) increases the bandwidth of a vibration isolation system as depicted in Figure 5.2 as well as the available energy [184].

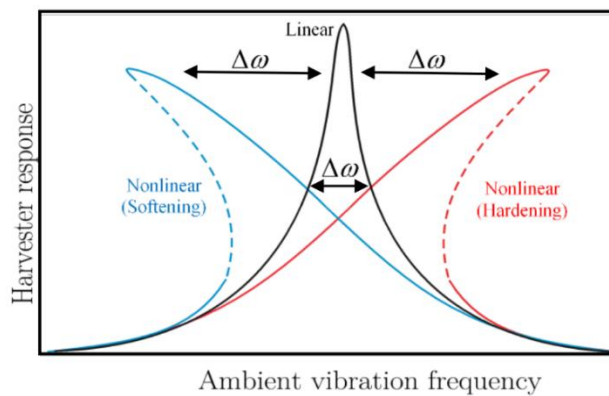


Figure 5.2: Effect of nonlinear stiffness on the resonant frequency

It is observed in Eq. (5.4), that an increase in the resonant frequency (frequency of interest) will result to an increase in the average power of the VEH system.

5.3 DETERMINATION OF THE OFRF STRUCTURE

Firstly, the OFRF representations of the output spectrum of system (5.2), $Z(j\omega)$ and the harvestable power of Eq. (5.4), P_{av} are obtained in terms of the design parameters, c_3 and k_3 . It is observed that system (5.2) belongs to the class of Volterra system of Eq. (2.4) in subsection 2.4.3 of Chapter 2, with $M = 3$ and $L = 2$. The system parameters are obtained as $c_{10}(2) = m$, $c_{10}(1) = c_1$, $c_{10}(0) = k_1$, $c_{30}(000) = k_3$, $c_{30}(111) = c_3$, and $c_{01}(0) = -m\omega^2 Y$.

If the set of monomials in the OFRF representation of the n th-order output spectrum of system (5.2) is denoted by \mathfrak{M} and the complex-valued OFRF coefficients denoted by $\Theta(j\omega)$, the OFRF representation can therefore be written as

$$Z(j\omega) = \mathfrak{M} \cdot \Theta(j\omega) \quad (5.5)$$

Applying the algorithm, as presented in subsection 2.4.3 of Chapter 2, to obtain the OFRF monomials, \mathfrak{M} up to the 7th-order, yields

$$\begin{aligned} E_1 &= [1] \\ E_3 &= [c_3 \quad k_3] \\ E_5 &= [c_3^2 \quad c_3 k_3 \quad k_3^2] \\ E_7 &= [c_3^3 \quad c_3^2 k_3 \quad c_3 k_3^2 \quad k_3^3] \end{aligned} \quad (5.6)$$

Therefore, $\mathfrak{M} = \bigcup_{n=1}^{s_N} E_n = [1, c_3, k_3, c_3^2, c_3 k_3, k_3^2, c_3^3, c_3^2 k_3, c_3 k_3^2, k_3^3]$

It should be noted that for improved accuracy, higher orders can be considered. Furthermore, the OFRF representation, as stated in Eq. (5.5), which comprises the monomials obtained, as presented in Eq. (5.6), and its respective OFRF coefficients, $\Theta_{n|r}(j\omega)$ (yet to be determined), can be represented in the form

$$Z_{\text{OFRF}}(j\omega) = \sum_{n=1}^{s_N} E_{n|r} \cdot \Theta_{n|r}(j\omega) \quad (5.7)$$

where $r = 0, 2, \dots, h$ and h is the maximum number of elements in E_n . Rewriting Eq. (5.7) yields

$$\begin{aligned} Z_{\text{OFRF}}(j\omega) &= \Theta_{10}(j\omega) + c_3 \cdot \Theta_{31}(j\omega) + k_3 \cdot \Theta_{32}(j\omega) \\ &+ c_3^2 \cdot \Theta_{51}(j\omega) + c_3 k_3 \cdot \Theta_{52}(j\omega) + k_3^2 \cdot \Theta_{53}(j\omega) + c_3^3 \cdot \Theta_{71}(j\omega) \\ &+ c_3^2 k_3 \cdot \Theta_{72}(j\omega) + c_3 k_3^2 \cdot \Theta_{73}(j\omega) + k_3^3 \cdot \Theta_{74}(j\omega) \end{aligned} \quad (5.8)$$

Therefore, to determine the OFRF coefficients, $\Theta_{nr}(j\omega)$, the ALEs of system (5.2) is first computed up to the 7th-order. In the next section, the evaluation of the ALEs for an NDE system is shown.

5.4 EVALUATION OF THE ASSOCIATED LINEAR EQUATIONS

For a nonlinear system of the Volterra class given by system (5.2), the following substitutions can be made

$$z(t) = \sum_{n=1}^{\infty} z_n(t) \quad (5.9)$$

Rewriting system (5.2) in a general form by leaving all the linear elements on the LHS and substituting Eq. (5.9) yields

$$\begin{aligned} m \sum_{n=1}^{\infty} \ddot{z}_n + c_1 \sum_{n=1}^{\infty} \dot{z}_n + k_1 \sum_{n=1}^{\infty} z_n = \\ m\omega^2 Y \sin(\omega t) - \sum_{j=3}^L c_j \left(\sum_{n=1}^{\infty} \dot{z}_n \right)^j - \sum_{j=3}^L k_j \left(\sum_{n=1}^{\infty} z_n \right)^j \end{aligned} \quad (5.10)$$

The ALEs of system (5.10) can be obtained for the n th-order, for $n = 1, 2, \dots, S_N$, where S_N is the maximum order of the system nonlinearity considered, as demonstrated in [181], thus

$$\begin{aligned} m \sum_{n=1}^{S_N} \ddot{z}_n + c_1 \sum_{n=1}^{S_N} \dot{z}_n + k_1 \sum_{n=1}^{S_N} z_n = \\ m\omega^2 Y \sin(\omega t) \\ - \sum_{n=1}^{S_N} \sum_{j=3}^{n-3} c_j \sum_{\dot{z}_1=1}^{n-j+1} \dots \sum_{\dot{z}_{j-1}=1}^{n-l+i-\dot{z}_1-\dots-\dot{z}_{j-1}} \dots \sum_{\dot{z}_j=0}^{n-\dot{z}_1-\dots-\dot{z}_{j-1}-\dot{z}_j} \dot{z}_{\dot{z}_1} \dot{z}_{\dot{z}_2} \dots \dot{z}_{\dot{z}_j} \\ - \sum_{n=1}^{S_N} \sum_{j=3}^{n-3} k_j \sum_{z_1=1}^{n-j+1} \dots \sum_{z_{j-1}=1}^{n-j+i-\dot{z}_1-\dots-\dot{z}_{j-1}} \dots \sum_{z_j=0}^{n-\dot{z}_1-\dots-\dot{z}_{j-1}-z_j} z_{z_1} z_{z_2} \dots z_{z_j} \end{aligned} \quad (5.11)$$

where the summation of all the sub-indices of \dot{z}_j and z_j on the RHS has to equal n i.e. $(\underline{j}_1 + \dots + \underline{j}_l = n)$ and $(\underline{j}_1 + \dots + \underline{j}_l = n)$. In computing the ALEs, the low-order output responses contribute to the immediate higher-order responses up to the maximum order considered.

For an estimation of the total output responses up to the S_N th-order and its corresponding output spectrums,

$$\begin{cases} z(t) = \sum_{n=1}^{S_N} z_n(t) \\ Z(j\omega) = \sum_{n=1}^{S_N} Z_n(j\omega) \end{cases} \quad (5.12)$$

For $S_N = 7$, the following ALEs are obtained

$$\begin{cases} m\ddot{z}_1 + c\dot{z}_1 + kz_1 = m\omega^2 Y \sin(\omega t) \\ m\ddot{z}_3 + c\dot{z}_3 + kz_3 = -k_3 z_1^3 - c_3 \dot{z}_1^3 \\ m\ddot{z}_5 + c\dot{z}_5 + kz_5 = -3k_3 z_1^2 z_3 - 3c_3 \dot{z}_1^2 \dot{z}_3 \\ m\ddot{z}_7 + c\dot{z}_7 + kz_7 = -3k_3 (z_1 z_3^2 + z_1^2 z_5) - 3c_3 (\dot{z}_1 \dot{z}_3^2 + \dot{z}_1^2 \dot{z}_5) \end{cases} \quad (5.13)$$

The continuous-time output response of system (5.2) and its corresponding output spectrum, where $Z_n(j\omega) = \text{fft}(z_n(t))$, are respectively expressed as

$$\begin{cases} z(t) = z_1(t) + z_3(t) + z_5(t) + z_7(t) \\ Z(j\omega) = Z_1(j\omega) + Z_3(j\omega) + Z_5(j\omega) + Z_7(j\omega) \end{cases} \quad (5.14)$$

The cumulative structure of the individual n th-order ALE contributions up to the 7th - order is presented in Figure 5.3. Similarly, Figure 5.4 shows the output spectrum for each n th-order contribution of the ALE decompositions up to the 7th-order. It is observed that at resonance there is a significant contribution by the various decompositions.

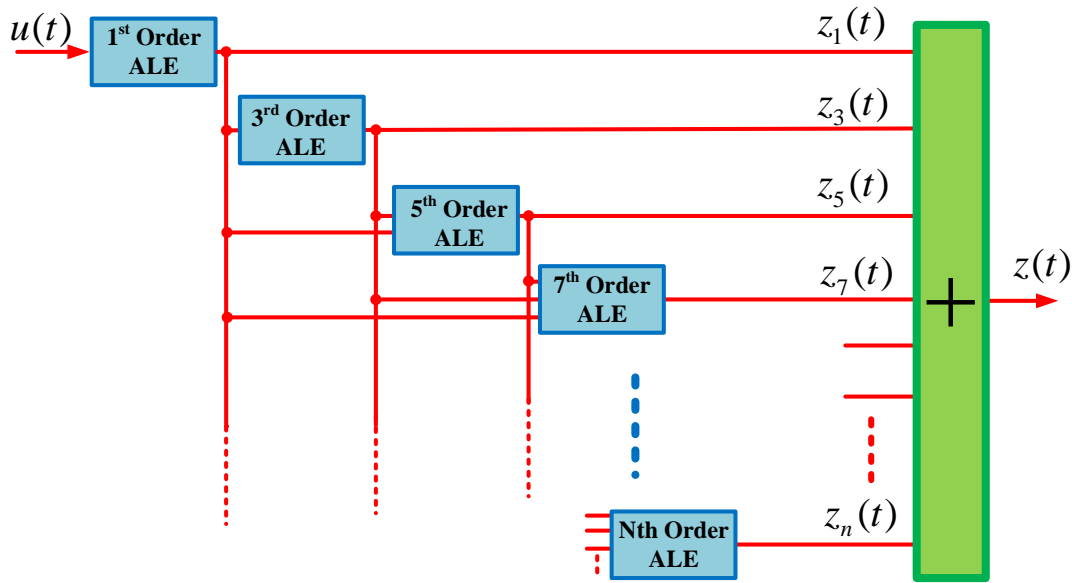


Figure 5.3: A representation of the individual ALE contributions to the general output response of system (5.2).

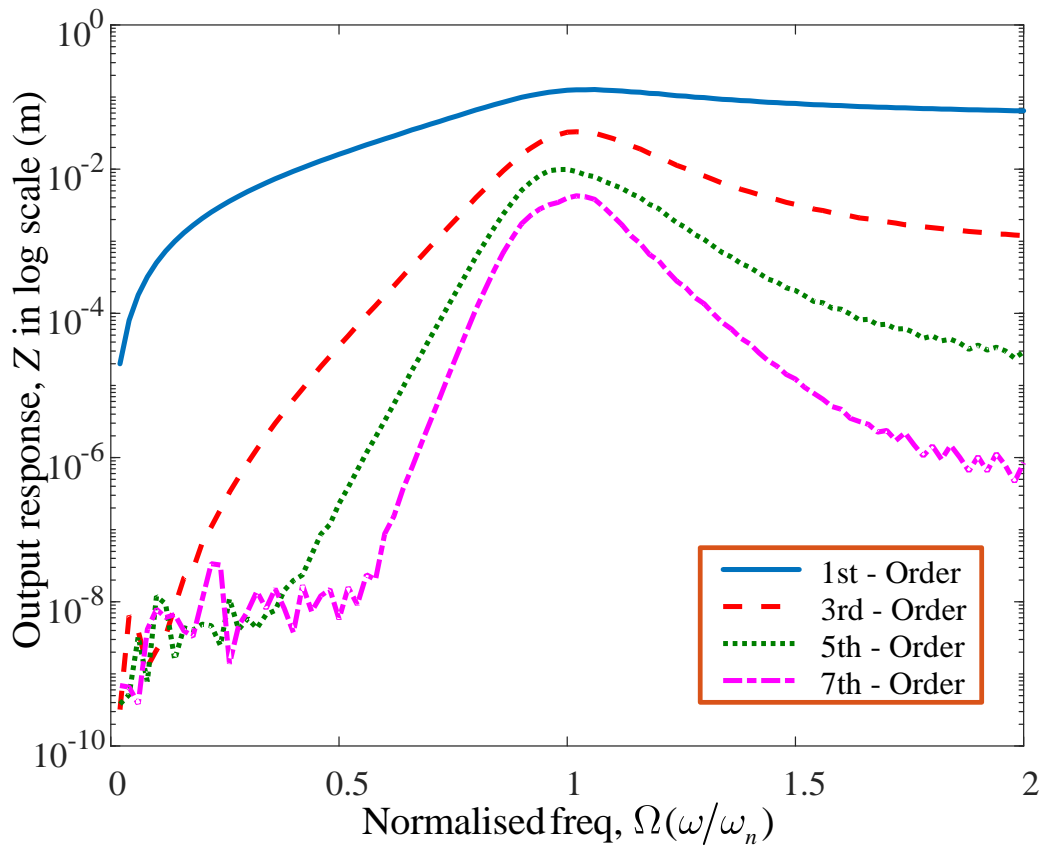


Figure 5.4: Graph of individual nth-order ALE contributions to the output response of system (5.2) at the fundamental frequency.

5.5 DETERMINATION OF THE OFRF USING THE ALES

Equation (5.14) shows the output spectrum of system (5.2) determined from the fft of the ALE contributions obtained. The n th-order output spectrum of each ALE contribution is equal to the corresponding n th-order component of the OFRF representation thus

$$\begin{cases} Z_{\text{ALES}}(j\omega) = Z_{\text{OFRF}}(j\omega) \\ \sum_{n=1}^{S_N} Z_n(j\omega) = \sum_{n=1}^{S_N} E_{n/r} \cdot \Theta_{n/r}(j\omega) \end{cases} \quad (5.15)$$

From Eq. (5.15), it can be deduced that

$$\begin{aligned} Z_1(j\omega) &= \Theta_{10}(j\omega) \\ Z_3(j\omega) &= c_3 \cdot \Theta_{31}(j\omega) + k_3 \cdot \Theta_{32}(j\omega) \\ Z_5(j\omega) &= c_3^2 \cdot \Theta_{51}(j\omega) + c_3 k_3 \cdot \Theta_{52}(j\omega) + k_3^2 \cdot \Theta_{53}(j\omega) \\ Z_7(j\omega) &= c_3^3 \cdot \Theta_{71}(j\omega) + c_3^2 k_3 \cdot \Theta_{72}(j\omega) + c_3 k_3^2 \cdot \Theta_{73}(j\omega) \\ &\quad + k_3^3 \cdot \Theta_{74}(j\omega) \end{aligned} \quad (5.16)$$

Subsequent analysis in this study has been done using the following system parameter values; $m = 1\text{kg}$, $k_1 = 25\text{Nm}^{-1}$, $c_1 = 2\text{Nsm}^{-1}$, $Y = 0.05\text{m}$, $\omega_n = 5\text{rads}^{-1}$, $\Omega = \omega / \omega_n$.

To obtain the OFRF coefficients up to the 7th-order, five simulations are required using five different values of $c_3(c_{3r})$ and $k_3(k_{3r})$ {where $r = 1, 2, 3, 4, 5.$ } as given in Table 5.1.

Table 5.1: Simulation (Training) values of model design parameters

Model nonlinear parameter	Sim1 value	Sim2 value	Sim3 value	Sim4 value	Sim5 value
c_3 ($\text{N}\cdot\text{s}^3\cdot\text{m}^{-3}$)	0.300	0.325	0.350	0.375	0.400
k_3 ($\text{N}\cdot\text{m}^{-3}$)	0	55	110	165	220

The OFRF coefficients can be determined for any frequency of interest using Eq. (5.17) given as

$$\begin{aligned}
\Theta_{10}(\mathbf{j}\omega) &= Z_1(\mathbf{j}\omega) \\
\begin{bmatrix} \Theta_{31}(\mathbf{j}\omega) \\ \Theta_{32}(\mathbf{j}\omega) \end{bmatrix} &= \begin{bmatrix} c_{31} & k_{31} \\ c_{32} & k_{32} \end{bmatrix}^{-1} \begin{bmatrix} Z_{31}(\mathbf{j}\omega) \\ Z_{32}(\mathbf{j}\omega) \end{bmatrix} \\
\begin{bmatrix} \Theta_{51}(\mathbf{j}\omega) \\ \Theta_{52}(\mathbf{j}\omega) \\ \Theta_{53}(\mathbf{j}\omega) \end{bmatrix} &= \begin{bmatrix} c_{31}^2 & c_{31}k_{31} & k_{31}^2 \\ c_{32}^2 & c_{32}k_{32} & k_{32}^2 \\ c_{33}^2 & c_{33}k_{33} & k_{33}^2 \end{bmatrix}^{-1} \begin{bmatrix} Z_{51}(\mathbf{j}\omega) \\ Z_{52}(\mathbf{j}\omega) \\ Z_{53}(\mathbf{j}\omega) \end{bmatrix} \\
\begin{bmatrix} \Theta_{71}(\mathbf{j}\omega) \\ \Theta_{72}(\mathbf{j}\omega) \\ \Theta_{73}(\mathbf{j}\omega) \\ \Theta_{74}(\mathbf{j}\omega) \end{bmatrix} &= \begin{bmatrix} c_{31}^3 & c_{31}^2k_{31} & c_{31}k_{31}^2 & k_{31}^3 \\ c_{32}^3 & c_{32}^2k_{32} & c_{32}k_{32}^2 & k_{32}^3 \\ c_{33}^3 & c_{33}^2k_{33} & c_{33}k_{33}^2 & k_{33}^3 \\ c_{34}^3 & c_{34}^2k_{34} & c_{34}k_{34}^2 & k_{34}^3 \end{bmatrix}^{-1} \begin{bmatrix} Z_{71}(\mathbf{j}\omega) \\ Z_{72}(\mathbf{j}\omega) \\ Z_{73}(\mathbf{j}\omega) \\ Z_{74}(\mathbf{j}\omega) \end{bmatrix}
\end{aligned} \tag{5.17}$$

Therefore, the ALE-generated OFRF representation of the output spectrum of system (5.2) can be expressed as

$$\begin{aligned}
Z(\mathbf{j}\omega; c_3, k_3) &= \Theta_{10}(\mathbf{j}\omega) + c_3 \cdot \Theta_{31}(\mathbf{j}\omega) + k_3 \cdot \Theta_{32}(\mathbf{j}\omega) + c_3^2 \cdot \Theta_{51}(\mathbf{j}\omega) \\
&+ c_3k_3 \cdot \Theta_{52}(\mathbf{j}\omega) + k_3^2 \cdot \Theta_{53}(\mathbf{j}\omega) + c_3^3 \cdot \Theta_{71}(\mathbf{j}\omega) + c_3^2k_3 \cdot \Theta_{72}(\mathbf{j}\omega) \\
&+ c_3k_3^2 \cdot \Theta_{73}(\mathbf{j}\omega) + k_3^3 \cdot \Theta_{74}(\mathbf{j}\omega)
\end{aligned} \tag{5.18}$$

The OFRF coefficients of Eq. (5.18) have been determined using the ALEs approach. The benefit of using the ALEs approach is that the number of numerical simulations required to determine the OFRF of the system is significantly reduced. To obtain the respective OFRF representation of the average power harvestable by the VEH system via the nonlinear damping system, the OFRF representation of the output spectrum in Eq. (5.18) is substituted in Eq. (5.4) to yield

$$P_{av}(\omega, c_3, k_3) = \frac{3}{8} c_3 \omega^4 |Z(\mathbf{j}\omega; c_3, k_3)|^4 \tag{5.19}$$

The OFRF representation of the quartic magnitude of the output spectrum, $|Z(\mathbf{j}\omega; c_3, k_3)|^4$ can also be derived and represented in a polynomial form as

$$|Z(\mathbf{j}\omega; c_3, k_3)|^4 = \sum_{\bar{n}=0}^7 \sum_{\bar{m}=0}^{\bar{n}} v_{\bar{m}, \bar{n}-\bar{m}}(\omega) c_3^{\bar{m}} k_3^{\bar{n}-\bar{m}} \tag{5.20}$$

where $\underline{N} = 7$ is the maximum nth order nonlinearity while $v_{\bar{m}, \bar{n}-\bar{m}}$ are functions of frequency and represent the OFRF coefficients of $|Z(\mathbf{j}\omega; c_3, k_3)|^4$.

Therefore, the average power can be represented as

$$P_{av}(\omega, c_3, k_3) = \frac{3}{8} \omega^4 \cdot \sum_{\bar{n}=0}^7 \sum_{\bar{m}=0}^{\bar{n}} v_{\bar{m}, \bar{n}-\bar{m}}(\omega) c_3^{\bar{m}+1} k_3^{\bar{n}-\bar{m}} \quad (5.21)$$

The OFRF-based results are obtained and compared with that determined using the *Runge-Kutta 4* algorithm (ODE45 in MATLAB) for the output spectrum of system (5.2) and the average power harvestable by the VEH system. The comparisons were conducted for different combinations of parameter values beyond the training set for c_3 and k_3 . The results are presented in Figure 5.5 and Figure 5.6 for the pair of parameters, $c_3 = 0.45 \text{ N.s}^3.\text{m}^{-3}$, $k_3 = 250 \text{ N.m}^{-3}$ and $c_3 = 0.25 \text{ N.s}^3.\text{m}^{-3}$, $k_3 = 270 \text{ N.m}^{-3}$, respectively.

5.6 RESULTS AND DISCUSSION

The OFRF representation of the output spectrum, Z of system (5.2) was derived using the ALE decompositions evaluated from the same system. The OFRF representation of the output spectrum was subsequently used to estimate the average power absorbed by the electromagnetic damper. This was performed for a pair of nonlinear parameter values, c_3 and k_3 , beyond the range over which the OFRF representation was determined i.e. $c_3 \in [0.3, 0.4] \text{ N.s}^3.\text{m}^{-3}$ and $k_3 \in [0, 220] \text{ N.m}^{-3}$. As observed in Figure 5.5 and Figure 5.6, the OFRF representation accurately represents the actual output spectrum and average power of the VEH respectively. These results clearly demonstrate a good match between the OFRF representation and the more accurate numerical simulation result. This demonstrates the benefits of the OFRF methodology as it evidently describes the system dynamics over the entire spectrum. Note that the wobbles observed around the resonant regions in Figures 5.5 and 5.6 are due to the use of parameters beyond the design (training) range. Using parameters further beyond the design range (marginally) will cause the system to approach instability.

In the implementation of such a nonlinear VEH system, the cubic damping nonlinearity can be contributed by an electromagnetic damper whose characteristics is dependent on that of the load resistance in the energy harvesting circuit. The hardening stiffness nonlinearity can be incorporated by the application of magnetic springs whereby a mass of permanent magnet is levitated between two stationary magnets

[185]. However, such magnetic springs can also contribute a damping component typically referred to as magnetic damping [186].

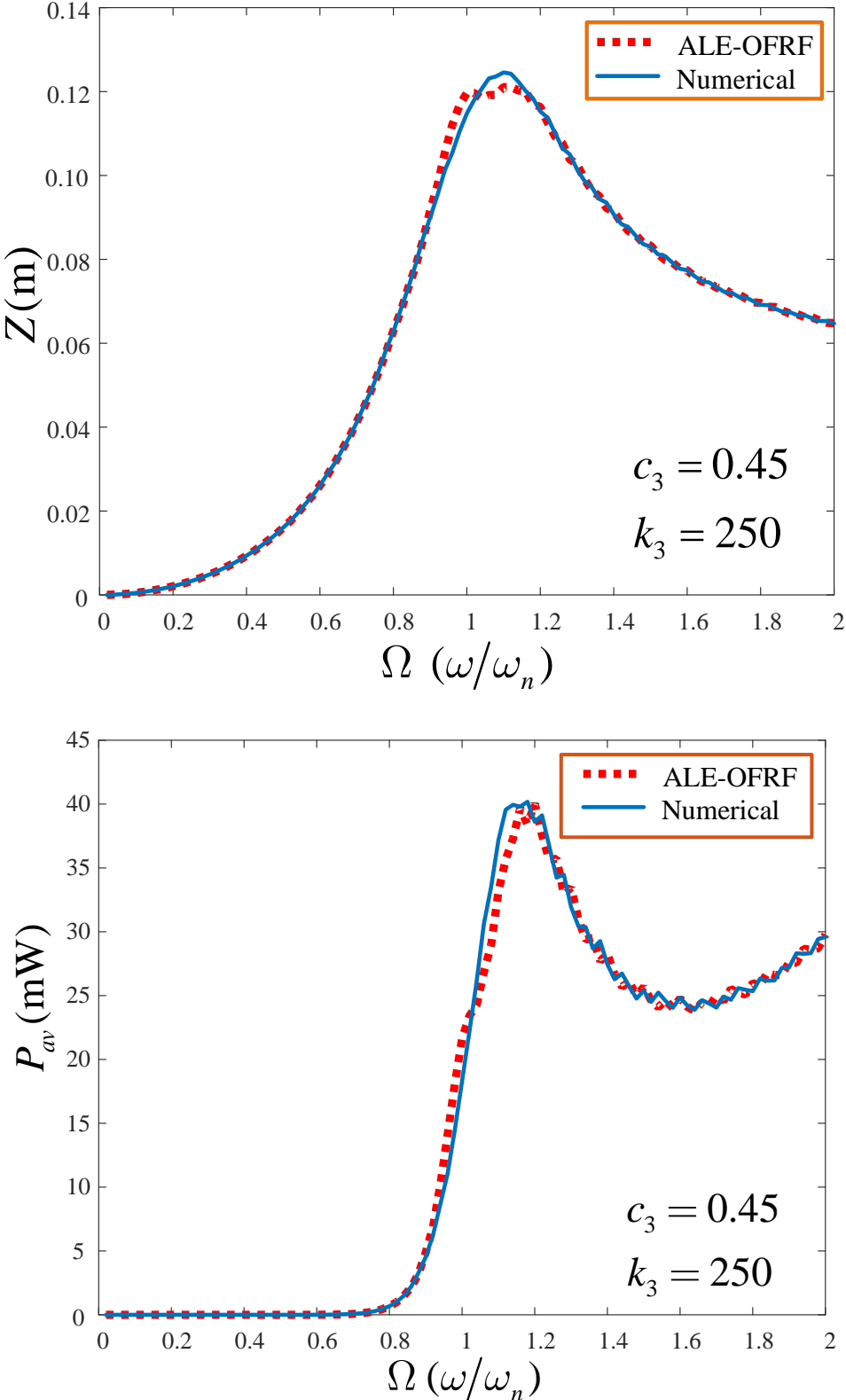


Figure 5.5: ALE-OFRF vs numerical simulation results for the output spectra and average power respectively at $c_3 = 0.45$ and $k_3 = 250$.

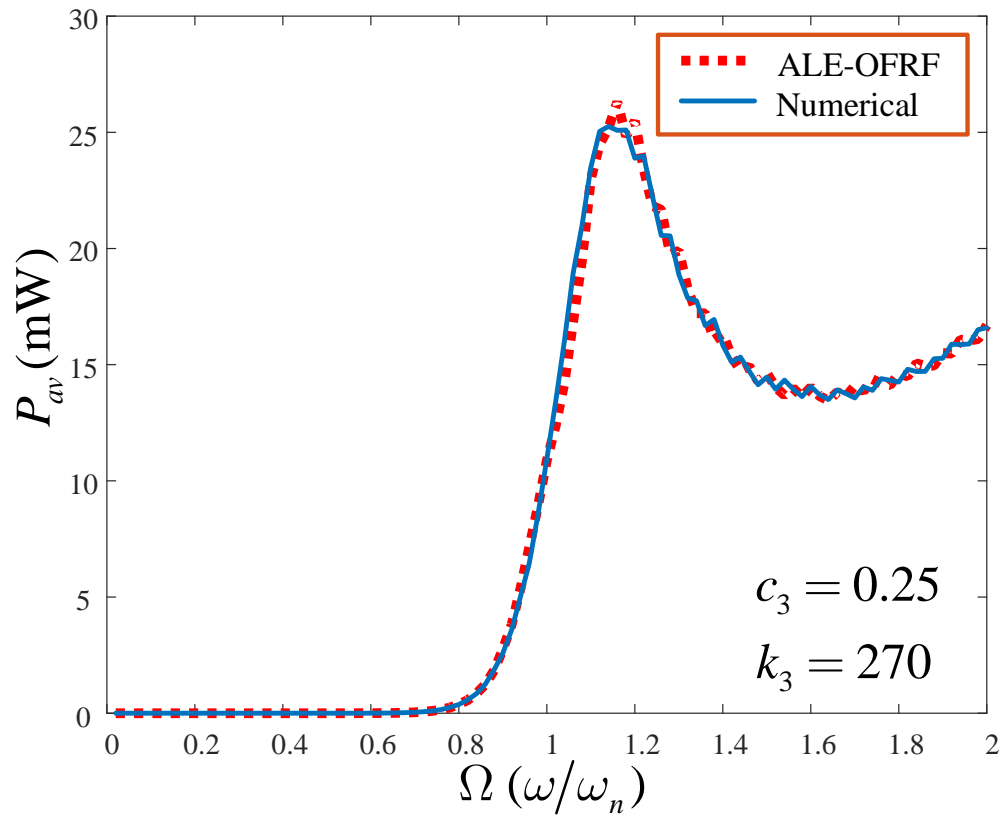
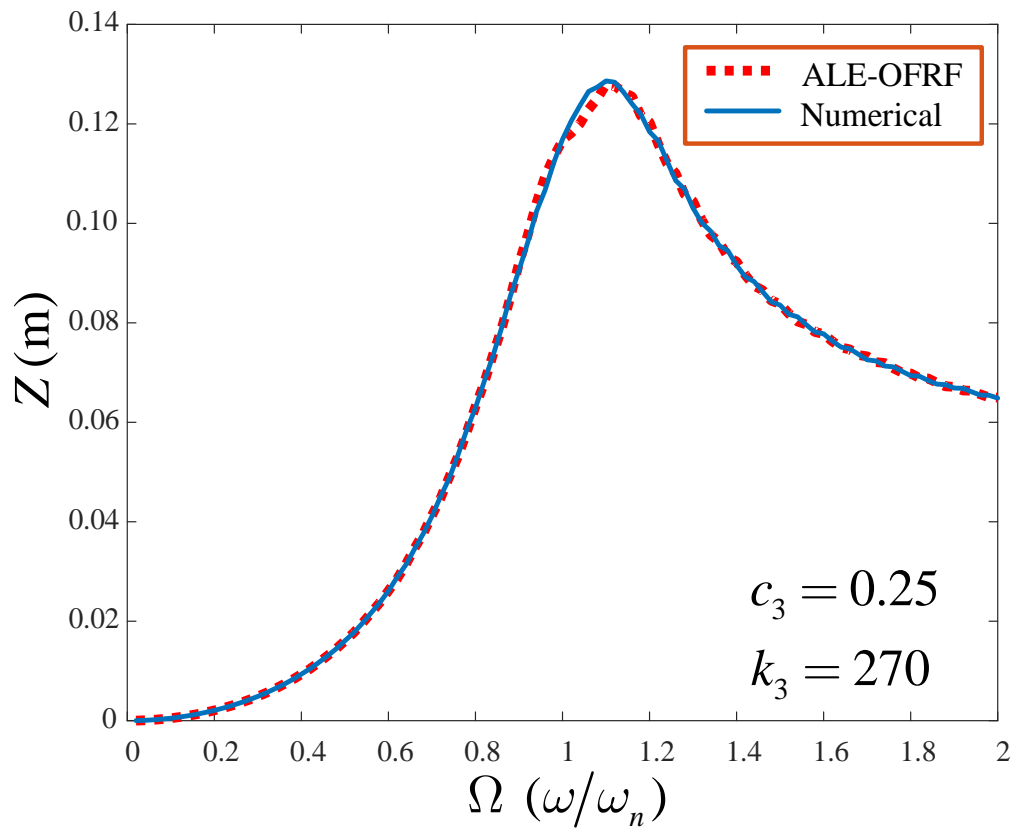


Figure 5.6: ALE-OFRF vs numerical simulation results for the output spectra and average power respectively at $c_3 = 0.25$ and $k_3 = 270$.

5.6.1 Effects of hardening spring on VEH systems with cubic damping

Hardening spring nonlinearities have been integrated into standard linear harvester devices to expand the bandwidth over which power is harvested which is due to a shift in the resonant frequency to higher frequencies [133], [145], [174], [176]. To demonstrate the effect of integrating a hardening-type stiffness characteristic to the dynamics of a VEH system with cubic damping nonlinearity, numerical studies are conducted. The integration of a hardening spring effect can be implemented by employing magnetic springs [186], [185]. Using the OFRF representations expressed in Eqns. (5.8) and (5.19), the effect of the stiffness parameter, k_3 can be observed in Figure 5.7. It is clearly seen to extend the operational bandwidth of the nonlinear VEH system due to the shift in the resonant frequency of the output spectra. The operational bandwidth of the VEH system with and without stiffness characteristic are given as $\Delta\Omega_2$ and $\Delta\Omega_1$ respectively. In addition to this, an apparent increase in the dynamic range of the nonlinear VEH system can also be observed. This is logical as the average power of the nonlinear VEH system, given in Eqn. (5.19), is a function of the excitation frequency, ω . Much of the current literature focused on increasing the bandwidth of linear devices with the integration of a hardening stiffness and compared the duffing-type harvesters with standard linear harvesters.

This study incorporates a hardening stiffness to a VEH system with cubic damping nonlinearity. Nonetheless, a comparison of the VEH with damping and stiffness nonlinearities against a linear system has not been considered here. This is due to the unavailability of a basis for such comparison to be made. Such a comparison has never been reported for VEH devices with damping and stiffness nonlinearities to the best of my knowledge.

Furthermore, most studies in literature considered the Duffing-type harvesters that exhibit the jump phenomenon and they were majorly designed to operate within the larger stable branch. Nevertheless, it is imperative to note that if the VEH model experiences a jump phenomenon, the sum of the ALE decompositions will not converge to the actual output spectrum around the jump region. Therefore, the OFRF representations will poorly describe the actual output spectra of the system and, consequently, will be inappropriate for system analysis and design. However, this

problem is solved here due to the presence of both linear and nonlinear damping characteristics.

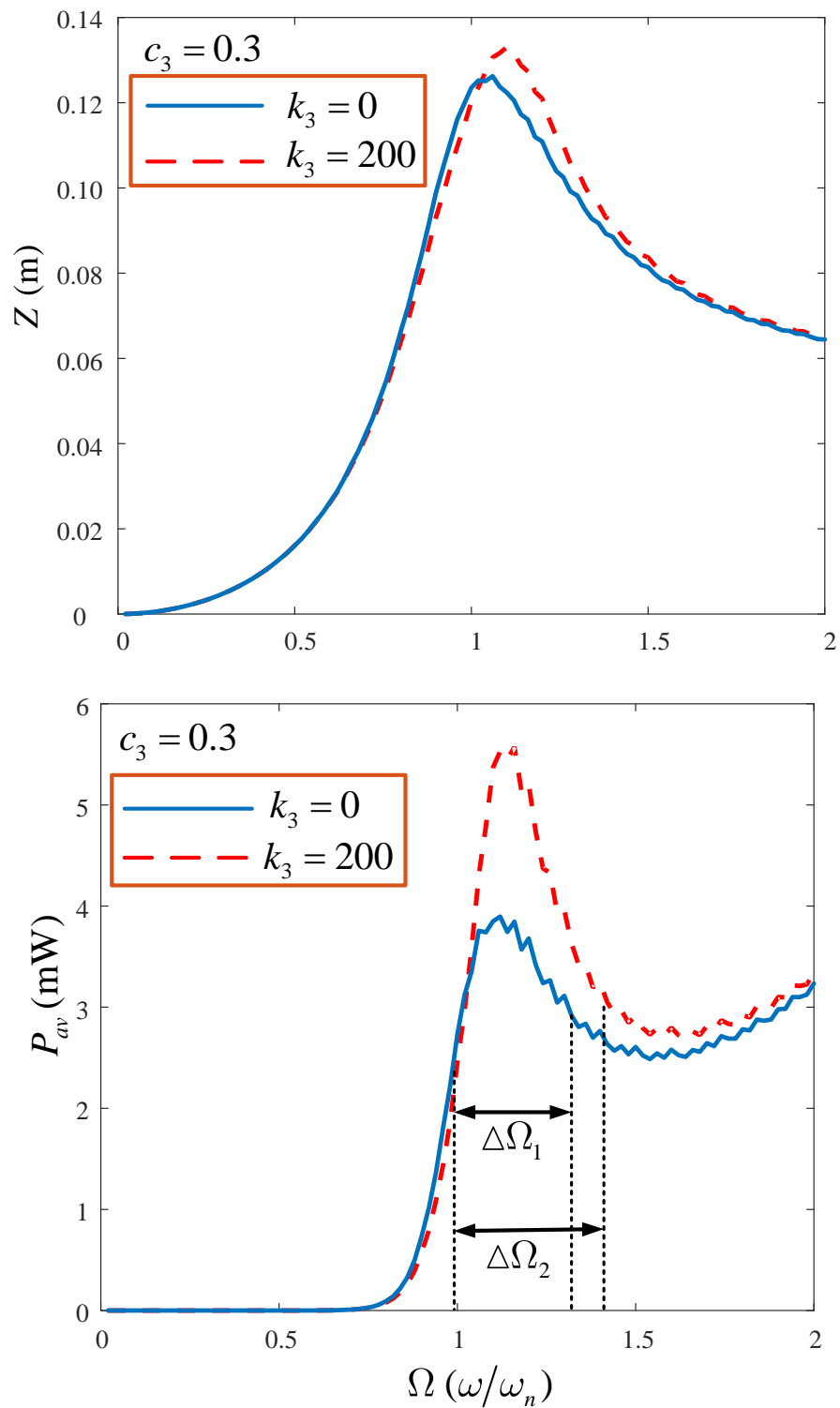


Figure 5.7: Effect of hardening stiffness on the output spectrum and average power of the nonlinear VEH system.

5.6.2 Optimisation of an unconstrained nonlinear VEH system

Using the OFRF representation of the average power as determined in Eq. (5.21), an optimisation problem can be formulated as;

$$\begin{aligned} \max_{c_3, k_3} & P_{av}(\omega_r, c_3, k_3) \\ \text{s.t.} & \begin{cases} 0.3 \leq c_3 \leq 0.4 \\ 0 \leq k_3 \leq 220 \end{cases} \end{aligned} \quad (5.22)$$

The solution to the unconstrained optimisation problem is simple and can be determined using the MATLAB *fminsearch* or *fmincon* function. Moreover, using the OFRF representations of Eqns. (5.18) and (5.21), the relationships between the design parameters, c_3 , k_3 and the output spectrum and average power can be established. These are presented in Figure 5.8 and Figure 5.9. It can be deduced from Figure 5.10 that the average power is significantly sensitive to the nonlinear stiffness characteristic, k_3 and less sensitive to the nonlinear damping characteristic, c_3 .

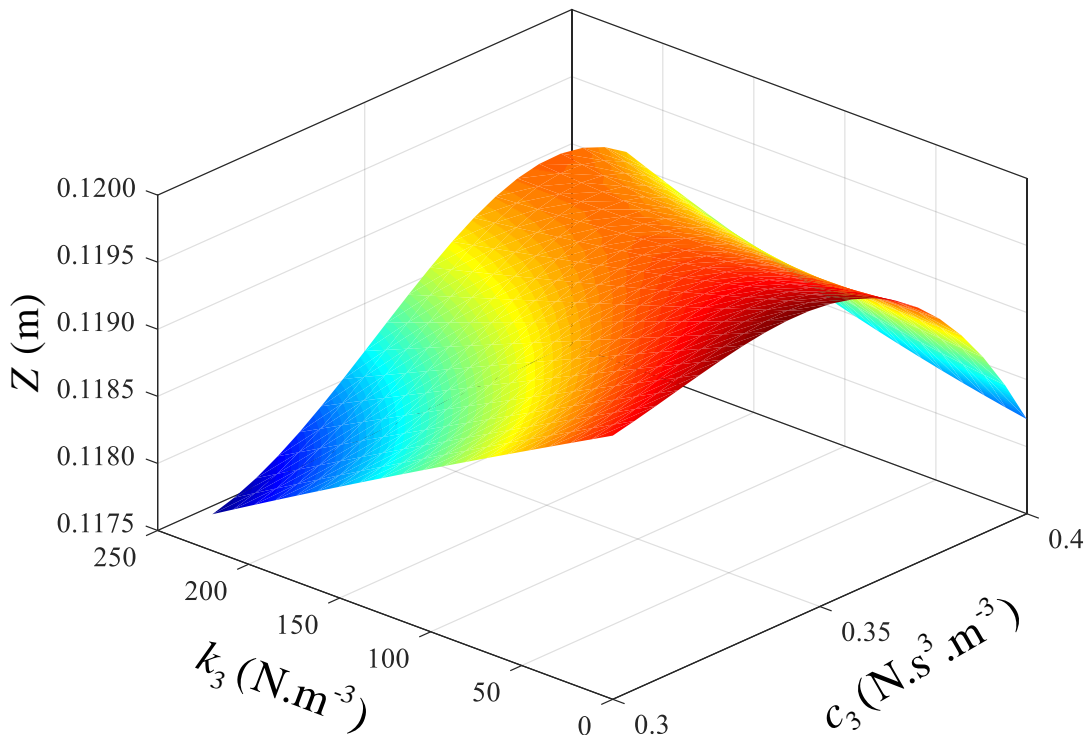


Figure 5.8: Output spectrum of system (5.2) versus a variation of c_3 and k_3 at $\Omega = 1$.

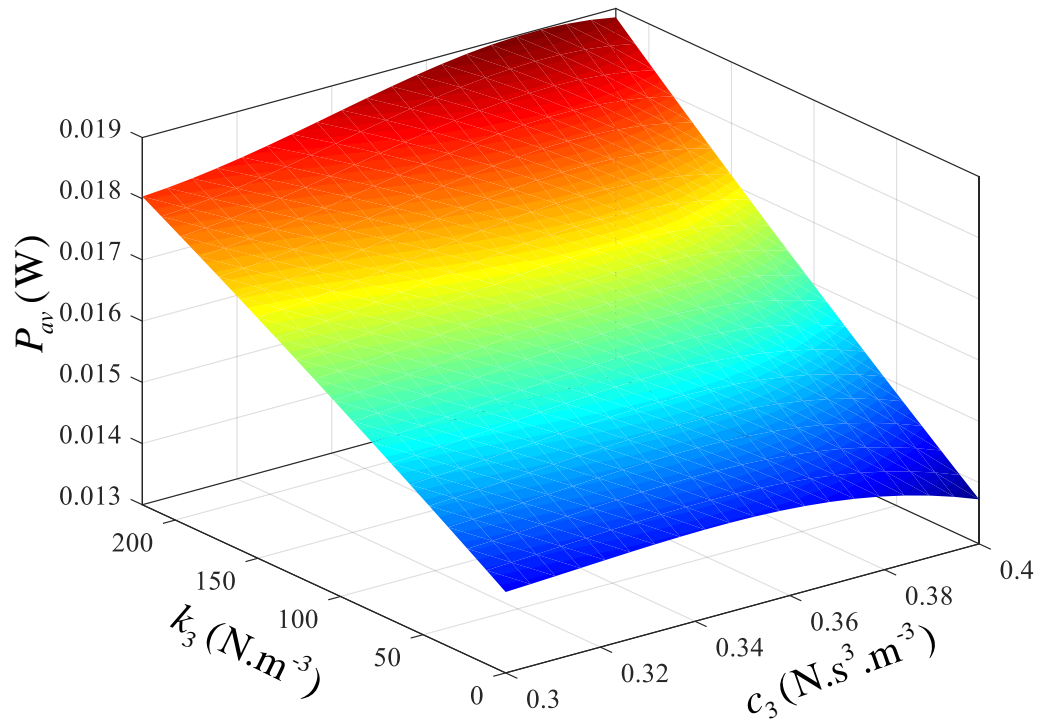


Figure 5.9: Average power of VEH versus a variation of c_3 and k_3 at $\Omega=1$.

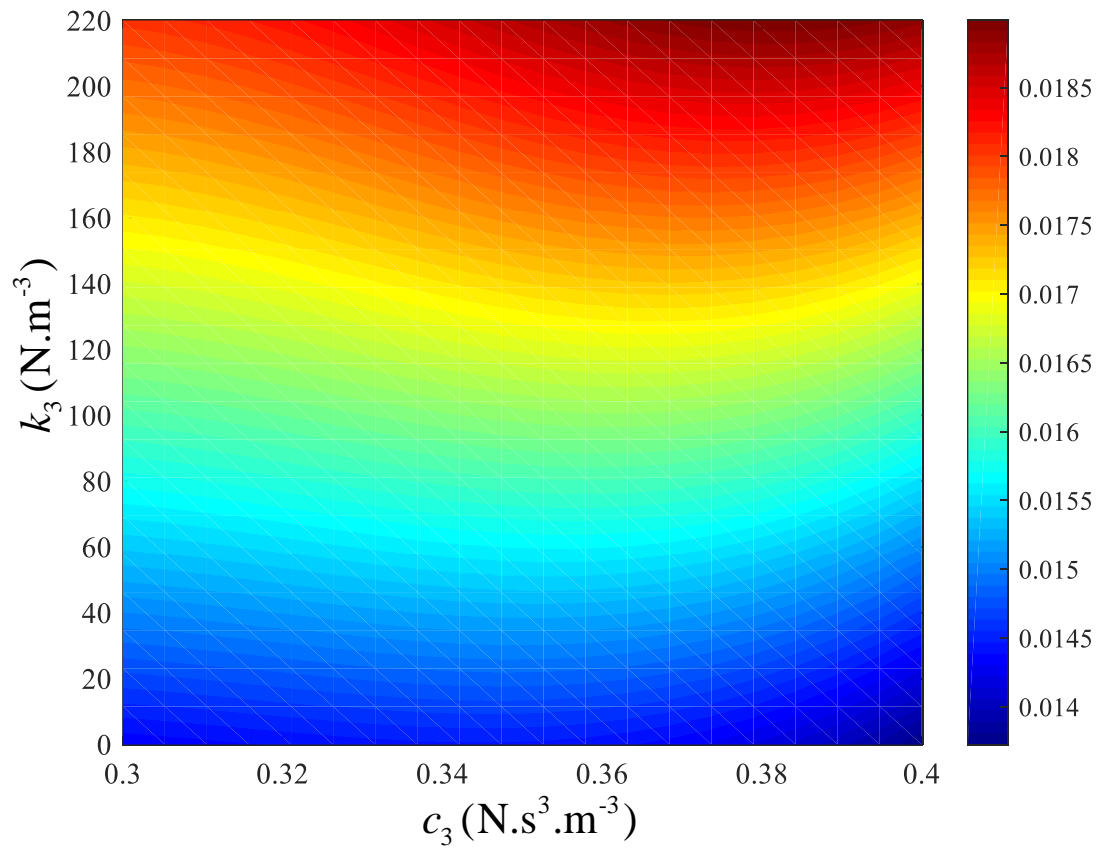


Figure 5.10: Y-X view of the Average power of VEH for a variation of c_3 and k_3 at $\Omega=1$.

5.7 CONCLUSIONS

In this study, the analysis and design of a vibration energy harvester with damping and stiffness nonlinearities was considered. Nonlinear stiffness was introduced into the mechanical subsystem of a vibration energy harvester with cubic damping to improve the operational frequency range (bandwidth) of the VEH system.

A polynomial representation of the system model, i.e. Output Frequency Response Function (OFRF), was derived. However, the OFRF representation was determined using the Associated Linear Equations (ALEs) decompositions of the system model. It was observed that by using the ALEs method, the number of numerical simulations needed to determine the OFRF of the actual system was considerably reduced. Subsequently, the ALE-generated OFRF representation of the actual system was verified to ensure it evidently represented the system output spectra.

The effect of hardening stiffness nonlinearity on the VEH system with cubic damping was investigated. The application of low-level excitation for this study ensured no jump phenomenon was exhibited. This is because the ALE and OFRF concepts are applicable only to a class of nonlinear systems stable at zero equilibrium and which can be described by a Volterra series model. The exhibition of a jump by the system model will nullify the suitability of the methods employed in this study.

The results obtained in this study show that the nonlinear stiffness characteristic extends the operational bandwidth as well as the harvested power of the VEH system hence improving its performance. Using the OFRF representation, optimal values of the VEH design parameters can be determined for any desired power level within and beyond the design range. Future studies will focus on the design of VEH systems with damping and stiffness nonlinearities subject to mass-displacement constraints inherent in practical VEH systems.

The key contribution in this work, and which is the first attempt in literature, to the best of the authors' knowledge, a VEH device is investigated with the integration of both damping and stiffness nonlinearities. Furthermore, a novel application of the OFRF method was employed. However, in this study, the OFRF model was derived using the ALE decompositions of the actual system model.

Chapter 6: Analysis, design and optimisation of a dual-function vibration isolation and energy harvesting system

6.1 INTRODUCTION

In Chapter 3, a vibration isolation system was considered as the system of interest where key system nonlinear parameters were designed to meet a desired specification. In Chapters 4 and 5, vibration energy harvesters were the focus of study as different nonlinearities were integrated into the system models in order to improve the performance of the systems. In this chapter, a dual-function system is considered. A dual-purpose vibration isolation and energy harvesting (VI-EH) system is studied. The primary function of the system is vibration isolation while the secondary function is energy harvesting. Dr Hamzeh Bardaweel and Mehdi Mofidian, of the Institute for Manufacturing, Louisiana Tech University, USA, are collaborators to this study.

Recently, there has been an increasing attention in the development of dual-function systems that are capable of both vibration isolation and energy harvesting [138], [187]–[194]. This attention is motivated by the continuous improvement in electronics manufacturing which led to deployment of onboard low-power devices and gadgets [195]–[198]. For instance, equipment and structures, such as highway bridges and moving vehicles have onboard sensing units are currently installed on them to monitor operating conditions such as temperature, pressure, stress, strain, and humidity [199], [200]. Undesired destructive vibrations are also present in these structures as a result of their dynamic interaction and engagement with the surroundings. While it is desirable to suppress or attenuate these vibrations, nonetheless, these oscillations represent free form of kinetic energy. Thus, creating dual-function systems that are capable of isolating undesired vibrations while simultaneously converting some of the kinetic energy contained in these oscillations into electric power has been sought [138], [187]–[194]. To this end, Li et al. developed a mechanical metamaterial dual-function system comprising a square array

of free-standing piezoelectric cantilevers to simultaneously harvest energy and isolate undesired vibrations [191]. Hu et al. presented an analytical model of a dual-function acoustic-elastic metamaterial structure [201]. The proposed structure exhibited a stop band gap for wave transmission while simultaneously achieving energy harvesting by integrating the metamaterial with piezoelectric energy-harvesting element. Davis and McDowell proposed a passive vibration isolation device that harvests energy using post-buckled beam and piezoelectric elements [190]. Approximately, $0.36 \mu\text{W}$ electric power was harvested at 2% transmissibility. Li et al. proposed an energy harvesting shock damper system to attenuate vibrations transferred from vehicle-road interaction while simultaneously generate power using a unidirectional rotational mechanism using a mechanical motion rectifier rather than an electrical rectifier to generate DC current [202]. Similarly, Ali and Adhikari studied, theoretically, the performance of regenerative vibration absorber device supplemented with a piezoelectric stack for power recovery [188]. In Ref. [203] the feasibility of integrating vibration absorber with piezoelectric stack for power generation under random excitations was investigated using probabilistic linear random vibration theory. Results from this theoretical study showed that the recovered power increases with increase in the mass of structure. Moreover, a dual-function device was developed to isolate micro vibrations and harvest energy from micro-jitters for space applications [138]. The dual-function device was able to isolate the desired mass and recovered $5.84 \mu\text{W}$ of vibration energy into electric energy. Also, a semi-active energy harvesting vibration suppression system using piezoelectric platform was proposed [204]. Additionally, in previous work Mofidian and Bardaweel introduced a novel vibration isolation energy harvesting (VI-EH) system using a combination of magnetic and mechanical springs, and viscous and magnetic dampers [194]. While the study was focused on fabrication and proof-of-concept, experimental results from their work showed that the fabricated device was able to attenuate oscillations higher than 12.5 [Hz] and recover 0.115 [mW] at 9.81 m.s^{-2} , respectively. This study, which is a collaboration with the authors of [194], is an extension of the work in [194].

The abovementioned discussion reveals the growing interest and the rising need for dual-function VI-EH systems. Therefore, there is a necessity to investigate the design aspects and perform optimisation process for dual-function VI-EH systems. This is especially true since these systems are required to perform two functions

simultaneously: Vibration isolation (primary function) and energy harvesting (secondary function). Thus, an optimisation process is a mandate to ensure that maximum amount of energy contained in these oscillations is recovered without jeopardizing the ability of the system to prevent these oscillations from traveling through the structure and causing serious damage. Therefore, this work is focused on optimisation of a representative dual-function VI-EH system using a frequency-based approach known as Output Frequency Response Function (OFRF). Model formulation using OFRF is described in Section. 6.2; an analysis of the VI-EH System is presented in Section 6.3; experimental model validation is presented in Section. 6.4; System design and optimisation process are presented in Section. 6.5; effects of load resistance on the performance metrics are demonstrated in Section 6.6; then finally some concluding remarks are provided in Section 6.7.

6.2 MODEL FORMULATION

Dynamic Model formulation and performance metrics for the VI-EH system are described in this section. Additionally, the OFRF method is used to analyse the dynamic performances of the VI-EH system. Relative displacement transmissibility, absolute displacement transmissibility, energy conversion efficiency, input power, and output power needed for system optimisation are introduced and formulated using the OFRF method.

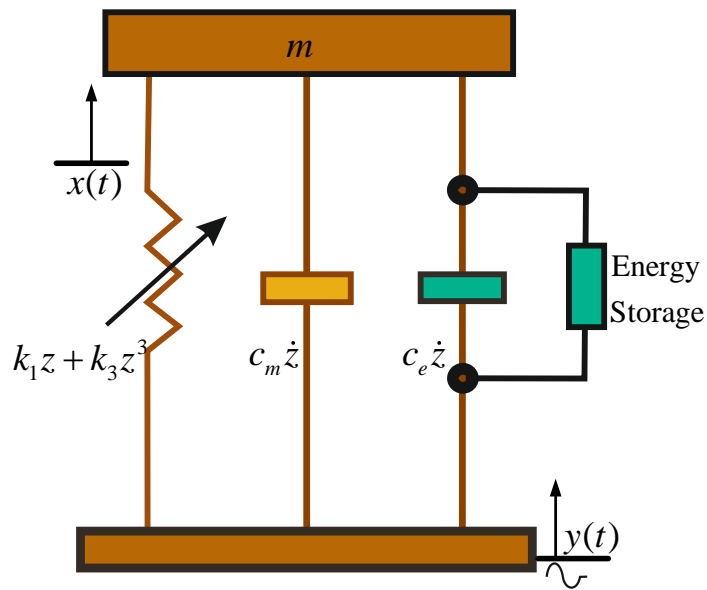


Figure 6.1: Model schematic of the dual-function VI-EH system.

Figure 6.1 shows a representative model of a dual-function VI-EH system. The system represents a single-degree-of-freedom (SDOF) with mass, m connected to a linear damper of damping coefficient c_1 and nonlinear spring characterized by linear, k_1 and nonlinear, k_3 stiffness coefficients, respectively. It is assumed that lateral vibrations are absent and, therefore, the effective mass, m , is displaced vertically in response to ground excitation, $y(t)$. Therefore, the equation of motion of the moving mass is given by:

$$m\ddot{z} + c_1\dot{z} + k_1z + k_3z^3 = -m\ddot{y} \quad (6.1)$$

where $z = x - y$, and $c_1 = c_e + c_m$ is the total magnetic and mechanical damping in the system, i.e. c_e and c_m respectively. For a ground harmonic excitation input, i.e. $y = Y \sin(\omega t)$, Eq. (6.1) becomes

$$m\ddot{z} + c_1\dot{z} + k_1z + k_3z^3 = m\omega^2 Y \sin(\omega t) \quad (6.2)$$

For the dual-function VI-EH system, displacement transmissibility, T_a and energy conversion efficiency, η_e are the two main performance metrics sought in this work. Displacement transmissibility is a measure of the effectiveness of vibration isolation and relates the amount of oscillations transmitted from the source of excitation to the isolated mass, i.e. $T_a = \left| \frac{Z + Y}{Y} \right|$. The average amount of mechanical power input to the VI-EH system from ground harmonic excitation is given as [205]–[208].

$$P_{in} = \frac{1}{\pi} m\omega^3 Y^2 \quad (6.3)$$

Typically, energy conversion is performed using either electrostatic [117], [209], piezoelectric [210], or electromagnetic transducers [211], [212]. Assuming electromagnetic transduction unit with coil resistance, R_C , is responsible for energy harvesting in the VI-EH system, the average output (harvested) power across a load resistance, R_L is given by

$$P_{out} = \frac{1}{2} \cdot \left[\frac{k_t \omega Z}{R_C + R_L} \right]^2 \cdot R_L \quad (6.4)$$

where $k_t = BNI$ and l is the length of the coil per turn, N is the number of coil turns, and B is the average magnetic flux density in the air gap between the moving magnet mass and the coil. Considering the average output power, P_{out} of the VI-EH system when subject to ground harmonic excitation with average input mechanical power of P_{in} , the energy conversion efficiency η_e of the VI-EH system is, then, given by

$$\eta_e (\%) = \frac{P_{out}}{P_{in}} \times 100 \quad (6.5)$$

Next section describes the OFRF approach used to analyse the dynamic model of the VI-EH system (6.2). The OFRF representation of the relative displacement transmissibility, absolute displacement transmissibility, average output power, and energy conversion efficiency are derived, respectively.

6.3 VI-EH SYSTEM ANALYSIS

In this section, the OFRF method is used in the analytical study of the VI-EH system described by Eq. (6.2) which is representative of the Duffing equation. Dynamic model of the system (6.2) is a special case of Eq. (2.4) with $L = 2$ and $M = 3$ with system parameters obtained as $c_{10}(2) = m$, $c_{10}(1) = c_1$, $c_{10}(0) = k_1$, $c_{30}(000) = k_3$, $c_{01}(0) = -m\omega^2 Y$, else $c_{p,m-p} = 0$. Applying the algorithm for obtaining the OFRF structure (monomials) as presented in Eq. (2.8) and (2.9) to system (6.2) up to 7th-order i.e. $N = 15$, yields the following monomials;

$$\mathfrak{M} = \bigcup_{n=1}^N M_n = [1, k_3, k_3^2, k_3^3, k_3^4, k_3^5, k_3^6, k_3^7] \quad (6.6)$$

Using the method developed and discussed in [31], [85], [148], the frequency function vector $\Phi(j\omega)$ is computed, with a training set $k_3 = [0:0.1:1.4] \times 10^6$ as

$$\Phi(j\omega) = \begin{bmatrix} \phi_0(j\omega) \\ \phi_1(j\omega) \\ \vdots \\ \phi_6(j\omega) \\ \phi_7(j\omega) \end{bmatrix} = \psi^T \psi^{-1} \psi^T \cdot \begin{bmatrix} Z(j\omega)|_{k_3(1)} \\ Z(j\omega)|_{k_3(2)} \\ \vdots \\ Z(j\omega)|_{k_3(14)} \\ Z(j\omega)|_{k_3(15)} \end{bmatrix} \quad (6.7)$$

where

$$\psi = \begin{bmatrix} 1 & k_3(1) & k_3^2(1) & \cdots & k_3^6(1) & k_3^7(1) \\ 1 & k_3(2) & k_3^2(2) & \cdots & k_3^6(2) & k_3^7(2) \\ \vdots & \vdots & \vdots & \ddots & \vdots & \vdots \\ 1 & k_3(15) & k_3^2(15) & \cdots & k_3^6(15) & k_3^7(15) \end{bmatrix} \quad (6.8)$$

and $Z(j\omega)|_{k_3(i)}$ represents the output spectrum of the system when $k_3 = k_3(i) = (i-1) \times 10^5$.

Therefore, the OFRF of system (6.2) derived for each (four) excitation level, $s = 0.25\text{g}, 0.5\text{g}, 0.75\text{g}$ and 1g [m/s^2], is given as

$$\begin{cases} Z^{(s)}(j\omega, k_3) = \phi_0^{(s)}(j\omega) + \phi_1^{(s)}(j\omega)k_3 + \phi_2^{(s)}(j\omega)k_3^2 + \phi_3^{(s)}(j\omega)k_3^3 + \cdots + \phi_6^{(s)}(j\omega)k_3^6 + \phi_7^{(s)}(j\omega)k_3^7 \\ Z^{(s)}(j\omega, k_3) = \sum_{r=0}^R \phi_r^{(s)}(j\omega)k_3^r \text{ where } R = 7 \text{ and } s = 0.25\text{g}, 0.5\text{g}, 0.75\text{g} \text{ and } 1\text{g} [\text{m/s}^2] \end{cases} \quad (6.9)$$

where $\phi_r^{(s)}(j\omega)$ are the frequency functions dependent on the s th system input level and linear characteristic parameters, c_1 and k_1 . Moreover, the squared magnitudes of the output response of Eq. (6.9) are described as in [85]

$$\begin{cases} |Z^{(s)}(j\omega, k_3)|^2 = Z^{(s)}(j\omega, k_3) \cdot Z^{(s)}(-j\omega, k_3) = \left(\sum_{r=0}^R \phi_r^{(s)}(j\omega)k_3^r \right) \left(\sum_{r=0}^R \phi_r^{(s)}(-j\omega)k_3^r \right) \\ = \phi_0^{(s)}\phi_0^{(s)*} + \sum_{t=1}^{\infty} \left(k_3^t \sum_{\tau=0}^t \phi_{\tau}^{(s)}\phi_{t-\tau}^{(s)*} \right) \\ = \delta_0^{(s)} + \delta_1^{(s)}k_3 + \delta_2^{(s)}k_3^2 + \cdots + \delta_{13}^{(s)}k_3^{13} + \delta_{14}^{(s)}k_3^{14} \\ = \sum_{r=0}^{\tilde{R}} \delta_r^{(s)}(\omega)k_3^r \quad , \text{ where } \tilde{R} = 14 \text{ and } s = 0.25\text{g}, 0.5\text{g}, 0.75\text{g} \text{ and } 1\text{g} [\text{m/s}^2] \end{cases} \quad (6.10)$$

Substituting Eq. (6.10) in Eq. (6.4) yields

$$\left\{ \begin{aligned} P_{out}^{(s)}(\omega, k_3) &= \frac{1}{2R_L} \cdot \left[\frac{k_t \omega R_L}{R_C + R_L} \right]^2 \cdot |Z^{(s)}|^2 \\ &= \frac{1}{2R_L} \cdot \left[\frac{k_t \omega R_L}{R_C + R_L} \right]^2 \cdot \left[\sum_{r=0}^{\tilde{R}} \delta_r^{(s)}(\omega) k_3^r \right] \\ &= \alpha(\omega) \cdot \left[\sum_{r=0}^{\tilde{R}} \delta_r^{(s)}(\omega) k_3^r \right] \quad \text{where } \alpha(\omega) = \frac{1}{2R_L} \cdot \left[\frac{k_t \omega R_L}{R_C + R_L} \right]^2 \end{aligned} \right. \quad (6.11)$$

Similarly, substituting Eq. (6.3) and Eq. (6.11) in Eq. (6.5) yields

$$\left\{ \begin{aligned} \eta_e^{(s)}(\omega, k_3) &= \frac{\frac{1}{2R_L} \cdot \left[\frac{k_t \omega R_L}{R_C + R_L} \right]^2 \cdot \left[\sum_{r=0}^{\tilde{R}} \delta_r^{(s)}(\omega) k_3^{\tilde{r}} \right]}{\frac{1}{\pi} m \omega^3 Y^2} \\ &= \frac{\pi \omega}{2mR_L \omega^2 Y^2} \cdot \left[\frac{k_t \omega R_L}{R_C + R_L} \right]^2 \cdot \left[\sum_{r=0}^{\tilde{R}} \delta_r^{(s)}(\omega) k_3^{\tilde{r}} \right] \\ &= \lambda(\omega) \cdot \left[\sum_{r=0}^{\tilde{R}} \delta_r^{(s)}(\omega) k_3^{\tilde{r}} \right] \quad \text{where } \lambda(\omega) = \frac{\pi \omega}{2mR_L \omega^2 Y^2} \cdot \left[\frac{k_t \omega R_L}{R_C + R_L} \right]^2 \end{aligned} \right. \quad (6.12)$$

From Eq. (6.11) and Eq. (6.12), the following representations for P_{out} and η_e can be made.

$$\left\{ \begin{aligned} P_{out}^{(s)}(\omega, k_3) &= \sum_{r=0}^{\tilde{R}} \varphi_r^{(s)}(\omega) \cdot k_3^r \quad \text{where } \varphi_r^{(s)}(\omega) = \alpha(\omega) \cdot \delta_r^{(s)}(\omega) \\ \eta_e^{(s)}(\omega, k_3) &= \sum_{r=0}^{\tilde{R}} \beta_r^{(s)}(\omega) k_3^{\tilde{r}} \quad \text{where } \beta_r^{(s)}(\omega) = \lambda(\omega) \cdot \delta_r^{(s)}(\omega) \end{aligned} \right. \quad (6.13)$$

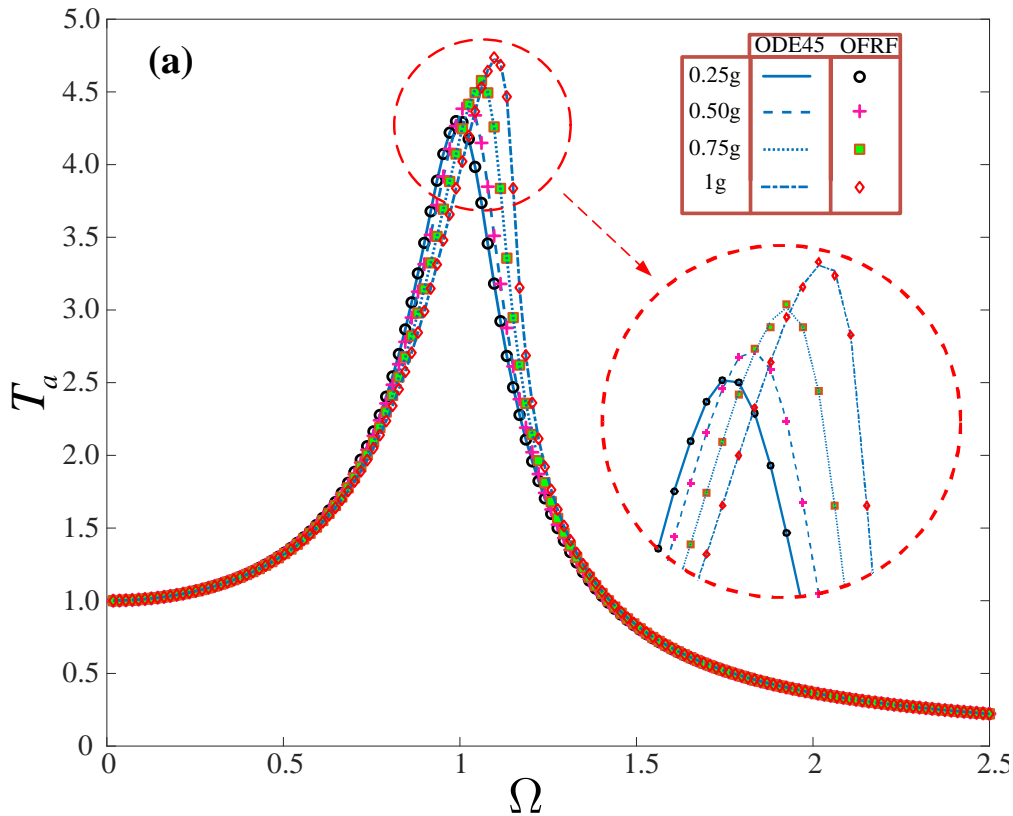
Equation (6.13) shows the OFRF representation for the average output power, P_{out} and the energy conversion efficiency, η_e of the VI-EH system (6.2), respectively for each acceleration level, s . The corresponding OFRF for the absolute displacement transmissibility, T_a , under excitation s is then given as

$$T_a^{(s)}(\omega, k_3) = \sum_{r=0}^R \rho_r^{(s)}(\omega) \cdot k_3^r \quad (6.14)$$

where $\varphi_r^{(s)}(\omega)$, $\beta_r^{(s)}(\omega)$ and $\rho_r^{(s)}(\omega)$ are frequency functions dependent on the system input and linear characteristic parameters and ω is the driving frequency of interest.

It should be noted that the OFRF representation of the system performance indices of interest is each unique for one of the four specific input acceleration levels of $s = 0.25g, 0.5g, 0.75g$ and $1g$ [m/s^2] considered in this work.

The OFRF is a polynomial representation of the system performance. A comparison of the OFRF results with that obtained using the *Runge-Kutta 4* algorithm (ODE45 in MATLAB) over the system parameter values beyond the OFRF training range (in this case, $k_3 = 1.5 \times 10^6$ N m^{-3}) is shown in Figure 6.2(a-c) indicating that the OFRF provides a very good representation for the actual system performance.



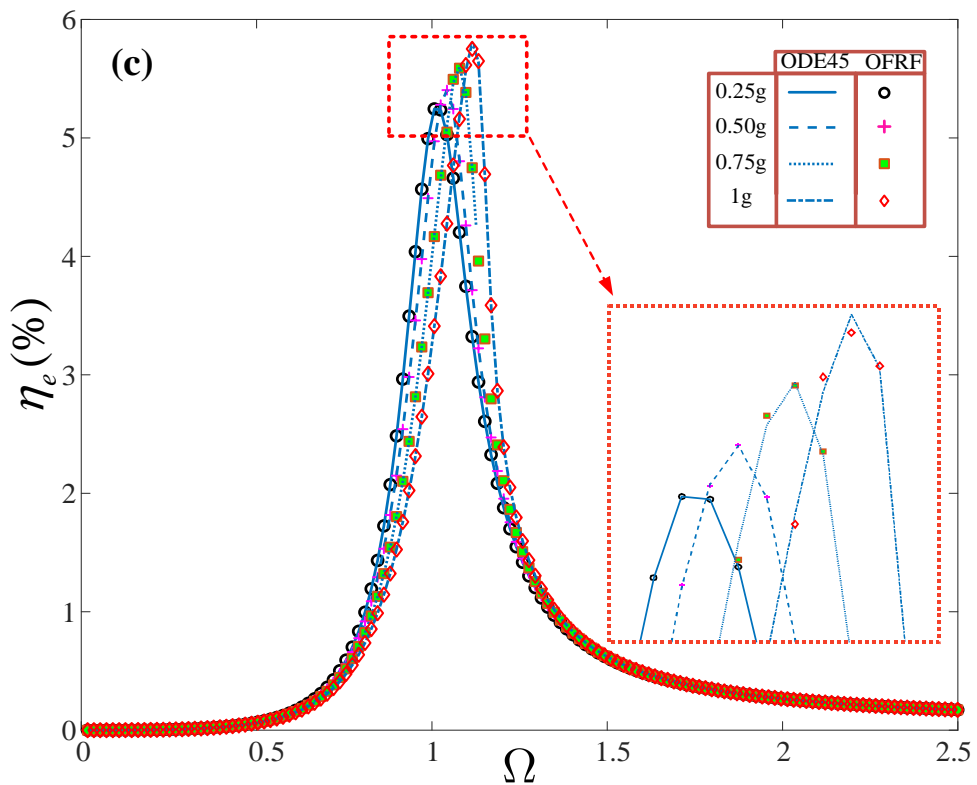
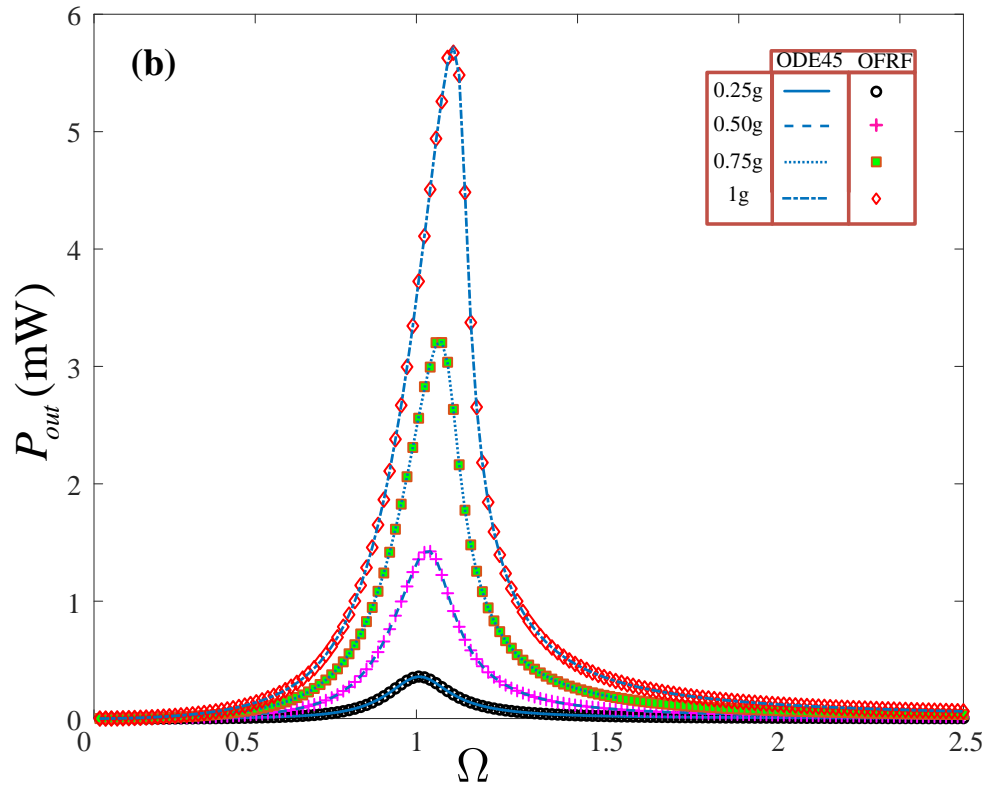


Figure 6.2: Comparison between the OFRF analytical and Runge-Kutta numerical solution: a) Transmissibility, b) Output power, and c) Energy conversion efficiency at four acceleration levels 0.25g, 0.50g, 0.75g, and 1.0g [m.s⁻²].

6.4 EXPERIMENT FOR MODEL VALIDATION

This section describes the experimental work carried out by the collaborators, to obtain necessary design parameters that can be used as a starting point to perform the optimisation process for the VI-EH system. It should be noted that the experiment carried out was for model validation only.

6.4.1 Device

Figure 6.3 shows the representative dual-function VI-EH device fabricated and adopted in this work. A group of magnets, an elastic mechanical spring, coils, and air holes constitute the major components of the adopted design. The three magnets are arranged in a repulsive manner causing the solid magnet to levitate between the top and bottom fixed ring magnets. The mechanical spring guides the movement of the levitated magnet and prevents it from realigning itself with the top and bottom fixed ring magnets. A rod is used to connect the mechanical and magnetic springs to the isolated mass as shown in Figure 6.3.

External disturbance of the system causes the levitated magnet to move vertically. Viscous damping is then the result of air being pushed through the air holes. Energy harvesting is achieved using stationary coils fixed around the rest position of the levitated magnet. As the levitated magnet moves, voltage is induced in the coil. Thus, the kinetic energy from the oscillations is converted into electric energy. The coils not only serve as a mechanism for power extraction but also introduce additional damping force as a result of eddy currents induced in the coil because of variation in magnetic flux as the levitated magnet is displaced [213]. Thus, the dual-functionality of the device is achieved through a combination of elastic and magnetic springs as well as viscous damping due to airflow, and magnetically-induced damping due to levitated magnet movement inside the coil. The damping (viscous and magnetic) and stiffness (mechanical and magnetic spring) form the platform for vibration isolation. Simultaneously, the levitated magnet movement inside the coil forms the base for converting the kinetic energy of vibrations into electric charge.

This design was recently introduced by Mofidian and Bardaweel [194]. This representative dual-function design is adopted because it offers unique features that are essential for vibration isolation and energy harvesting. Of these unique features is the use of magnetic components to achieve its dual-functionality. For example, an

essential limitation of piezoelectric is their inherently large internal resistance [214]. Consequently, large load resistance is required to obtain optimum power transfer.

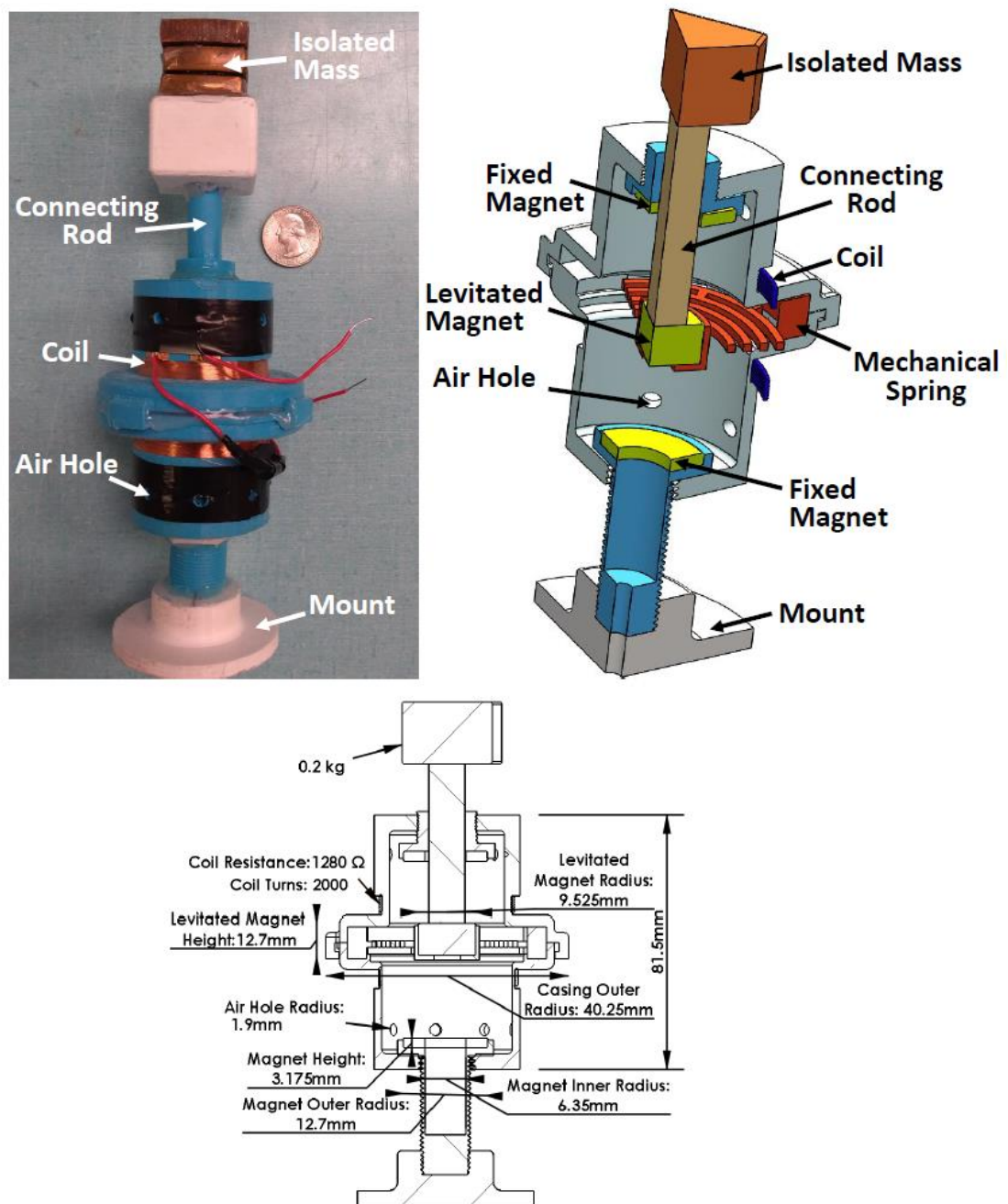


Figure 6.3: The representative dual-function VI-EH device fabricated and adopted in this work: a) Fully fabricated and assembled VI-EH device, b) Cross-sectional view of the VI-EH device, and c) 2D sketch of the VI-EH device with detailed geometries and dimensions.

This results in very small output currents that are well below the threshold of currents required to operate onboard sensors, i.e. 10-50 mA [214]. Unlike electrostatic and piezoelectric-based devices, electromagnetic-type devices have significantly lower

output impedance [215]. This results in no further required impedance matching at the output stage and, therefore, simpler circuitry. On the other hand, magnetic field-based devices offer larger energy densities [216]. In addition, electromagnetic energy harvesters do not need external voltage supply necessary for electrostatic energy harvesters. The mass of the magnet itself also reduces the resonant frequency of the dual-function device which further enables low frequency specialization [217]. Therefore, the use of electromagnetic energy harvesting unit, instead of piezoelectric, in the dual-function device makes it most suitable for real-world applications [218], [219].

Additive manufacturing was used to fabricate the exterior casing and the mechanical spring using Polylactic acid (PLA) thermoplastic filament and Thermoplastic Poly-Urethane (TPU) rubber-like filament, respectively. Neodymium iron boron (NdFeB) magnets were used to structure the magnetic spring. The stationary coil was 40 AWG copper coil positioned around the equilibrium position of the levitated magnet. Detailed geometry, dimensions, and design specifications are shown in Figure 6.3c.

6.4.2 Determination of system parameters

Essential for model validation and optimisation process of the representative VI-EH system shown in Figure 6.3 is the determination of system parameters including, k_1 , k_3 , c_1 etc. Figure 6.4 shows the experiment setup used to estimate restoring forces of both mechanical and magnetic springs. A test stand (SHIMPO FGS-250W), displacement sensor (KEYENCE IL-100), digital force sensor (SHIMPO FG-3006), data acquisition system (NI myDAQ), power supply, and a PC constitute the experiment setup used to measure restoring forces. Figure 6.5 shows the restoring forces of both mechanical and magnetic springs measured using the experiment setup shown in Figure 6.4. The total restoring force was then fitted to a third order polynomial of the form $k_1 z + k_3 z^3$ and the stiffness coefficients, k_1 and k_3 were then extracted. Natural frequency, ω_n and total damping, c_1 , of the system were also estimated. This was done by holding the dual-function VI-EH device firmly in place, bringing it to a predetermined height, and then releasing it. In this experiment no external excitation was applied, and therefore, the dual-purpose device acted as damped un-driven oscillator. The logarithmic decrement method [115], [220], [221]

was then used to estimate the total damping of the system, c_1 , and natural frequency, ω_n . Note that the logarithmic decrement method is only valid for linear systems. However, the nonlinear system in this study was approximated as a linear system for small displacements and acceleration levels. Then the logarithmic decrement method was used to estimate the damping. Measured system parameters of the fabricated dual-function VI-EH device and properties are summarized in Table 6.1. These measured values were then used in model validation and as the starting points of the system optimisation process.

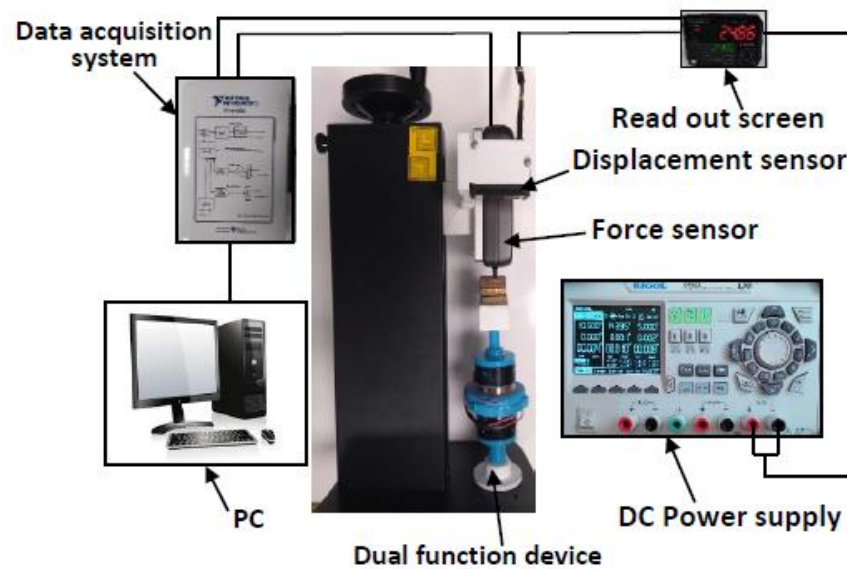


Figure 6.4: Experiment setup used to estimate restoring forces of the VI-EH device.

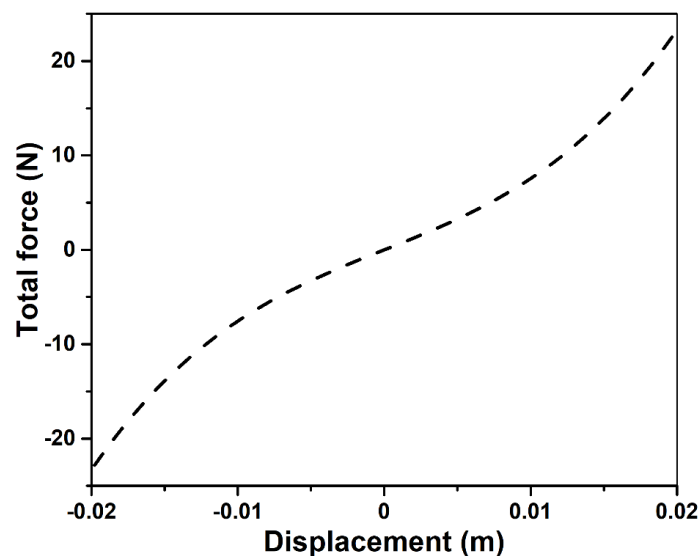


Figure 6.5: Measured total restoring force of the VI-EH device.

Table 6.1: Systems parameters and properties of the fabricated multi-function VI-EH device.

Parameter	Properties
Coil resistance (R_C) [Ω]	1280
Load resistance (R_L) [Ω]	1280
Coil turns	2000
Coil material	Copper, 40 AWG
Isolated mass (kg)	0.2
Mechanical spring material	Thermoplastic poly-Urethane (TPU)
k_3 [N m^{-3}]	1.368e+06
k_1 [N m^{-1}]	618
c_1 [$\text{N s}^{-1} \text{m}^{-1}$]	2.7
f_n [Hz]	8.85
B [T]	0.0286

6.4.3 Model validation against measured data

In order to validate the developed model (Section 6.2) both displacement transmissibility, T_a and energy conversion efficiency, η_e of the dual-function device were measured simultaneously. The apparatus used for these tests is shown in Figure 6.6 and consisted of a shaker table (VT-500, SENTEK DYNAMICS), power amplifier (LA-800, SENTEK DYNAMICS), vibration controller (S81B-P02, SENTEK DYNAMICS), two accelerometers (PCB333B30 model, PCB Piezotronics), data acquisition system (NI myDAQ), and a PC. The dual-function device was firmly fixed on the shaker table top and driven at accelerations of $0.5g$ [m/s^2]. The voltage output from the dual-function device across load resistance, R_L , and the acceleration level transmitted to the isolated mass were simultaneously measured. Induced voltage was measured across a load resistance using a decade box (GLOBAL SPECIALTIES RDB-10) and extracted power, P_{out} was then estimated. It should be noted that decade boxes are test instruments that use a series of resistors, capacitors, or inductors to simulate very specific electrical values.

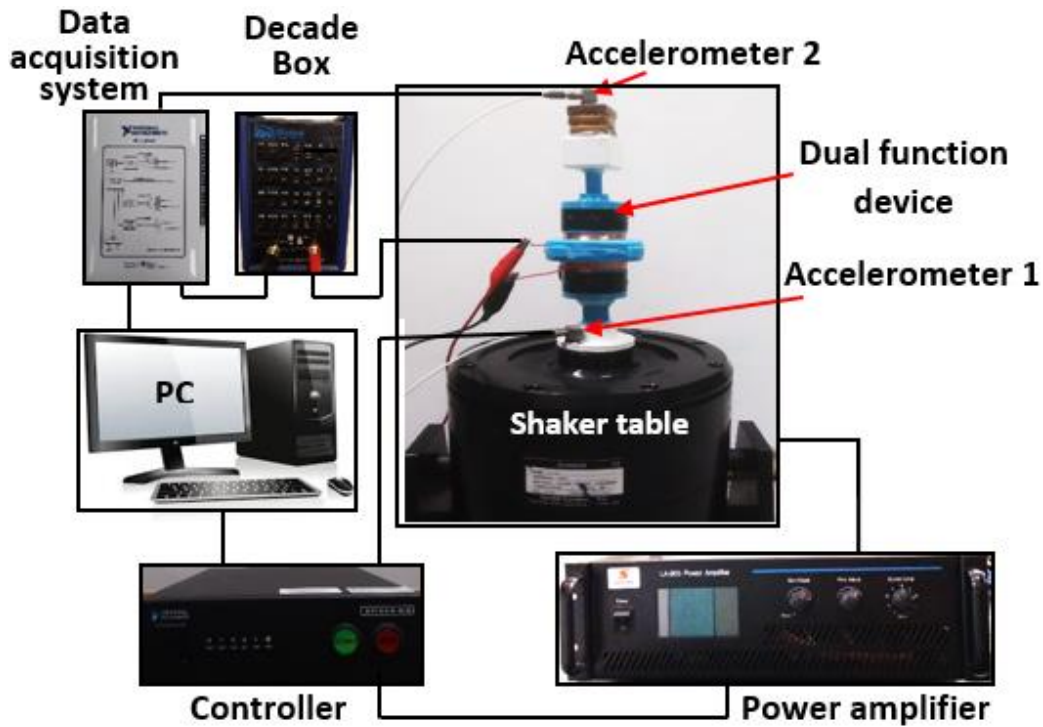


Figure 6.6: Apparatus used for dynamic characterization of the VI-EH device.

Measured displacement transmissibility, and power extracted by the dual-function device are shown in Figure 6.7 and Figure 6.8, respectively. Additionally, model predictions are compared to measured data as shown in Figure 6.7 and Figure 6.8. Results reveal good agreement between experimental data and model simulated results. Figure 6.7 demonstrates that transmissibility of the dual-function device drops to less than unity, i.e. $T_a < 1$ at corresponding frequencies, $\omega \cong 79 \text{ rad.s}^{-1}$ when loading level is $0.5g$ [m/s^2]. The ability of the dual-function device to extract electric power from the ground excitation during the dynamic operation is also evident in Figure 6.8. The power extracted during the dynamic operation of the dual-function device was measured across a load resistance, $R_L = 1280$ [Ω]. The power produced by the device when transmissibility dropped to unity, i.e. $T_a = 1$ was approximately 0.34 [mW] at $0.5g$ [m/s^2]. This demonstrates the ability of the dual-function device to simultaneously isolate the mass and scavenge kinetic energy from these oscillations. Optimisation process of the VI-EH system will be discussed next in Section 6.5.

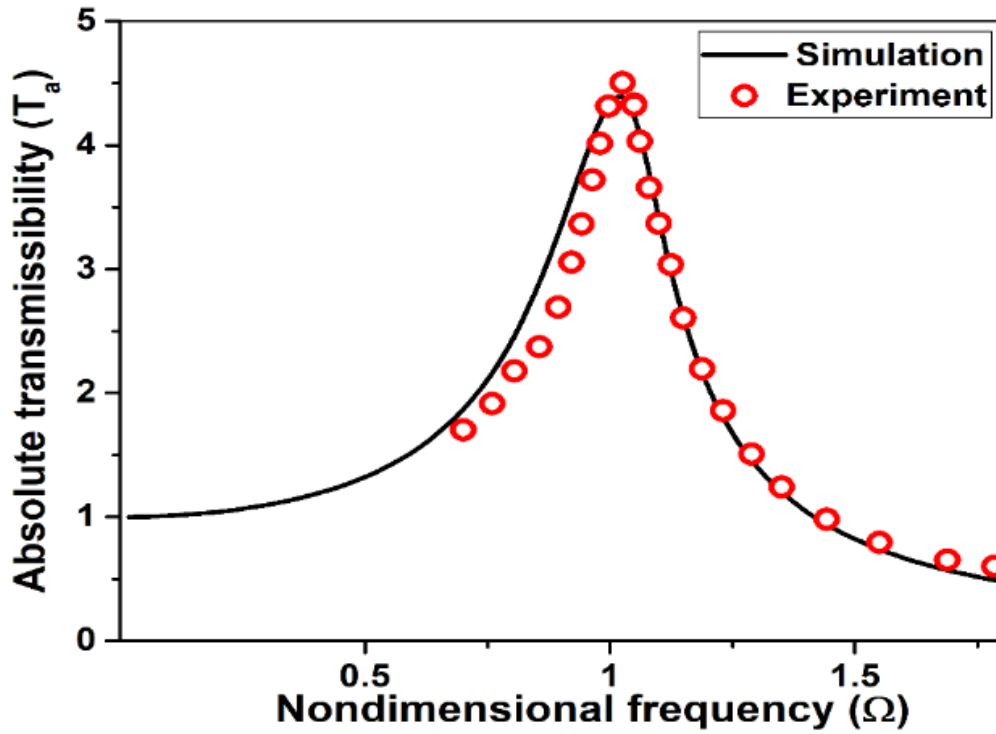


Figure 6.7: Measured and modelled simulated displacement transmissibility of the VI-EH device at $0.5g$ [$m.s^{-2}$].

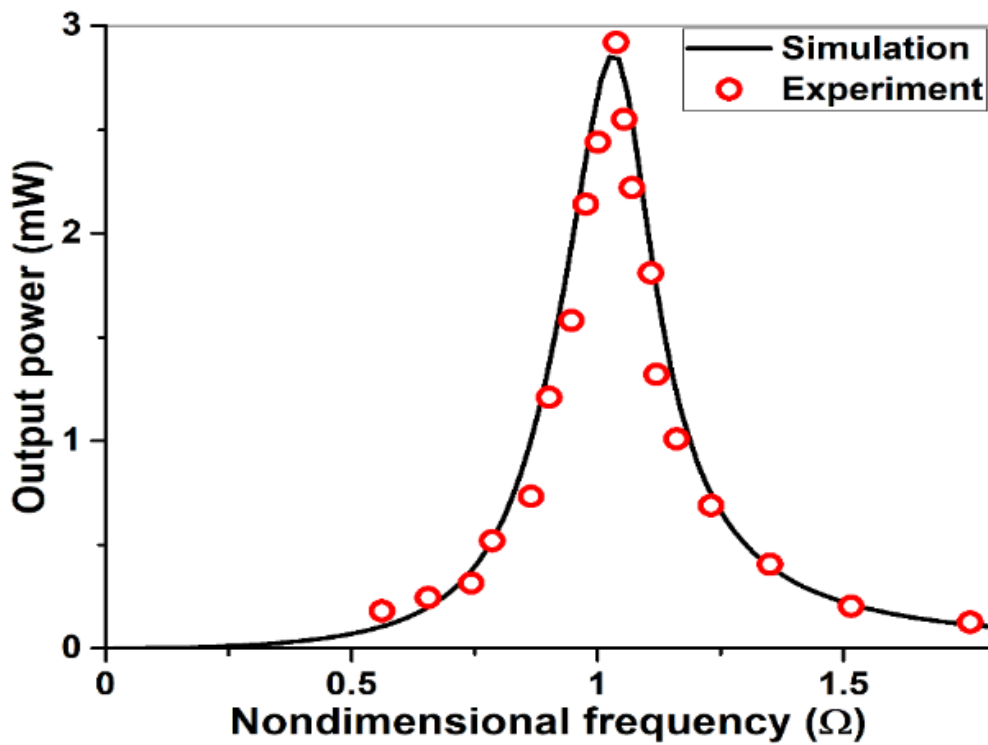
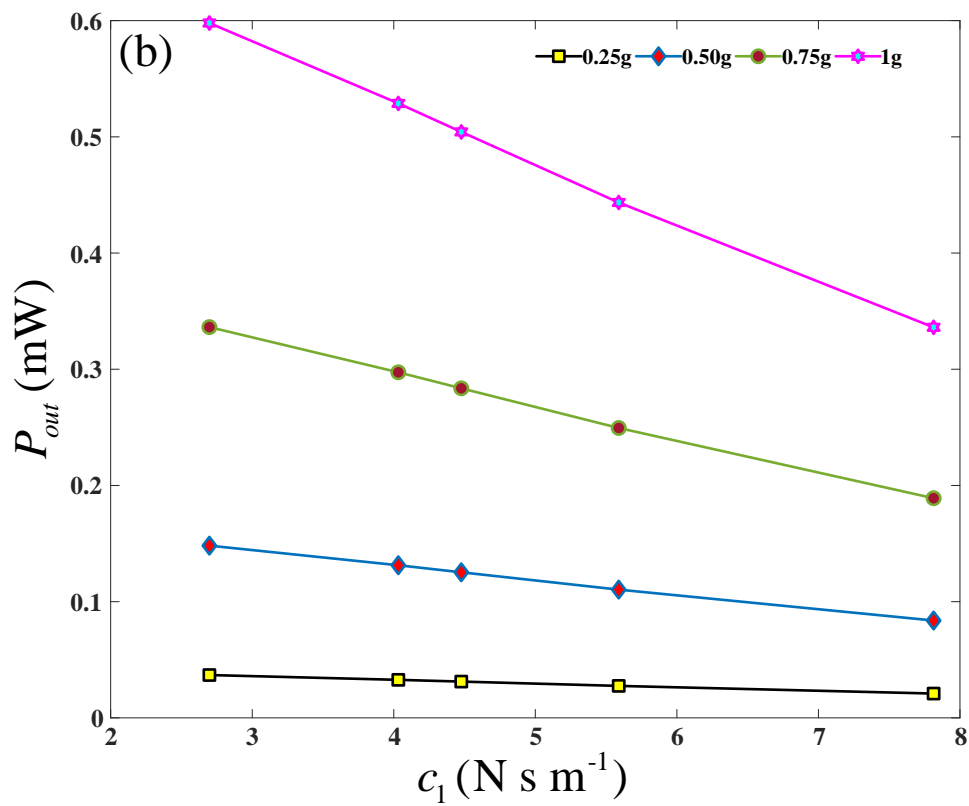
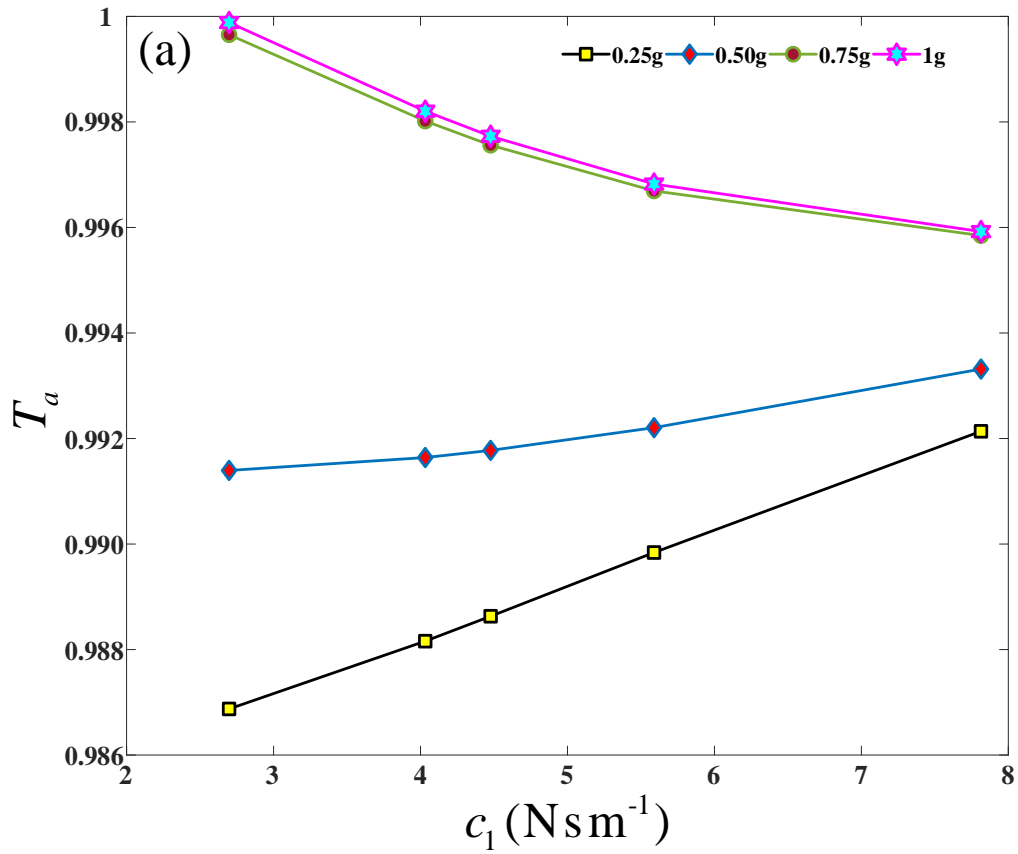


Figure 6.8: Measured and modelled output power from the VI-EH device at $0.5g$ [$m.s^{-2}$].

6.5 SYSTEM DESIGN AND OPTIMISATION

A simulation study of the performance of the VI-EH system subject to variation in linear damping, c_1 around the experimentally measured value of $c_1 = 2.7 \text{ [N.m.s}^{-1}\text{]}$ while keeping k_3 fixed as $1.368 \times 10^6 \text{ [N.m}^{-3}\text{]}$ is shown in Figure 6.9(a-c). In designing the VI-EH system over the isolation region ($\omega > \omega_n \sqrt{2}$), it is apparent, as presented in Figure 6.9a that at low levels of acceleration, i.e. 0.25g and 0.5g, transmissibility, T_a , increased slightly as the linear damping c_1 increased. On the other hand, at higher level of acceleration (0.75g and 1.0g), an increase in linear damping, c_1 leads to decrease in transmissibility values. This becomes an important feature of the nonlinear VI-EH system in comparison to a linear system. That is, an inherent limitation of typical linear isolation systems ($k_3 = 0$) is that its absolute displacement transmissibility increases as linear damping is increased for all acceleration levels. Figure 6.9b suggests that, for fixed acceleration level, the average output power decreases at higher linear damping. Nonetheless, as the linear damping, c_1 increases the rate of decay in output power P_{out} is larger at higher levels of excitations. It also reveals that, for fixed damping, the average output power increases as the excitation level increases. Nonetheless, a closer inspection of Figure 6.9c shows that while the energy conversion efficiency, η_e is sensitive to linear damping, c_1 , it is independent of the excitation level. This is possibly due to the fact that an increase in input mechanical power at higher acceleration is accompanied by increase in the output power. Overall, for low acceleration levels, lower damping values are favourable and yield higher energy conversion efficiencies (Figure 6.9c) and improved vibration isolation (Figure 6.9a). At higher acceleration levels, there is a trade-off where lower damping values worsen vibration isolation characteristics of the VI-EH system (Figure 6.9a) but yield higher energy conversion efficiencies (Figure 6.9c).



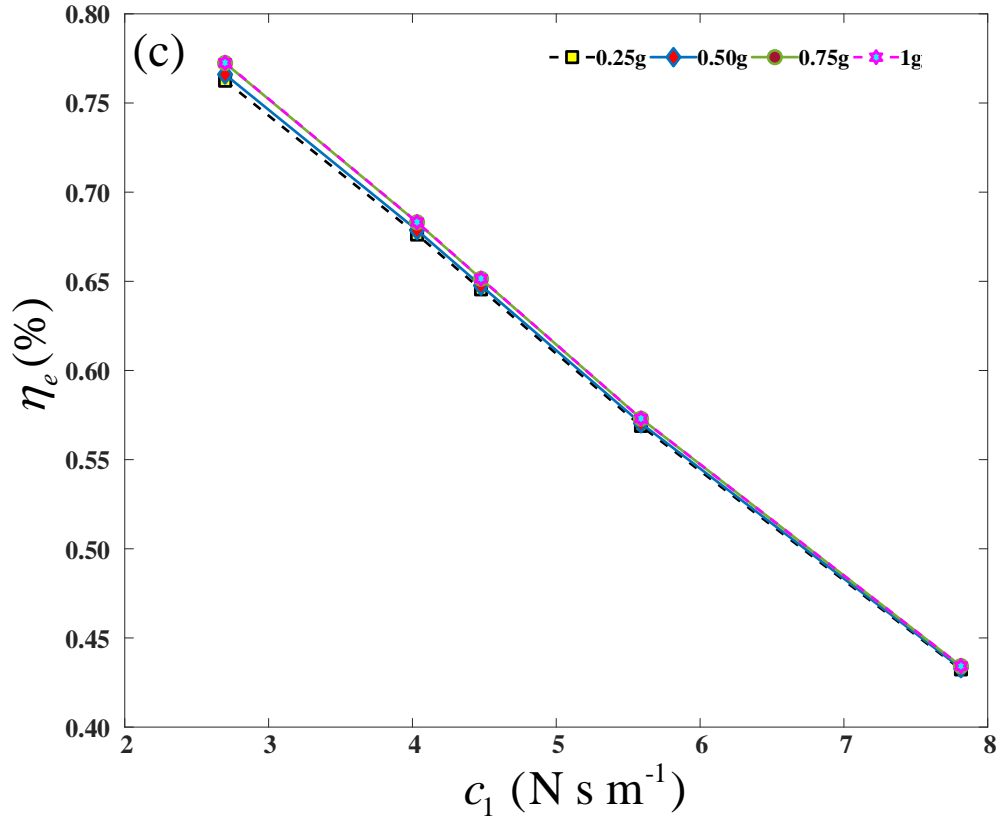


Figure 6.9: Model simulation of the performance of the VI-EH system subject to variation in linear damping, c_1 while keeping k_3 fixed: a) Transmissibility, b) Output power, and c) Energy conversion efficiency at 4 acceleration levels 0.25g, 0.50g, 0.75g, and 1.0g [m.s⁻²].

Next, the linear damping parameters are, first, designed under low base-excitation and, then, used to design and optimize the nonlinear stiffness k_3 at different excitation levels. Using the measured natural frequency, $\omega_n = 55.6$ rad.s⁻¹ and design criteria for the system, i.e.

$T_a = 0.9855$ when $\omega = \omega_n \sqrt{2}$, or $\Omega = \frac{\omega}{\omega_n} = 1.42$, then k_1 and c_1 are obtained as:

$$\left\{ \begin{array}{l} k_1 = m\omega_n^2 \\ c_1 = 2\xi m\omega_n \\ \text{where } \xi \text{ is determined from the equation} \\ T_a = \sqrt{\frac{1 + 2\xi\Omega^2}{1 - \Omega^2 + 2\xi\Omega^2}} \end{array} \right. \quad (6.15)$$

Using the system linear parameters k_1 and c_1 , thus determined, the OFRF in terms of the nonlinear parameter k_3 is employed for the design and optimisation of the VI-EH system as follows.

From the OFRF representation for the energy conversion efficiency and the absolute displacement transmissibility obtained in Section 6.3, the optimisation problem for nonlinear parameter k_3 can be formulated as;

$$\begin{aligned} \max_{k_3} \quad & \eta_e^s(\omega, k_3) \\ \text{s.t.} \quad & \begin{cases} k_3 - 1.4 \times 10^6 \leq 0 \\ \sum_{r=0}^R \rho_r^s(\omega) \cdot k_3^r - 1 < 0 \end{cases} \end{aligned} \quad (6.16)$$

where $\omega = \omega_n \sqrt{2} = 79 \text{ rad.s}^{-1}$, which is an essential constraint for vibration isolation characteristics of the VI-EH system (primary function). The solution to the optimisation problem (6.16) under each of the four levels of ground acceleration inputs of $s = 0.25\text{g}$, 0.5g , 0.75g and 1g [m/s^2] is presented in Table 6.2.

Table 6.2: Maximum energy conversion efficiency attainable at specific nonlinear stiffness value subject to the system constraints at predetermined base accelerations

Base acceleration Level [m.s^{-2}]	Absolute displacement transmissibility, T_a	Max. Energy conversion efficiency, $\eta_{e_{\max}}$ (%)	Average output power, P_{out} (mW)	Nonlinear stiffness, k_3 (N.m^{-3})
0.25g	0.9869	0.7624	0.037	1.4×10^6
0.50g	0.9914	0.7659	0.148	1.4×10^6
0.75g	0.9996	0.7723	0.336	1.4×10^6
1.00g	0.9999	0.7724	0.598	0.8×10^6

From Table 6.2, it is evident that the maximum nonlinear stiffness coefficient $k_3 = 1.4 \times 10^6 \text{ N.m}^{-3}$ results in a maximum conversion efficiency, $\eta_{e_{\max}}$ at the first three levels of acceleration, that is, 0.25g , 0.5g and 0.75g [m.s^{-2}], respectively. Nonetheless, at acceleration level of 1.0g [m.s^{-2}], increasing the nonlinear stiffness coefficient, k_3 beyond $0.8 \times 10^6 \text{ N.m}^{-3}$ causes the transmissibility to grow beyond unity, which violates the second constraint of design. Therefore, the optimal solution is

$k_3 = 0.8 \times 10^6 \text{ N.m}^{-3}$. Overall, the maximum energy conversion efficiency of the VI-EH system is less than 1%, which is relatively low. This is because the primary function (vibration isolation) of the VI-EH system is to maintain transmissibility to be less than unity, i.e. $T_a < 1$. However, it is worth pointing out that even though the conversion efficiency is low, converting some of the free and abundant kinetic energy using a stack of VI-EH devices could still be useful for onboard low-power sensors and gadgets.

The above optimisation problem (6.16) was solved for each of the four input levels. If a design needs to take into account all the four input levels, a weighted sum of the objective functions associated with each input level such that

$$\begin{cases} T_a^K = \kappa_1 \cdot T_a^{(0.25g)} + \kappa_2 \cdot T_a^{(0.5g)} + \kappa_3 \cdot T_a^{(0.75g)} + \kappa_4 \cdot T_a^{(1g)} \\ P_{out}^K = \kappa_1 \cdot P_{out}^{(0.25g)} + \kappa_2 \cdot P_{out}^{(0.5g)} + \kappa_3 \cdot P_{out}^{(0.75g)} + \kappa_4 \cdot P_{out}^{(1g)} \\ \eta_e^K = \kappa_1 \cdot \eta_e^{(0.25g)} + \kappa_2 \cdot \eta_e^{(0.5g)} + \kappa_3 \cdot \eta_e^{(0.75g)} + \kappa_4 \cdot \eta_e^{(1g)} \end{cases} \quad (6.17)$$

where $\kappa_1 + \kappa_2 + \kappa_3 + \kappa_4 = 1$ can be used. Eq (6.17) can be further written as

$$\begin{cases} T_a^K = \sum_{r=0}^{\tilde{R}} \left[\kappa_1 \rho_r^{(0.25g)}(\omega) + \kappa_2 \rho_r^{(0.5g)}(\omega) + \kappa_3 \rho_r^{(0.75g)}(\omega) + \kappa_4 \rho_r^{(1g)}(\omega) \right] \cdot k_3^r \\ P_{out}^K = \sum_{r=0}^{\tilde{R}} \left[\kappa_1 \varphi_r^{(0.25g)}(\omega) + \kappa_2 \varphi_r^{(0.5g)}(\omega) + \kappa_3 \varphi_r^{(0.75g)}(\omega) + \kappa_4 \varphi_r^{(1g)}(\omega) \right] \cdot k_3^r \\ \eta_e^K = \sum_{r=0}^{\tilde{R}} \left[\kappa_1 \beta_r^{(0.25g)}(\omega) + \kappa_2 \beta_r^{(0.5g)}(\omega) + \kappa_3 \beta_r^{(0.75g)}(\omega) + \kappa_4 \beta_r^{(1g)}(\omega) \right] \cdot k_3^r \end{cases} \quad (6.18)$$

Consider, for example, the conversion efficiency as the design objective. Then, the optimisation problem, taking into account all four loading conditions, can be formulated as

$$\begin{aligned} \max_{k_3} \quad & \eta_e^K \\ \text{s.t.} \quad & \begin{cases} k_3 - 1.4 \times 10^6 \leq 0 \\ \sum_{r=0}^{\tilde{R}} \left[\kappa_1 \rho_r^{(0.25g)}(\omega) + \kappa_2 \rho_r^{(0.5g)}(\omega) + \kappa_3 \rho_r^{(0.75g)}(\omega) + \kappa_4 \rho_r^{(1g)}(\omega) \right] \cdot k_3^r - 1 < 0 \end{cases} \end{aligned} \quad (6.19)$$

where $\omega = \omega_n \sqrt{2} = 79 \text{ rad.s}^{-1}$

The solutions to the optimisation problem (6.19) under the following three choices of the weights

$$\kappa_1 = \kappa_2 = \kappa_3 = \kappa_4 = 0.25$$

$$\kappa_1 = \kappa_2 = 0.5, \kappa_3 = \kappa_4 = 0$$

and

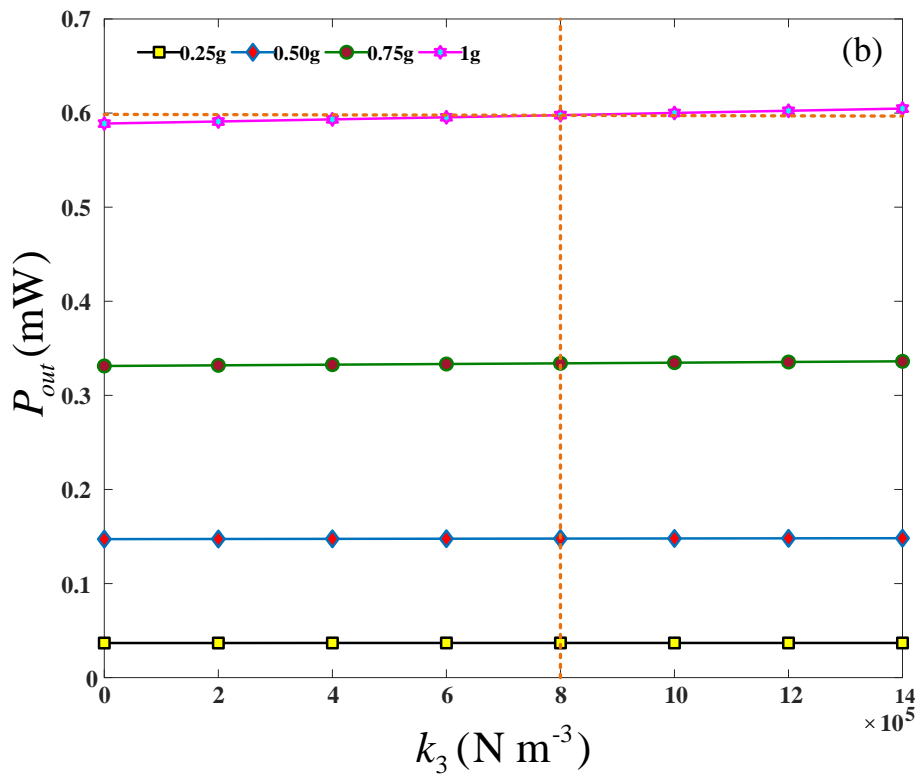
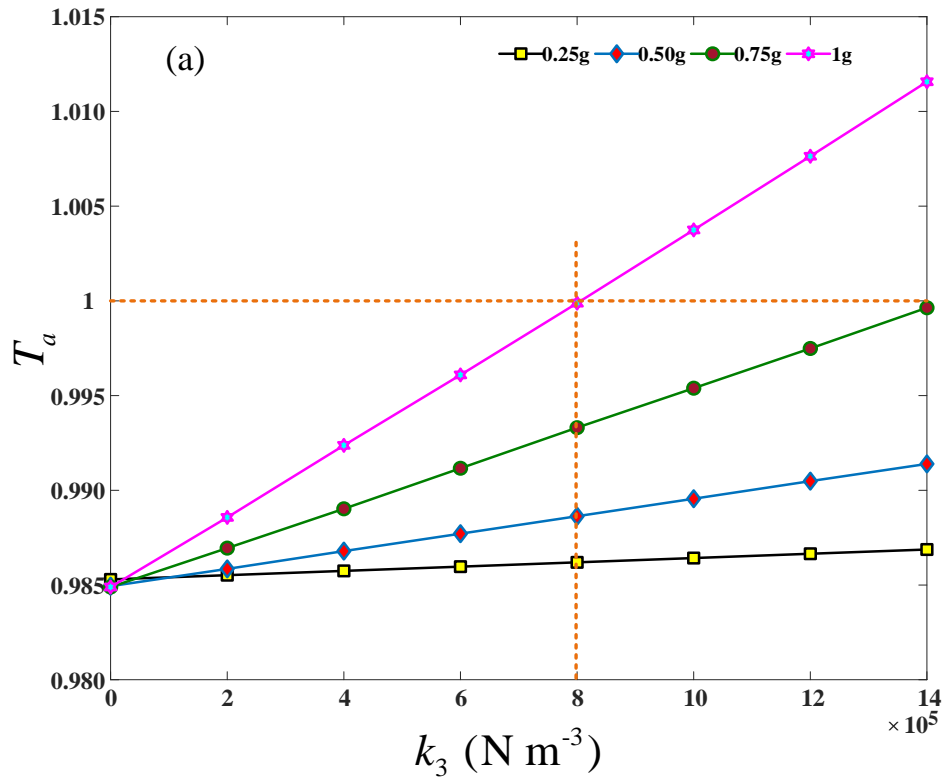
$$\kappa_1 = \kappa_2 = 0, \kappa_3 = \kappa_4 = 0.5$$

are shown in Table 6.3. The results indicate that the conversion efficiency is almost the same in all the cases. But, in the case of $\kappa_1 = \kappa_2 = 0.5, \kappa_3 = \kappa_4 = 0$, where two lowest input levels are considered for the optimal design, the average power output is the lowest; In the case of $\kappa_1 = \kappa_2 = \kappa_3 = \kappa_4 = 0.25$ where all the four loading levels are considered, the average power output become larger; In the case of $\kappa_1 = \kappa_2 = 0, \kappa_3 = \kappa_4 = 0.5$ where the two largest input levels are considered, the average power output is the highest. These are all fully consistent with considerations from the perspective of physics.

Table 6.3: Maximum energy conversion efficiency attainable at specific nonlinear stiffness value subject to the system constraints considering the normalized weight contribution of each excitation.

Set of normalized weight contributions, $\underline{\mathbb{K}}$	Absolute displacement transmissibility, T_a^K	Max. energy conversion efficiency, $\eta_{e_{\max}}^K$ (%)	Average output power, P_{out}^K (mW)	Nonlinear stiffness, k_3 (N.m ⁻³)
$\kappa_1 = \kappa_2 = \kappa_3 = \kappa_4 = 0.25$	0.9974	0.7705	0.282	1.4×10^6
$\kappa_1 = \kappa_2 = 0.5, \kappa_3 = \kappa_4 = 0$	0.9891	0.7641	0.0925	1.4×10^6
$\kappa_1 = \kappa_2 = 0, \kappa_3 = \kappa_4 = 0.5$	0.9996	0.7722	0.471	1×10^6

The optimal designs introduced above were conducted based on an OFRF representation of the transmissibility, conversion efficiency, and output power of the VI-EH system in terms of the system's nonlinear stiffness coefficient, k_3 . The advantage of this design approach over other techniques is that an explicit relationship between the design objective and design parameter is exploited to find an optimal solution to the design. Figure 6.10 shows these OFRF representations.



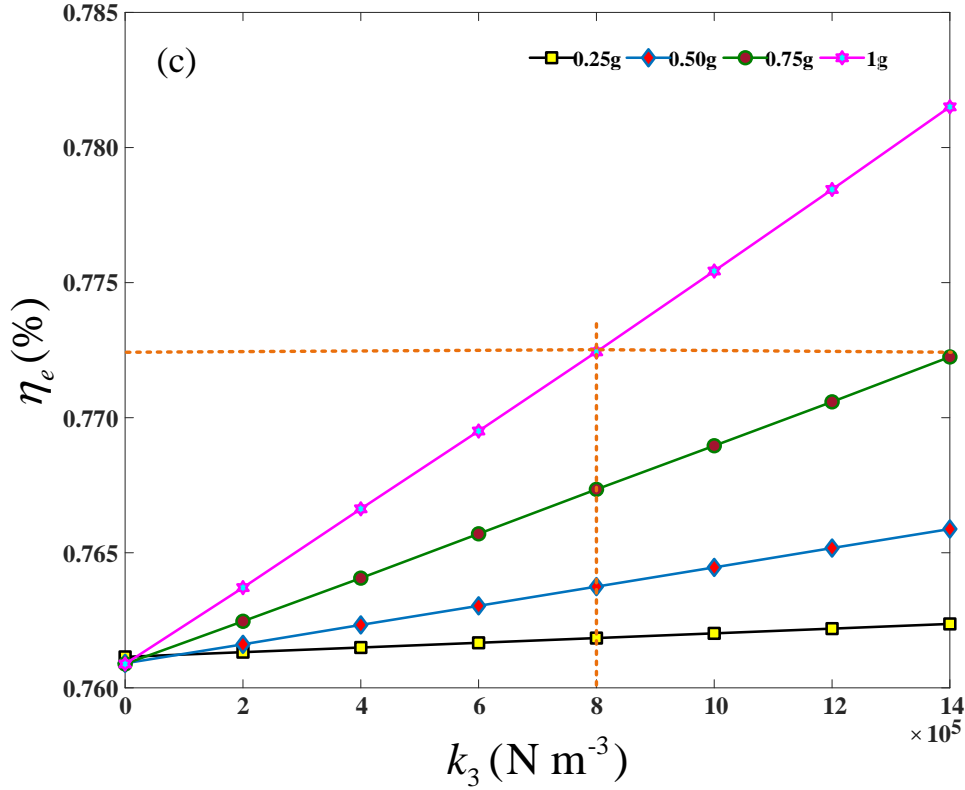


Figure 6.10: Design criteria for the nonlinear stiffness coefficient, k_3 : a) Transmissibility, b) Output power, and c) Energy conversion efficiency at four acceleration levels 0.25g, 0.50g, 0.75g, and 1.0g [m.s^{-2}].

In Figure 6.10a, the effect of k_3 on transmissibility T_a is evident. For a fixed acceleration, an increase in k_3 yields higher transmissibility, T_a (Figure 6.10a) and higher efficiency (Figure 6.10c). Also, the rates of increase in transmissibility T_a and efficiency become larger (steeper) as the acceleration level is increased. This is primarily due to the stiffness hardening nonlinearity effects which manifest itself at higher accelerations. It is worth mentioning that for the case of linear stiffness (i.e. $k_3 = 0$), the VI-EH transmissibility, T_a is independent of the excitation level as depicted in Figure 6.10a. On the other hand, Figure 6.10b suggests that, at all excitation levels, the output power, P_{out} is insensitive to nonlinear stiffness coefficient, k_3 . However, Figure 6.10b shows that the output power, P_{out} is very sensitive to the excitation level, making significant improvement in harvested power when increasing the excitation level. Overall, Figure 6.10 reveals that for fixed acceleration level, increasing the nonlinear stiffness coefficient, k_3 , results in higher conversion

efficiencies (Figure 6.10c) but worsens the vibration isolation of the VI-EH system, transmitting more vibration to the isolated mass (Figure 6.10a).

These observations further confirm the validity of the optimal solutions that have been obtained above by solving optimisation problems (6.16) and (6.19), respectively and demonstrate that the OFRF based optimisation has good potential to be applied for the optimal design of the VI-EH systems in practice.

6.6 EFFECTS OF LOAD RESISTANCE ON PERFORMANCE METRICS

The influence of the load resistance, R_L on the output power and efficiency of the VI-EH system are discussed in this section. The optimum load resistance required to achieve the maximum output power is determined by evaluating the zero of the derivatives with respect to R_L of Eq. (6.4) which gives

$$\begin{cases} \frac{dP_{out}}{dR_L} = \left[\frac{k_t \omega Z}{R_C + R_L} \right]^2 \cdot \left[\frac{R_C + 3R_L}{2(R_C + R_L)} \right] = 0 \\ \Rightarrow R_L = R_C \end{cases} \quad (6.20)$$

Similarly, the effect of the load resistance to the energy conversion efficiency of the VI-EH system can be investigated. Substituting Eq. (6.3) and Eq. (6.4) into Eq. (6.5) and then equating its derivative, with respect to R_L , to zero yields

$$\begin{cases} \eta_e = \frac{50\pi}{m\omega^3 Y^2} \cdot \left[\frac{k_t \omega Z}{R_C + R_L} \right]^2 \cdot R_L \\ \frac{d\eta_e}{dR_L} = \frac{50\pi}{m\omega^3 Y^2} \cdot \left[\frac{k_t \omega Z}{R_C + R_L} \right]^2 \cdot \left[\frac{R_C + 3R_L}{2(R_C + R_L)} \right] = 0 \\ \Rightarrow R_L = R_C \end{cases} \quad (6.21)$$

As can be seen from Eqs. (6.20) and (6.21), to obtain the maximum output power level and efficiency of the VI-EH system, the load resistance must equal the coil resistance of the VI-EH system. The results, as revealed, for the output power and efficiency of the VI-EH system are presented in Figure 6.11 and Figure 6.12 respectively. Furthermore, from Figure 6.11 it is evident that the output power of the VI-EH system is sensitive to the base acceleration level on the system. However, this is not the case for its efficiency as it is non-sensitive to the base acceleration level.

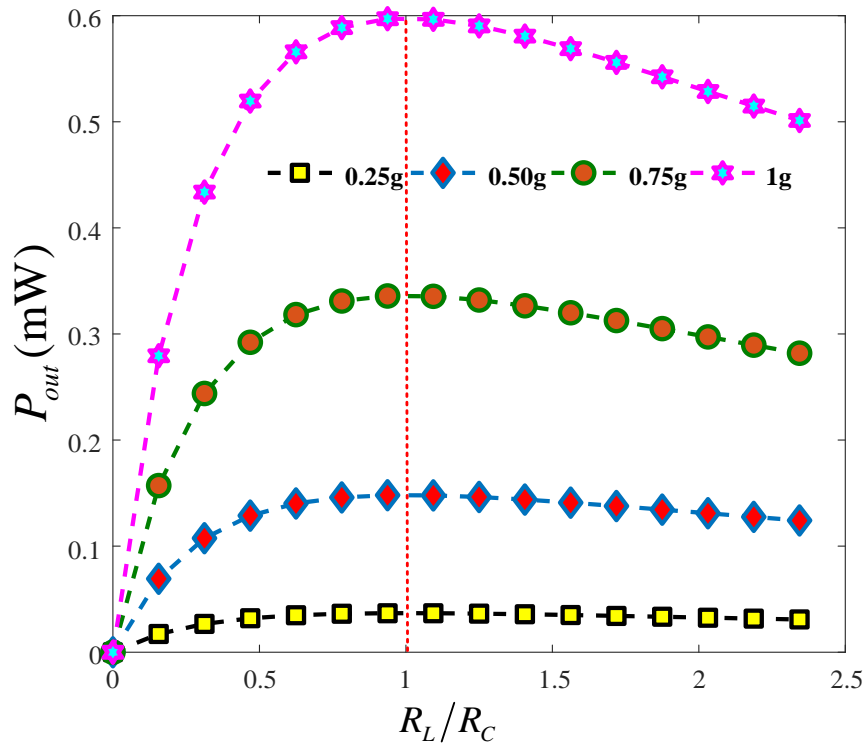


Figure 6.11: The Output power of the VI-EH system as a function of R_L while keeping k_3 fixed at the optimum value for four acceleration levels 0.25g, 0.5g, 0.75g and 1.0g [m.s^{-2}].

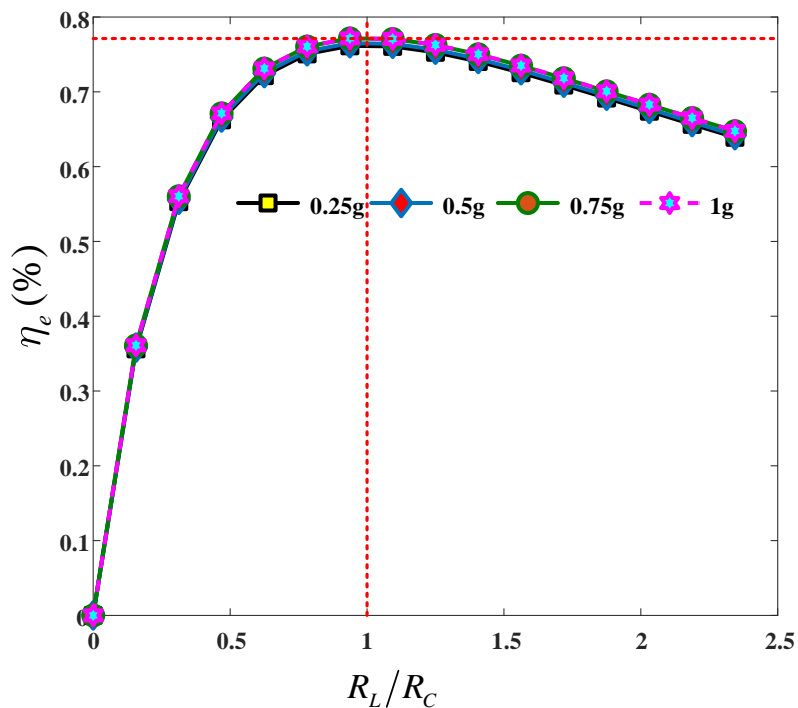


Figure 6.12: Effect of the Energy conversion efficiency of the VI-EH system to variation in R_L while keeping k_3 fixed at the optimum value for four acceleration levels 0.25g, 0.5g, 0.75g and 1.0g [m.s^{-2}].

6.7 CONCLUSIONS

Driven by the growing interest in simultaneous vibration isolation and energy harvesting this work has focused on optimisation of a representative dual function VI-EH system. A mathematical model of the VI-EH system has been developed and analysed using a nonlinear system frequency analysis approach known as Output Frequency Response Function (OFRF). Performance metrics including displacement transmissibility, energy conversion efficiency, and subsequently, output electric power have been formulated using the OFRF. A prototype of a representative VI-EH system was fabricated and used for model validation. An OFRF based optimisation process has then been performed to maximize vibration energy conversion (secondary function) of the VI-EH system while maintaining its vibration transmissibility to less than unity (primary function). Results reveal that the maximum attainable energy conversion efficiency of the VI-EH system is inherently low and in the order of 1%. Nonetheless, since the primary function (vibration isolation) of the VI-EH system is achieved harvesting some of the free and abundant kinetic energy contained in these oscillations (secondary function) may be useful in the future as power requirements for onboard sensors is continuously dropping. Finally, the effects of the load resistance on the performance metrics, output power and energy conversion efficiency, were investigated and the results show that the VI-EH system performed best when the load and coil resistances are equal. Other design improvements may lead to improved power metrics. For example, future work will focus on investigating VI-EH systems with nonlinear damping element as well as softening stiffness nonlinearities as possible route to improve their performance metrics.

In this chapter, an optimisation process has been performed to maximise the amount of energy harvested by a dual-function VI-EH system while ensuring vibrations are suppressed to limits that meet the design criteria. The ease of the design and optimisation process demonstrates the benefits of the OFRF methodology in nonlinear system design and optimisation. This key contribution is the first effort to tackle the issue of simultaneous vibration isolation and energy harvesting system using an analytical approach (the OFRF method).

Chapter 7: Conclusions and Future work

This chapter concludes the thesis discourse and also comprises some ongoing fabrication work of a VEH test rig for some proposed future experimental studies on vibration isolation and vibration energy harvesting. It is therefore structured in the following format: Section 7.1 provides concluding remarks concerning the motivations for the works reported in this thesis and also a brief discussion of the objectives accomplished. Section 7.2 highlights the major contributions in this work on a chapter basis and based on the research objectives stated in Chapter 1:. Section 7.3 presents recommendations and future works. This includes an ongoing fabrication work of a VEH test-rig based on some of the contributions made in this thesis as well as extensions of some of the major contributions reported in this thesis.

7.1 CONCLUSIONS

Vibration is ubiquitous in nature and also inherent in all engineering systems and structures. However, depending on the level of vibration present within the system or structure, it can have destructive effects. Many vibration isolation techniques have been developed over the years to mitigate the destructive effects of such structural vibrations. Such techniques employ vibration isolation elements which mainly comprises a mass (typically the payload), spring and damper system. While the mass and spring dictate a natural frequency for the system, the damper has a secondary effect on it. These linear isolation elements ensure the disturbing vibration is totally isolated from the device requiring protection or reduced to tolerable limits. Each vibration isolation method is unique in its way, however, similarities between methods may exist. Vibration isolation methods are broadly classified into three main categories; passive, semi-active and active. Though the active method provides excellent isolation performance compared to other methods, its complexity, cost and power requirement discourage its popularity. This has led to a shift in attention to the semi-active method which, just as the active method, require some control inputs generated from sensor-measurement data. Nevertheless, with the integration of nonlinearities in the dynamic characteristics of the isolation elements, the passive method has received significant attention in recent times. This has inspired the application of nonlinear system analysis

methods for the design of vibration isolation systems. Such methods include; the harmonic balance method, nonlinear normal forms method, perturbation method, method of averaging and the recently developed output frequency response function method. To ensure the desired vibration isolation performance is achieved, several configurations (geometric and physical) of nonlinear vibration isolation systems have been proposed. Although vibration isolation systems can either be force or base-excited, subject to the source and location of the input force, this thesis focuses on base-excited systems.

The need to improve the performance of vibration isolation systems is of significant importance. Typical isolation elements are designed to minimise the input energy to the system which in turn reduces the acceleration in the structure. This is commonly achieved by reducing the force transmitted to the payload, through the isolation elements, to an acceptable level. Nonetheless, some of the input energy can be absorbed and converted to a form of beneficial use by employing electric generators such as electromagnetic dampers. Electromagnetic dampers possess a dual functionality. They can function as a vibration isolation element as well as an electric generator which is required in vibration energy harvesters. Furthermore, the constant development in electronics manufacturing has inspired the need to develop standalone sources of power which has motivated the interest in energy harvesting.

This thesis has provided a comprehensive review of past studies on both vibration isolation and energy harvesting systems. Some nonlinear configurations of these systems were discussed including methods adopted in their analytical studies. Based on past studies in the literature, nonlinear characteristics of a dynamic system can be achieved from the geometric configuration of the linear components (elements) integrated into the system. It can also be realised from inherent nonlinearity in the component design or material structure. The output frequency response function methodology was employed for the studies reported in this thesis.

In Chapter 3, a vehicle suspension system, which is representative of a vibration isolation system, was considered. The main objective was to investigate the energy dissipation level of the designed nonlinear suspension system. The suspension system was designed to minimise the force transmitted by the isolation elements, to acceptable limits (a specified threshold). The energy dissipation capability of the designed suspension system was explored for a nonlinear suspension system, as less attention

has been paid to this area recently. This analysis provided some insight into the amount of energy available to be harvested into electricity. The OFRF method was employed for this study.

In Chapter 4, the main objective of the study was to analyse, design, and optimise a vibration energy harvesting system using, for the first time, the OFRF method. The thesis provided an analysis, design, optimisation, and implementation process for a nonlinear VEH system, which was shown to outperform an equivalent linear device. It was demonstrated that such a system performs better, regardless of the excitation level. This is because it provides the same average power as an equivalent linear device at the maximum excitation level and performed significantly better than the equivalent linear device at base excitations below the maximum level. The OFRF method was also employed in this study for the optimal design of the parameter of interest at the maximum excitation level. With the designed parameter and at the frequency of interest, a SIMULINK model was developed. This model is the corresponding electromechanical analogy of the VEH system which provides the same dynamic characteristic as the mechanical analogy of the VEH system.

The study in Chapter 5 extended the performance of the nonlinear VEH system considered in Chapter 4. To the best of the knowledge of the author of this thesis, this is the first attempt to consider, simultaneously, nonlinear damping and stiffness in VEH systems. In this study, the objective was to broaden the frequency range over which a VEH device with cubic damping characteristic can function which was realised by the integration of a hardening stiffness component. The OFRF method was employed again in this study, however, this time the OFRF representation was derived using the Associated Linear Equation method. The ALE-generated OFRF model provides the exact polynomial representation of the actual system. This is because the ALE decompositions represent the exact n th order nonlinearities of the actual system. However, the typical OFRF representation is determined using the Least Squares approach involving much less unknowns.

In Chapter 6, the design and optimisation of a combined vibration isolation (primary function) and energy harvesting (secondary function) device was investigated. The primary objective was to analytically investigate the dual-function VI-EH, which is, to the best of the author's knowledge, the first effort to consider this. The design and optimisation process was performed based on four input levels with

respect to the design parameter, which is a hardening stiffness component. In the optimisation problem, two cases were considered; the first case considered each input level (independent of others) while the second case considered all the four input levels (based on a weighted sum). Finally, effects of the resistive load on the performance metrics of the VI-EH system was demonstrated. The next section highlights the main contributions in this thesis.

7.2 HIGHLIGHTS OF MAIN CONTRIBUTIONS

Major contributions collated from the respective chapters are presented here for ease of identification.

❖ Chapter 3

The major contribution of the study presented in this chapter is the novel investigation of the Energy dissipation level of a designed vehicle suspension system using the OFRF method. This also involved a Hysteresis analysis of the vehicle suspension system based on the OFRF design. Using the OFRF method, it was demonstrated that the energy dissipation level, for a designed vehicle suspension system, can be estimated. The effect of each nonlinear design parameter was also demonstrated.

❖ Chapter 4

The major contribution of the research work presented in this chapter, is the novel application of the OFRF method in the analysis, design and optimisation of a nonlinear VEH system. In this study, a cubic damping characteristic was considered and a systematic way of proceeding from the design stage to implementation stage, is demonstrated.

❖ Chapter 5

In this chapter, and for the first time, a VEH device is investigated with the integration of both damping and stiffness nonlinearities. Furthermore, a novel application of the OFRF method was employed. However, in this study, the OFRF model was derived using the ALE decompositions of the actual system model.

❖ Chapter 6

This chapter considered a dual-function vibration isolation and energy harvesting system. The novel OFRF method was employed in the analysis, design and

optimisation of the dual-function VI-EH system. The system was optimised for the nonlinear stiffness parameter. This work is the first effort to tackle the issue of simultaneous vibration isolation and energy harvesting system using an analytical approach (the OFRF method).

7.3 RECOMMENDATIONS AND FUTURE WORKS

7.3.1 Ongoing fabrication work of a VEH test rig

In addition to the studies reported in this thesis, a design and fabrication work has been ongoing, concurrently. The test-rig designed and fabricated is a vibration energy harvester which will be integrated with a nonlinear load resistive circuit (still under design). A Computer Aided Design (CAD) model of the test rig is presented in Figure 7.1 in geometric and right-side view.

The nonlinear load resistive circuit will be designed using DC-DC converters and power electronic circuit elements. The major components of the proposed test rig are discussed below.

- ❖ **Shaker:** This is a device employed in vibration analysis for exciting a system or structure while performing a model test, endurance test or some other vibration test. Table 7.1 outlines its specifications.

Table 7.1: Shaker device specifications

Max. Sine Force (pk) (N)	Max. Random Force (rms) (N)	Max. Shock Force (N)	Max. Acceleration (Sine) (m/s ²)	Maximum Velocity (m/s)	Displacement (Peak - Peak)	Freq. Range (Hz)
17.8	5.9	17.8	892.4	1.49	5	DC-1.8e ⁴

- ❖ **Electromagnetic Damper:** This is a unique U Channel-type of linear motor with two parallel magnet tracks (magnets placed on steel) facing each other with a forcer (rotor) incorporated between the plates. A bearing system supports the forcer in the magnet track. The forcer contains the coil windings encapsulated in epoxy, a thermistor (temperature sensor), and the electrical connections. Linear guide rails preserve the locus of the forcer in the magnetic field of the magnet track. The EMD also has a continuous force from 0-184.0 N and is presented in Figure 7.2.

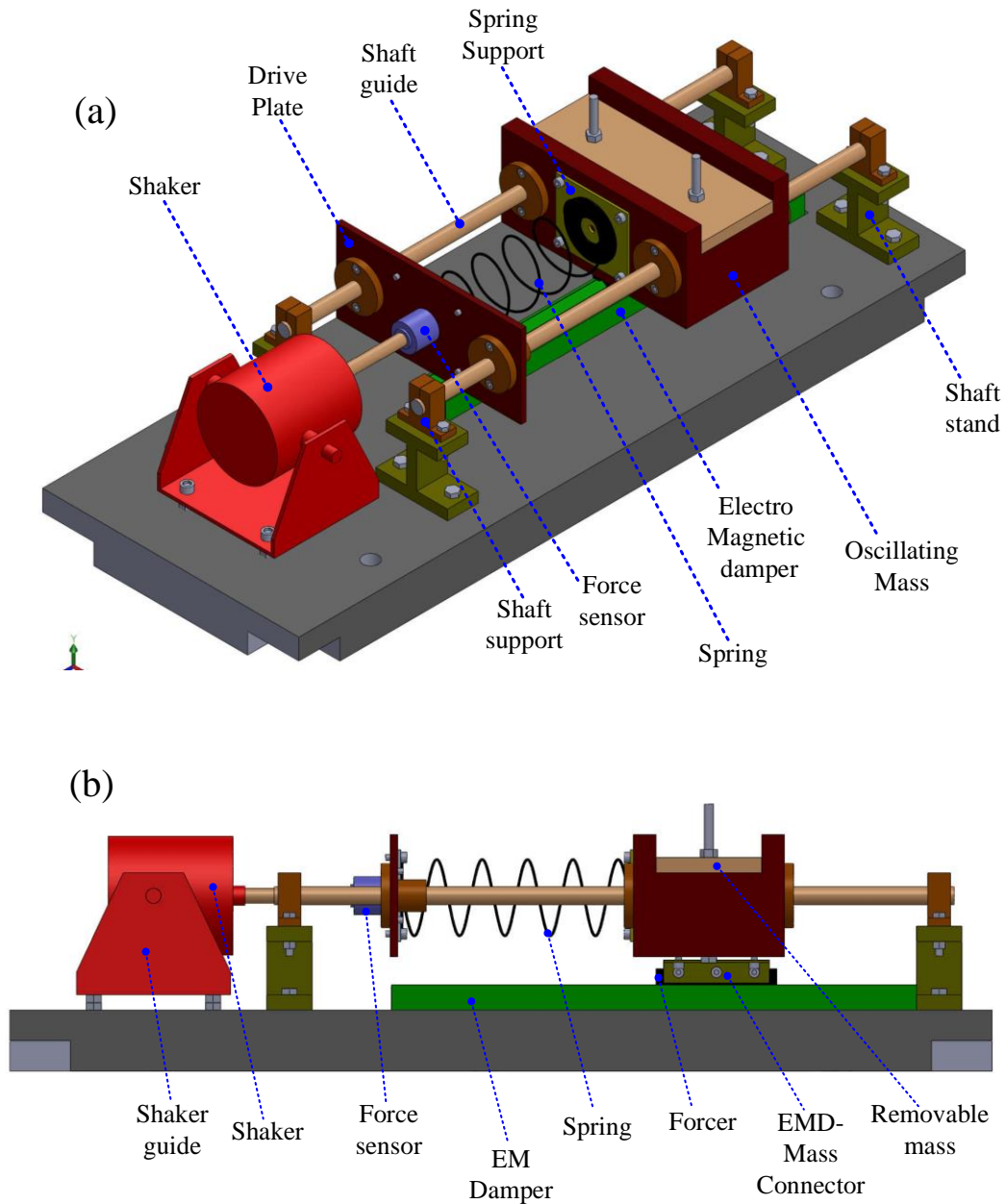


Figure 7.1: CAD model of (a) geometric and (b) right-side views of the proposed vibration energy harvester test rig.

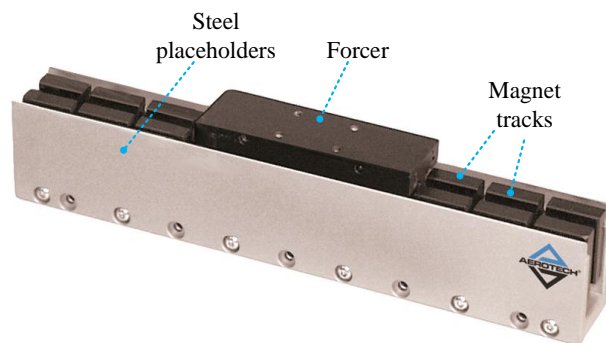


Figure 7.2: Electromagnetic damper by Aerotech, Inc.

- ❖ **Helical Spring:** The helical spring, like typical springs, absorb energy from shocks and subsequently releases it. The spring used for the test rig provides a stiffness value of 220 N.m^{-1} .

In addition to the aforementioned components, a force sensor is also integrated to measure the actual force input from the shaker to the VEH system. Figure 7.3 provides additional camera views of the test rig CAD model as well as a snap-shot of the actual fabricated test rig which is close to completion.

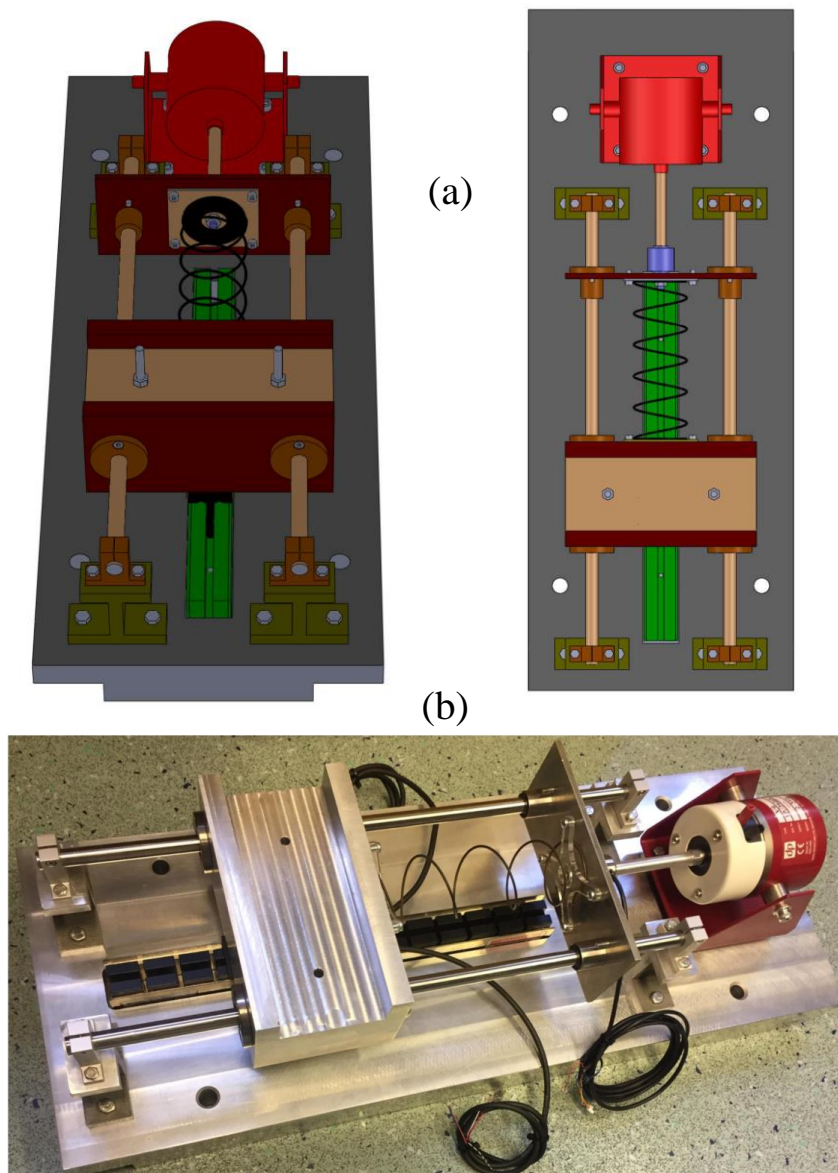


Figure 7.3: CAD models (a) and actual assembly (b) of the vibration energy harvester test rig

7.3.2 Extensions of research works for future consideration

The studies presented here have several possible extensions to them especially the consideration of other loading conditions such as random excitation, impulse excitation etc. These will be discussed on a chapter basis.

❖ Chapter 3

In this study, the design of a vehicle suspension system was considered. This involved the design and parameter optimisation of a vehicle suspension system with respect to the design criteria. The investigation also considered an estimation of the energy dissipation estimation by the isolation elements based on the designed parameters. In an extended study, a feedback control may be integrated to control and implement the damping characteristic. This can be implemented using a controllable damper such as a magnetorheological damper.

❖ Chapter 4

This research study concerned the use of a nonlinear cubic damping characteristic to extend the power available to the VEH system. An extension of this work will consider the investigation of the effect of other forms of damping nonlinearities such as a displacement-velocity dependent damping characteristic. However, the electrical implementation of such damping characteristic may be challenging as the characteristic of the resistive load circuit determines the characteristic of the EMD.

❖ Chapter 5

This study was an extension of the research work discussed in Chapter 4. However, an additional extension to this study would include more in-depth analysis of the effect of incorporating a hardening stiffness to the nonlinear VEH system considered. A further study can consider the optimisation of key components of the VEH system such as the resistive load circuit, the nonlinear damping parameter and the suspended mass.

❖ Chapter 6

This study considered a dual-function VI-EH system with vibration isolation as its primary function and energy harvesting as its secondary function. An optimisation process was conducted to provide the best dual performance based on the designed nonlinear stiffness characteristics. Nonetheless, the integration of a nonlinear damping characteristic will be considered in a future work. It is expected to improve the vibration isolation performance (primary function) of the VI-EH system.

Bibliography

- [1] Inman D. J., and Ramesh C.S., *Engineering vibration*. Vol. 3. Englewood Cliffs, NJ: Prentice Hall, 1994.
- [2] Harris C. M., and Allan G. P., *Harris' Shock and vibration handbook*. Vol. 5. New York: Mcgraw-hill, 2002..
- [3] Rivin E. I., *Dynamic Properties of Vibration Isolation Systems*. Asme press, 2003.
- [4] Inman D. J., *Vibration with control*. John Wiley & Sons, 2017.
- [5] Liu C., Jing X., Daley S., and Li F., Recent advances in micro-vibration isolation. *Mechanical Systems and Signal Processing*, 56, (2015): 55-80.
- [6] Garoi F., Winterflood J., Ju L., Jacob J., and Blair D.G., "Passive vibration isolation using a Roberts's linkage". *Review of Scientific Instruments*, 74(7), (2003): 3487-3491.
- [7] Collette C., Janssens S., and Artoos K., "Review of active vibration isolation strategies". *Recent patents on Mechanical engineering*, 4(3), (2011): 212-219.
- [8] Preumont A., Francois A., Bossens F., and Abu-Hanieh A., "Force feedback versus acceleration feedback in active vibration isolation". *Journal of sound and vibration*, 257(4), (2002): 605-613.
- [9] Preumont A., *Vibration control of active structures* (Vol. 2). Dordrecht: Kluwer academic publishers,1997.
- [10] Cobb R.G., Sullivan J.M., Das A., Davis L.P., Hyde T.T., Davis T., Rahman Z.H., and Spanos J.T., "Vibration isolation and suppression system for precision payloads in space". *Smart Materials and Structures*, 8(6), (1999): 798.
- [11] Zhu W.H., Tryggvason B., and Piedboeuf J.C., "On active acceleration control of vibration isolation systems". *Control Engineering Practice*, 14(8), (2006): 863-873.
- [12] Dyke S.J. and Spencer B.F., "A comparison of semi-active control strategies for the MR damper". In *Proceedings Intelligent Information Systems. IIS'97* (1997): 580-584, IEEE.

- [13] Karnopp D., Crosby M.J., and Harwood R.A., "Vibration control using semi-active force generators". *Journal of engineering for industry*, 96(2), (1974): 619-626.
- [14] Fischer D. and Isermann R., "Mechatronic semi-active and active vehicle suspensions". *Control engineering practice*, 12(11), (2004): 1353-1367.
- [15] Karnopp D., "Active and semi-active vibration isolation". In *Current Advances in Mechanical Design and Production VI* (1995): 409-423.
- [16] Liu Y., Matsuhisa H., and Utsuno H., "Semi-active vibration isolation system with variable stiffness and damping control". *Journal of sound and vibration*, 313(1-2), (2008)16-28.
- [17] Cottone F., Vocca H., and Gammaitoni L., "Nonlinear energy harvesting". *Physical Review Letters*, 102(8), (2009): 080601.
- [18] Zuo L. and Tang X., "Large-scale vibration energy harvesting". *Journal of intelligent material systems and structures*, 24(11), (2013): 1405-1430.
- [19] Boisseau S., Despesse G., and Seddik B.A., "Electrostatic conversion for vibration energy harvesting". *Small-Scale Energy Harvesting*, (2012): 1-39.
- [20] Aljadiri R.T., Taha L.Y., and Ivey P., "Electrostatic energy harvesting systems: a better understanding of their sustainability". *Journal of Clean Energy Technologies*, 5(5), (2017): 409-416.
- [21] Shevtsov S.N., Soloviev A.N., Parinov I.A., Cherpakov A.V., and Chebanenko V.A., *Piezoelectric Actuators and Generators for Energy Harvesting*. Springer IP AG, (2018).
- [22] Cook-Chennault K.A., Thambi N., and Sastry A.M., "Powering MEMS portable devices—a review of non-regenerative and regenerative power supply systems with special emphasis on piezoelectric energy harvesting systems". *Smart materials and structures*, 17(4), (2008): 043001.
- [23] Sadiku M.N., *Elements of electromagnetics*. Oxford university press, (2014).
- [24] Mitropolsky I.A., "Averaging method in non-linear mechanics". *International Journal of Non-Linear Mechanics* 2, no. 1 (1967): 69-96.
- [25] Kamel A.A., "Perturbation method in the theory of nonlinear oscillations". *Celestial Mechanics* 3, no. 1 (1970): 90-106.

- [26] Nayfeh A.H. and Sayed D.H., "The method of multiple scales and non-linear dispersive waves". *Journal of Fluid Mechanics* 48, no. 3 (1971): 463-475.
- [27] Asfar O.R. and Nayfeh A.H., "The application of the method of multiple scales to wave propagation in periodic structures". *SIAM Review* 25, no. 4 (1983): 455-480.
- [28] Leung A.Y. and Chui S.K., "Non-linear vibration of coupled duffing oscillators by an improved incremental harmonic balance method". *Journal of Sound and Vibration* 181, no. 4 (1995): 619-633.
- [29] Beléndez A., Hernández A., Beléndez T., Alvarez M.L., Gallego S., Ortuño M., and Neipp C., "Application of the harmonic balance method to a nonlinear oscillator typified by a mass attached to a stretched wire". *Journal of Sound and Vibration* 302, no. 4-5 (2007): 1018-1029.
- [30] Lang Z.Q. and Billings S.A., "Output frequency characteristics of nonlinear systems". *International Journal of Control* 64, no. 6 (1996): 1049-1067.
- [31] Lang Z.Q., Billings S.A., Yue R., and Li J., "Output frequency response function of nonlinear Volterra systems". *Automatica* 43, no. 5 (2007): 805-816.
- [32] Ho C., Lang Z.Q., and Billings S.A., "A frequency domain analysis of the effects of nonlinear damping on the Duffing equation". *Mechanical Systems and Signal Processing* 45, no. 1 (2014): 49-67.
- [33] Beeby S.P., Tudor M.J., and White N.M., "Energy harvesting vibration sources for microsystems applications". *Measurement science and technology* 17, no. 12 (2006): R175.
- [34] Saadon S., and Sidek O., "A review of vibration-based MEMS piezoelectric energy harvesters". *Energy Conversion and Management* 52, no. 1 (2011): 500-504.
- [35] Arnold D.P., "Review of microscale magnetic power generation". *IEEE Transactions on Magnetics* 43, no. 11 (2007): 3940-3951.
- [36] Yildirim T., Ghayesh M.H., Li W., and Alici G., "A review on performance enhancement techniques for ambient vibration energy harvesters". *Renewable and Sustainable Energy Reviews* 71 (2017): 435-449.

- [37] Shaikh F.K., and Zeadally S., "Energy harvesting in wireless sensor networks: A comprehensive review". *Renewable and Sustainable Energy Reviews* 55 (2016): 1041-1054.
- [38] Zhou M., Al-Furjan M.S.H., Zou J., and Liu W., "A review on heat and mechanical energy harvesting from human—Principles, prototypes and perspectives". *Renewable and Sustainable Energy Reviews* 82 (2018): 3582-3609.
- [39] Wei C. and Jing X., "A comprehensive review on vibration energy harvesting: Modelling and realization". *Renewable and Sustainable Energy Reviews* 74 (2017): 1-18.
- [40] Abdelkareem M.A.A., Xu L., Ali M.K.A., Elagouz A., Mi J, Guo S., Liu Y., and Zuo L., "Vibration energy harvesting in automotive suspension system: A detailed review". *Applied energy* 229 (2018): 672-699.
- [41] Gripp J.A.B. and Rade D.A., "Vibration and noise control using shunted piezoelectric transducers: A review". *Mechanical Systems and Signal Processing* 112 (2018): 359-383.
- [42] Nelson F.C. "Vibration isolation: A review, I. Sinusoidal and random excitations". *Shock and Vibration* 1, no. 5 (1994): 485-493.
- [43] Diala U.H. and Ezeh G.N., "Nonlinear damping for vibration isolation and control using semi active methods". *Academic Research International* 3, no. 3 (2012): 141.
- [44] Kamesh D., Pandiyan R., and Ghosal A., "Passive vibration isolation of reaction wheel disturbances using a low frequency flexible space platform". *Journal of Sound and Vibration* 331, no. 6 (2012): 1310-1330.
- [45] Yu Y., Naganathan N.G., and Dukkipati R.V., "A literature review of automotive vehicle engine mounting systems". *Mechanism and machine theory* 36, no. 1 (2001): 123-142.
- [46] Den Hartog J.P., *Mechanical vibrations*. Addison Wesley, 1985.
- [47] Williams K., Chiu G., and Bernhard R., "Adaptive-passive absorbers using shape-memory alloys". *Journal of Sound and Vibration* 249, no. 5 (2002): 835-848.

- [48] Williams K.A., Chiu G.T.C., and Bernhard R.J., "Nonlinear control of a shape memory alloy adaptive tuned vibration absorber". *Journal of Sound and Vibration* 288, no. 4-5 (2005): 1131-1155.
- [49] Liu Y., Waters T.P., and Brennan M.J., "A comparison of semi-active damping control strategies for vibration isolation of harmonic disturbances". *Journal of Sound and Vibration* 280, no. 1-2 (2005): 21-39.
- [50] dos Santos M.B., Coelho H.T., Neto F.P.L., and Mafhoud J., "Assessment of semi-active friction dampers". *Mechanical Systems and Signal Processing* 94 (2017): 33-56.
- [51] Verros G., Natsiavas S., and Papadimitriou C., "Design optimization of quarter-car models with passive and semi-active suspensions under random road excitation". *Modal Analysis* 11, no. 5 (2005): 581-606.
- [52] Wu T.H. and Lan C.C., "A wide-range variable stiffness mechanism for semi-active vibration systems". *Journal of Sound and Vibration* 363 (2016): 18-32.
- [53] Gawthrop P.J., Neild S.A., and Wagg D.J., "Semi-active damping using a hybrid control approach". *Journal of Intelligent Material Systems and Structures* 23, no. 18 (2012): 2103-2116.
- [54] Yao G. Z., Yap F.F., Chen G., Li W., and Yeo S.H., "MR damper and its application for semi-active control of vehicle suspension system". *Mechatronics* 12, no. 7 (2002): 963-973.
- [55] Rakheja S. and Sankar S., "Vibration and shock isolation performance of a semi-active "on-off" damper". *Journal of Vibration, Acoustics, Stress, and Reliability in Design* 107, no. 4 (1985): 398-403.
- [56] Setareh M., "Floor vibration control using semi-active tuned mass dampers". *Canadian Journal of Civil Engineering* 29, no. 1 (2002): 76-84.
- [57] Popov G. and Sankar S., "Modelling and analysis of non-linear orifice type damping in vibration isolators". *Journal of sound and vibration* 183, no. 5 (1995): 751-764.
- [58] Mallik A.K., Kher V., Puri M., and Hatwal H., "On the modelling of non-linear elastomeric vibration isolators". *Journal of Sound and Vibration* 219, no. 2 (1999): 239-253.

- [59] Alhan C., and Gavin H., "A parametric study of linear and non-linear passively damped seismic isolation systems for buildings". *Engineering structures* 26, no. 4 (2004): 485-497.
- [60] Kovacic I., Brennan M.J., and Waters T.P., "A study of a nonlinear vibration isolator with a quasi-zero stiffness characteristic". *Journal of sound and vibration* 315, no. 3 (2008): 700-711.
- [61] Ibrahim R.A., "Recent advances in nonlinear passive vibration isolators". *Journal of sound and vibration* 314, no. 3-5 (2008): 371-452.
- [62] Shekhar N.C., Hatwal H., and Mallik A.K., "Response of non-linear dissipative shock isolators". *Journal of Sound and Vibration* 214, no. 4 (1998): 589-603.
- [63] Jing X.J., Lang Z.Q., Billings S.A., and Tomlinson G.R., "Frequency domain analysis for suppression of output vibration from periodic disturbance using nonlinearities". *Journal of Sound and vibration* 314, no. 3-5 (2008): 536-557.
- [64] Jing X.J. and Lang Z.Q., "Frequency domain analysis of a dimensionless cubic nonlinear damping system subject to harmonic input". *Nonlinear Dynamics* 58, no. 3 (2009): 469.
- [65] Ho C., Lang Z.Q., and Billings S.A., "The benefits of nonlinear cubic viscous damping on the force transmissibility of a Duffing-type vibration isolator". In *Control (CONTROL), 2012 UKACC International Conference on*, pp. 479-484. IEEE, 2012.
- [66] Gatti G., Kovacic I., and Brennan M.J., "On the response of a harmonically excited two degree-of-freedom system consisting of a linear and a nonlinear quasi-zero stiffness oscillator". *Journal of Sound and Vibration* 329, no. 10 (2010): 1823-1835.
- [67] Ho C., Lang Z.Q., and Billings S.A., "Design of vibration isolators by exploiting the beneficial effects of stiffness and damping nonlinearities". *Journal of Sound and Vibration* 333, no. 12 (2014): 2489-2504.
- [68] Zhu Y. and Lang Z.Q., "Design of Nonlinear Systems in the Frequency Domain: An Output Frequency Response Function-Based Approach". *IEEE Transactions on Control Systems Technology* 26, no. 4 (2018): 1358-1371.

- [69] Guo P.F., Lang Z.Q., and Peng Z.K., "Analysis and design of the force and displacement transmissibility of nonlinear viscous damper based vibration isolation systems". *Nonlinear Dynamics* 67, no. 4 (2012): 2671-2687.
- [70] Jing X.J., Lang Z.Q., and Billings S.A., "Frequency domain analysis for non-linear Volterra systems with a general non-linear output function". *International Journal of Control* 81, no. 2 (2008): 235-251.
- [71] Guo Y., Guo L.Z., Billings S.A., Coca D., and Lang Z.Q., "Characterizing Nonlinear Spatio-Temporal Systems in the Frequency Domain". *International Journal of Bifurcation and Chaos* 22, no. 02 (2012): 1230009.
- [72] Peng Z.K., Lang Z.Q., and Billings S.A., "Crack detection using nonlinear output frequency response functions". *Journal of Sound and Vibration* 301, no. 3-5 (2007): 777-788.
- [73] Billings S.A., Stansby P.K., Swain A.K., and Baker M., "Accurate prediction of non-linear wave forces: Part II (Responding cylinder)". *Mechanical systems and signal processing* 12, no. 3 (1998): 487-498.
- [74] Wu Q., Yue H., Liu R., Zhang X., Ding L., Liang T., and Deng Z., "Measurement model and precision analysis of accelerometers for maglev vibration isolation platforms". *Sensors* 15, no. 8 (2015): 20053-20068.
- [75] Wu X.F., Lang Z.Q., and Billings S.A., "Analysis of output frequencies of nonlinear systems". *IEEE Transactions on signal processing* 55, no. 7 (2007): 3239-3246.
- [76] Lang Z.Q. and Billings S.A., "Output frequencies of nonlinear systems". *International Journal of Control* 67, no. 5 (1997): 713-730.
- [77] Jing X.J., Lang Z.Q., and Billings S.A., "Nonlinear influence in the frequency domain: alternating series". *Systems & Control Letters* 60, no. 5 (2011): 295-309.
- [78] Lang Z.Q., Jing X.J., Billings S.A., Tomlinson G.R., and Peng Z.K., "Theoretical study of the effects of nonlinear viscous damping on vibration isolation of SDOF systems". *Journal of Sound and Vibration* 323, no. 1-2 (2009): 352-365.
- [79] Peng Z.K., Meng G., Lang Z.Q., Zhang W.M., and Chu F.L., "Study of the effects of cubic nonlinear damping on vibration isolations using harmonic balance

method". *International Journal of Non-Linear Mechanics* 47, no. 10 (2012): 1073-1080.

[80] Chen Y., Jing X.J., and Cheng L., "Investigation of nonlinear vehicle suspension systems using a frequency domain method". (2011).

[81] Xiao Z., Jing X., and Cheng L., "The transmissibility of vibration isolators with cubic nonlinear damping under both force and base excitations". *Journal of Sound and Vibration* 332, no. 5 (2013): 1335-1354.

[82] Tang B. and Brennan M.J., "A comparison of two nonlinear damping mechanisms in a vibration isolator". *Journal of Sound and Vibration* 332, no. 3 (2013): 510-520.

[83] Pazooki A., Goodarzi A., Khajepour A., Soltani A., and Porlier C., "A novel approach for the design and analysis of nonlinear dampers for automotive suspensions". *Journal of Vibration and Control* 24, no. 14 (2018): 3132-3147.

[84] Lang, Z. Q., Guo P.F., and Takewaki I., "Output frequency response function based design of additional nonlinear viscous dampers for vibration control of multi-degree-of-freedom systems". *Journal of Sound and Vibration* 332, no. 19 (2013): 4461-4481.

[85] Jing X.J., Lang Z.Q., and Billings S.A., "Output frequency response function-based analysis for nonlinear Volterra systems". *Mechanical systems and signal processing* 22, no. 1 (2008): 102-120.

[86] Jing X.J., Lang Z.Q., and Billings S.A., "Output frequency properties of nonlinear systems". *International Journal of Non-Linear Mechanics* 45, no. 7 (2010): 681-690.

[87] Laalej H. and Lang Z.Q., "Numerical investigation of the effects of mr damper characteristic parameters on vibration isolation of SDOF systems under harmonic excitations". *Journal of Intelligent Material Systems and Structures* 21, no. 5 (2010): 483-501.

[88] Laalej H., Lang Z.Q., Daley S., Zazas I., Billings S.A., and Tomlinson G.R., "Application of non-linear damping to vibration isolation: an experimental study". *Nonlinear Dynamics* 69, no. 1-2 (2012): 409-421.

- [89] Bajkowski J., Nachman J., Shillor M., and Sofonea M., "A model for a magnetorheological damper". *Mathematical and computer modelling* 48, no. 1-2 (2008): 56-68.
- [90] Laalej H. and Lang Z.Q., "Study of the effects of nonlinear characteristics of MR dampers on vibration isolation using the output frequency response function". In *Control Conference (ECC), 2009 European*, pp. 1432-1437. IEEE, 2009.
- [91] Zhou N. and Liu K., "A tunable high-static–low-dynamic stiffness vibration isolator". *Journal of Sound and Vibration* 329, no. 9 (2010): 1254-1273.
- [92] Drezet C., Kacem N., and Bouhaddi N., "Design of a nonlinear energy harvester based on high static low dynamic stiffness for low frequency random vibrations". *Sensors and Actuators A: Physical* 283 (2018): 54-64.
- [93] Shaw A. D., Neild S.A., and Wagg D.J., "Dynamic analysis of high static low dynamic stiffness vibration isolation mounts". *Journal of Sound and Vibration* 332, no. 6 (2013): 1437-1455.
- [94] Dong G., Zhang X., Xie S., Yan B., and Luo Y., "Simulated and experimental studies on a high-static-low-dynamic stiffness isolator using magnetic negative stiffness spring". *Mechanical Systems and Signal Processing* 86 (2017): 188-203.
- [95] Dong G., Zhang Y., Luo Y., Xie S., and Zhang X., "Enhanced isolation performance of a high-static–low-dynamic stiffness isolator with geometric nonlinear damping". *Nonlinear Dynamics* (2018): 1-18.
- [96] Huang X., Liu X., Sun J., Zhang Z., and Hua H., "Effect of the system imperfections on the dynamic response of a high-static-low-dynamic stiffness vibration isolator". *Nonlinear Dynamics* 76, no. 2 (2014): 1157-1167.
- [97] Cheng C., Li S.M., Wang Y., and Jiang X.X., "Performance analysis of high-static-low-dynamic stiffness vibration isolator with time-delayed displacement feedback". *Journal of Central South University* 24, no. 10 (2017): 2294-2305.
- [98] Sun X. and Jing X., "A nonlinear vibration isolator achieving high-static-low-dynamic stiffness and tunable anti-resonance frequency band". *Mechanical Systems and Signal Processing* 80 (2016): 166-188.
- [99] Carrella A., "Force transmissibility of a nonlinear vibration isolator with high-static-low-dynamic-stiffness". (2011).

- [100] Abbasi A., Khadem S.E., and Bab S., "Vibration control of a continuous rotating shaft employing high-static low-dynamic stiffness isolators". *Journal of Vibration and Control* 24, no. 4 (2018): 760-783.
- [101] Kovacic I. and Brennan M.J., *The Duffing equation: nonlinear oscillators and their behaviour*. John Wiley & Sons, 2011.
- [102] Xu D., Yu Q., Zhou J., and Bishop S.R., "Theoretical and experimental analyses of a nonlinear magnetic vibration isolator with quasi-zero-stiffness characteristic". *Journal of Sound and Vibration* 332, no. 14 (2013): 3377-3389.
- [103] Wu W., Chen X., and Shan Y., "Analysis and experiment of a vibration isolator using a novel magnetic spring with negative stiffness". *Journal of Sound and Vibration* 333, no. 13 (2014): 2958-2970.
- [104] Zheng Y., Zhang X., Luo Y., Yan B., and Ma C., "Design and experiment of a high-static-low-dynamic stiffness isolator using a negative stiffness magnetic spring". *Journal of Sound and Vibration* 360 (2016): 31-52.
- [105] Zheng Y., Zhang X., Luo Y., Zhang Y., and Xie S., "Analytical study of a quasi-zero stiffness coupling using a torsion magnetic spring with negative stiffness". *Mechanical Systems and Signal Processing* 100 (2018): 135-151.
- [106] Alabuzhev P. M., *Vibration protection and measuring systems with quasi-zero stiffness*. CRC Press, 1989.
- [107] Carrella A., Brennan M.J., and Waters T.P., "Optimization of a quasi-zero-stiffness isolator". *Journal of Mechanical Science and Technology* 21, no. 6 (2007): 946.
- [108] Carrella A., Brennan M.J., and Waters T.P., "Static analysis of a passive vibration isolator with quasi-zero-stiffness characteristic". *Journal of sound and vibration* 301, no. 3-5 (2007): 678-689.
- [109] Carrella A., Brennan M.J., Kovacic I., and Waters T.P., "On the force transmissibility of a vibration isolator with quasi-zero-stiffness". *Journal of Sound and Vibration* 322, no. 4-5 (2009): 707-717.
- [110] Brennan M. J., Kovacic I., Carrella A., and Waters T.P., "On the jump-up and jump-down frequencies of the Duffing oscillator". *Journal of Sound and Vibration* 318, no. 4-5 (2008): 1250-1261.

- [111] Galayko D. and Basset P., "A general analytical tool for the design of vibration energy harvesters (VEHs) based on the mechanical impedance concept". *IEEE Transactions on Circuits and Systems I: Regular Papers* 58, no. 2 (2011): 299-311.
- [112] Williams C. B., and Yates R.B., "Analysis of a micro-electric generator for microsystems". *Sensors and actuators A: Physical* 52, no. 1-3 (1996): 8-11.
- [113] Shearwood C. and Yates R.B., "Development of an electromagnetic microgenerator". *Electronics Letters* 33, no. 22 (1997): 1883-1884.
- [114] Scully B., Zuo L., Shestani J., and Zhou Y., "Design and characterization of an electromagnetic energy harvester for vehicle suspensions". In *ASME 2009 International Mechanical Engineering Congress and Exposition*, pp. 1007-1016. American Society of Mechanical Engineers, 2009.
- [115] Nammari A., Caskey L., Negrete J., and Bardaweel H., "Fabrication and characterization of non-resonant magneto-mechanical low-frequency vibration energy harvester". *Mechanical Systems and Signal Processing* 102 (2018): 298-311.
- [116] Mehr T.H., Tabesh A., and Ghadamyari M.A., "Design and Implementation of a Hybrid Electromagnetic Vibration to Electricity Energy Harvester for AC Power Lines Sensors". *Power MEMS 2011*, Seoul, South Korea, Nov. 2011.
- [117] Tao K., Lye S.W., Miao J., and Hu X., "Design and implementation of an out-of-plane electrostatic vibration energy harvester with dual-charged electret plates". *Microelectronic Engineering* 135 (2015): 32-37.
- [118] Nammari A. and Bardaweel H., "Design enhancement and non-dimensional analysis of magnetically-levitated nonlinear vibration energy harvesters". *Journal of Intelligent Material Systems and Structures* 28, no. 19 (2017): 2810-2822.
- [119] Stabile A., Aglietti G.S., Richardson G., and Smet G., "Design and verification of a negative resistance electromagnetic shunt damper for spacecraft micro-vibration". *Journal of Sound and Vibration* 386 (2017): 38-49.
- [120] Yang J., Yu Q., Zhao J., Zhao N., Wen Y., Li P., and Qiu J., "Design and optimization of a bi-axial vibration-driven electromagnetic generator". *Journal of Applied Physics* 116, no. 11 (2014): 114506.

- [121] Spreemann D. and Manoli Y., *Electromagnetic vibration energy harvesting devices: Architectures, design, modeling and optimization*. Vol. 35. Springer Science & Business Media, 2012.
- [122] Khaligh A., Zeng P., and Zheng C., "Kinetic energy harvesting using piezoelectric and electromagnetic technologies—state of the art". *IEEE Transactions on Industrial Electronics* 57, no. 3 (2010): 850-860.
- [123] Mitcheson P.D., Green T.C., Yeatman E.M., and Holmes A.S., "Architectures for vibration-driven micropower generators". *Journal of microelectromechanical systems* 13, no. 3 (2004): 429-440.
- [124] Stephen N.G., "On energy harvesting from ambient vibration". *Journal of sound and vibration* 293, no. 1-2 (2006): 409-425.
- [125] Roundy S., Wright P.K., and Rabaey J., "A study of low-level vibrations as a power source for wireless sensor nodes". *Computer communications* 26, no. 11 (2003): 1131-1144.
- [126] Harne R.L. and Wang K.W., "A review of the recent research on vibration energy harvesting via bistable systems". *Smart materials and structures* 22, no. 2 (2013): 023001.
- [127] Mateu L. and Moll F., "Review of energy harvesting techniques and applications for microelectronics". In *VLSI Circuits and Systems II*, vol. 5837, pp. 359-374. International Society for Optics and Photonics, 2005.
- [128] Roundy S. and Zhang Y., "Toward self-tuning adaptive vibration-based microgenerators". In *Smart Structures, Devices, and Systems II*, vol. 5649, pp. 373-385. International Society for Optics and Photonics, 2005.
- [129] Challa V.R., Prasad M.G., Shi Y., and Fisher F.T., "A vibration energy harvesting device with bidirectional resonance frequency tunability". *Smart Materials and Structures* 17, no. 1 (2008): 015035.
- [130] Cammarano A., Burrow S.G., Barton D.A., Carrella A., and Clare L.R., "Tuning a resonant energy harvester using a generalized electrical load". *Smart Materials and Structures* 19, no. 5 (2010): 055003.

- [131] Zhu D., Tudor M.J., and Beeby S.P., "Strategies for increasing the operating frequency range of vibration energy harvesters: a review". *Measurement Science and Technology* 21, no. 2 (2009): 022001.
- [132] Nguyen S.D. and Halvorsen E., "Nonlinear springs for bandwidth-tolerant vibration energy harvesting". *Journal of Microelectromechanical Systems* 20, no. 6 (2011): 1225-1227.
- [133] Ramlan R., Brennan M.J., Mace B.R., and Kovacic I., "Potential benefits of a non-linear stiffness in an energy harvesting device". *Nonlinear dynamics* 59, no. 4 (2010): 545-558.
- [134] Tehrani M.G. and Elliott S.J., "Extending the dynamic range of an energy harvester using nonlinear damping". *Journal of Sound and Vibration* 333, no. 3 (2014): 623-629.
- [135] Hendijanizadeh M., Elliott S.J., and Ghandchi-Tehrani M., "The effect of internal resistance on an energy harvester with cubic resistance load". *The 22nd International Congress on Sound and Vibration (ICSV22)*, Italy, (2015).
- [136] Hendijanizadeh M., Elliott S.J., and Ghandchi-Tehrani M., "Extending the dynamic range of an energy harvester with a variable load resistance". *Journal of Intelligent Material Systems and Structures* 28, no. 20 (2017): 2996-3005.
- [137] Simeone L., Ghandchi Tehrani M., Elliott S.J., and Hendijanizadeh M., "Nonlinear damping in an energy harvesting device". *Conference on Noise and Vibration Engineering (ISMA2014)*, Belgium, (2014).
- [138] Kwon S.C. and Oh H.U., "Experimental validation of satellite micro-jitter management strategy in energy harvesting and vibration isolation". *Sensors and Actuators A: Physical* 249 (2016): 172-185.
- [139] Zhu S., Shen W.A., and Xu Y.L., "Linear electromagnetic devices for vibration damping and energy harvesting: Modeling and testing". *Engineering Structures* 34 (2012): 198-212.
- [140] Han B., Vassilaras S., Papadias C.B., Soman R., Kyriakides M.A., Onoufriou T., Nielsen R.H., and Prasad R., "Harvesting energy from vibrations of the underlying structure". *Journal of Vibration and Control* 19, no. 15 (2013): 2255-2269.

- [141] Tang X. and Zuo L., "Simulation and experiment validation of simultaneous vibration control and energy harvesting from buildings using tuned mass dampers". In *American Control Conference (ACC), 2011*, pp. 3134-3139. IEEE, 2011.
- [142] Lefeuvre E., Audigier D., Richard C., and Guyomar D., "Buck-boost converter for sensorless power optimization of piezoelectric energy harvester". *IEEE Transactions on Power Electronics* 22, no. 5 (2007): 2018-2025.
- [143] Hu H., Dowell E.H., and Virgin L.N., "Resonances of a harmonically forced Duffing oscillator with time delay state feedback". *Nonlinear Dynamics* 15, no. 4 (1998): 311-327.
- [144] Erturk A. and Inman D.J., "Broadband piezoelectric power generation on high-energy orbits of the bistable Duffing oscillator with electromechanical coupling". *Journal of Sound and Vibration* 330, no. 10 (2011): 2339-2353.
- [145] Cammarano A., Neild S.A., Burrow S.G., Wagg D.J., and Inman D.J., "Optimum resistive loads for vibration-based electromagnetic energy harvesters with a stiffening nonlinearity". *Journal of Intelligent Material Systems and Structures* 25, no. 14 (2014): 1757-1770.
- [146] Mofidian S.M. and Bardaweel H., "Displacement transmissibility evaluation of vibration isolation system employing nonlinear-damping and nonlinear-stiffness elements". *Journal of Vibration and Control* 24, no. 18 (2018): 4247-4259.
- [147] Xiong Y.P., Xing J.T., and Price, W.G., "Power flow analysis of complex coupled systems by progressive approaches". *Journal of Sound and Vibration*, 239, no. 2 (2001): 275-295.
- [148] Jing X.J., Lang Z.Q., Billings S.A., and Tomlinson G.R., "The parametric characteristic of frequency response functions for nonlinear systems". *International Journal of Control* 79, no. 12 (2006): 1552-1564.
- [149] Peng Z.K. and Lang Z.Q., "The effects of nonlinearity on the output frequency response of a passive engine mount". *Journal of Sound and Vibration* 318, no. 1-2 (2008): 313-328.
- [150] Peng Z.K., Lang Z.Q., Meng G., and Billings S.A., "Reducing force transmissibility in multiple degrees of freedom structures through anti-symmetric nonlinear viscous damping". *Acta Mechanica Sinica* 28, no. 5 (2012): 1436-1448.

- [151] Peng Z.K., Lang Z.Q., and Meng G., "Evaluation of transmissibility for a class of nonlinear passive vibration isolators". *Frontiers of Mechanical Engineering* 7, no. 4 (2012): 401-409.
- [152] Peng Z.K., Lang Z.Q., Jing X.J., Billings S.A., Tomlinson G.R., and Guo L.Z., "The transmissibility of vibration isolators with a nonlinear antisymmetric damping characteristic". *Journal of Vibration and Acoustics* 132, no. 1 (2010): 014501.
- [153] Boyd S. and Chua L., "Fading memory and the problem of approximating nonlinear operators with Volterra series". *IEEE Transactions on circuits and systems* 32, no. 11 (1985): 1150-1161.
- [154] Lu Z.Q., Chen L.Q., Brennan M.J., Li J.M., and Ding H., "The Characteristics of Vibration Isolation System with Damping and Stiffness Geometrically Nonlinear". In *Journal of Physics: Conference Series*, vol. 744, no. 1, p. 012115. IOP Publishing, 2016.
- [155] Zhu Y. and Lang Z.Q., "The effects of linear and nonlinear characteristic parameters on the output frequency responses of nonlinear systems: The associated output frequency response function". *Automatica* 93 (2018): 422-427.
- [156] Gavin H.P., "Vibrations of single degree of freedom systems". *Department of Civil and Environmental Engineering, Duke University* (2014).
- [157] Tao J.S., Liu G.R., and Lam K.Y., "Design optimization of marine engine-mount system". *Journal of Sound and vibration* 235, no. 3 (2000): 477-494.
- [158] Soliman J.I. and Ismailzadeh E., "Optimization of unidirectional viscous damped vibration isolation system". *Journal of sound and vibration* 36, no. 4 (1974): 527-539.
- [159] Jazar G.N., Narimani A., Golnaraghi M.F., and Swanson D.A., "Practical frequency and time optimal design of passive linear vibration isolation mounts". *Vehicle system dynamics* 39, no. 6 (2003): 437-466.
- [160] Alleyne A. and Hedrick J.K., "Nonlinear adaptive control of active suspensions". *IEEE transactions on control systems technology* 3, no. 1 (1995): 94-101.

- [161] Jazar G.N., Houim R., Narimani A., and Golnaraghi M.F., "Frequency response and jump avoidance in a nonlinear passive engine mount". *Journal of Vibration and Control* 12, no. 11 (2006): 1205-1237.
- [162] Borowiec M., Litak G., and Friswell M.I., "Nonlinear response of an oscillator with a magneto-rheological damper subjected to external forcing". In *Applied Mechanics and Materials*, vol. 5, pp. 277-284. Trans Tech Publications, 2006.
- [163] Jones J.P., "Automatic computation of polyharmonic balance equations for non-linear differential systems". *International Journal of Control* 76, no. 4 (2003): 355-365.
- [164] Elliott A.M., Bernstein M.A., Ward H.A., Lane J., and Witte R.J., "Nonlinear averaging reconstruction method for phase-cycle SSFP". *Magnetic resonance imaging* 25, no. 3 (2007): 359-364.
- [165] Stanzhitskii A.N. and Dobrodzii T.V., "Study of optimal control problems on the half-line by the averaging method". *Differential Equations* 47, no. 2 (2011): 264-277.
- [166] Xing X. and Zhang D., "Realization of Nonlinear Describing Function Method Virtual Experiment System Based on LabVIEW". *International Conference of China Communication (ICCC2010)*, (2010).
- [167] Attari M., Haeri M., and Tavazoei M.S., "Analysis of a fractional order Van der Pol-like oscillator via describing function method". *Nonlinear dynamics* 61, no. 1-2 (2010): 265-274.
- [168] Milovanovic Z., Kovacic I., and Brennan M.J., "On the displacement transmissibility of a base excited viscously damped nonlinear vibration isolator". *Journal of Vibration and Acoustics* 131, no. 5 (2009): 054502.
- [169] Denoël V. and Degée H., "Analysis of linear structures with non-linear dampers". In *Proceeding of the Eurodyn Conference 2002*. 2002.
- [170] Priya S. and Inman D.J., eds. *Energy harvesting technologies*. Vol. 21. New York: Springer, 2009.
- [171] Beeby S.P., Torah R.N., Tudor M.J., Glynne-Jones P., O'donnell T., Saha C.R., and Roy S., "A micro electromagnetic generator for vibration energy harvesting". *Journal of Micromechanics and microengineering* 17, no. 7 (2007): 1257.

- [172] Hendijanizadeh M., Sharkh S.M., Elliott S.J., and Moshrefi-Torbati M., "Output power and efficiency of electromagnetic energy harvesting systems with constrained range of motion". *Smart Materials and Structures* 22, no. 12 (2013): 125009.
- [173] Hendijanizadeh M., Moshrefi-Torbati M., and Sharkh S.M., "Constrained design optimization of vibration energy harvesting devices". *Journal of Vibration and Acoustics* 136, no. 2 (2014): 021001.
- [174] Su D., Nakano K., Zheng R., and Cartmell M.P., "On electrical optimisation using a Duffing-type vibrational energy harvester". *Proceedings of the Institution of Mechanical Engineers, Part C: Journal of Mechanical Engineering Science* 229, no. 18 (2015): 3308-3319.
- [175] Mitcheson P.D., Toh T.T., Wong K.H., Burrow S.G., and Holmes A.S., "Tuning the resonant frequency and damping of an electromagnetic energy harvester using power electronics". *IEEE Transactions on Circuits and Systems II: Express Briefs* 58, no. 12 (2011): 792-796.
- [176] Cammarano A., Neild S.A., Burrow S.G., and Inman D.J., "The bandwidth of optimized nonlinear vibration-based energy harvesters". *Smart Materials and Structures* 23, no. 5 (2014): 055019.
- [177] Cammarano A., Gonzalez-Buelga A., Neild S.A., Burrow S.G., and Inman D.J., "Bandwidth of a nonlinear harvester with optimized electrical load". In *Journal of Physics: Conference Series*, vol. 476, no. 1, p. 012071. IOP Publishing, 2013.
- [178] Fernando J.S. and Sun Q., "Bandwidth widening of vibration energy harvesters through a multi-stage design". *Journal of Renewable and Sustainable Energy* 7, no. 5 (2015): 053110.
- [179] Diala U., Pope S., and Lang Z.Q., "Analysis and design of a nonlinear vibration-based energy harvester-a frequency based approach". In *Advanced Intelligent Mechatronics (AIM), 2017 IEEE International Conference on*, pp. 1550-1555. IEEE, 2017.
- [180] Diala U., Lang Z.Q., and Pope S., "Analysis, design and optimization of a nonlinear energy harvester". In *24th International Congress on Sound and Vibration 2017 (ICSV 24)*. (2017)

- [181] Feijoo J.V., Worden K., and Stanway R., "Associated linear equations for Volterra operators". *Mechanical Systems and Signal Processing* 19, no. 1 (2005): 57-69.
- [182] Feijoo J.V., Worden K., and Stanway R., "Analysis of time-invariant systems in the time and frequency domain by associated linear equations (ALEs)". *Mechanical Systems and Signal Processing* 20, no. 4 (2006): 896-919.
- [183] Ibrahim N.N.L.N. and Lang Z.Q., "A new and efficient method for the determination of Output Frequency Response Function of nonlinear vibration systems", *Transforming the Future of Infrastructure through Smarter Information: Proceedings of the International Conference on Smart Infrastructure and Construction*, (2016).
- [184] Stanton S.C., McGehee C.C., and Mann B.P., "Reversible hysteresis for broadband magnetopiezoelectric energy harvesting". *Applied Physics Letters* 95, no. 17 (2009): 174103.
- [185] Mofidian S.M., and Bardaweel H., "Investigation of Damping Nonlinearity in Duffing-Type Vibration Isolation System with Geometric and Magnetic Stiffness Nonlinearities". In *ASME 2017 International Mechanical Engineering Congress and Exposition*, American Society of Mechanical Engineers, 2017.
- [186] Mofidian S.M. and Bardaweel H., "Theoretical study and experimental identification of elastic-magnetic vibration isolation system". *Journal of Intelligent Material Systems and Structures* 29, no. 18 (2018): 3550-3561.
- [187] Tang X. and Zuo L., "Simultaneous energy harvesting and vibration control of structures with tuned mass dampers". *Journal of Intelligent Material Systems and Structures* 23, no. 18 (2012): 2117-2127.
- [188] Ali S.F. and Adhikari S., "Energy harvesting dynamic vibration absorbers". *Journal of Applied Mechanics* 80, no. 4 (2013): 041004.
- [189] Gonzalez-Buelga A., Clare L.R., Cammarano A., Neild S.A., Burrow S.G., and Inman D.J., "An optimised tuned mass damper/harvester device". *Structural Control and Health Monitoring* 21, no. 8 (2014): 1154-1169.
- [190] Davis R.B. and McDowell M.D., "Combined Euler column vibration isolation and energy harvesting". *Smart Materials and Structures* 26, no. 5 (2017): 055001.

- [191] Li Y., Baker E., Reissman T., Sun C., and Liu W.K., "Design of mechanical metamaterials for simultaneous vibration isolation and energy harvesting". *Applied Physics Letters* 111, no. 25 (2017): 251903.
- [192] Chen Z., Guo B., Yang Y., and Cheng C., "Metamaterials-based enhanced energy harvesting: A review". *Physica B: Condensed Matter* 438 (2014): 1-8.
- [193] Shen W., Zhu S., Xu Y.L., and Zhu H.P., "Energy regenerative tuned mass dampers in high-rise buildings". *Structural Control and Health Monitoring* 25, no. 2 (2018): e2072.
- [194] Mofidian S.M. and Bardaweel H., "A dual-purpose vibration isolator energy harvester: Experiment and model". *Mechanical Systems and Signal Processing* 118 (2019): 360-376.
- [195] Patel S., Park H., Bonato P., Chan L., and Rodgers M., "A review of wearable sensors and systems with application in rehabilitation". *Journal of neuroengineering and rehabilitation* 9, no. 1 (2012): 21.
- [196] Knight C., Davidson J., and Behrens S., "Energy options for wireless sensor nodes". *Sensors* 8, no. 12 (2008): 8037-8066.
- [197] Zuo L. and Cui W., "Dual-functional energy-harvesting and vibration control: electromagnetic resonant shunt series tuned mass dampers". *Journal of vibration and acoustics* 135, no. 5 (2013): 051018.
- [198] Nammari A., Doughty S., Savage D., Weiss L., Jaganathan A., and Bardaweel H., "Design and analysis of a small-scale magnetically levitated energy harvester utilizing oblique mechanical springs". *Microsystem Technologies* 23, no. 10 (2017): 4645-4657.
- [199] Sazonov E., Li H., Curry D., and Pillay P., "Self-powered sensors for monitoring of highway bridges". *IEEE Sensors Journal* 9, no. 11 (2009): 1422-1429.
- [200] Park G., Rosing T., Todd M.D., Farrar C.R., and Hodgkiss W., "Energy harvesting for structural health monitoring sensor networks". *Journal of Infrastructure Systems* 14, no. 1 (2008): 64-79.
- [201] Hu G., Tang L., Banerjee A., and Das R., "Metastructure with piezoelectric element for simultaneous vibration suppression and energy harvesting". *Journal of Vibration and Acoustics* 139, no. 1 (2017): 011012.

- [202] Li Z., Zuo L., Kuang J., and Luhrs G., "Energy-harvesting shock absorber with a mechanical motion rectifier". *Smart Materials and Structures* 22, no. 2 (2012): 025008.
- [203] Madhav C. and Ali S.F., "Harvesting energy from vibration absorber under random excitations". *IFAC-PapersOnLine* 49, no. 1 (2016): 807-812.
- [204] Makihara K., Onoda J., and Minesugi K., "A self-sensing method for switching vibration suppression with a piezoelectric actuator". *Smart Materials and Structures* 16, no. 2 (2007): 455.
- [205] Wang X.Y., Palagummi S., Liu L., and Yuan F.G., "A magnetically levitated vibration energy harvester". *Smart Materials and Structures* 22, no. 5 (2013): 055016.
- [206] Palagummi S., Zou J., and Yuan F.G., "A horizontal diamagnetic levitation based low frequency vibration energy harvester". *Journal of Vibration and Acoustics* 137, no. 6 (2015): 061004.
- [207] Palagummi S. and Yuan F.G., "An optimal design of a mono-stable vertical diamagnetic levitation based electromagnetic vibration energy harvester". *Journal of Sound and Vibration* 342 (2015): 330-345.
- [208] Palagummi S. and Yuan F.G., "Magnetic levitation and its application for low frequency vibration energy harvesting". In *Structural Health Monitoring (SHM) in Aerospace Structures*, pp. 213-251. 2016.
- [209] Bu L., Wu X., Wang X., and Liu L., "Non-resonant electrostatic energy harvester for wideband applications". *IET Micro & Nano Letters* 8, no. 3 (2013): 135-137.
- [210] Anton S.R. and Sodano H.A., "A review of power harvesting using piezoelectric materials (2003–2006)". *Smart materials and Structures* 16, no. 3 (2007).
- [211] Mallick D., Amann A., and Roy S., "A nonlinear stretching based electromagnetic energy harvester on FR4 for wideband operation". *Smart Materials and Structures* 24, no. 1 (2014): 015013.
- [212] Yang B., Lee C., Xiang W., Xie J., He J.H., Kotlanka R.K., Low S.P., and Feng H., "Electromagnetic energy harvesting from vibrations of multiple

frequencies". *Journal of Micromechanics and Microengineering* 19, no. 3 (2009): 035001.

[213] Sodano H.A., Bae J.S., Inman D.J., and Belvin W.K., "Concept and model of eddy current damper for vibration suppression of a beam". *Journal of Sound and Vibration* 288, no. 4-5 (2005): 1177-1196.

[214] Gao M., Wang Y., Wang Y., and Wang P., "Experimental investigation of non-linear multi-stable electromagnetic-induction energy harvesting mechanism by magnetic levitation oscillation". *Applied Energy* 220 (2018): 856-875.

[215] Rahimi A., Zorlu Ö., Muhtaroglu A., and Kulah H., "Fully self-powered electromagnetic energy harvesting system with highly efficient dual rail output". *IEEE Sensors Journal* 12, no. 6 (2012): 2287-2298.

[216] Zahn M., "Magnetic fluid and nanoparticle applications to nanotechnology". *Journal of nanoparticle research* 3, no. 1 (2001): 73-78.

[217] Zorlu Ö., Topal E.T., and Kulah H., "A vibration-based electromagnetic energy harvester using mechanical frequency up-conversion method". *IEEE Sensors Journal* 11, no. 2 (2011): 481-488.

[218] Liu M., Lin R., Zhou S., Yu Y., Ishida A., McGrath M., Kennedy B., Hajj M., and Zuo L., "Design, simulation and experiment of a novel high efficiency energy harvesting paver". *Appl. Energy*, vol. 212, no. January, pp. 966–975, 2018.

[219] Zhang Z., Zhang X., Chen W., Rasim Y., Salman W., Pan H., Yuan Y., and Wang C., "A high-efficiency energy regenerative shock absorber using supercapacitors for renewable energy applications in range extended electric vehicle". *Applied Energy* 178 (2016): 177-188.

[220] Gutierrez M., Shahidi A., Berdy D., and Peroulis D., "Design and characterization of a low frequency 2-dimensional magnetic levitation kinetic energy harvester". *Sensors and Actuators A: Physical* 236 (2015): 1-10.

[221] Berdy D.F., Valentino D.J., Peroulis D., "Design and optimization of a magnetically sprung block magnet vibration energy harvester". *Sensors and actuators A: Physical* 218 (2014): 69-79.